
AFRL-RB-WP-TR-2008-3101

# A JOINED-WING FLIGHT EXPERIMENT

**Maxwell Blair, Jason Robinson, William A. McClelland, and Jason C. Bowman**

**Design and Analysis Methods Branch**
**Structures Division**

**FEBRUARY 2008**
**Final Report**



**AIR FORCE RESEARCH LABORATORY**
**AIR VEHICLES DIRECTORATE**
**WRIGHT-PATTERSON AIR FORCE BASE, OH 45433-7542**
**AIR FORCE MATERIEL COMMAND**
**UNITED STATES AIR FORCE**

# NOTICE AND SIGNATURE PAGE

Using Government drawings, specifications, or other data included in this document for any purpose other than Government procurement does not in any way obligate the U.S. Government. The fact that the Government formulated or supplied the drawings, specifications, or other data does not license the holder or any other person or corporation; or convey any rights or permission to manufacture, use, or sell any patented invention that may relate to them.

This report was cleared for public release by the Wright-Patterson Air Force Base (WPAFB) Public Affairs Office and is available to the general public, including foreign nationals. Copies may be obtained from the Defense Technical Information Center (DTIC) (http://www.dtic.mil).

AFRL-RB-WP-TR-2008-3101 HAS BEEN REVIEWED AND IS APPROVED FOR PUBLICATION IN ACCORDANCE WITH ASSIGNED DISTRIBUTION STATEMENT.

*//Signature//

MAXWELL BLAIR
Aerospace Engineer
Design and Analysis Methods Branch
Structures Division

//Signature//

FRANK C. WITZEMAN
Chief
Design and Analysis Methods Branch
Structures Division

*//Signature//

JOHN A. BOWLUS
Chief, Structures Division
Air Vehicles Directorate

This report is published in the interest of scientific and technical information exchange, and its publication does not constitute the Government's approval or disapproval of its ideas or findings.

*Disseminated copies will show "//signature//" stamped or typed above the signature blocks.

# REPORT DOCUMENTATION PAGE

*Form Approved*
*OMB No. 0704-0188*



| 1. REPORT DATE *(DD-MM-YY)* | 2. REPORT TYPE | 3. DATES COVERED *(From - To)* |
|---|---|---|
| February 2008 | Final | 01 October 2003 – 30 September 2006 |

**4. TITLE AND SUBTITLE**
A JOINED-WING FLIGHT EXPERIMENT

**5a. CONTRACT NUMBER**
In-house

**5b. GRANT NUMBER**

**5c. PROGRAM ELEMENT NUMBER**
0602201

**6. AUTHOR(S)**
Maxwell Blair and Jason Robinson (AFRL/RBSD)
William A. McClelland (AFRL/RBCC)
Jason C. Bowman (AFRL/RBSA)

**5d. PROJECT NUMBER**
A03H

**5e. TASK NUMBER**

**5f. WORK UNIT NUMBER**
0A

**7. PERFORMING ORGANIZATION NAME(S) AND ADDRESS(ES)**
Design and Analysis Methods Branch (AFRL/RBSD)
Structures Division
Control Systems Development and Applications Branch (AFRL/RBCC)
Flight Controls Division
Advanced Structural Concepts Branch (AFRL/RBSA)
Structures Division
Air Force Research Laboratory, Air Vehicles Directorate
Wright-Patterson Air Force Base, OH 45433-7542
Air Force Materiel Command, United States Air Force

**8. PERFORMING ORGANIZATION REPORT NUMBER**
AFRL-RB-WP-TR-2008-3101

**9. SPONSORING/MONITORING AGENCY NAME(S) AND ADDRESS(ES)**
Air Force Research Laboratory
Air Vehicles Directorate
Wright-Patterson Air Force Base, OH 45433-7542
Air Force Materiel Command
United States Air Force

**10. SPONSORING/MONITORING AGENCY ACRONYM(S)**
AFRL/RBSD

**11. SPONSORING/MONITORING AGENCY REPORT NUMBER(S)**
AFRL-RB-WP-TR-2008-3101

**12. DISTRIBUTION/AVAILABILITY STATEMENT**
Approved for public release; distribution unlimited.

**13. SUPPLEMENTARY NOTES**
PAO Case Number: WPAFB 08-3320; Clearance Date: 20 May 2008. Report contains color.

**14. ABSTRACT**
This report summarizes several design and analysis studies surrounding the flight test of a 7% geometric scale of a notional high-altitude, long-endurance (HALE) variant that targeted the AFRL SensorCraft mission. Established procedures were modified to accommodate low-cost testing with giant-scale radio-controlled technology as an approach to reduce high risk associated with new technologies, such as the joined-wing concept. The flight test vehicle reported here was rigid. The second successful flight ended in deep stall due to under-powered design. Minimal data was extracted from the flight test. Significant experience was gained. This report motivates and describes the next step toward low-cost aeroelastic scaling of joined-wing concepts where geometric non-linear structures is a key component.

**15. SUBJECT TERMS**
Flight Testing, Joined-Wing, SensorCraft, Stability, Design, Aeroelasticity, Finite Elements

| 16. SECURITY CLASSIFICATION OF: | | | 17. LIMITATION OF ABSTRACT: | 18. NUMBER OF PAGES | 19a. NAME OF RESPONSIBLE PERSON (Monitor) |
|---|---|---|---|---|---|
| a. REPORT | b. ABSTRACT | c. THIS PAGE | | | Maxwell Blair |
| Unclassified | Unclassified | Unclassified | SAR | 216 | 19b. TELEPHONE NUMBER *(Include Area Code)* N/A |

**Standard Form 298 (Rev. 8-98)**
Prescribed by ANSI Std. Z39-18

## Table of Contents

## LIST OF FIGURES

## LIST OF TABLES

# FOREWORD

This technical report is a compilation of a number of previously cleared reports.

1) Jason Robinson, "Structural Testing and Analysis of a Joined Wing Technology Demonstrator", AFRL-VA-WP-TR-2004-3048, April 2004 (DTIC AD number A425641)
2) Jason Bowman, "STABILITY & CONTROL ANALYSIS OF THE AFRL RADIO-CONTROLLED JOINED WING"
3) William A. McClelland, Captain, USAF, "INERTIA MEASUREMENT AND DYNAMIC STABILITY ANALYSIS OF A RADIO-CONTROLLED JOINED-WING AIRCRAFT", (AFIT/GA/ENY/06-M07 ), (DTIC: ADA451280) (cleared for public release, unlimited distribution)
4) M. Blair, D. Garmann, V. Bond, R. Canfield, P. Pereira, A. Suleman, "Non-Linear Aeroelastic Scaling of a Joined-Wing Concept", AIAA-2007-1887, Cleared for Public Release: by AFRL/WS Public Affairs. Disposition Date: 8/1/2006. Document Number AFRL-WS 06-1857)

**Contributions from inside AFRL:**

Hank Baust designed, set up and conducted the motor/propeller calibration testing in the vertical wind tunnel. Hank also compiled and formatted the test results. This flight test program would not have happened without his encouragement and substantial contributions. His contributions are reported in Section VIII, "Ground Testing" under subsection "Propulsion Testing". Jason Bowman made significant contributions with his analysis for stability and control of the flight test vehicle.

Several AFRL engineers played key roles as pilot and structural restoration. These experts are Mike Pilkenton (pilot), Santiago Panzardi, Joe Mekina, Keith Numbers, This flight test program would not have happened without their substantial contributions. The following AFRL engineers also provided much appreciated support as Flight Test Personnel, Capt David "Walker" Callaway, 1Lt Mark D. Stevenson, 1Lt Carrie Clewett and 1Lt Alexis Nelson.

Much appreciation goes to Purdue University co-op students: Etan Karni, Beth Newsom, Elizabeth Mikolaj. Beth designed and fabricated the balsa and foam prototypes which formed the geometric specifications for low-cost fabrication. Elizabeth was a key contributor in developing the test plan and execution. Both contributed to the larger joined-wing design and analysis effort.

This flight test would not have happened without the structural re-design and analysis of co-author Jason Robinson, co-op from Wright State University. Jason wrote Section VI, "Model Structural Analysis" and the portion of Section VIII "Ground Testing" under "Static Structural Testing". Mike Ooten, now at Ohio State University, came to us under the Wright Scholar Program to support this flight test in many practical ways.

**Contributions from outside of AFRL:**

Early guidance came from Naval Research Lab: Richard J. Foch, Head of Vehicle Research Section. David Patko of AeroComposites in Medway Ohio fabricated the flight test vehicle under delivery order contract F33615-95-D-3215, "Design and Fabrication of Scaled Joined-Wing Prototype". The builder was Mr. Ed Noble. This project benefited with guidance from Tom Cimanto of MaxCim Motors in sizing the electric motor and propeller.

Much appreciation goes to Lt Col. Robert A. Canfield of AFIT for leading graduate student theses and support as flight test personnel and contributions to Section X, " An Aeroelastically Scaled Flight Test Concept". Much appreciation also goes to Lt. Col. Vanessa Bond (formerly Maj. Vanessa Rebello) for her expertise in Flight Testing, which is reflected in Section IX "Flight Testing" and contributions to Section X. Co-author Capt William A. McClelland authored portions of section VIII, "Ground Testing" in the area of "Inertial Testing", as well as the bulk of Section VII, "Model Stability & Control Analysis" in collaboration with co-author Jason Bowman.

# 1. Introduction

## 1.1. SensorCraft

The AFRL SensorCraft program envisions a single platform to perform the missions served by several wide-body aircraft. Many SensorCraft technologies target a consolidated flight profile with 30 hours of endurance at 2000 nautical miles range. The aerodynamics community generated technologies to radically improve aero-efficiency. Structural technologies target aeroelastic performance criteria. Materials technologies target a number of mechanical, thermal and optical criteria. Electromagnetic technologies target remote sensing and radar functions. Configuration designers packaged all this technology in an uninhabited military aircraft. Together, the combined system requirements drive a reduction in size, weight and power. See Reference [1][Lucia] for additional background on SensorCraft.

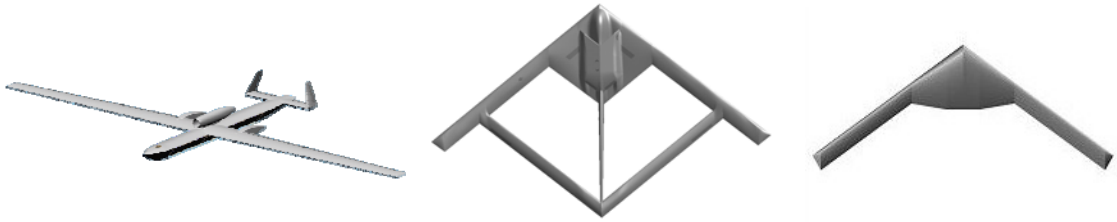

Figure (1) Three SensorCraft Concept Configuration Variants

SensorCraft technologies were integrated into any of several focus concepts depicted in Figure (1). Figure (2) provides an additional view of the Boeing Joined-Wing SensorCraft concept.

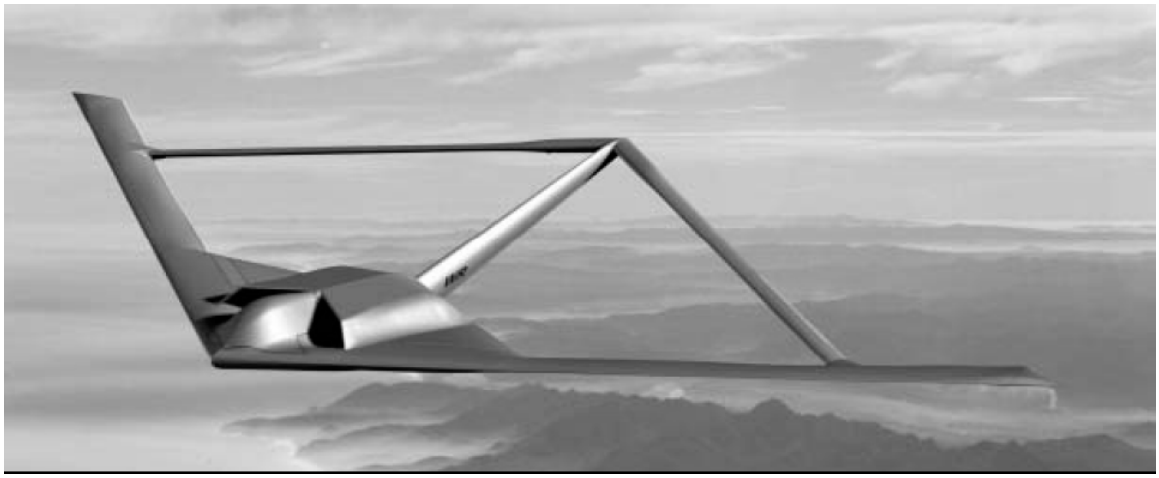

Figure (2) Boeing Joined-Wing SensorCraft Concept

Mission critical needs include long range (50 to 60 hour missions) and high altitude (65,000 feet) flight capabilities [Johnson][2].The joined-wing configuration offers two potential advantages: (a) Full, unobstructed, 360 degree azimuth sensor field-of-regard capability when sensor apertures are embedded in all four wing panels. (b) Joined-wing proponents believe the concept offers significant reduction in wing structural weight and an associated reduction in induced drag relative to a conventional wing-body-tail configuration in the same payload and endurance class [Wolkovitch][3][4].

The inventor of the joined-wing concept, Julian Wolkovitch, promoted his design as more structurally and aerodynamically efficient than conventional wing-tail designs. Potential uses for such a configuration include commercial transport or intelligence surveillance and reconnaissance (ISR). A conformal radar antenna array embedded in such a wing-tail combination provides a natural 360 degree radar coverage at low frequency (long wave length). The AFRL Sensorcraft program has funded a joined-wing concept as the basis for technology development and is a current area of research at the Air Force Research Laboratory (AFRL).

High-Altitude Long-Endurance (HALE) concepts are typically prone to aeroelastic effects. The SensorCraft HALE joined-wing concept is not an exception. However, the joined-wing is characterized by unusual structural load paths that have a fundamental influence on all aspects of the design. As it turns out, the critical load case is associated with aerodynamic gusts at low altitude. Thus, gust load alleviation (GLA) technologies promise a major structural benefit. The research described here ultimately points to a scaled flight test of a joined-wing which incorporates GLA technologies.

The theoretical advantages inherent to the joined-wing structure also introduce significant developmental risks. A number of aeroelastic design studies have focused on the joined-wing. Early studies highlight the unusual structural load paths that follow lines near to and parallel with the leading and trailing edges. These loads form compressive and tensile pairs that account for the additional stiffness inherent to the joined-wing. In a vertical gust, the leading edge will be in compression, eventually leading to geometric non-linear behavior (e.g. buckling). [Blair, Canfield, Roberts] published an optimized joined-wing design study demonstrating that the structure is gust critical and the response is non-linear. There are a number of aeroelastic consequences. Wolkovitch's promise for significant structural weight savings will materialize once we develop confidence in our ability to analyze, validate and design aeroelastic fail-safe joined-wing configurations.

There are a number of approaches toward risk reduction, involving a combination of analysis and testing. In the end, analysis codes can be formally validated in highly controlled environments with streams of data. Validation can be very expensive. Significant risk can be reduced with simple preliminary experiments. High risk experiments are compatible with low cost experiments.

A number of computational developments (involving aeroelastic and structural optimization) have been published. These represent low-cost approaches that increase our insight into the unusual load paths of the joined-wing.

This report describes a preliminary step toward an experimental flight program that reduces the aeroelastic uncertainty associated with joined-wing design. Here, low cost is achieved with recent advances in giant-scale radio-controlled flight (the hobby guys with lots of expendable cash). These advances have come in the form of low-cost propulsion, data acquisition, telemetry, autonomous control, materials etc. All together, it is now possible to conduct low speed aeroelastic flight testing for perhaps 1/100 (one hundredth) the cost of past aeroelastic flight tests. However, such cost reduction can only be realized with modified test procedures that allow for higher probability of failure (without risk to people or property).

Figure (3) VA-1 Remote-Controlled Joined-Wing Aircraft [[14]]

This report describes all the activities that went into the successful flight test of a "rigid" joined-wing variant with 14 foot span depicted in Figure (3). Again, this test represents an increment towards an aeroelastically scaled variant of the Boeing SensorCraft depicted in Figure (2). The aircraft in Figure (3) does not appear to geometrically scale the Boeing configuration in Figure (2). However, they both feature a joined-wing planform, a significant leap of confidence in and of itself. The Boeing configuration would require significantly more cost with dual thrusters and complex assembly. The AFRL configuration in Figure (3) was designed to accommodate a simple pusher propeller with an electric motor. Construction was low cost using foam, balsa and plywood materials.

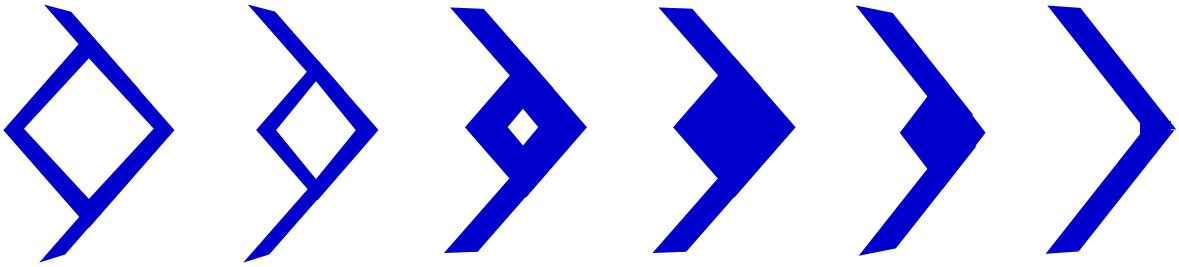

Figure (4) Sample of SensorCraft Design Variants

As an initiative into affordable, fast-response scaled aircraft prototype production, Air Vehicles Division of the Air Force Research Laboratory began design of the Air Vehicles Joined Wing Technology Demonstrator (VA VA-1). The VA-1 is a scaled version of the joined wing SensorCraft candidate in development by Dr Blair of AFRL and Lt. Col. Robert Canfield of the Air Force Institute of Technology [5].

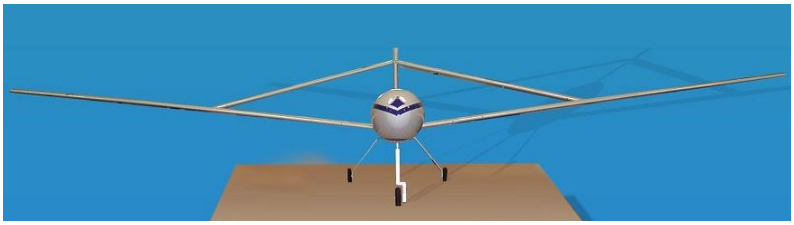

Figure (5) Front View of the Joined Wing Technology Demonstrator

## 1.2. Early Research on the Joined-Wing

Dr. Julian Wolkovitch [4], the original patent holder of the joined wing configuration, created the first proof of concept joined wing vehicles in 1983 through a contract between ACA Industries and Unmanned Systems of East Texas, Inc. In 1986, Dr. Wolkovitch [3] defined the joined wing aircraft configuration as "an airplane that incorporates tandem wings arranged to form diamond shapes in both plan and front views." An example of this diamond shape in the front view can be seen in the picture above. Through mere geometric considerations alone, this configuration lends itself to the SensorCraft application inasmuch as the diamond shaped wing from the plan view gives 360° coverage for possible radar applications.

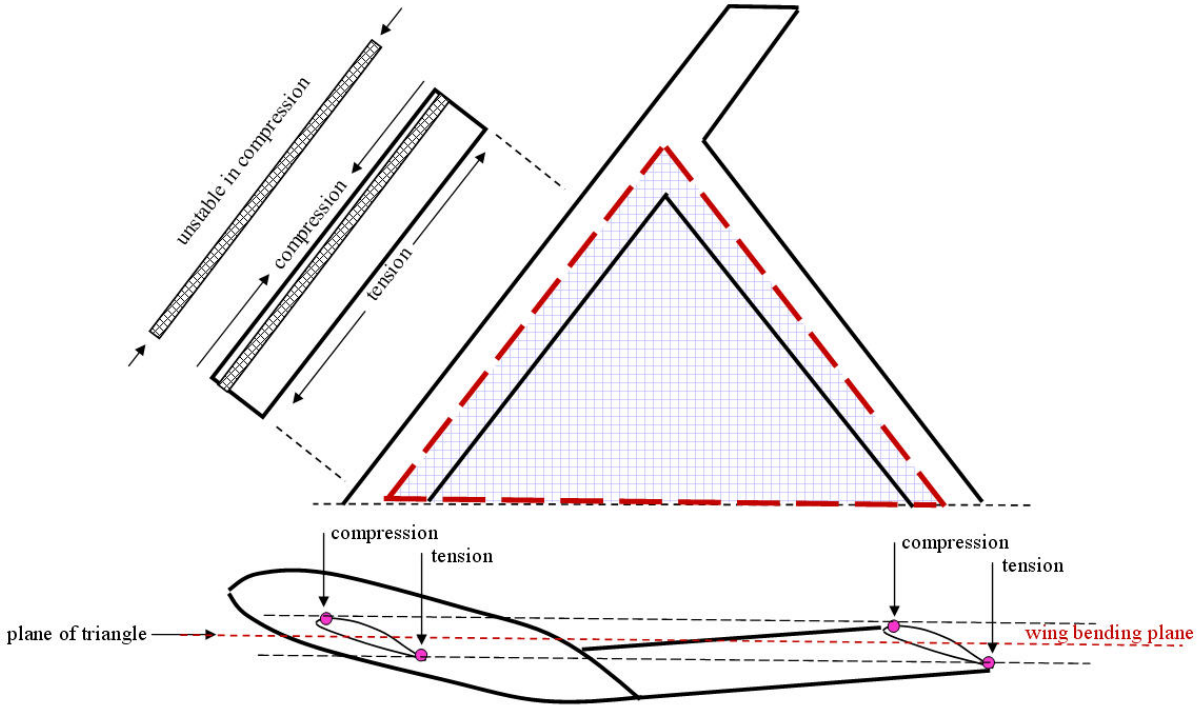


Figure (6) The Wolkovitch Effect

Figure (6) depicts a side and top view of a joined-wing airplane. The dashed triangle outlines a planar surface. The plane is also indicated in the side view. In general, the joined-wing deforms about the plane of least resistance. Thus, in the side view, we see the leading and trailing edges

will be in the most stress due to bending about the plane of least resistance. For upward bending, we see, in both views, that the leading edge is in compression and the trailing edge is in tension. This is the Wolkovitch effect. Subsequent research reviewed in Section 1.4 has identified the role of geometric bend-twist coupling and an unconventional buckling mechanism.

It is hypothesized that with the loads concentrated along the leading and trailing edges, thin airfoil designs may be possible. But, the relationship is not so easily explored and optimized.

Wolkovitch first introduced the joined-wing concept in 1976. He published some of his research findings later in 1986 and described the potential benefits of the joined-wing configuration. He found that joined-wing aircraft could to be up to 25% lighter and have less induced drag than a conventional wing-tail design. The weight savings were contested by Samuels [6] and by Gallman [7]. Wolkovitch also claimed the configuration possessed good stability and control characteristics [3]. Smith et al, however, discovered a pitch up instability near stall angles of attack [8]. The optimal joint location was found to be from 60-100% of the span. For stability, Wolkovitch recommended the front wing stall slightly before the aft wing achieved $Cl_{max}$ [3].

Samuels [6] reported a slightly lower structural weight savings than Wolkovitch regarding joined-wing design. She found a joined wing was 12-22% lighter than a reference, Boeing 727, conventional wing plus tail combination. The study was conducted by building a finite-element model of each respective wing and comparing the weights of them both.

Gallman, Kroo and Smith published research results of an aerodynamic and structural study of joined-wing aircraft. The most promising joint location appeared to be between 60-75% of the semi span. High aft wing compression forces were discovered and Gallman recommended examining aft wing buckling in closer detail. The authors concluded the joined-wing configuration had no real significant advantages over its conventional counterpart, but that the joined-wing concept was definitely worth further investigation[7].

Kroo, et al later conducted a structural study that accounted for the structural weight needed to prevent aft wing buckling [10]. In their study the aft wing was used for both pitch control and structural support for the forward wing. In comparison to an equivalent conventional design, they discovered the joined-wing needed a larger forward wing to improve takeoff field length performance and a larger tail to prevent buckling. The extra weight yielded a 3.2 % higher direct operating cost for the joined-wing. They concluded the joined-wing design was inferior to a comparable conventional wing.

Smith, Cliff and Kroo designed a joined-wing flight demonstrator aircraft called JW-1 and successfully tested a one sixth scale wind-tunnel model of their design. In the design stage they used a vortex-lattice method (VLM) program called LinAir to obtain aerodynamic lift and drag coefficients and found reasonable agreement with wind-tunnel data. By contrast, this research used the VLM approach with a different program called HASC and did not verify the computations with wind tunnel tests. Wind tunnel tests revealed that JW-1, with vortilons added had satisfactory flying qualities for a flight demonstrator aircraft [8].

The JW-1 wing had a linear twist distribution to minimize induced drag with an elliptical lift distribution. A secondary objective of the twist was to achieve takeoff and landing without the fuselage hitting the ground. However, the swept and tapered high aspect ratio wing led to a minor unstable pitch up during stall. Wolkovitch, by contrast, simply stated that joined wings in general would have good stability and control characteristics and did not address this issue [3].

Wing twist was adjusted, at the cost of increased induced drag during cruise, to maintain good handling qualities and improve stall behavior [8]. VA-1 was similar to JW-1 in many aspects. A detailed comparison is made in the detailed geometrical description of VA-1. One key difference was that VA-1 had zero aerodynamic and geometric twist. As a result VA-1 is expected to have a less stable pitch up near stall angles of attack than JW-1.

JW-1 design modifications failed to completely eliminate the unstable stall problem and it re-emerged during wind-tunnel tests. Vortilons were installed on the front wing and produced a "profound improvement" in the post-stall pitching moment. They also found the positive dihedral effect from the wing was reduced as the wing stalled and the lateral stability above stall was influenced by the negative dihedral contribution from the tail. They concluded the impact of this loss on lateral stability on the post-stall handling qualities should be investigated [8].

In the end Smith, Cliff and Kroo sacrificed cruise performance to get better stall characteristics as good handling was considered more important. On its final flight the VA-1 experienced an unrecoverable deep stall during a turn, resulting in a hard landing that suspended flight testing indefinitely. This study did not address post stall pitch up characteristics as HASC does not model viscous effects. However, a preliminary analysis of stall during turns was conducted.

Nangia et al examined configurations and conducted design studies of high aspect ratio Sensorcraft vehicle. He evaluated uncambered wing sections and then wings with designed camber and twist using an inverse design method. He found aerodynamic interference effects between the wing and tail. For an uncambered configuration the leading edge suction was higher on the outboard tip of the front wing, whereas it was higher at the root of the aft wing. In addition, the wing tip experienced a higher loading than expected for an elliptical lift distribution. This effect was reduced when twist and camber were modified to make the spanwise lift more elliptical. Finally, an inverse wing design method using 3-D membrane analogy for joined-wings was discussed. Nangia demonstrated this design method's ability to quickly design wing twist and camber distribution [11].

Nangia et al examines six different Joined-Wing planforms and their effects on aircraft performance both at cruise, takeoff and landing. The configurations included forward and aft swept outer wing versions of a constant chord planforms, AR = 17.46, with leading edge extensions at fore and aft wing roots, and the "lambda-joined-wing" concept. They assumed laminar flow during cruise and examined thick laminar flow airfoil wings both with and without camber. They found that the constant chord planforms, with optimized twist and camber to achieve laminar flow during cruise, had the lowest drag. This planform geometry was similar to the VA-1 planform, except the AFRL version has no camber and no twist and had a lower AR = 14. Both AR calculations utilized combined front and aft wing areas [26].

Reich et al studied the idea of an Active Aeroelastic Wing control method to control wing and therefore antenna deformation. Their study found that six control surfaces could feasibly minimize antenna deformations while simultaneously trimming the aircraft. Furthermore they performed three more variations of progressively subdividing the control surfaces into smaller sections, gradually approaching a morphing type of wing [10].

## 1.3. Aeroelastic Design Challenges

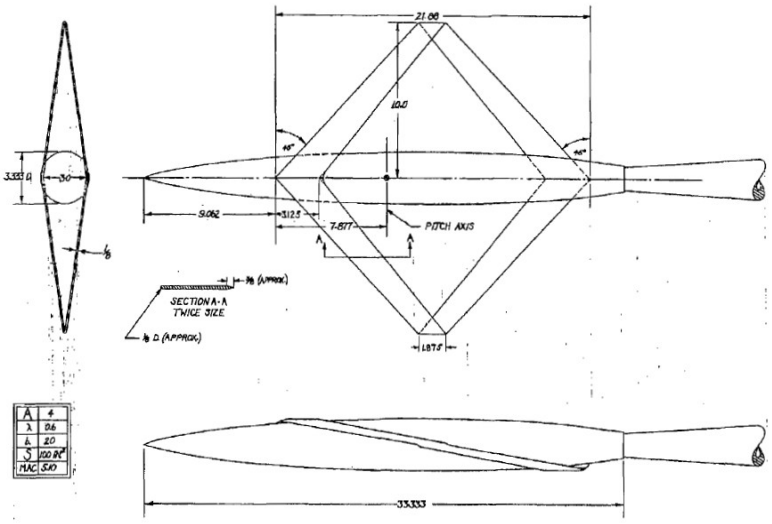


Figure (7) Cahill and Stead Joined-Wing Experiment

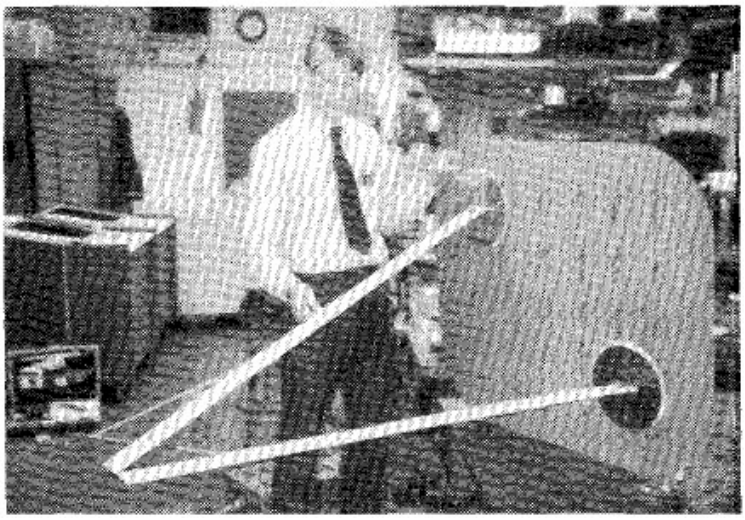

Figure (8) NASA Langley Joined-Wing Flutter Model. [7]

An early look at the transonic benefits of joined-wing technology was published in 1954 by Cahill and Stead [33]. The wind tunnel test model is shown in Figure (7). Following Wolkovitch's patent, testing was conducted at NASA Langley Transonic Dynamic Test (TDT) Facility. An early test model is shown in Figure (8). Figure (8), Figure (9) and Figure (10) are taken from Wolkovitch's overview [3] and represent various inspired experimental initiatives.

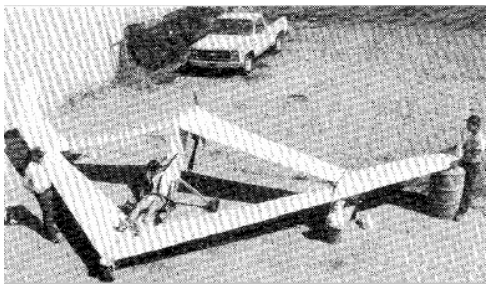

Figure (9) Summit Aircraft Corp. Trident Ultralight

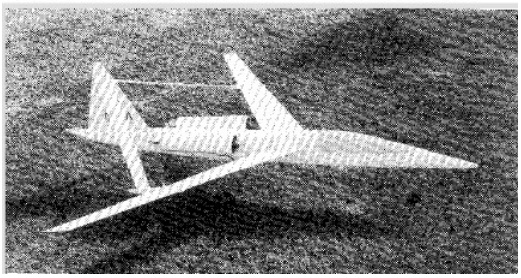

Figure (10) Radio-Controlled Model of JW-1 [8]

Much of the original interest was lost with conceptual studies that indicated a weight penalty associated with joined-wings on a commercial transport concept [7]. Interest was resurrected by the Boeing Company in response to the AFRL SensorCraft program objectives associated with persistent 360 degree radar coverage. Their joined-wing configuration is depicted in Figure 7.

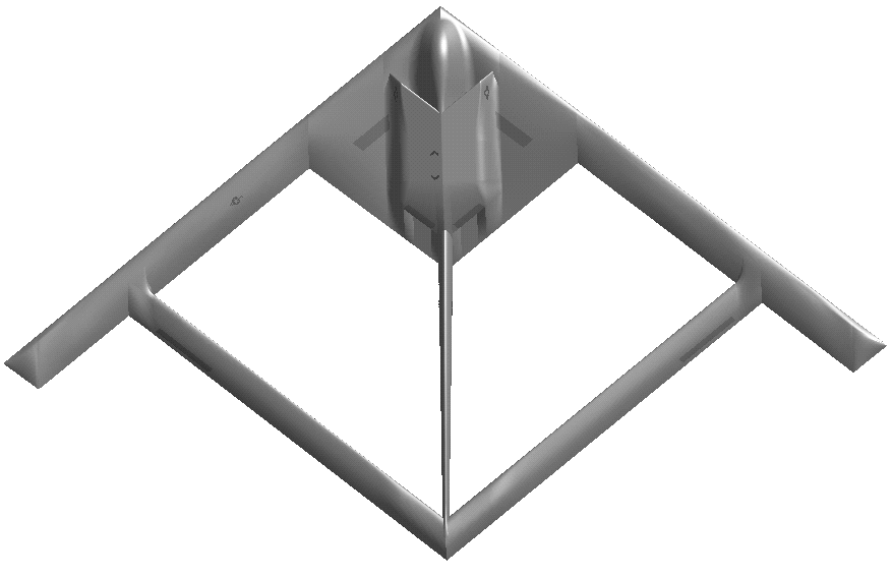

Figure (11) Boeing Joined-Wing SensorCraft Concept

The Joined-Wing concept has been resurrected as a noteworthy configuration alternative to meet the requirements laid out by the AFRL SensorCraft program. These requirements call for long-range, high-altitude missions with 360-degree azimuth for foilage penetration (FOPEN). The

Joined-Wing concept is not proven and will remain a high-risk configuration design alternative until significant research has been accomplished. This research calls for a combination of computational models and flight research for validation of this highly unusual concept. Recent advancements in electronic technologies open the possibilities for scaled flight research with unmanned air vehicles (UAV) with low risk and low cost.

The Joined-Wing literature provides many promised benefits with little validation to support the assertions. Past interest focused on a joined wing passenger aircraft. Simple linear analysis and regression models indicated the payoff over current passenger aircraft was discouraging. In contrast, the primary customer for the current effort is the AFRL SensorCraft Development Team and the primary benefit derives from the need for 360-degree antenna coverage. There are mission constraints where the joined-wing may prove beneficial. Our assertion is that with much non-linear design and development work, the Joined-Wing concept may provide the best range and longest endurance. With a view toward a 200-foot span SensorCraft vehicle, flexibility is certain to add to the many design challenges. Indeed, flexibility may actually enhance performance when properly understood and thereby intentionally designed into the system.

## 1.4. Joined-Wing Design Optimization at AFIT

Smallwood examined, first, how effective an embedded antenna array in a rigid joined-wing type aircraft might be and, second, compared those results to an elastic array with wing twisting and bending. He found that radiation patterns of an array that conformed to the surface of the front end aft wing section of the joined-wing underwent significant distortion due to typical wing deflections. Smallwood recommended active control of wing deformations as a method to improve beam steering but stated that structural changes may also be needed [27].

In her work, Sitz looked at the effectiveness of control surfaces used for roll and lift on a joined-wing aircraft. Her goal was to determine the best location for adequate control that averted control reversal. She found that, if used, conventional control surfaces were best placed on the outboard wing and concluded that conventional control surfaces on the inboard fore and aft sections may be unusable due to radar requirements. VA-1 did not strictly follow these criteria as it utilized a trailing edge flap device for elevator on its rear inboard wings. An alternative control method, twisting the rear wing, fell outside the scope of her study and she recommended further analysis in that area [28].

Rasmussen sought a weight optimized configuration of a Joined-Wing aircraft by varying the following six wing design parameters: front wing sweep, aft wing sweep, outboard wing sweep, joint location, vertical offset and thickness to chord ratio. He determined the optimal weight design had either high vertical offset and low thickness to chord ratio, or low vertical offset and high thickness to chord ratio. He found the joint should ideally be located between ½ and ¾ of the span. He also recommended avoiding high wing sweep angles for both the fore and aft wings [12].

Craft researched three different conceptual design methods for predicting drag of joined-wing type aircraft. His most accurate prediction method was broken into three parts. Wing drag was computed in the Aerospace Vehicle Technology Integration Environment, AVTIE. AVTIE, created by Blair, used Pan Air to predict wing induced drag and XFOIL to determine wing parasite drag [5]. Since AVTIE only accounted for the wing, Roskam's drag buildup approach was then used to find the drag of the fuselage and vertical tail. Total aircraft drag was the

combination of wing, fuselage and vertical tail drag. Craft recommended a CFD analysis to validate his drag predictions [13].

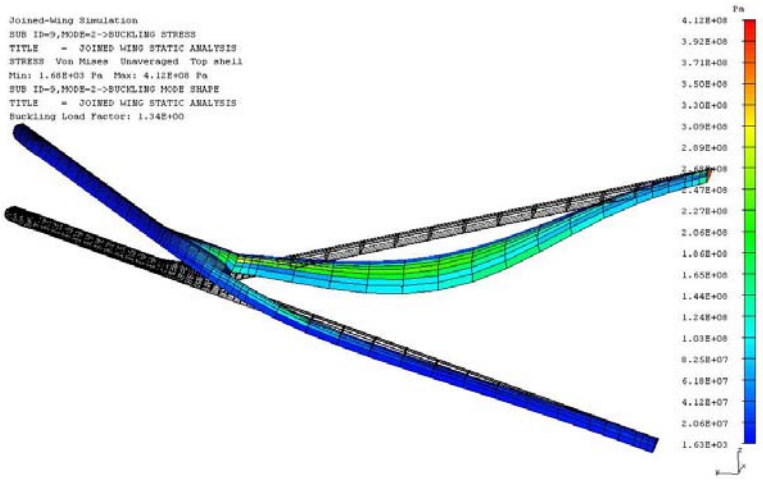


Figure (12) Critical Buckling of the Fully-Stressed Non-Linear FEM

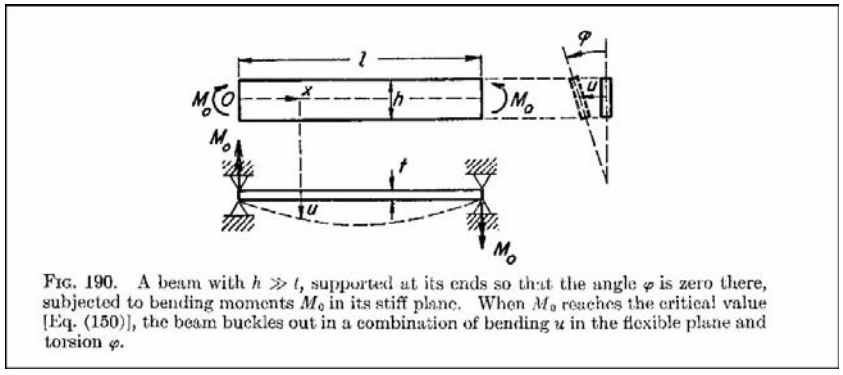


FIG. 190. A beam with $h \gg t$, supported at its ends so that the angle $\varphi$ is zero there, subjected to bending moments $M_0$ in its stiff plane. When $M_0$ reaches the critical value [Eq. (150)], the beam buckles out in a combination of bending $u$ in the flexible plane and torsion $\varphi$.

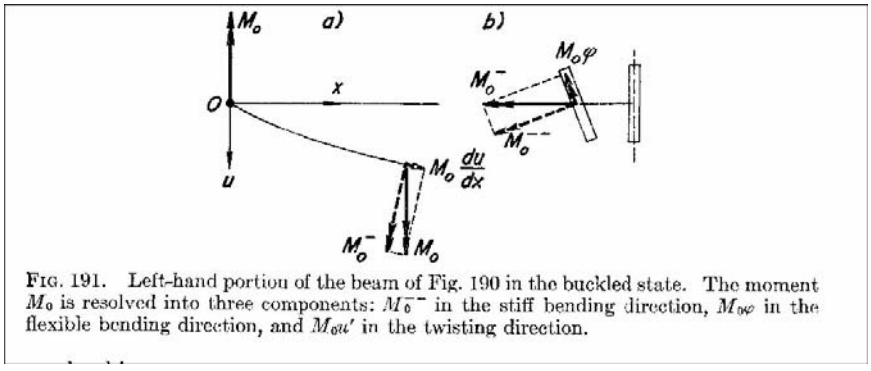


FIG. 191. Left-hand portion of the beam of Fig. 190 in the buckled state. The moment $M_0$ is resolved into three components: $M_0^-$ in the stiff bending direction, $M_0\varphi$ in the flexible bending direction, and $M_0 u'$ in the twisting direction.

Figure (13) Den Hartog's Illustration of Beam in Bend-Twist Coupling

This research used a similar approach to modeling the drag of the different configurations. Craft [13] found that Roskam's method [29] for finding induced drag on the wing was not as accurate

as a panel-method computer code. HASC was used to determine the induced drag of the front and rear wings, while Roskam's drag buildup approach was used to determine parasite drag caused by the wings, fuselage, vertical tails and landing gear.

In parallel with the Boeing SensorCraft study, the AFRL and AFIT conducted a number of in-house research studies to explore the mechanics of joined-wing designs. Reference [5] concluded that joined-wing designs have built-in geometric non-linearity and when the trimmed static aeroelastic vehicle is optimized, there is a noteworthy weight penalty associated with buckling from follower forces or (i.e. geometric non-linearity) Figure (12).

Subsequent study points to Den Hartog's example[37] of a beam in a coupled bend-twist buckled state, depicted in Figure (13). This simple insight points to the correct buckling mechanism for structural design optimization of a joined-wing configuration. The buckling depends on out-or-plane bending stiffness (EI) and torsional stiffness (GJ) alone. Section [8] in this report describes an aeroelastic scaling procedure for the linear representation that should replicate the geometric non-linear response.

# 2. Joined-Wing Flight Test Program

The Joined-Wing concept requires an alternative approach toward controlling the flexibility. However, the mechanics of joined-wing aeroelasticity are not well understood. These mechanics are tightly linked to the configuration and are likely dominated by non-linear behavior.

## 2.1. Phase I Program Objective Overview and Critical Technical Issues

The overall goal of the program is to evaluate the flight characteristics of an aeroelastically-scaled Joined-Wing concept with the lowest risk for aeroelastic flight research in anticipation of future Joined-Wing programs where the cost will be high by necessity.

The Joined-Wing community will benefit from a proven flying baseline. A flying baseline, in contrast to a paper study, removes all doubt about the flight worthiness, thus allowing for well focused follow-on discussion, design and developments. In contrast to a conventional transport vehicle, the joined-wing configuration varies with a myriad of design variables. Each engineering discipline alone tends to bias the airplane into an unnatural configuration. The design put forth for this program blends a number of factors including aerodynamics, structures and flight controls.

Very large airplanes are inherently flexible. Indeed structural flexibility leads to exaggerated aeroelastic behavior that dominates over structural strength as the critical design factor. While the Joined-Wing configuration is thought to be stiffer than a straight wing configuration, the full-scale design will still be dominated by flexibility. There is one important complicating factor. How to incorporate inherent geometric non-linear structural behavior that is unique to Joined-Wing design. This structural behavior causes numerous unconventional design choices that are ultimately realized in flight experimentation. This aspect is discussed in Section [8].

Here, low risk is realized with low-cost with respect to manufacturing and man-hours. Rapid Prototyping will prove valuable in joined-wing development.

Phase I, which is also broken down into sub-phases, includes all flight-testing that will occur with the 7% scaled Joined-Wing model. Phase I activity will follow an incremental build-up starting with Phase I-A in which the model will be the least cost in order to offset the high level of fundamental uncertainty which exists in spite of our best efforts. Indeed, a successful Phase I-A program will significantly aid in the development of mathematical models of the vehicle flight behavior.

### 2.1.1. Phase I-A Program Objective and Critical Technical Issues

Because this particular vehicle concept has never been flown, the test configuration will be used to establish baseline aerodynamic behavior with rigid structures. Technical issues to be resolved will be controllability (control surface layout, sizing and mixing), propulsion in the form of a battery-driven electric motor and fixed propeller, aero performance in terms of speed and duration, direct-lift takeoff-and landing with a pusher propeller, and mass balance with respect to controllability and stability. The placement of the trailing edge control surface on the aft wing cuts into the main structural load path. This is a characteristic of the joined-wing structural design introduced in Reference 2.1. We will explore the effectiveness of the outboard elevon as

the sole pitch effecter. The Technology Readiness Level of this program falls under experimental Research & Development.

Critical Technical Issues: Power, balance, stability, turning performance, pitch effectiveness, operations. Phase I-A will involve taxi tests, test hops, and flying a pattern. This is discussed in detail in Section [7]. Overall confidence in flight-worthiness will be established in Phase I-A at the lowest cost in time and materials.

### 2.1.2. Phase I-B Objective

Autonomous navigation and control will be considered as a first step toward expanding the vehicle envelope. An expanded envelope will also require many vehicle enhancements with respect to power generation and telemetry. Lessons will be learned in Phase I-A and significant redesigns of the current joined-wing configuration are also in order.

Phase I-B flight testing should take place at an established flight test facility. Phase I-B was not yet initiated at the time of this report.

### 2.1.3. Phase I-C Objective

The vehicle in phase I-B will be retrofitted with an aeroelastic wing that will replicate the gust response. The goal will be the development of a practical gust alleviation system in order to validate potential full-scale vehicle weight reductions. This level of technical fidelity will require the design to incorporate significant instrumentation (strain gauges, accelerometers, pitot, on-board camera to monitor wing deflection), data acquisition capability and enhanced telemetry. Aeroelastic scaling is discussed in Section [8].

## 2.2. Test Goal: Risk Reduction with Scaled Testing

The goal of this effort is to demonstrate the basic practicality of joined-wing design for high-altitude, long endurance (HALE) missions with basic research to uncover unrealized aeroelastic behavior. The focus will be on the structural response and flight characteristics of a stiffness scaled joined-wing concept with low-speed flight tests. The inexpensive proposed platform complements ongoing full-scale baseline design developments to realize the practicality of joined-wing design with non-linear aeroelastic behavior.

The AFRL SensorCraft initiative will benefit with development of new HALE concepts that invite the development of multifunctional antenna technology. This proposal supports the VA focus on UAV technologies.

The AFRL Air Vehicle Directorate has spent considerable effort in studies in support of the AFRL SensorCraft project. This was initially a project to integrate the activities of the Multidisciplinary Technologies (MDT) Center. This project, however, shows considerable promise as a potentially valuable reconnaissance platform, with significant operational effectiveness (see below), and deserves further development. There is concern, however, about the effects of the flexibility of the wing structure, and how this could modify antenna performance. The aeroelastic effects have been modeled computationally, but it is felt that this must be substantiated experimentally and in a cost-effective manner. Sub-scale UAVs could be used to do this, but AFRL's experience with such vehicles is limited.

### 2.2.1. Relevance to the War Fighter

Joined-wing technology is relevant to the proposed SensorCraft program because the vehicle configuration facilitates broadband sensor technologies, while extending altitude, range and endurance. The long leading wing structure supports a low-frequency antenna while the diamond structure provides structural support for higher-frequency imagery with 360 degrees of coverage. It is difficult to envisage an alternative configuration that will give such overall vehicle efficiency for such a mission. In order to realize the maximum performance achievable, aeroelastic effects will contribute an important influence on vehicle range, maneuverability, and sensor pointing accuracy. Scaled prototypes are the affordable and low-risk approach in development of joined wing technology where aeroelastic effects may predominate. The scientific questions answered in this proposed program will be an integral part of a successful SensorCraft concept development.

### 2.2.2. Scientific Merit

The stability and control of any HALE concept is highly influenced by the aeroelastic behavior. The aeroelastic behavior of a joined-wing concept is known to be highly non-linear. The software analysis tools are far from proven.

The principal physics to be investigated are non-linear (geometric) static and dynamic aeroelasticity. Joined wing mechanics can involve non-linear structural behavior associated with compressed structures and large deformations. The focus here is on non-linear structural response arising from deformation-dependent stiffness that subsequently results in non-linear aeroelastic behavior. Many unanswered questions follow. Does the non-linear aeroelastic system tend to equilibrate or destabilize? What is the dynamic gust response of such a system? What are the critical modes of dynamic instability (e.g. flutter) and how do we mathematically characterize them for follow-on design efforts. What is the response of the non-linear aeroservoelastic system? The proposed research team integrates both design and scientific backgrounds in order to effectively address all these questions.

The static and dynamic physics of non-linear aeroelastic joined-wing configurations are not currently understood. These unexplored physical phenomena require development of a theoretical basis, computational models, scaling rules and testing. Full scale testing is not the affordable approach. Scaled vehicle prototypes are affordable and provide a scientifically valid approach to reduce risk for a system development. There exists a significant scientific need for scaling laws that relate model predictions to full-scale vehicle design. This proposal fills this need. The scientific issue of scaling laws for non-linear structural dynamics needs to be rigorously investigated and validated before accurately scaled vehicles can be designed and fabricated. The identification of scaling principles associated with aeroelastic behavior and sensor pointing will facilitate the development of affordable scaled air vehicle prototypes, thus significantly reducing program risks of full-sized aircraft.

### 2.2.3. Benefits Expected to Accrue from this Effort:

Benefits will be incremental and leading to the ability to control non-linear aeroelastic behavior on joined-wing concepts in support of the AFRL SensorCraft Program. From another perspective, students may continue their focus on aeroelastic modeling in their graduate studies

and future work with AFRL. The demonstration in 2004 provided groundwork in developing an extremely low-cost environment conducive to in-house research to advance UAV technologies and attract creative talent. The AFRL has a role to play in the discovery of non-linear interactions before the benefits of joined-wing technology will be realized.

### 2.2.4. Proposed Cost

| **Material Item** | **Cost** |
|---|---|
| Raw Materials | $200 |
| (Foam, Fiberglass and Wood) | |
| Tools and Work Surfaces | $300 |
| Hot Wire Foam Cutter | $200 |
| Low Temp Resins | $500 |
| Vacuum-Bagging Materials | $500 |
| Vacuum System | $800 |
| Radio Control System | $500 |
| MaxCim Electric Motors & Controllers (2) | $2500 |
| Propellers (3) | $200 |
| Static Propeller Test Stand | $500 |
| Ref Books and Media | $300 |
| **TOTAL MATERIALS** | $6500 |
| **FY02 Labor** | **Cost** |
| Required to complete 14 foot rigid variant: 350 hrs shop time | |
| 350 hrs AeroComposites Inc @$65/hr | $22,750 |
| **Indirect (ASSIST Contract)** | **Cost** |
| 16% fee on $22,750 | $3,640 |
| **TOTAL PROPOSED COST:** | **$32,890** |

Table (1) Initial Cost Estimate

# 3. Concept Design Activities

Using this knowledge of the possibility of a thin airfoil, the VA-1 was designed during the summer of 2002 as a 7% scale design of the full-scale SensorCraft candidate from Blair and Canfield. This resulted in an aircraft with a 14-foot span and fore and aft wings swept at ± 30°, respectively. The fore wings are placed at a 9° dihedral, and the aft wings are placed at a 7.8° anhedral. Using inexpensive materials to facilitate a build-up approach with some trial-and-error, the vehicle consists of construction materials found in nearly all remotely controlled aircrafts on the commercial market. The VA-1 also contains many off-the-shelf items, such as its motor, servos, and other pieces of R/C equipment.

Figure (14) The Joined Wing Technology Demonstrator as Delivered Under Contract with AeroComposites, Inc.

Analysis of VA-1 geometry was important for ensuring the HASC model matched the actual dimensions as closely as possible. The VA-1 was a seven percent scaled model of a larger design [5]. It had a takeoff weight of 31.5 lbs, 168 in. wingspan and an 80 in. long fuselage. The 2.95 horsepower electric power plant was a MaxCim MegaMax 3.7 Brushless Motor installed in a pusher configuration [14]. An inlet was placed just below the nose to provide cooling air to the electric engine. The cooling air was let out the tail end of the fuselage. A 28 in. propeller with an 18 degree pitch at the root was used during the flight test. The wheels were configured for a direct lift takeoff (e.g. B-52 and Predator) as shown in Figure (14).

In the design stage the VA-1 initial takeoff weight was 26 lbs. The takeoff weight, however, increased slightly due to minor design modifications. After Bowman's stability analysis revealed a weakness in yaw stability, a lower vertical tail was added to simultaneously improve lateral stability and protect the propeller during takeoff rotation. Removing the lower vertical tail puts the propeller at risk of striking the ground. Flight test video confirmed that the lower vertical tail would hit the ground on takeoff rotation, successfully preventing damage to the propeller. A Global Positioning System (GPS) recording device was added inside the fuselage. Finally, the number of batteries used was increased to extend the engine life during the test.

VA-1 was damaged a number of times. Repairs reconnected the fuselage and lower vertical tail and resulted in slightly increased the aircraft weight. After the final flight and before inertial testing the fuselage was restored and the weight was 31.5 lbs.

The front and aft wings were created using a XF 60-100 airfoil shape with a constant streamwise chord of 9.24 in. The FX 60-100 airfoil was initially designed as a low-speed laminar flow airfoil. FX airfoils were named after Franz Xaver Wortmann, who designed the airfoils specifically for gliders. The nomenclature did not follow rigid guidelines, so not all designations had the same meaning. Usually the first two numbers designated the year of the design and the last three yield thickness in 1/1000's of chord [15]. The wings had a taper ratio of one and zero spanwise twist. Each wing section had the same camber along the span except at the joint, where the same camber was simply scaled to fit the new chord length and blended as smoothly as possible with the adjoining wing sections.

One area for potential confusion was the mean aerodynamic chord. The wing joint allowed a number of possible ways to compute the mean chord because it was part of both the front and rear wings. For this research, the mean aerodynamic chord was calculated from the front wing as though the rear wing did not connect at the joint. Since the root chord and tip chord were the same, the taper ratio was one. Hence the mean geometric chord was the same as the root chord, 9.24 in., and will be denoted as c in this study.

| Parameter | VA-1 | JW-1 |
|---|---|---|
| Front Wing Sweep | 30º | 30.5º |
| Aft Wing Sweep | -30º | 32º |
| Front Wing Dihedral | 7.5º | 5º |
| Aft Wing Dihedral | -15º | -20º |
| AR | 12.7 | 11.25 |
| Joint Location (% semispan) | 54% | 60% |
| $S_R/S_F$ | 0.44 | 0.3 |
| Re cruise | $3.14 \times 10^5$ | $1.0 \times 10^6$ |
| Static Margin, SM | 0.4 | 0.35 |
| Control Surface Chord (% of total chord) | 28% (38% for rudder) | 20% |

Table (2) Comparison of VA-1 with JW-1 [8].

The front wing planform had 30 degrees aft sweep and the rear wing had 30 degrees forward sweep. Front and aft wing dihedral were 9.0 and -7.8 degrees respectively. The front wing leading edge started 19 in. from the nose and the rear wing leading edge started at 71.75 in. Vertically, the front wing root was positioned 1.6 in. below the fuselage center line, while the aft wing root was 12 in. above the centerline. The front and rear wing sections joined at approximately 56% of the semispan. Note the VA-1 geometry was similar to the JW-1 geometry, tabulated for easy reference in Table (2). Stability derivatives will be compared later in the dynamic stability analysis. One crucial difference between the two designs was that the JW-1 wing was optimized in twist, airfoil and camber distribution to minimize induced drag and improve stability, while the VA-1 wing was not optimized in this way.

There was potential for confusion regarding wing areas and aspect ratios. The term rear-wing will be used to denote the aft portion of the wing that is located where the horizontal tail would

ordinarily be. The subscripts F and R were used to denote forward and rear wing sections respectively. Total wing area, S = SF + SR, was computed by combining the total planform surface area of both front and aft wings. The front wing area, SF, was computed as if only the front of the joint section existed and the front wing had a constant chord from the aircraft centerline to the outboard wing tip. The rear wing area, SR, was simply the difference between the total area and the front wing. The aspect ratio, AR = b2/S, was computed using total wing area. This wing area convention was used throughout this research effort.

From VA-1 geometry we can see that the spanwise lift distribution was not designed to be elliptic. This means that twisting the wing offers the possibility of both reduced induced drag and reducing a potential pitch-up instability near stall angles of attack. The zero twist possibly made the wing prone to tip stall, which in the case of VA-1, could cause loss of elevator effectiveness in stall. Smith et al discussed an unstable pitch-up problem when they built and collected wind tunnel data on their JW-1 design. They washed the forward wingtip in and the forward wing root out to reduce this effect. Eventually vortilons were added to bring the pitch up instability to acceptable levels [8]. Due to unique aerodynamic characteristics of joined-wing aircraft, careful wing aerodynamic design plays a critical role in flight worthiness of such aircraft. Redesigning the VA-1 wing with these aerodynamic effects in mind could yield both a drag reduction and improved stall characteristics.

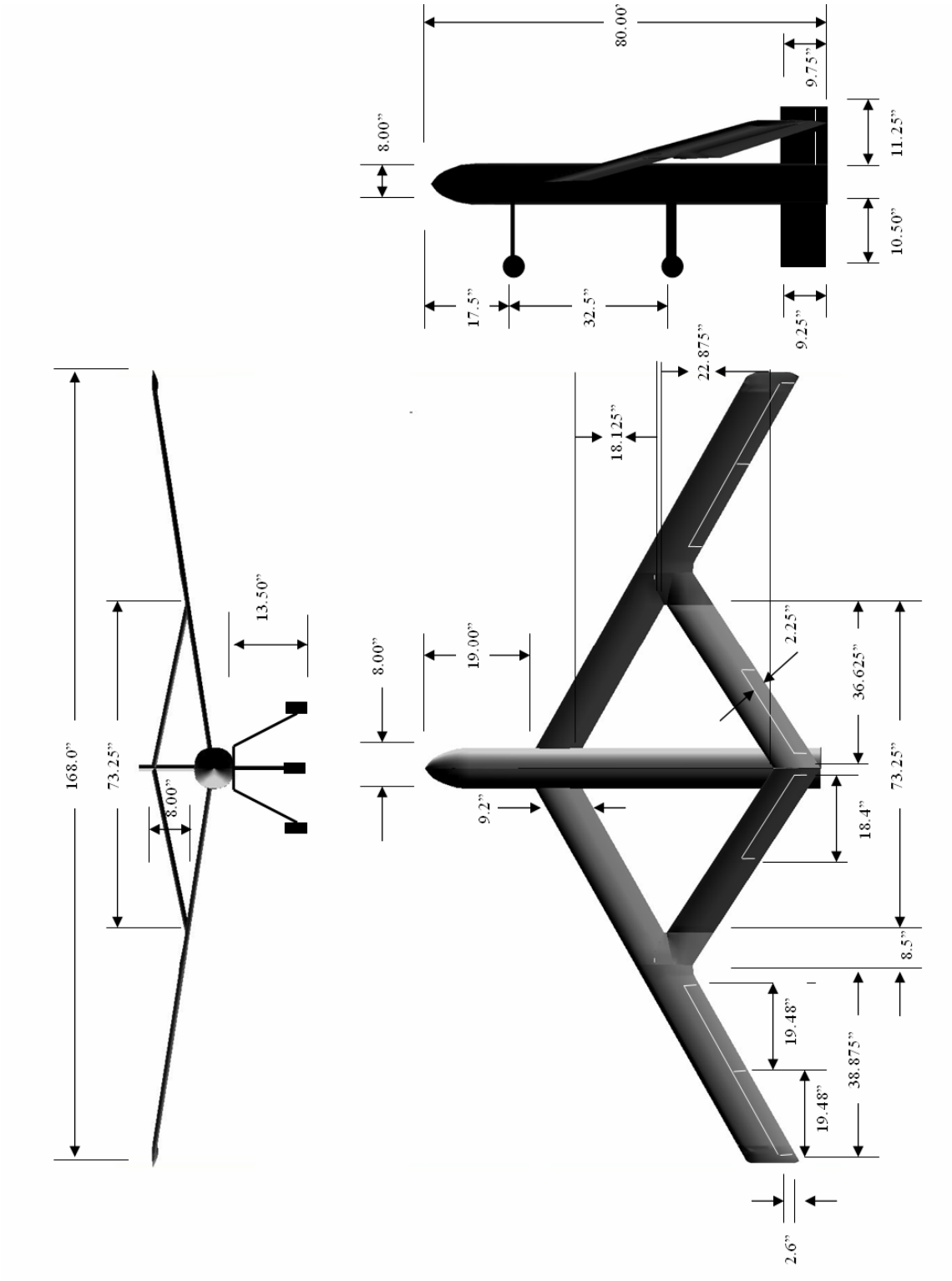


Figure (15) VA-1 Geometry

## 3.1. Design for Modularity

A key design consideration of the VA-1 was modularity of its wings, due to the cumbersome nature of a 14-foot aircraft. The design called for three removable wing sections: right fore wing, left fore wing, and aft wing. The fore wings were to be attached to the fuselage by means of a male carry-through spar (made of a carbon fiber composite) running spanwise across the fuselage and a female double-sided lap joint section on each wing. The lap joints were to receive the male portion of the carry-through spar and two bolts were to connect them. This lap joint is shown below in Figure (16). The single spar design was a critical flaw that required significant modification.

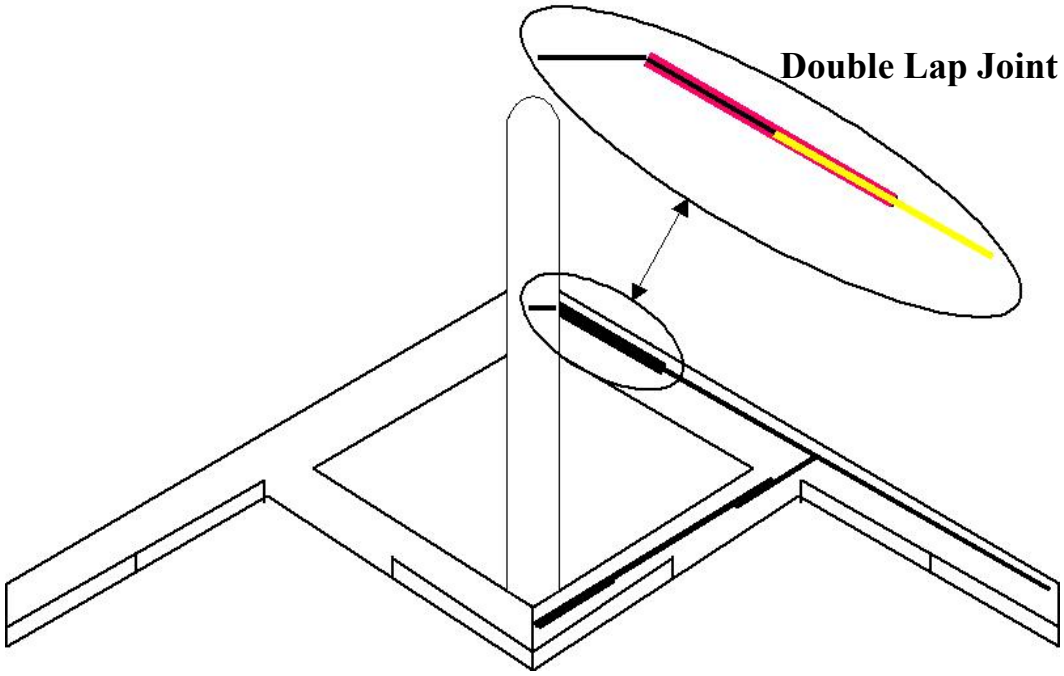


Figure (16) Double Lap Joint in Wing-Fuselage Connection

## 3.2. Cruise Velocity Estimate

The motor and propeller of the VA-1 were tested in a wind tunnel at speeds from 0 mph to 45 mph, where thrust was the key output data. Refer to Section [6.2] for more details. From this testing, it was found that at zero velocity, the motor and 28-18 propeller are able to create 11.5 pounds of thrust. At 45 mph, the motor and propeller are able to produce 4 pounds of thrust. If a linear decrease in thrust with respect to velocity and a lift to drag ratio of 10 are assumed (see Appendix A), the maximum flight speed of the vehicle can be estimated. The following linear formula relates thrust to velocity.

(1) $$V = \left[\frac{45}{4-11.5}\right](T-11.5) = -6T + 69$$

In order to maintain a static velocity, thrust must equal drag and lift must equal the weight of the vehicle. It follows that we require 26 lbs of lift leading to an estimation of 2.6 lbs of drag. Thus equation (1) specifies a maximum velocity of 53 mph at 2.6 lbs of thrust.

Unfortunately, the wind tunnel data may be slightly skewed by the absence of airflow interference around the wings and fuselage of the VA-1. The maximum airspeed of the VA-1 is estimated to be approximately 50 miles per hour.

## 3.3. Redesigned Concept

In conceiving a redesign plan for the VA-1, the design team's main focus was to reduce the likelihood of failures similar to those found in the static load test. The fore wing root quickly became the center of attention. As the wing was simply fastened to a single spar (of relatively low thickness), all the loads were passed through that spar into the fuselage. Because it was not thick, the carry-through spar presented very low resistance to twisting in the wing. These are the two main problems accounted for in the redesign of the wing-fuselage attachment. See Section 5.1.9 for a detailed description of the repair process. A new section, created from foam and balsa, was placed spanwise around the original carry-through spar. This addition, upon subsequent reinforcement, would then serve as mounting point connecting the wing to the fuselage. After constructing new foam and balsa carry-through structure, the wing was reinforced at four hard-points. A hard-point is a section of significant structural integrity (i.e. a hard wood) adhered to the foam and balsa in order to act as a structural connection. The hard-point is a way to distribute the load of the connection throughout the balsa and foam structure whereas it would be impossible to mount directly to foam and balsa, due to their relatively low abilities to resist failure due to high stress concentrations. Four hard points in total would be added to the wings – two on either side of the center axis of the plane. Each set of hard points would have one directly in front of the other. These hard-points would in turn be bolted directly onto a horizontal bulkhead within the fuselage. This bulkhead would replace the vertical bulkhead damaged in the static load test. By setting these hard points away from each other (one near the leading edge and one near the trailing edge of the wing), they would act to reinforce the wing root against the torque that led to the delamination of the lap joint within the wing.

Unlike the single carry-through spar design, the new design would not allow all load paths to channel themselves through a small area. This is done by the addition of the large connection base to the fuselage. In creating that large base, the issue of torque has been circumvented as well.

To create an extra bit of assurance against stress failure, and to reduce unwanted flexibility within the wing, several degrees of fiberglass reinforcement would be added. These fiberglass layers would be added incrementally, and to different sections of the wing, according to necessity.

The first layer of fiberglass to be added is reinforcement tape. Two strips of thick fiberglass tape would run near the leading and trailing edges of the wing on both the top and bottom of the wing. This layer would be added only from the wing root section out to midway between the root and the wing merge section. This section would aid in the reinforcement of the joint at the wing root.

The second layer of fiberglass would both reinforce the root joint and act as a stiffener for the entire wing. This layer would be composed of a single sheet of 2 oz. fiberglass that covers the entire surface of the wing from the wing root to the wing merge.

Up to three additional layers of 2 oz. fiberglass sheets would be added to the wing root. They would run spanwise to half the distance between the root and the wing merge section. These layers would also both reinforce the joint at the wing root and add needed stiffness to the wing.

Between the fiberglass reinforcement and the updated mounting section of the wing, it would appear that all problems exhibited by the VA-1 during static load testing had been addressed by the redesigned mounting configuration.

## 3.4. Final Repair Prior to Inertial Testing

The VA-1 joined-wing airplane was damaged upon a hard landing after the second flight. This is reported in Section 7.12. The model was repaired in order to properly develop an analysis model of the inertial characteristics. (This was conducted by co-author McClelland as part of his AFIT Master's thesis).

VA-1 had an unusual geometry and heavy interior components that made predicting the center of gravity more difficult. In addition repairs to the front of the fuselage after the hard landing could have shifted the center of gravity. Figure (17) and Figure (18) show the fuselage repair work. The effect of the repairs on center of gravity, if any, was unknown. Aircraft c.g. was measured using two different methods to ensure accurate results.

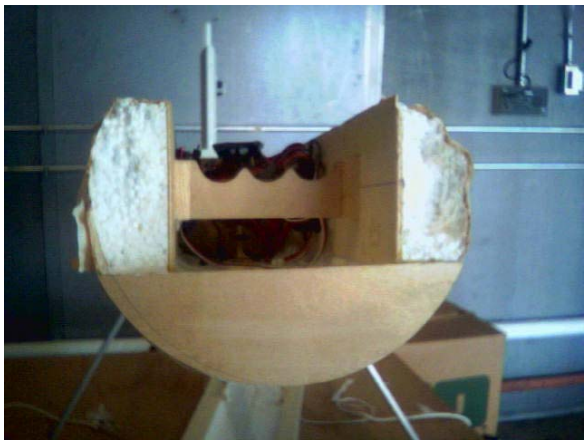

Figure (17) Fuselage Cross Section Prior to Completed Repairs.

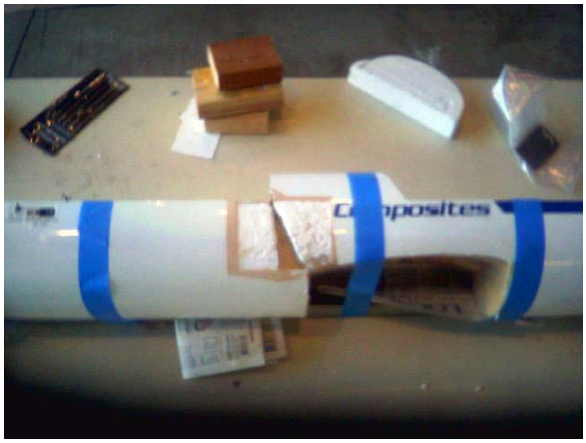

Figure (18) Fuselage Section Reconnected With Glue and Internal Braces.

# 4. Model Fabrication and Delivery


Figure (19) Balsa Concept for Initial Estimate of Aerodynamic Trim Requirement

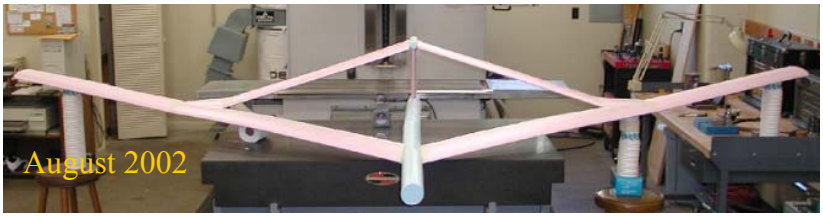


Figure (20) Styrofoam Prototype Delivered to Fabricator

The carry-through spar was inserted into the fuselage by imbedding it in a structural bulkhead. The bulkhead consisted of three layers of plywood. The middle layer had a section removed that was the height of the carry-through spar. The spar was bonded in that removed section within bulkhead with an epoxy adhesive.

The aircraft was constructed under contract with AeroComposites Inc. and delivered on 30 March 2003. Although the model was accepted by AFRL, there were concerns about flexibility of the airplane. It was far more flexible than expected by the design team, leading to concern over structural integrity of the vehicle.

## 4.1. Test Item Description

The Joined-Wing vehicle is shown in Figure (21) below.

The completed vehicle was delivered by the contractors with the specifications listed in Table (3).

The vehicle has two interchangeable configurations. First is as shown in Figure (21). The second Figure (15) moves the aft wheel struts forward to near the center of mass and the addition of a vertical tail under the aft fuselage (also serves to protect propeller from striking ground). Do not fly without propeller protection from ground strike.

Figure (21) The Delivery of the Joined-Wing Vehicle: 30 March 2003

| | |
|---|---|
| Wing Span | 14 ft |
| Wing Area | 15.2 $ft^2$ |
| Fuselage Length | 6.67 ft |
| Vehicle Weight | 26 lbs |
| Propeller Diameter – Pitch | 28-18 |
| Motor Rotation Speed | 2500 RPM |
| Motor | MaxCim MegaMax 3.7 |
| Motor Output Power | 3 HP (2200 watts) |
| Power System | 36 NiMH cells |
| Power System Output | 48 Volts at 30 amps |

Table (3) VA-1 Delivery Specifications

The manufacturer's specifications are listed below.

- Wing Span: 14 ft
- Wing Area: 15.2 ft^2
- Fuselage Length: 80 in
- Vehicle Weight: 26 lb
- Propeller Diameter: 28-18 (diameter-pitch)
- Propeller Rotation: 2500 RPM

- Motor: MaxCim MegaMax 3.7 (2200 watts / 3 Hp)
- Power: 36 NiMH cells configured to produce 48 volts at 30 amps

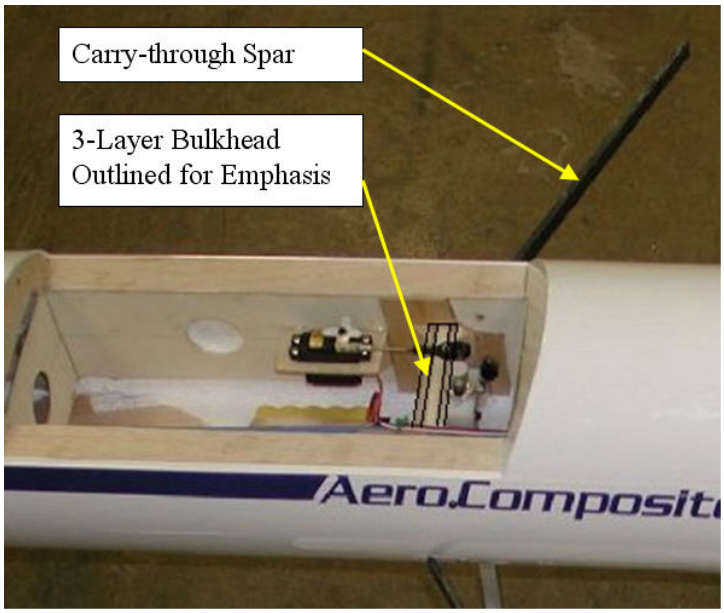


Figure (22) Carry-Through Spar and Bulkhead System

## 4.2. Electronic Components

Flight Controls: The radio controller for the Joined-Wing is the JR XP8103 shown in Figure (23). The radio can carry up to 8 activity channels. The frequency range of the controller is the 72-73 MHz R/C band which comprises fifty 20 kHz channels.

The radio transmitter is programmable for mixing of actuation with respect to control input on the transmitter. Thus, the aft flaps can be mixed with the throttle for vehicle trim. Also, the rudder and ailerons can be mixed for coordinated turns. Also, the (wing inboard) ailerons and (wing outboard) elevons can be mixed and traded for best blend of pitch and roll authority. Trailing edge control surfaces are incompatible with joined-wing structural design (inboard of joint). We will explore the effectiveness of the outboard elevon alone (aft wing flap locked out).

PCM receiver is programmable for fail safe flight in event signal is lost. See Section 10 "Flight Termination Procedure" for additional details.


Figure (23) Radio Transmitter

# 5. ANALYSIS

The VA-1 was analyzed for structural integrity and flight dynamic stability following design and delivery of the VA-1 Joined-Wing flight vehicle. The strategy was to use standard model airplane techniques to scale up the simple balsa glider and the foam prototypes pictured in Figure (19) and Figure (20). The goal of this first flight concept (described in Section 2.1) was to establish flight worthiness in the least time with the least cost. While analysis is an absolutely integral part of a flight certification program, high fidelity (FEM etc) analysis is not typically used to design model airplanes. The VA-1 was constructed from low cost materials using rapid fabrication techniques with the expectation that the model airplane could very well experience structural damage due to hard landings. A significant part of flight test cost comes from data acquisition. The VA-1 was designed without data acquisition, thus keeping with low cost as a way to manage high risk.

From a time/cost/benefit perspective, analysis of model airplanes begins to make sense in the context of perfecting performance. This will be especially true in the design of an aeroelastically scaled concept where significant expensive instrumentation will be incorporated to measure the flexible flight vehicle response and thereby validate full-scale design models.

## 5.1. Structural Analysis of the Scaled Model [57]

The airplane was delivered in March 2003 with modular wings. Each wing contained a single graphite spar. The wing spars connected to a single graphite carry-through spar encased in resin between two plywood bulkheads in the fuselage. As it turns out, a single spar design has disastrous structural consequences.

A key design consideration of the VA-1 was modularity of its wings, due to the cumbersome nature of a 14-foot aircraft. The design called for three removable wing sections: right fore wing, left fore wing, and aft wing. The fore wings were to be attached to the fuselage by means of a male carry-through spar (made of a carbon fiber composite) running spanwise across the fuselage and a female double-sided lap joint section on each wing. The lap joints were to receive the male portion of the carry-through spar and two bolts were to connect them. This lap joint is shown in Figure (16).

The carry-through spar was inserted into the fuselage by imbedding it in a structural bulkhead. The bulkhead consisted of three layers of plywood. The middle layer had a section removed that was the height of the carry-through spar. The spar was bonded in that removed section within bulkhead with an epoxy adhesive. The spar and bulkhead system are shown in Figure (22).

The wing structure delivered in March 2003 was extremely flexible in bending. The wings were not nearly as stiff as one normally associates with model aircraft with foam core wing construction. It was clear that this airplane was not flight-worthy in the aeroelastic sense. However, the airplane was accepted upon delivery. It was clear we needed to test the wings before engaging in a full flight test. Because it was clear the wings were not flight-worthy, it made sense to test to failure and then analyze the wing failure with finite element analysis. With a validated FEM model, the wing could then be redesigned and structurally modified and retested. This procedure is described below.

### 5.1.1. Structural Load Requirement

The VA-1 test plan calls for a series of pre-flight ground tests. These tests are more than one normally associates with RC airplane development, but less than required for certified aircraft. The ground tests are intended to balance the requirement for safety with practicality. The first of the series of tests is a 2G-maneuver load test.

The rationale behind a 2G load testing is based on the calculation of flight loads at the minimum radius and maximum speed predicted for the flight-testing. The aircraft flying around a radius, r, at a speed, V, must create the proper amount lift, L, that will maintain its flight pattern. Calculating this needed lift will allow us to find the amount of Gs the aircraft must withstand. $F_C$ is the inertial load of the vehicle, and θ is its bank angle.

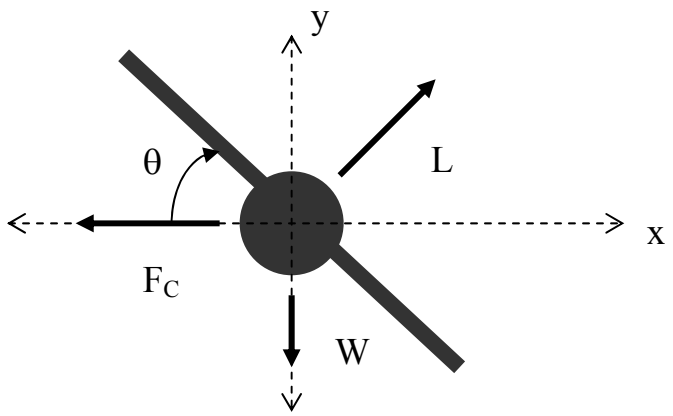


Figure (24) Free Body Diagram of Aircraft in Radial Flight Pattern

To calculate lift, we must also calculate bank angle. We make this calculation by balancing forces shown in the free body diagram of Figure (24).

(2) $$\sum F_X = 0 = L\sin\theta - F_C = L\sin\theta - ma_c$$

The aircraft is making a coordinated turn with a radius, r. The inertial acceleration must be centripetal acceleration.

$$ma_C = m\frac{v^2}{r}$$

(3) $$L\sin\theta - m\frac{v^2}{r} = 0$$

$$L\sin\theta = m\frac{v^2}{r}$$

(4) $$\sum F_y = 0 = L\cos\theta - W = L\cos\theta - mg$$

$$L\cos\theta = mg$$

With two equations and two unknowns, our aerodynamic load can be obtained.

(5)
$$\sin\theta = \frac{mv^2}{Lr}$$
$$\cos\theta = \frac{mg}{L}$$
$$\sin^2\theta + \cos^2\theta = 1 \Rightarrow \left(\frac{mv^2}{Lr}\right)^2 + \left(\frac{mg}{L}\right)^2 = 1$$

(6)
$$\Rightarrow \sqrt{\left(\frac{mv^2}{Lr}\right)^2 + \left(\frac{mg}{L}\right)^2} = 1 \Rightarrow \sqrt{\left(\frac{m}{L}\right)^2}\sqrt{\left(\frac{v^2}{r}\right)^2 + g^2} = 1$$

(7)
$$\frac{m}{L}\sqrt{\left(\frac{v^2}{r}\right)^2 + g^2} = 1$$

(8)
$$L = m\sqrt{\left(\frac{v^2}{r}\right)^2 + g^2}$$

This value is the lift that must be created by the aircraft to maintain velocity, v, around a turn of radius, r. The maximum lift is caused when the radius is minimized and the velocity is maximized. As found in wind-tunnel testing of the motor and by using an engineering approximation, the maximum speed at which the VA-1 is able to make this maneuver is approximately 50 miles per hour (nearly its maximum speed). The vehicle will make a turn with a radius of 200 feet during it elliptical flight path. Using Equation (8), the lift needed for that maneuver is 33.9 lbs, or 130% of the aircraft's weight. Adding a margin of safety of 50%, the plane must be able to withstand loads up to 200% of its own weight, equivalent to a 2G symmetric pull-up maneuver.

In order to create an environment in which incremental loads could be added to the wings, the VA-1 was inverted during static load testing. Using Figure (25), a 2G-wing load is calculated as follows:

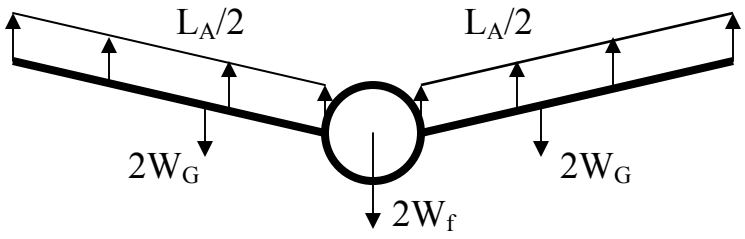


Figure (25) Free-body Diagram of VA-1 Under 2G Loading

(9)
$$\sum F_Z = L_A - \left(2W_G + 2W_f + 2W_G\right) = 0$$
$$L_A = 4W_G + 2W_f \qquad L_A/2 = 2W_G + W_f$$

Where $L_A$ is the aerodynamic lift force, $W_G$ is the weight of each wing, and $W_f$ is the weight of the fuselage. Upon inverting the fuselage, the needed testing force can be found. From the above equations, we can find that the total force experienced by the wing under a 2G maneuver is $F_W$:

$$(10) \qquad F_W = {}^{L_A}\!/_{2} - 2W_G = \left(W_F + 2W_G\right) - 2W_G = W_F$$

Under test conditions, the plane is inverted and the test load, $L_T$ is applied to the bottom of the wings. $L_T$ is the weight of the sandbags to be used during testing and will be calculated in this derivation. Inverting the plane and adding the test load creates the following free body diagram.

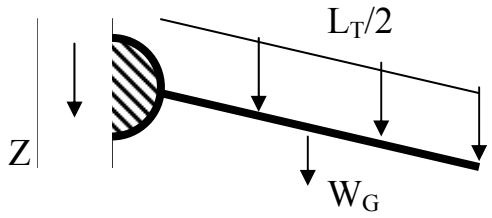


Figure (26) Free-body Diagram of VA-1 Under Ground Testing Conditions

Using the free-body diagram in Figure (26) to calculate the force experienced by the inverted wing, we find $F_W$' as follows:

$$(11) \qquad F_W' = {}^{L_T}\!/_{2} + W_G$$

In order for the wing to experience the same forces during the static load test as it would in the prescribed flight maneuver, we must equate the forces experienced by the wing under each circumstance (inverted and not).

$$F_W = F_W'$$

$$(12) \qquad W_f = {}^{L_T}\!/_{2} + W_G$$

$$L_T = 2\left(W_f - W_G\right)$$

The total weight of the VA-1 is 26 lbf, where the weight of each wing is 1.5 lbf, bringing the weight of the fuselage to 23 lbf. Finally, the testing weight if found as follows:

$$(13) \qquad F_T = 2W_f - 2W_G = 2\left(23lbf\right) + 2\left(1.5\ lbf\right) = 43\ lbf$$

where half the testing load is applied to each wing.

Due to the research nature of the load tests, it was imperative that the loads be applied at small increments so the results of progressively increased loads could be documented. Also, in the case of test failure, a single application of the testing load could cause catastrophic failure without any forewarning. On the other hand, an incremental application of the load may show lesser signs of failure before the aircraft would break beyond repair.

A set of one-pound sandbags was created that would be placed along the wing at even intervals as the loads were applied. During testing, these one-pound sandbags were placed symmetrically along the wings, two at a time – one on the right wing and one on the left wing, at the same

distance from the fuselage. Starting at the root of the wing, leading outward, the load was placed at even intervals until reaching the wing tip. This loading was placed on both the fore and aft wings.

As indicated, the wings were tested after delivery and before structural analysis. They failed, as described in Section 6.3.2.6 (Static Structural Ground Test). This failure lead to the wing redesign effort. This time done correctly.

### 5.1.2. Analysis Model of the Baseline Wing

During the time of construction, computer based structural analysis of the full-scale joined wing configuration was near completion, but since analysis was not yet finished, it was left to conventional knowledge and common R/C construction practices to complete the design and building of the VA-1. This will be discussed in further detail as it directly lead to the failure of the VA-1 under static load testing.

Upon seeing that the first static load test of the VA-1 would end in failure, it was believed to be a lapse in structural analysis that led the design to its demise. In order to ensure a successful redesign, the VA-1 was to be subjected to a series of finite elements studies. This finite elements work focused on the point of the structural failure – the root of the fore wing – and integrated the structural redesign concepts into the model. With new knowledge of structural loading and a reassurance of the aircraft's structural integrity after modifications, the finite element studies should help create an aircraft with improved structural performance under prescribed flight conditions.

A finite element study would be performed to match baseline model behavior with the behavior of the VA-1 under static load testing. From here, the baseline finite element model would be modified to reflect the redesign concepts mentioned above. It is thought that having properly matched the behavior of the baseline model, any advantages seen by the modifications in the finite elements analysis would also be seen in the real model upon modification.

In order to subject an aircraft to such a study, one must create a finite elements model of that aircraft. This model consists of a 3-Dimensional geometric model, which gets meshed into the finite elements. A model is created via a pre-processor within the finite elements software package or within a separate modeling program that can export the model to the software package. The model of the VA-1 was created using a 3D computer aided design package, named SolidWorks. SolidWorks creates solid geometries that can be exported to the software module COSMOSWorks to be studied as finite element models. The benefit of SolidWorks over other preprocessor driven model generation packages is its relative ease of use. Someone with only a small amount of training can accurately capture geometries of quite complex objects.

### 5.1.3. Geometric Model

Within SolidWorks, all three structural components of the VA-1 wing are created as separate part files. The foam core, balsa sheeting, and carbon-fiber spar system are then merged into one assembly of parts with perfect precision. The model is created so that it is an idealized version of the VA-1, whereas any imperfections in construction are neglected.

In order to reduce computation time, the airfoil was reduced in complexity (only one out of ten data points of the fully smoothed airfoil cross-section were used to create its cross-sectional

geometry), but still maintained the shape of the actual airfoil. This cross-sectional geometry was extruded to the proper angles and lengths in order to create the foam core entity. The balsa sheeting was created by means of an outward shelling process. Knowing that the balsa sheeting is 1/16 of an inch thick, and it covers the foam, the foam core entity was used to create the balsa skin. The foam core was expanded by the thickness of the balsa and left hollow. This created an accurate representation of the balsa skin used on the VA-1. In creating the spars, an entity was created that modeled the geometry of the spars. This exact shape was removed from the foam and balsa entities, allowing for the recess in which the spar sits. These three entities were brought together in one assembly to create the 3-Dimensional model of the VA-1 wing. This assembly of the three basic wing sections will now be referred to as the baseline geometric model.

In order to perform any series of finite element analyses, the baseline geometric model must be converted to a finite elements model by means of creating a mesh and assigning material properties to the different wing components. From the point of completing baseline geometric model, the assembly is loaded into the COSMOSWorks software module. This module is a piece of add-on software that allows a user to analyze a model within the SolidWorks graphical interface using the COSMOS finite elements solver algorithms.

### 5.1.4. Meshing

The mesh of the VA-1 finite elements model represents a departure from standard thin-wall aerospace analysis. The geometry of the foam wing core led to the use of solid elements to represent all components of the VA-1. The solid elements used are a standard tetrahedral element, with a standard edge length of 0.75 inches, allowing for a highly refined mesh. The edge length, however, was allowed to vary in the planar axis when the element needed to be thinner than the standard length, as was the case in the thin layer of balsa.

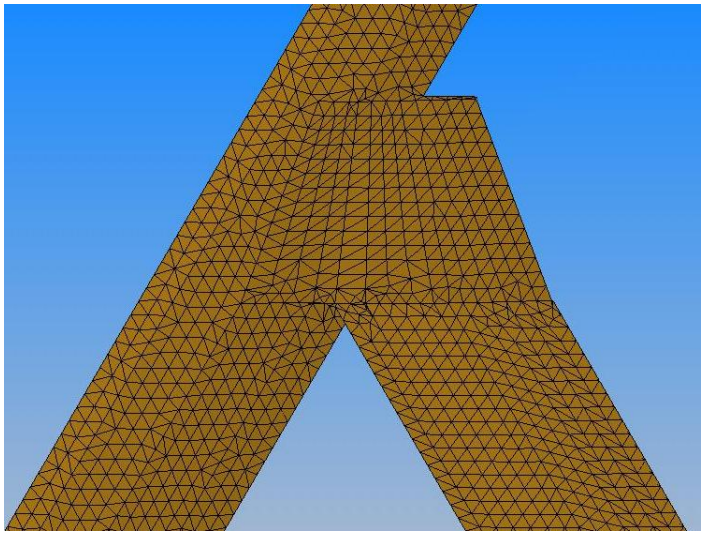

Figure (27) Top-view of VA-1 Finite Element Mesh

### 5.1.5. Verification of Solid Elements

In an attempt to verify the use of solid elements with such extreme aspect ratios, a study was conducted on a simple beam structure, as shown in Figure (27). The beam study compares solid elements and shell elements – the latter being more commonly used in aerospace analysis. Both maximum stress and displacement were recorded as the thickness was decreased and the aspect ratio of the solid elements reached that of the solid elements used in the balsa skin of the VA-1 model.

In the beam study, the final result compares solid and shell elements at the aspect ratio used in the thin balsa layer of the VA-1 finite element model. The beam was made incrementally thinner until it the ratio of the standard top edge length of the solid elements to the thickness of the beam matched the same ratio as seen on the balsa elements of the VA-1 model. In the case of the VA-1 model, the average planar edge length of each element is approximately 0.75 inches. The balsa sheeting is one sixteenth of an inch thick. The average planar edge length used in the beam study is equal to that used in the VA-1 model; therefore, the final thickness – which was incrementally decreased from 1 inch – was also one sixteenth of an inch. The final element aspect ratio can be observed in Figure (28).

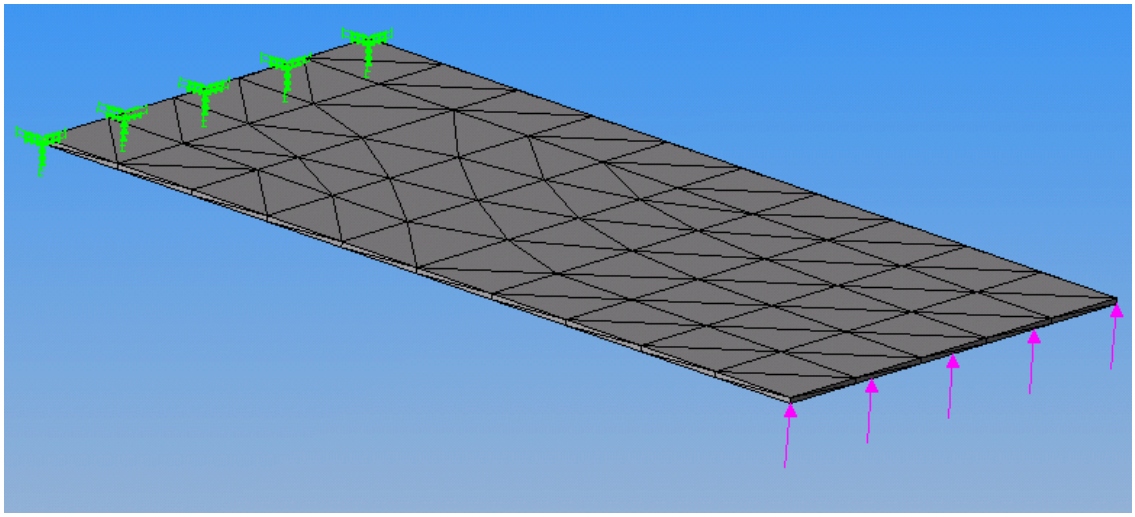

Figure (28) Final Aspect Ratio of Solid Elements Beam Used in the Solid to Shell Element Comparison Study

The results of the beam study show that the solid elements exhibit higher stiffness than the shell elements. The stress in the solid elements was approximately fifteen percent lower than that in the shell elements, regardless of element aspect ratio, whereas the displacement increased linearly with aspect ratio to a nearly seven percent deficit.

Also, the maximum displacement was plotted against the maximum stress for both types of elements. There was a nearly linear increase of displacement with respect to stress for both element types, of approximately the same slope. This indicates that it would be possible for one to correct for the added stiffness of solid elements by adjusting deflection and stress would adjust itself accordingly. This will also be noted when discussing the tuning of the finite elements model to match the results of the static load testing.

### 5.1.6. FEM Loads

Once the mesh was completed, it was necessary to model the wing loading to match that of the static load test. During the static load test, sandbags were distributed over the wing to simulate aerodynamic pressure during a simple pull-up maneuver. Since the sandbags were evenly spread across the wing, this discrete loading was mathematically modeled as an equivalent even pressure over the wing. This distribution of pressure was collocated as forces at all grid points along the bottom surface of the finite element model.

During static load testing, the maximum deflection was measured at a loading of twenty pounds on either wing. Therefore, the benchmark finite elements case involves 20 lbf of sandbags applied to the right wing, which computes to an equivalent 0.0143 psi pressure over the bottom skin. The load was applied in a vertical direction, the direction that gravity acted on the sand bags. Although the graphic below makes it appear as though the pressure is unevenly distributed along the merge section, this is simply due to the nature of the load visualization used. The pressure is added to several separated surfaces in that section, which is shown as a cluster of vectors. Each vector cluster only accounts for pressure on a section, and not the magnitude of the total applied force. This is why along the larger sections – e.g. the fore and aft wings – the load looks very sparse. This means that the smaller each section is, the more vectors will be shown.

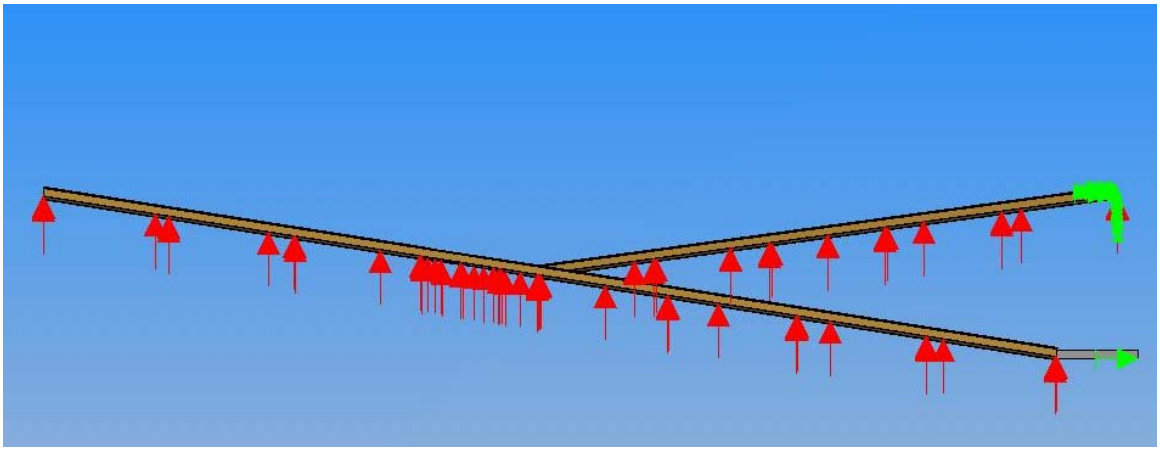

Figure (29) CosmosWorks Load Visualization for the VA-1 Finite Element Model

Because only half the spar is modeled, and the loads are added symmetrically to each side, symmetry boundary conditions could be applied. Another complication of the boundary conditions is the notion of spar twisting. When discussing the results of the static load testing, it was mentioned that the spar was found to have twisted within the plywood bulkhead. This is motion that must be accounted for within the finite elements model. In order to do so, a point on the top of the spar was constrained in the x-, y-, and z-directions. This allows for twisting about that point in any direction, but removes the possibility for translation. To model the symmetry of the spar, a constraint at the bottom of the spar root is placed to keep it from moving from the model's plane of symmetry. While this constrains the model from moving away from the plane of symmetry, it does nothing to stop the twisting of the wing, which is a desired effect in the

model. Because the connection of the aft wing was found to be far more rigid during static testing, every node of the aft wing is constrained from translation at its root.

### 5.1.7. Material Properties And Model Tuning

One peculiarity of this analysis is the fact that the materials used are not common engineering materials. Whereas the material properties of steels and other metals are easily found in materials handbooks, the same cannot be said about any material used in this analysis. Using sheets of expanded bead insulating foam for structural purposes is not the original intent for the product; therefore its structural properties have not been thoroughly tested nor published.

To further compound the issue, once the published material properties were actually found, both balsa and carbon fiber composites were shown to have a range of material properties. This is because balsa is an organic material; each section of wood has different properties. The difficulty with the carbon composite is that it is produced in a variety of methods, rendering different material properties for each, depending on the density of carbon fibers with respect to resin content.

Balsa wood has desirable strength-to-weight properties for use with small-scale airplane structures. Balsa wood material properties also come with significant variability. The specific gravity of balsa varies between [$0.06 < d < 0.22$]. The Young's modulus ($E_L$) is parametrically related to density as $E_L = [(5.5e6)\rho - 2.0e5]$ psi. Balsa is orthotropic and requires a transverse Young's modulus, which we take to be [$E_T = 0.015E_L$]. Also the shear modulus for balsa is $G_{LT} = 0.037E_L$. The strength of balsa is also variable.

| | Range (psi) |
|---|---|
| Tensile longitudinal strength ($S_{Lt}$) | [$1375 < S_{Lt} < 4525$] |
| Compressive longitudinal strength ($S_{Lc}$) | [ $500 < S_{Lc} < 2310$] |
| Tensile transverse strength is ($S_{Tt}$) | [ $72 < S_{Tt} < 223$] |
| Compressive transverse strength is ($S_{Tc}$) | [ $50 < S_{Tc} < 198$] |
| Shear strength ($S_{LT}$) | [ $158 < S_{LT} < 522$] |

Table (4) Material Properties of Balsa Wood

References: (http://www.cstsales.com/balsa_wood_properties.htm) and

US Dept of Agriculture Wood Handbook Handbook No. 72 produced by the Forest Products Laboratory of the Forest Service.

| | (psi) |
|---|---|
| Young's Modulus ($E_L$) | 768000 |
| Transverse Young's Modulus ($E_T$) | 11520 |
| Poisson's Ratio ($\eta_{xy}$) | 0.3 (no units) |
| Shear Modulus ($G_{LT}$) | 28416 |
| Tensile longitudinal strength ($S_{Lt}$) | 2500 |
| Compressive longitudinal strength ($S_{Lc}$) | 1750 |
| Tensile transverse strength is ($S_{Tt}$) | 125 |
| Compressive transverse strength is ($S_{Tc}$) | 100 |
| Shear strength ($S_{LT}$) | 350 |

Table (5) Balsa Material Properties Used in VA-1 Finite Element Model

The material properties for low-density foam (1 lbm/ft$^3$ white expanded bead - source unknown) are also not well specified. Engineering data is not commonly published for this kind of lightweight packing foam. Klegecell is an engineering foam with published isotropic properties indicated below.

| | |
|---|---|
| Young's Modulus (psi) | 3630 |
| Shear Modulus (psi) | 1450 |
| Poisson Ratio | 0.25 |
| Density (lbm/ft$^3$) | 2.5 |
| Tensile strength (psi) | 100 |
| Compressive strength (psi) | 60 |

Table (6) Material Properties of Foam

The properties for unidirectional graphite epoxy are also not calibrated, primarily due to undocumented resin content. These are the assumed properties.

| Graphite Properties | |
|---|---|
| Longitudinal Modulus (psi) | 2.63e+7 |
| Transverse Modulus (psi) | 1.49e+6 |
| Shear Modulus (psi) | 1.04e+6 |
| Poisson Ratio | 0.28 |
| Density (lbm/in$^3$) | 0.042 |
| Longitudinal strength (psi) | 5.0e+5 |
| Transverse strength (psi) | 5.0e+4 |
| Shear strength (psi) | 1.0e+5 |

Table (7) Material Properties of Graphite

Preliminary results indicated that the balsa skin properties strongly dominated the overall stiffness of the wing. With this in mind and the wide variability in balsa material properties

(factor of two), we chose to tune the baseline model by adjusting the stiffness of the balsa within a reasonable range. In the end, the FEM produced a wingtip deflection of 20.6 in. This matches very well with the experimental test deflection of 21" deflection. As discussed, we assume the non-linear shift in the tabulated test results were the result of the bulkhead failure with delamination. In this FEM, we assumed the spar was totally free to twist in the bulkhead following the bulkhead failure. Also, we feel that it is possible to obtain accurate stress information in the simple case of a cantilever beam by changing the deflection. If that statement is generalized, then the same principle can be applied to a model such as the VA-1.

### 5.1.8. Validation

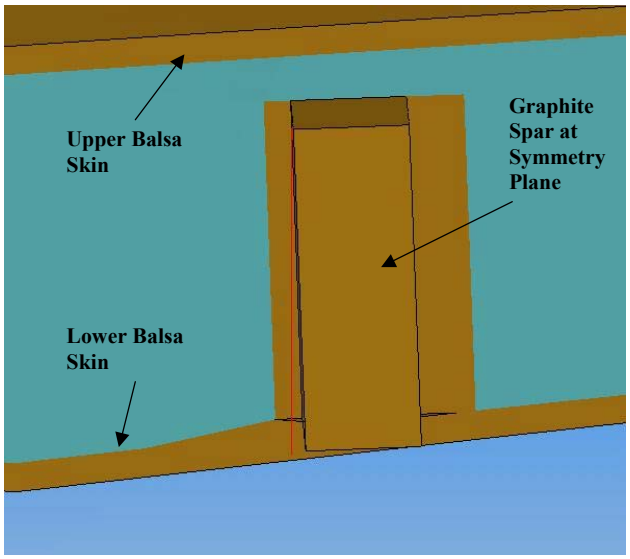


Figure (30) Twisting of the Wing Root Modeled with CosmosWorks

The wing deforms with both bending and twisting as the wing loading increases. Twisting is evident in the graphic above, Figure (30), where the structure twists away from the superimposed vertical red line. Again, we have assumed that this twisting caused the delamination of the multi-ply bulkhead in the fuselage and debonding between the wing spar and the interior foam.

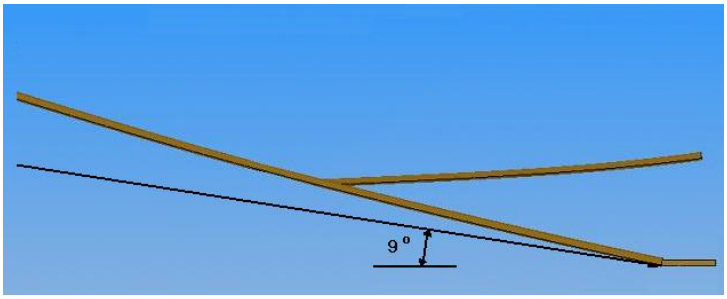


Figure (31) Deflection of Wing Modeled with CosmosWorks

As shown below, in Figure (31), the interface between the root of the wing and the carbon fiber spar has a very high stress concentration (as indicated by the color red) due to the twisting of the

spar at the wing's root. There is no load carried along the forward wing leading or trailing edges. This is expected, with no corresponding support and all loads transmitted through the spar.

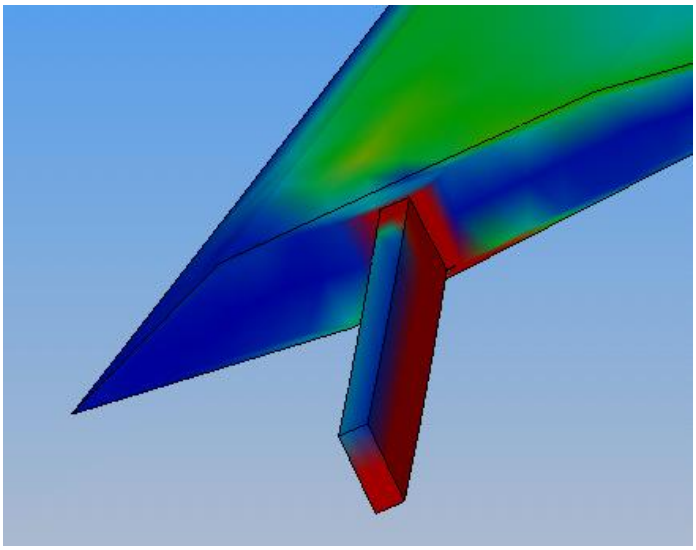

Figure (32) Von-Mises Stress Concentrations at Wing-Fuselage Connection

As shown in Figure (32), the maximum von-Mises stresses in the aft wing root occurs on the top of the wing along the leading edge and on the bottom of the wing along the trailing edge. The red sections of this chart are in the realm of 2000 psi. This is approaching the lower limit of the weakest balsa wood (see material properties table).

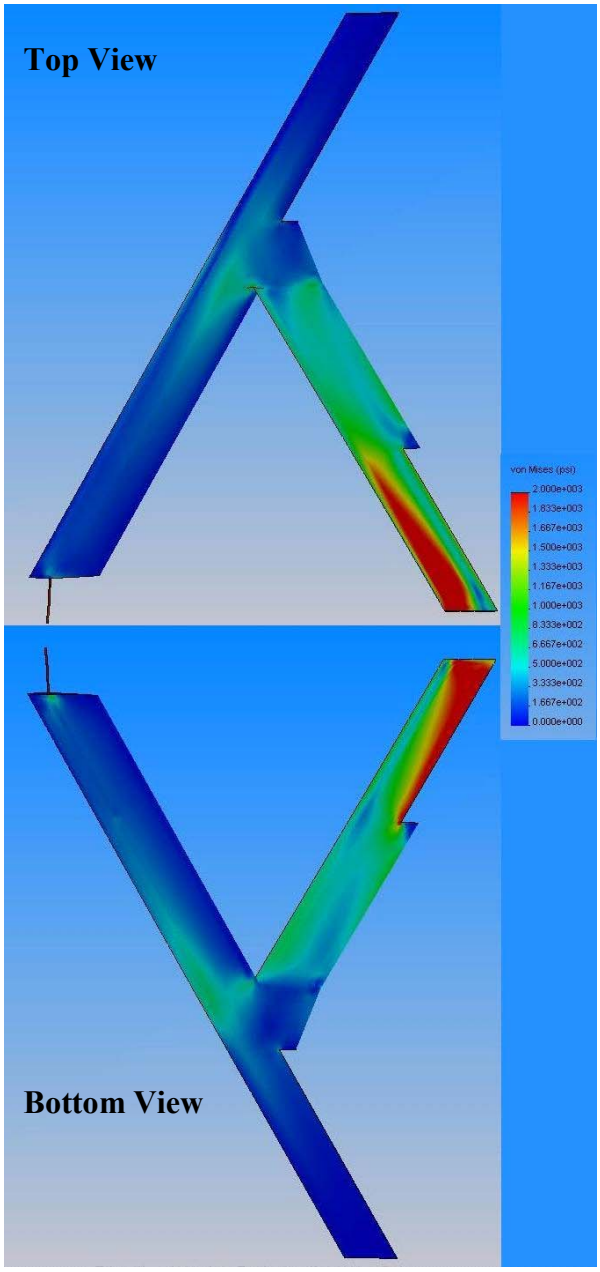


Figure (33) Top and Bottom Views of Stress Patterns in VA-1 Model

After taking note of all the results, the baseline finite elements model was found to be an acceptable model of the VA-1 under a static load test. This assumption is made based on two results: stress and displacement. After tuning the material properties of the balsa, the tip displacement of the model matched within two percent error of the measured value. Also, the rotational displacement of the wing's spar about a vertical axis is representative of the twisting spar within the fuselage of the VA-1. The stress analysis is thought to be accurate because of its placement and magnitude. There are high stress levels shown at the root of the forewing, where the spar enters the wing. This is consistent with the spar splaying the connections within the wing and the bulkhead. Also, the stress levels are not above the allowable stress levels of balsa

wood – which did not fracture during testing. Finally, the stress patterns in the aft wing are consistent with those published for the full-scale joined wing aircraft.

### 5.1.9. Structural Redesign

#### 5.1.9.1. Proposed Repair and Modification

The proposed modification is to extend the carry-through structure within a continuous wing. This procedure will result in a one-piece removable forward wing of 14 ft. span and a one-piece aft wing. Graphical representations will aid the interpretation of the following proposed repair and modification sequence.

- Restore the damaged bond between the wing and the carry-through spar
- Mark curve where wing and fuselage intersect (see fuselage modification)
- Remove the carry-through spar and wing assembly from the fuselage
- Cut foam core (airfoil shape minus skin) for carry-through
- Bond foam core to the wing and carry-through spar
- Bond 1/16 in balsa skin to carry-through foam core.
- Mill out balsa to receive 10 oz/yd fiberglass strips top and bottom
- Bond 10 oz fiberglass strips into balsa top and bottom
- Bond 2 oz/yd fiberglass on top and bottom of forward and rear wings (orient ±45°)
- Bond 2nd layer of 2 oz/yd fiberglass on top and bottom of forward and rear wings (orient ±45°)
- Finish wing surface to a smooth surface without ripples or bumps.
- Use a hole saw to cut 3/4 holes (quantity four) through wing and through 10 oz cloth as indicated
- Bond dowel rod segments in 3/4 holes.
- Drill 1/8 in centered holes in dowel segments to receive mounting bolts.
- Refer to fuselage modifications contained in the Statement of Work.
- Fasten modified wing to modified fuselage

A sketch of this repair technique is shown in the following sequence of schematics. A test article was constructed and is shown in Figure (33).

[Step 1]

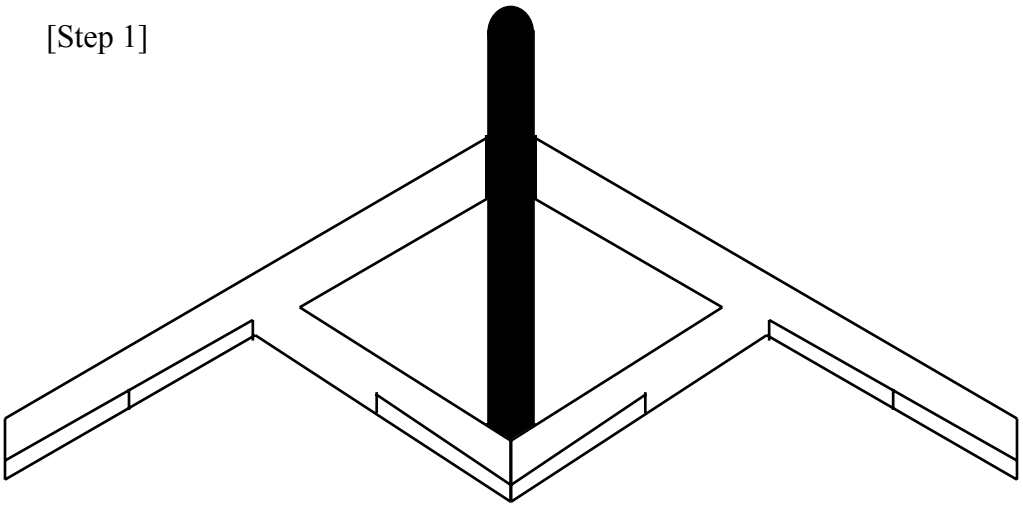

[Step 3]

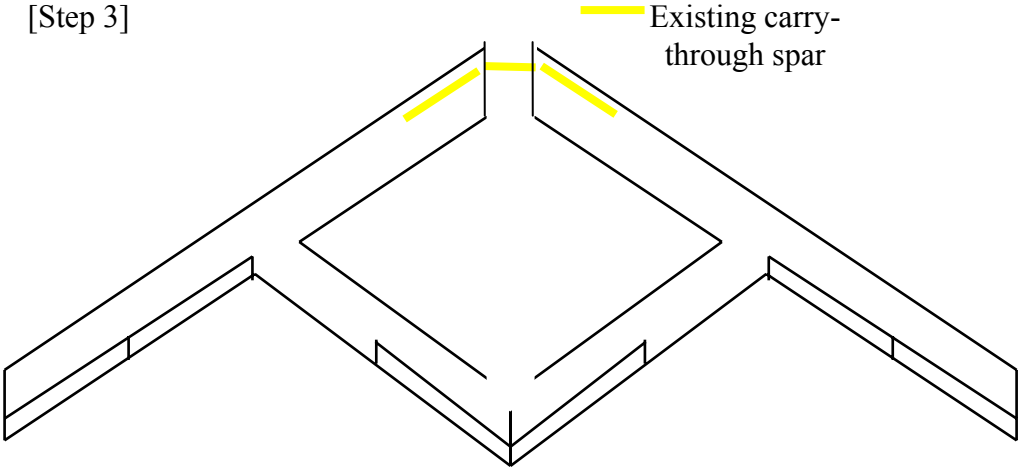

[Step 5]

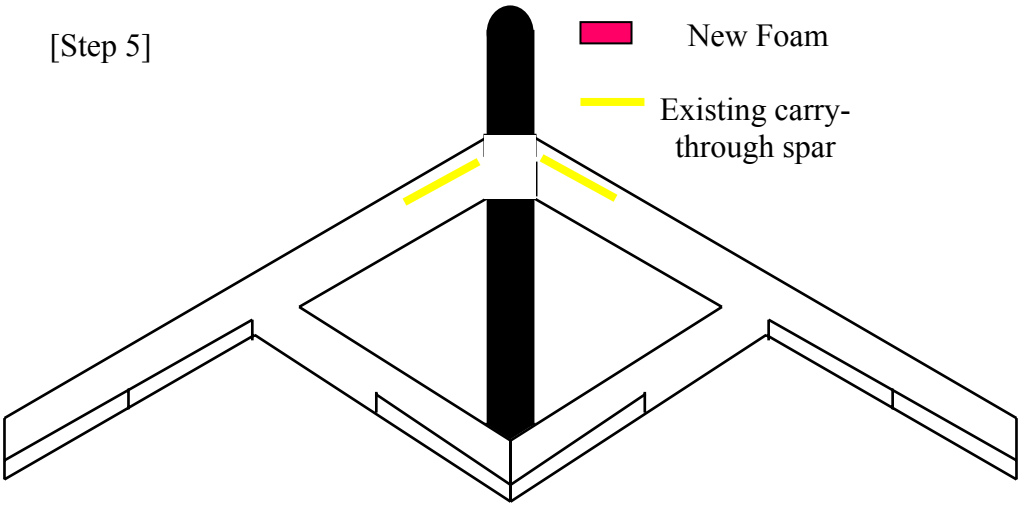


[Step 8]

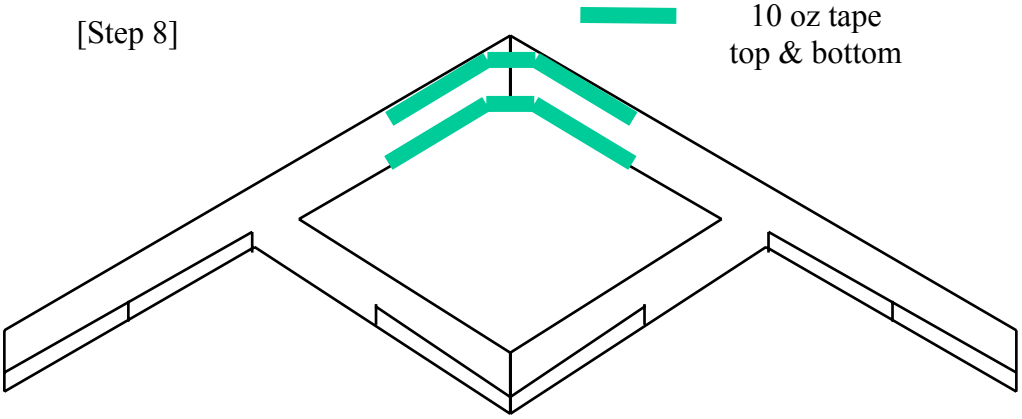


[Step 9]

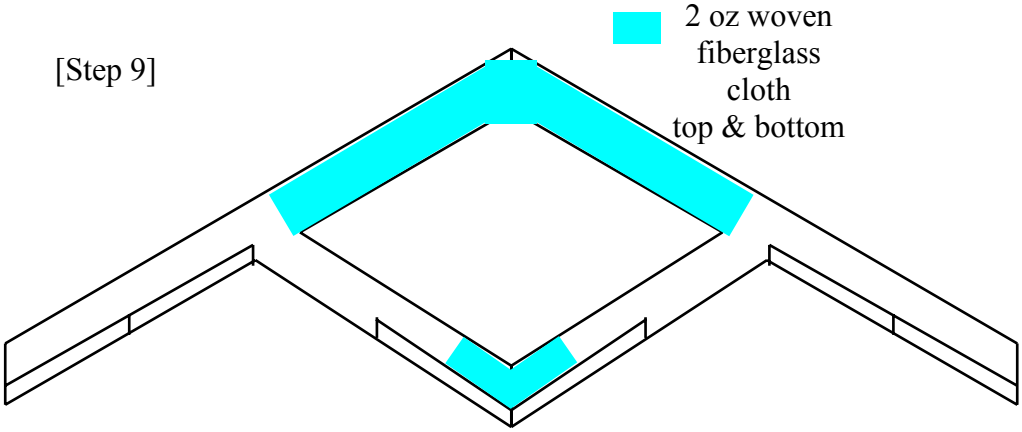

[Step 10]

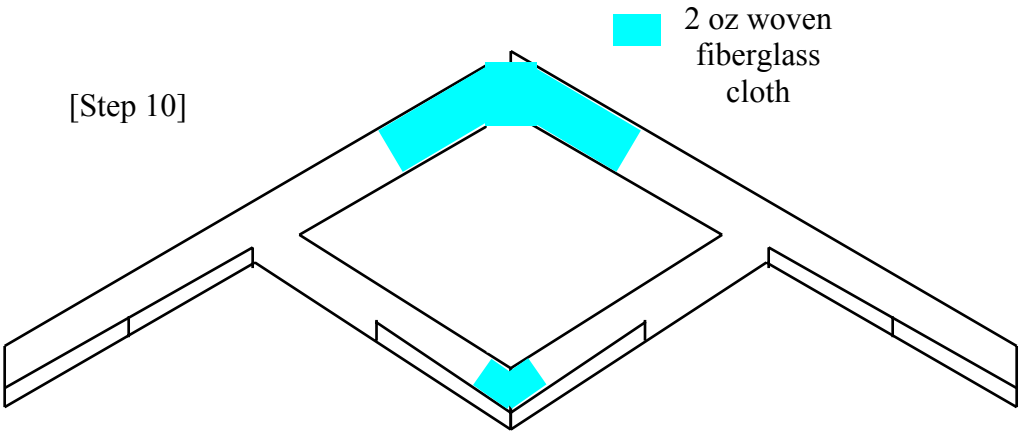


[Step 13]

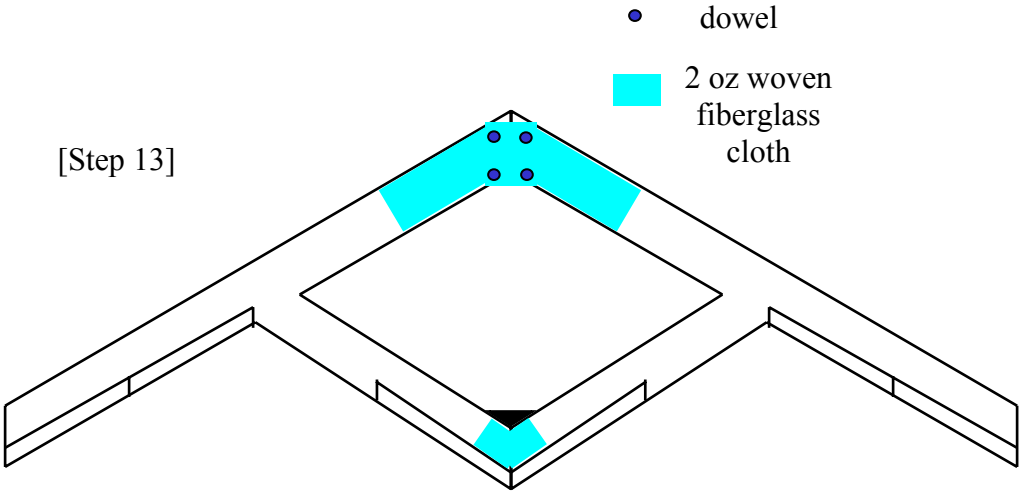


[Step 16]

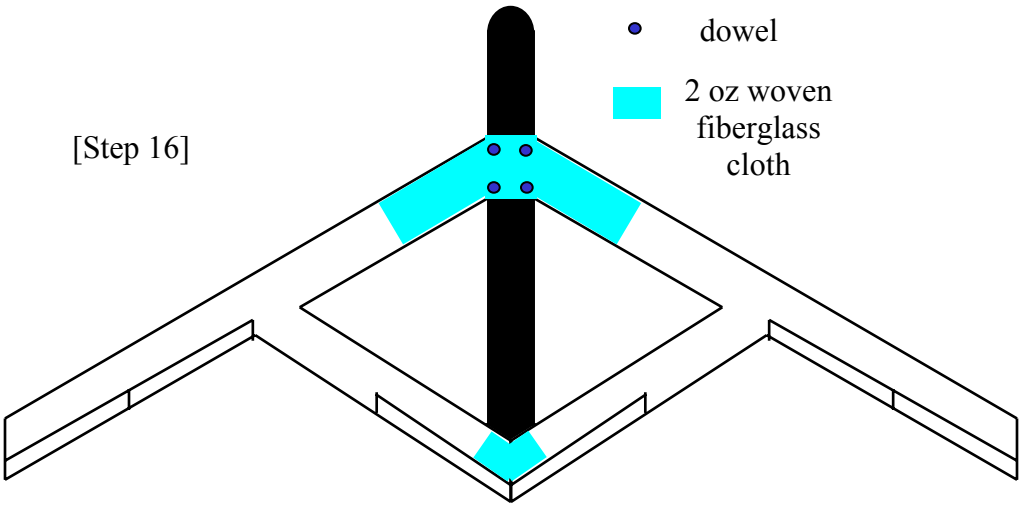

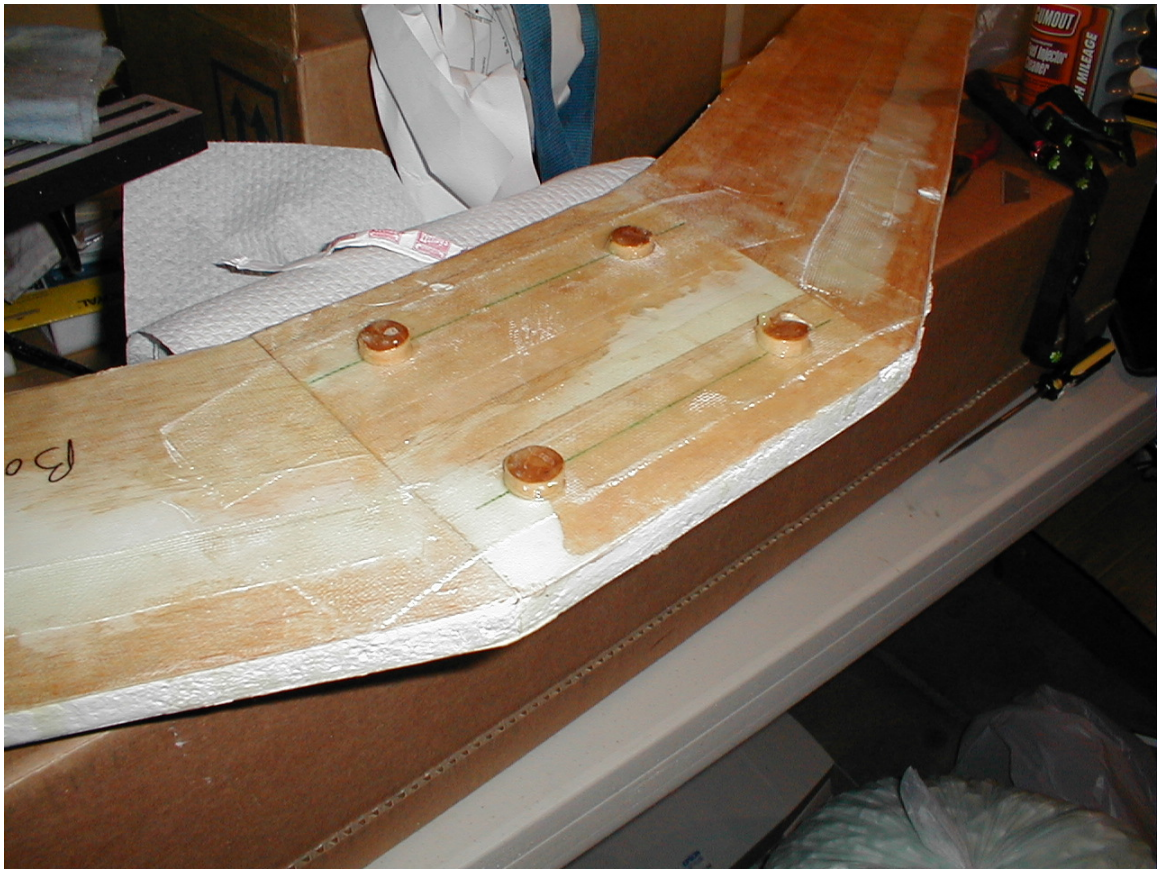

Figure (34) Bottom Side of Repair Test Article

The FEM indicated the structural flexibility was somewhat insensitive to the core (foam) material properties. However, structural flexibility is sensitive to the balsa skin properties. With this in mind and with results from the static load test, Robinson calibrated the balsa skin elements of the FEM for the unmodified wing to match the experimental deformation.

The wing design was modified with the application of fiberglass cloth to the balsa skin as roughly indicated in the cartoon Figure (34). (This was a work in progress with a large degree of uncertainty with the model builder's lack of experience with composites). The FEM was modified to reflect the new carry-though structure and the new fiberglass skin.

Distributed loads representing the static load test were applied to the FEM. The resulting deformation was dramatically reduced and the stress fell within limitations with 50% margin. Maximum principle stress on the wing skin is 700 psi. The manufacturer's published tensile strength allowable for fiberglass fabric is 33 kpsi. Allowing for 50% resin (strength allowable 8 kpsi), the composite wing skin tensile strength is 20.5 kpsi. Thus, the 700 psi predicted in the FEM model is far more than adequate. Stress contours are shown in Figure (36).

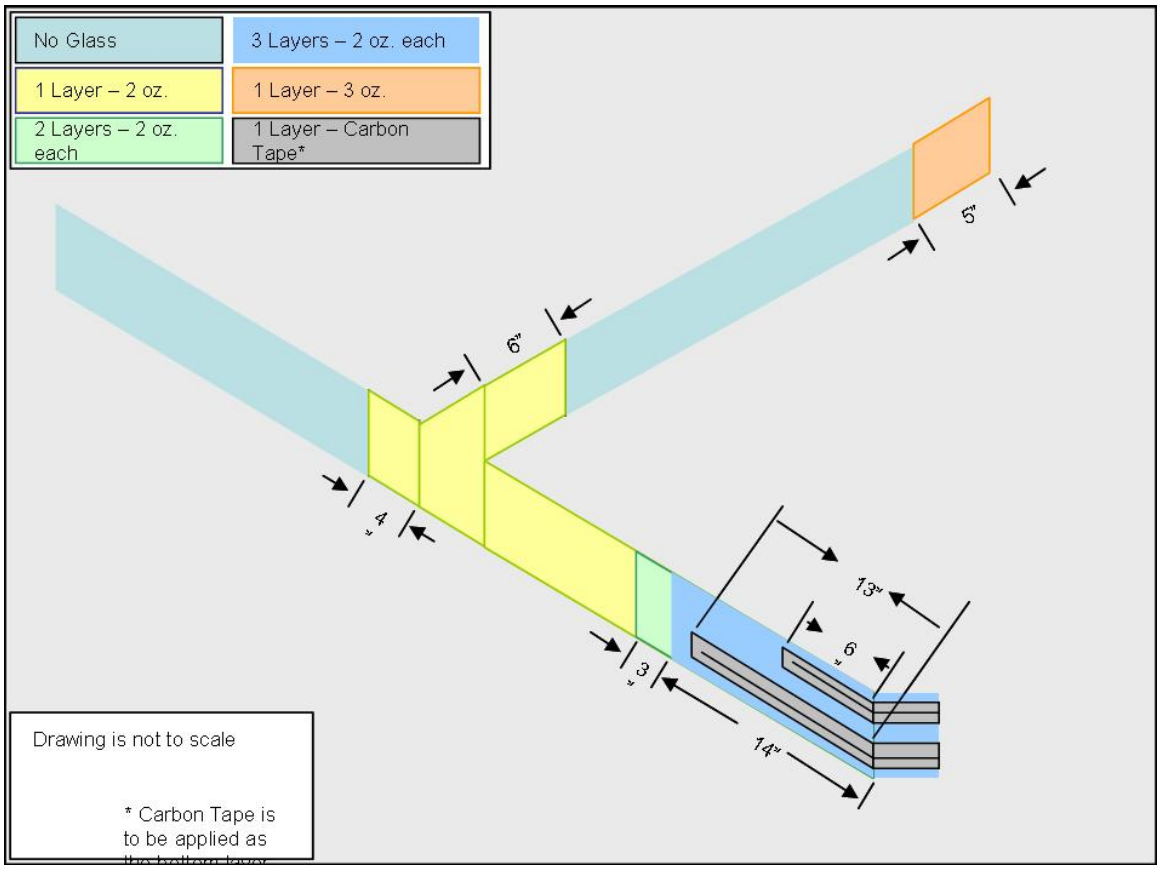


Figure (35) Composite Layup Plan for Wing Modification

### 5.1.10. Finite Element Analysis of the Redesigned Wing

After it was found that the baseline finite elements model properly captured the behavior of the VA-1 under static testing, modifications in step with the redesign plans were made. Both the left and right fore wings were extended to the centerline and connected with foam core covered with balsa. This is the first step in the redesign process. The finite element analysis was repeated with the wing root cantilevered.

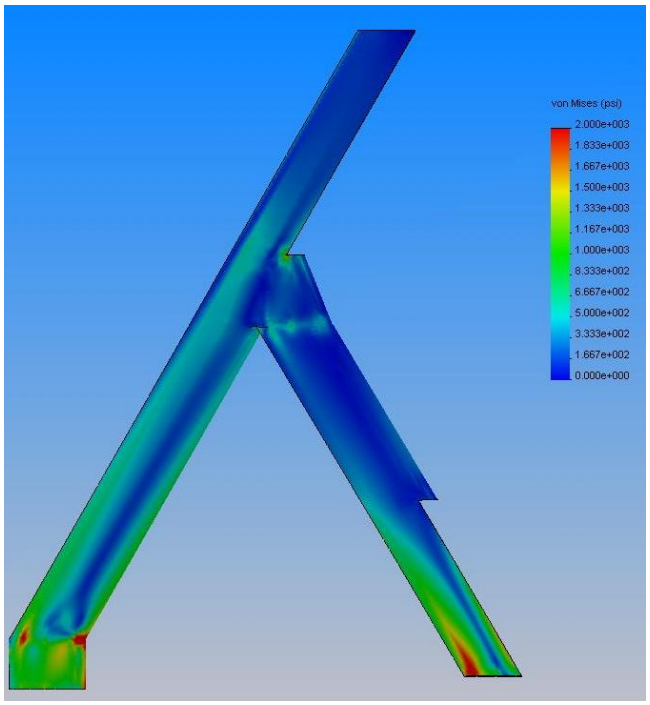


Figure (36) Top View of Stress Pattern Under Modified Boundary Conditions

The FEM displacements were very sensitive with respect to boundary conditions to reflect a case where the newly added center section is constrained. Both the fore and aft wings are constrained as cantilevers to the plane of symmetry in this case. In Figure 16, a stress contour (using the same color scale as the stress contour in the baseline study for continuity) is shown to have peaks in the stress contours along the leading and trailing edges of both the fore and aft wings. The stress concentrations shown are consistent with the location of the stress concentrations in the aft wing of the baseline study. Due to the new constraints on the fore wing (similar to those on the aft wing), it has stress concentrations in similar locations. These results are quite similar to the results of the full-scale finite elements analysis published at the time of completion of the VA-1.

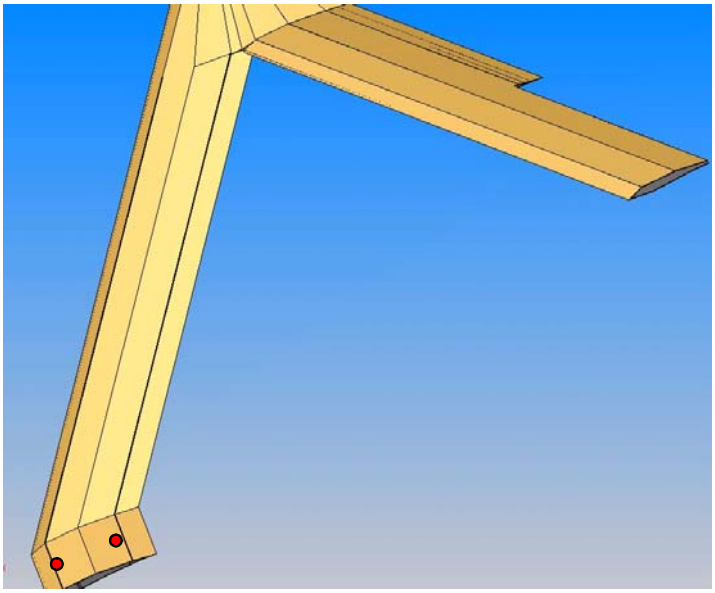

Figure (37) Positioning of Mounting Bolts Under Modified Mounting Conditions

Eventually this is modified to model a possible wing fastening design by adding four fasteners to clamp the wing to the fuselage. These bolts are fasteners that would be added at the approximate location of the red circles shown above, in Figure (37). This models the method of joining the wing to the fuselage called for in the redesign plan. This is modeled by fixing the wing at the positions indicated and applying a symmetry boundary condition to the root of the wing. The effects of changing this boundary condition are negligible in terms of stress concentrations. Although there is a slightly higher concentration at the position of the bolts, the rest of the wing experienced approximately the same stresses. This modification also did very little to affect the overall tip deflection, when compared to the totally cantilevered model.

The following table shows the effects of the different boundary conditions on deflection:

| Constraint | Tip deflection |
|---|---|
| Graphite spar (Baseline) | 20.61” |
| Entire Wing Root | 9.00” |
| Bolts | 9.01” |

Table (8) Boundary Conditions and Corresponding Tip Deflections

As a possible solution to the problem of excessive tip deflection and as reinforcement against torsion, it is suggested that fiberglass be applied to the inboard section of the fore wing of the VA-1. Adding fiberglass as shown, and allowing the boundary conditions to remain the same (a cantilevered center section) produce a decrease in tip deflection of the model. The fiberglass is added in two thicknesses. From the root to slightly inboard of the wing merge, a base layer is applied. Two additional layers are added from the root up to one quarter the distance to the wing merge. This results in thicknesses of 0.012 inches and 0.004 inches, respectively. Applying this modification to the baseline finite element model produces desirable results of decreasing tip

deflection even further than before. This reduction in tip deflection indicates the absence of structural failure due to excessive twisting within the wing. The fiberglass layout plan is shown in Figure (38).

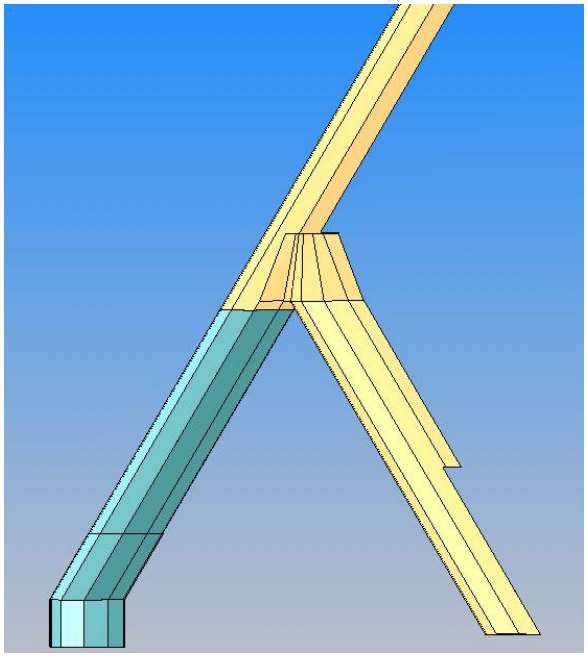

Figure (38) Layout of Fiberglass Reinforcement

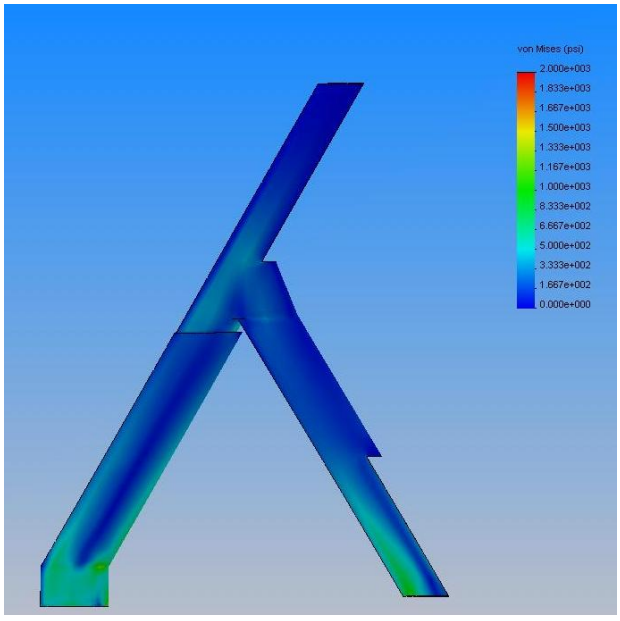


Figure (39) Top View of Stress Patterns in Fully Modified VA-1 Model

Another, more important, favorable effect of adding fiberglass is the stress reduction seen in the wing. As shown in the graphic in Figure (39), adding fiberglass to the wing structure allows for

a great decrease in the stress concentrations. Whereas the highest stress levels in the all the cases before adding fiberglass, the maximum stress levels were on the order of 2000 pounds per square inch. After adding fiberglass, and using the cantilevered boundary conditions, it's shown that the maximum stress concentration has a value of less than 700 pounds per square inch. This shows that adding fiberglass reduces stress by about 66%. While it was noted that solid elements are stiffer than shell elements, simply by their nature, this reduction in stress is a great sign for the confidence of the redesign plan. The maximum stress as indicated here is well within the design parameters of the materials used. This means that an even greater maximum stress is acceptable

### 5.1.11. Final Experimental Validation

The second (final) structural load test is described in Section [6.3.2.7]. As it turned out, the model builder did not comply with the above engineering specifications and it is not possible to correlate results with analysis. This discouraging disconnect probably points out the folly of requiring an amateur model builder to appreciate engineering requirements. However, to the model builder's credit, the modified wing structure did meet the load requirement.

## 5.2. Scaled Model Stability and Control Analysis [50]

The VA-1 was designed for vertical lift take-off (i.e. B-52 bomber and Predator). The bipod landing gear was positioned at the aft end of the fuselage, thus preventing the propeller from striking the ground upon takeoff. No fuselage rotation was envisioned on takeoff.

The VA-1 was rebuilt by a different model builder. There was personal concern, without analysis, that the vehicle would be unstable in yaw. Thus, an additional vertical tail was attached to the belly of the fuselage. The landing gear was moved forward in order to enable fuselage pitch-up rotation. This was done without regard for tail strike. The fuselage could only rotate a couple of degrees before the vertical tail dragged on the ground.

As it turned out in the flight test, this little bit of rotation was required to get the underpowered airplane airborne. But it is not clear the vertical tail was required. The idea was to conduct additional tests with the additional vertical tail removed.

Subsequent to the tail modification, analysis, presented here, also indicated a tendency for lateral instability. But not catastrophic.

The simple joined-wing balsa glider provided evidence that lateral stability would not be a factor.

A preliminary dynamic stability analysis was conducted prior to the flight test. Due to lack of inertia data, however, the dynamic stability analysis was not completed. This research completes the dynamic stability analysis of VA-1 and examined trimmed turning flight and related stall issues during the turn.

Figure (40) shows a flow chart outlining the research process.

Examining VA-1 geometry played an important role in ensuring the HASC model represented the aircraft well. Then aerodynamic coefficients were determined using a vortex-lattice method computer code called HASC-95 [16]. HASC output was used to calculate non-dimensional stability derivatives. A trim calculation used these derivatives to predict the cruise angle of attack and trim conditions for steady state level turns of various bank angles. Drag was modeled

by computing parasite drag on the wing, fuselage and vertical surfaces with empirical equations. Induced drag was found from HASC output with the cruise angle of attack. In order to evaluate dynamic stability, the mass moments of inertia of VA-1 were also required and measured experimentally. Inertia data, combined with stability derivates and the drag model, were input into a decoupled lateral and longitudinal 3-DOF state space model to estimate dynamic stability characteristics in straight and level flight. VA-1 was approximated as a rigid body and propeller effects were neglected. Dynamic stability characteristics of different combinations of aerodynamic surfaces were considered and recommendations made regarding which surfaces should be used or discarded for any potential future flight of VA-1.

Spanwise lift coefficients during a trimmed steady state turn were examined to see which wing sections potentially stalled first and to find the bank angle where stall began. For this process, trim conditions for the angle of attack, sideslip angle, all control deflections and angular rates were calculated for steady state level turns at different bank angles. The bank angles were increased until one or more wing sections stalled. This yielded the approximate bank angle for stall and located the wing section where stall began.

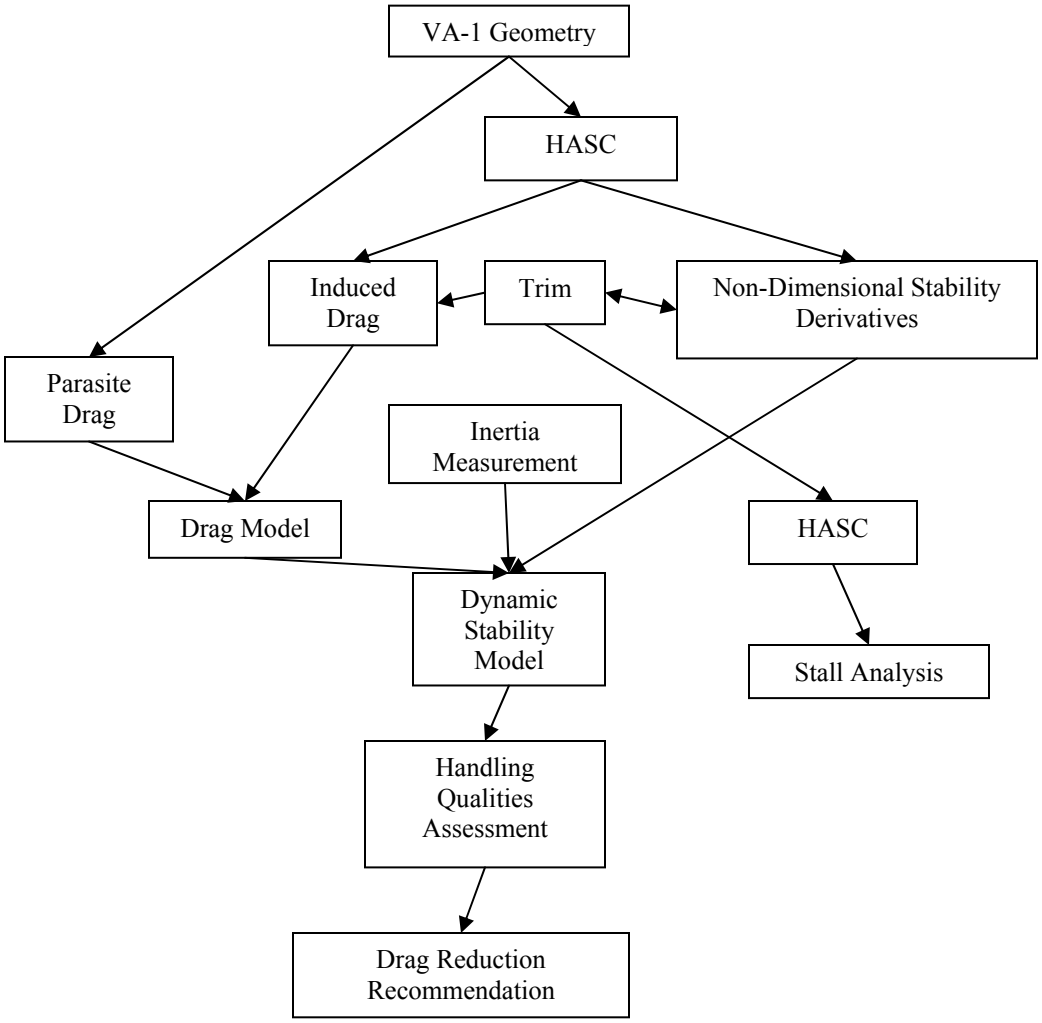


Figure (40) Research Process

### 5.2.1. Stability and Control Analysis

Due to initial concern regarding yaw stability, Bowman conducted a preliminary stability analysis on the AFRL Radio-Controlled Joined Wing aircraft . He utilized HASC [16], a vortex-lattice panel method computer code to predict the forces and moments on the aircraft in flight. Center of mass was varied longitudinally from 47 to 51 inches aft of the nose and several different combinations of aerodynamic surfaces were examined to include: reference geometry, reference geometry and fuselage, reference geometry and ventral fins, reference geometry and winglets and finally reference geometry and main gear strut-fins.

He concluded yaw stability, even with stability augmentation and strut fins, was likely too low for good flying qualities. In addition, at high angles of attack the yawing moments became small. If typical values of yaw moment due to sideslip range from 0.05 to 0.1 and higher values should be expected for radio-controlled aircraft, he argued, artificial yaw damping should be used. Furthermore, the modifications used to fix the yaw damping in his analysis caused the

spiral mode to become neutral or divergent and the modified vehicle would likely be prone to graveyard spirals [30]. This research will address VA-1 lateral stability in more detail.

Bowman predicted a longitudinally stable aircraft with Static Margin of 4% at the reference center of mass position. He stated that RC models typically need a static margin closer to 10% for the pilot to feel comfortable. He predicted a pitching moment coefficient below zero as long as the center of mass remained forward of a point approximately 50 inches aft of the nose. The fuselage was found to be destabilizing and he recommended the addition of winglets or strut fins, unless the center of mass was shifted forward [30].

Throughout his analysis it became clear that VA-1 stability was very sensitive to center of gravity location. Placing the center of mass too far forward made takeoff rotation difficult and too far aft made the plane unstable. For this reason, and to gather good inertia data, accurately measuring the center of mass became an important part of this research effort.

Bowman recommended simultaneous outboard aileron and rear wing elevator deflection for pitch control [30]. The inboard ailerons on the front wing section were used bilaterally for roll. This control scheme was used for the flight test and subsequently used when determining the stability derivatives with respect to aileron flap deflection.

A stability and control analysis was conducted using a vortex lattice model. Pitch stability and trim as well as yaw stability and lateral-directional behavior were examined.

**Yaw**: The baseline vehicle is predicted to be marginal in yaw stability in the trimmable and stable (pitch) CG range. $C_{N_\beta} \approx 0.01$ , which is approximately 5x to 10x lower than historical values for full scale vehicles at low Mach numbers. Given that rate damping on RC aircraft usually must be higher for the pilot to feel comfortable flying the vehicle, the predicted value may be 20x lower than a typical RC aircraft. With the addition of a COTS gyroscope (designed to work with the major brands of radio receivers) on the yaw channel, the yaw stability is still less than ideal but better than marginal. The exact effect is not known since a gyro was not available, but if the rudder is deflected 3° for every 1° of sideslip, $\Delta C_{N_\beta} \approx 0.03$ assuming ideal rudder effectiveness. With the addition of winglets or fins placed over the main wheel struts, $\Delta C_{N_\beta} \approx 0.02$. The addition of the winglets or strut fins introduces a spiral divergence at predicted cruise angles-of-attack, though. If during taxi tests and brief periods of flight it is determined that the yaw stability and damping is deemed insufficient, the winglets or strut fins can be added. Since the geometric solution would require structural modification to the vehicle, artificial stability augmentation should be attempted first. If geometric solutions are required, the potential spiral divergence is usually much more controllable than marginal yaw stability and damping. Consider installation of yaw gyro to augment yaw control

**Pitch**: The vehicle has approximately 4% static margin at the reference CG. If the CG is moved 1 inch forward (approximately 11% MAC), the static margin is 20%. The joined wing configuration has a higher than normal $C_{M_\alpha}$ due to the wing area being well forward and aft of the CG, which explains the sensitivity. At the higher static margins, the vehicle is predicted to trim in cruise and landing. **However, care should be taken to not get the vehicle too slow until it is certain the there is sufficient control effectiveness (pilot discretion)**. A control

effectiveness of 50% was assumed, but the effect of hinge gaps and low Reynolds numbers is uncertain.

**Lateral-Directional**: A dynamic analysis was not conducted, but the vehicle is predicted to have a positive dihedral effect. As previously mentioned, the addition of geometry to correct potential yaw stability and damping introduces a spiral divergence for angles-of-attack below 3° angle-of-attack (not much of a problem) for the winglets and below 8° (more of a problem) for the strut fins.

**Roll**: Bilateral deflection of the inboard surfaces should produce adverse yawing moments that do not exceed the capability of the rudder. However, if the rudder is also being used for yaw stability augmentation, full stability augmentation and/or adverse yaw control may not be possible. Given that the roll damping $C_{l_p} \approx -0.6$, which is 50% to 100% higher than normal, the roll acceleration and steady roll rate may be undesirable. However, the high damping should help limit entering situations where higher roll rates are necessary for recovery.

**Summary:** Pitch/roll mixing on the outboard surfaces may be necessary for the pilot to feel comfortable with the roll response. At all angles-of-attack, if both the inboard and outboard surfaces are used for roll, there are combinations that produce adverse yaw moments than exceed the capability of the rudder, especially at higher angles-of-attack (landing). The pilot may notice a marked decrease in roll/yaw/turning authority during the landing phase if a higher angle-of-attack is maintained. If programmable, the aileron on the side of the roll should have a higher deflection than its counterpart on the opposite side to mitigate the adverse yaw effects.

### 5.2.2. HASC Model and Stability Derivatives

This chapter discusses how the non-dimensional stability derivates used in the dynamic stability model were calculated. First, aerodynamic forces and moments for different combinations of angle of attack, sideslip angle and rotation rates were computed using HASC. Non-dimensional stability derivates were calculated from HASC output data using a excel spreadsheets that formed a derivative database. Many of the derivatives were slightly nonlinear with respect to angle of attack. The trim angle of attack solution, discussed in the next section, was iterated using the derivatives from this section and the non-dimensional stability derivates used for the dynamic stability model were then linearly interpolated from the derivative database for the cruise angle of attack.

The HASC program utilized a Vortex Lattice Method (VLM) to compute aerodynamic coefficients for a given aircraft geometry. HASC-95, an updated version, was used for this analysis and will be referred to as HASC throughout this discussion. HASC uses three primary methods to solve for the aerodynamic coefficients: VORLAX, VORLIF and VTXCLD. VORLAX is a generalized vortex lattice program, VORLIF is a semi-empirical strake/wing vortex analysis code and VTXCLD is a two dimensional, unsteady, separated flow analogy program for analyzing smooth forebody shapes [16].

In this research VORLAX was used exclusively. Use of VLM on joined-wing configurations is not entirely without precedent. Smith *et al* found VLM could predict aerodynamic coefficients for joined-wing type aircraft reasonably well [8]. This is probably because VLM method

neglects both thickness and viscosity effects, which usually cancel each other out [30]. Due to the preliminary nature of the VA-1 as only a demonstrator vehicle, HASC was deemed an appropriate tool to estimate the aerodynamic stability derivatives.

### 5.2.3. HASC VA-1 Model

A HASC input file from Bowman's preliminary dynamic stability analysis was used as the baseline configuration. Bowman's inputs for vertical and horizontal fuselage segments, all wing surfaces and the upper vertical tail were used as the baseline configuration. Bowman's strut-fin geometry was also used [30]. The strut-fins could potentially be used as fairings covering the main landing gear struts and were modeled as small 4 x 10 in. flat plates with zero camber. The horizontal fuselage plane was used to capture fuselage effects for longitudinal derivatives. A lower vertical tail (LVT) and strut-fins were evaluated as separate surfaces to determine their effect on the stability. The LVT configuration was actually used for the flight tests.

The most significant addition to the HASC model was the lower vertical tail (LVT). Bowman did not analyze this surface in his report [30]. Other adjustments were also made to the model. The strut-fins were moved forward to the main gear location used by the flight test team, as shown in Figure (41) shows both the LVT and strut-fin locations on VA-1. All measurements were closely verified from the actual vehicle. Wing geometry and camber remained unchanged. Propeller effects were neglected. The rudder was resized so that it ran the full vertical distance of the upper vertical tail. The c.g. was moved from 48 in. to 46.75 in. from the nose for all cases to reflect measured c.g. used for the inertia tests. HASC computed the aerodynamic moments about this point.

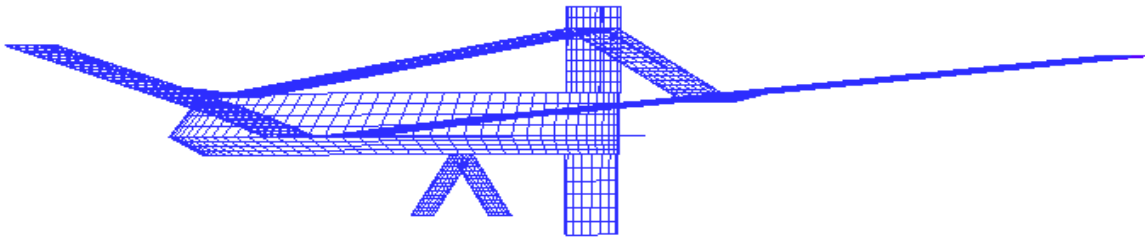

Figure (41) HASC input geometry with lower vertical tail and strut-fins.

The preliminary flight conditions used for the previous analysis assumed a Reynolds Number, Re, of 300000 and a Mach Number of 0.065. Perhaps due to increased weight or higher than anticipated drag, the actual flight velocity was a bit lower than the 57 mph calculated in the initial cruise velocity analysis [31]. The Palm Pilot GPS data in Figure (89) revealed, at the most consistent portion of the flight, an average speed of approximately 45 mph or 66 ft/s at full throttle was used. Note the GPS data sampling rate was not constant and varied between one and ten seconds. Accounting for field elevation and different speed, Re was approximated as 314000 for a Mach Number 0.06.

Each trailing edge device was assigned to one control function during the flight test. Figure (44) shows the elevators, ailerons and rudder control surfaces shaded green, red and blue respectively. Elevator control was assigned to the outboard control surfaces on the wingtips simultaneously with the trailing edge devices at the rear wing roots for a total of four elevator control surfaces. The rudder, on the vertical tail, ran the length of the vertical fin. Aileron control was bilateral

movement of the inboard trailing edge devices on the front wings for a total of two surfaces. The ailerons were positioned inboard of the elevator surfaces at the wingtips. This was unusual because most aircraft utilize the outboard trailing edge flap for aileron control. Bowman found, in his HASC analysis, the inboard aileron location was most effective for ailerons due to reduced lift at the wing tips [30]. This explains the unusual aileron placement

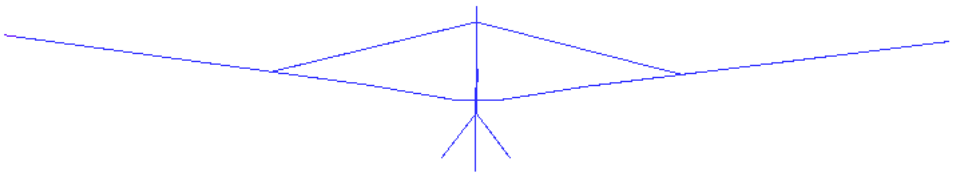

Figure (42) VA-1 HASC Model Frontview

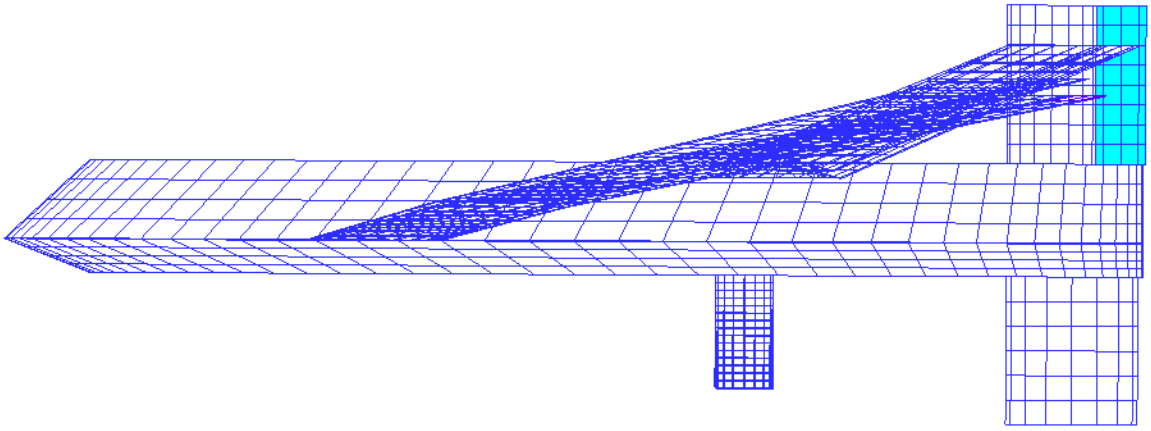

Figure (43) VA-1 HASC Model Sideview.

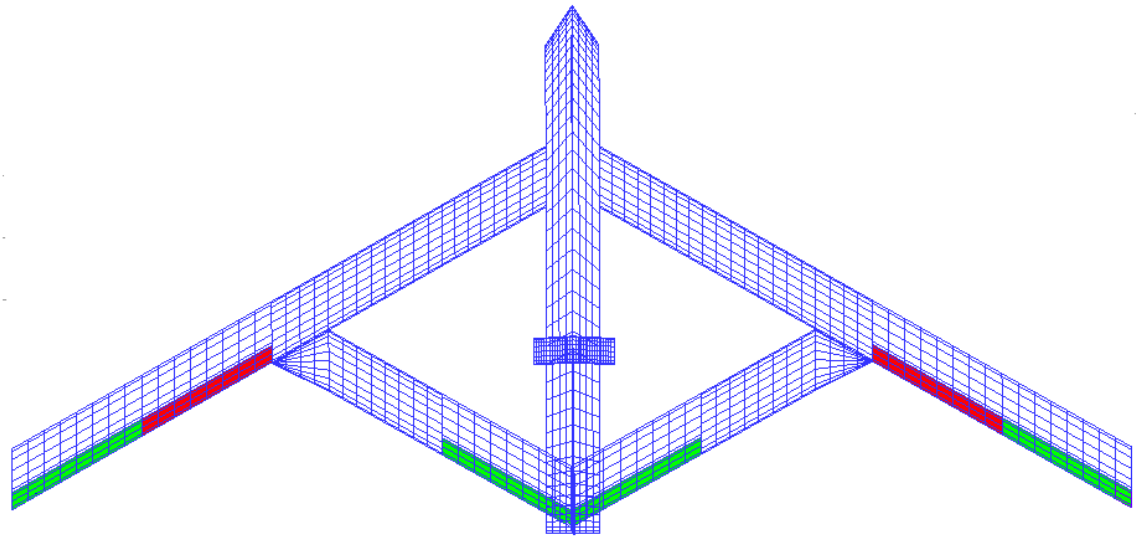

Figure (44) VA-1 HASC Model Top View.

### 5.2.4. Surfaces and Panels

HASC subdivides its surfaces and panels from largest to smallest with the following nomenclature: surfaces, panels, and subpanels[16]. VA-1 had eight surfaces: left forward wing (LFW), fuselage, right forward wing (RFW), left rear wing (LRW), strut-fins, lower vertical tail (LVT), vertical tail, and right rear wing (RRW). Each surface was then divided into panels depending on its size. Control surfaces were modeled as separate panels. Chordwise divisions on the subpanels were distributed so a total of ten chordwise subpanels existed at any spanwise station on the wing. Figure (42), Figure (43) and Figure (44) show the panel distribution.

Panels were subdivided into subpanels by specifying the number of spanwise and chordwise divisions for each subpanel. In general, each wing subpanel had ten chordwise divisions. For sections of wing with trailing edge flaps, the ten chordwise divisions were distributed in a 60% - 40% fashion. The front wing and trailing edge subpanels had six and four chordwise divisions respectively. At the wing joints, spanwise divisions were carefully matched to line up with fore and aft panel sections. Table (9) lists the spanwise and chordwise panel distributions for the major surfaces.

An important part of the HASC model is airfoil camber. Bowman's camber inputs for the FX 60-100 Airfoil were used in this HASC model. For wing sections with trailing edge devices, the camber was superimposed across the combined for and aft sections. At the joint, camber was simply scaled to the new chord length. In Figure (45) shows the non-dimensional camber lines for three different airfoil sections in relation to the surface coordinates for the FX60-100 airfoil. The specific data points plotted represent actual camber ordinates input into HASC.

| Surface Name | # of Surfaces | Spanwise Strips | Chordwise Strips | Subtotal |
|---|---|---|---|---|
| Forward Wing | 2 | 36 | 10 | 720 |
| Fuselage | 2 | 8 | 40 | 640 |
| Rear Wing | 2 | 20 | 10 | 400 |
| Strut-fin | 2 | 15 | 8 | 240 |
| LVT | 1 | 6 | 8 | 48 |
| Upper Vertical Tail | 1 | 8 | 12 | 96 |
| | | | **TOTAL** | **2144** |

Table (9) VA-1 HASC Subpanel Distribution

HASC outputs force and moment coefficients in the stability, wind and body axis systems. Stability axis coefficients were used to determine the non-dimensional stability derivatives. HASC used the total wing area, 2226 $in^2$, to non-dimensionalize its coefficients. The stability state space model used dimensional derivatives with respect to the body axis.

By comparison, Smith *et al* used VLM to analyze the JW-1 in LinAir. They input the complete aircraft geometry and had 20 spanwise by 5 chordwise panels for the front wing and 12 spanwise by 5 chordwise panels for the tail. Eight panels were used for the fuselage and engine nacelles for a total of 168 panels. The wind tunnel results for JW-1 matched the $C_{m_\alpha}$ and $C_{L_\alpha}$ predicted by LinAir fairly accurately between -4 and 3 degrees angle of attack [4].

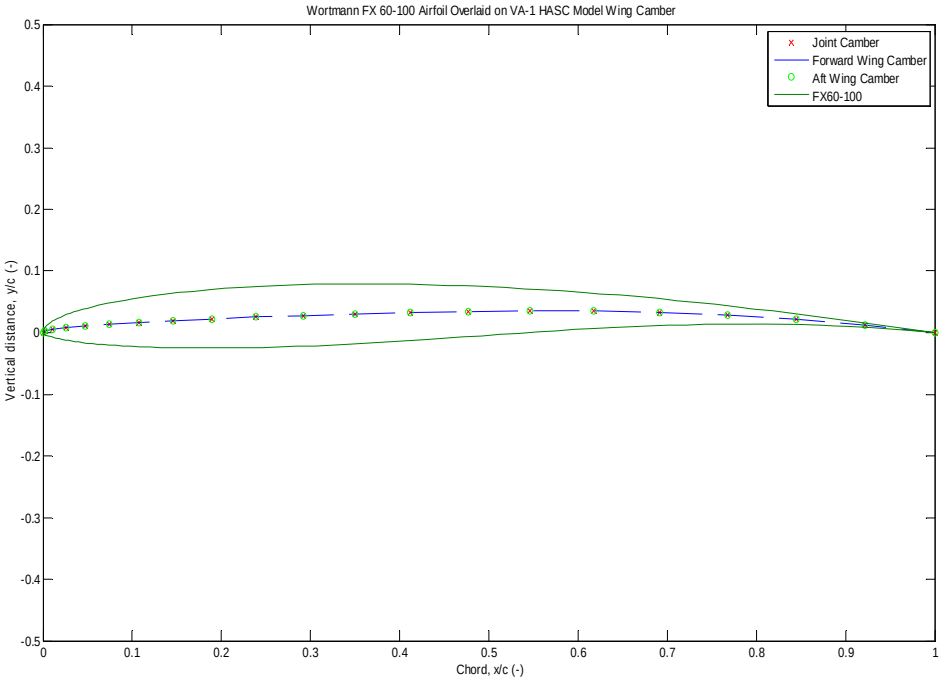


Figure (45) HASC camber lines compared to FX 60-100 Airfoil.

### 5.2.5. HASC Test Matrix

A range of variables were altered to produce stability coefficients through a range of angles of attack, sideslip angles, roll rates, pitch rates, yaw rates, elevator and aileron deflection angles. Angle of attack, $\alpha$, and sideslip angle, $\beta$, are in degrees. Positive angular rates mean right wing down for roll, nose up for pitch, and nose right for yaw. Surface deflections for elevator aileron and rudder are in degrees. Positive elevator deflection, $\delta e$, means trailing edge down. Positive aileron deflections, $\delta a$, were coordinated for a right roll. For example, an aileron deflection of five degrees was input as five degrees up on the right aileron and five degrees down on the left aileron. Positive rudder deflection, $\delta r$, means rudder trailing edge right and moves the nose right. This is opposite the normal rudder convention and more is discussed in the chapter on trim.

Entries with an arrow, →, denote a range of values incremented by the number after the comma, with the first and last value included. In the case where numbers were separated by commas, HASC did not automate the iterations and was run separately for each output. Table (10) and Table (11) show the combinations of variables run in HASC to find lateral and longitudinal stability derivatives. For all longitudinal cases $\beta = p = r = \delta a = \delta r = 0$.

| Angle of Attack (deg) | Pitch Rate (deg/s) | Elevator Deflection (deg) |
|---|---|---|
| -5→10, 1 | -5,0,5 | 0 |
| -5→10, 1 | 0 | -5,5 |

Table (10) HASC Test Matrix for Longitudinal Stability Derivatives.

| Angle of Attack (deg) | Sideslip (deg) | Roll Rate (deg/s) | Yaw Rate (deg/s) | Aileron Deflection (deg) | Rudder Deflection (deg) |
|---|---|---|---|---|---|
| -4→8, 2 | -5,0,5 | 0 | 0 | 0 | 0 |
| -4→8, 2 | 0 | -5,5 | 0 | 0 | 0 |
| -4→8, 2 | 0 | 0 | -5,5 | 0 | 0 |
| -4→8, 2 | 0 | 0 | 0 | -10,-5,5,10 | 0 |
| -4→8, 2 | 0 | 0 | 0 | 0 | -10,-5,5,10 |

Table (11) HASC Test Matrix for Lateral Stability Derivatives.

HASC outputs the force and moment coefficients, not the stability derivatives. The output files were put into an excel spreadsheet and stability derivates were computed by finding the slope between test points. For example, $C_{L_\alpha}$ was found by computing the rate of change in lift coefficient with respect to the change in angle of attack. Derivatives with respect to the angular rates $p$, $q$ and $r$ in radians/second were converted their corresponding non-dimensional roll, pitch and yaw rates: $pb/2u_1$, $qc/2u_1$ and $rb/2u_1$ respectively, where $u_1$ was the steady state velocity, $b$ was the wingspan and $c$ was the mean aerodynamic chord. The units for non-dimensional

angular rates were found in radians and the units for their respective derivatives were reported in units of 1/rad. Because the derivatives varied slightly with angle of attack, the trim angle of attack was needed to know which stability derivatives to use.

### 5.2.6. Non-Dimensional Longitudinal Stability Derivatives

As expected, the LVT had virtually no effect on the longitudinal derivatives. Small, yet insignificant changes were noted due to the strut-fins. Table (12) shows the differences in the non-dimensional derivative calculations between the baseline and strut-fin. JW-1 derivatives from wind tunnel data were also included for comparison. Units are 1/rad. Strut-fins made the pitching moment derivatives slightly more negative and slightly increased $C_{L_q}$. $C_{m_{\dot{\alpha}}}$ was estimated as $C_{L_q}$ ($d\varepsilon/d\alpha$) [19].

| Derivative | Baseline | Strut-fins | JW-1 |
|---|---|---|---|
| $C_{L_\alpha}$ | 4.842 | 4.888 | 4.64 |
| $C_{D_\alpha}$ | 0.426 | 0.428 | 0.267 |
| $C_{m_\alpha}$ | -1.072 | -1.093 | -1.153 |
| $C_{L_q}$ | 8.966 | 9.162 | N/A |
| $C_{m_q}$ | -25.593 | -25.593 | N/A |
| $C_{m_{\dot{\alpha}}}$ | -15.708 | -15.708 | N/A |
| $C_{L_{\delta e}}$ | 0.7795 | 0.7795 | 0.2 |
| $C_{m_{\delta e}}$ | -1.5383 | -1.5383 | N/A |

Table (12) Non-Dimensional Longitudinal Stability Derivatives For Different Configurations.

The change in downwash angle with respect to angle of attack, $d\varepsilon/d\alpha$, was found by comparing two HASC models: the first a rear wing and fuselage without a front wing attached, the second a complete front wing, fuselage and rear wing combination. Downwash angle, $\varepsilon$, was found by observing how much the downwash from the front wing effectively reduced the angle of attack on the rear wing. This approach is similar to that used in wind tunnels [18].

First, the lift curve slope of the rear wing without the downwash effects of the front wing was found by removing the front wing from the HASC model. Aircraft angle of attack was fixed to zero degrees and rear wing incidence angle was set to zero and five degrees respectively. The slope of the change in rear wing lift coefficient, $C_{L_R}$, with respect to angle of attack, $\Delta C_{L_R}/\Delta\alpha$, was computed. At this point $C_{L_R}$ without the front wing downwash is known for zero and five degrees angle of attack.

Next, with the front wing attached, $C_{L_R}$ was computed at zero and five degrees angle of attack. With downwash effects of the front wing included, the new $C_{L_R}$ values were slightly reduced

from the case with the front wing removed. This reduction in $C_{L_R}$ was due to downwash angle. The change in $C_{L_R}$ was divided by the lift curve slope of the rear wing to find the change in angle of attack required to match the reduced lift coefficient. This change in angle of attack was the downwash angle.

The change in downwash angle with respect to aircraft angle of attack was found by computing a downwash angle for two separate angles of attack:

$$\frac{d\varepsilon}{d\alpha} = \frac{\varepsilon_2 - \varepsilon_1}{\alpha_2 - \alpha_1} \quad (14)$$

Where $\varepsilon_2$ is the downwash when $\alpha = 5$ deg and $\varepsilon_1$ is the downwash when $\alpha = 0$ deg. For VA-1 $d\varepsilon/d\alpha$ turned out to be approximately 0.61.

### 5.2.7. Non-Dimensional Lateral Stability Derivatives

The different configurations had five noticeable effects on the lateral stability derivatives. Table (13) shows the results in units of 1/rad. Derivatives with respect to $\beta$ seemed to vary the most. As expected, derivatives with respect to non-dimensional pitch rate did not change much. Some minor variations occurred in the derivatives with respect to non-dimensional yaw rate.

Addition of the LVT and strut-fins made $C_{y_\beta}$ more negative. This made sense as both surfaces increase the surface area facing the sideslip angle and more positive sideslip would generate more negative sideforce. A balance between $C_{l_\beta}$ and $C_{n_\beta}$ for good Dutch roll stability is required.

The dihedral derivative, $C_{l_\beta}$, usually ranges from about -0.4 to 1.0 per radian [17] and VA-1 sits well in this range. The dihedral derivative became less negative as the LVT and strut-fins were added. This made sense because adding surface area below the fuselage centerline would cause a resistance to any rolling motion induced by sideslip. Think of the fuselage and one vertical tail on top. Positive sideslip would cause a negative roll moment, or a left roll. Now add a mirror image of the vertical fin pointing down. The roll moments caused by sideslip on both vertical surfaces would then tend to cancel each other out.

More negative dihedral derivative values usually mean the aircraft will be more stable in the Dutch roll mode. In general the LVT and strut-fins tended to decrease Dutch roll stability with respect to this derivative. This was possibly due to the increased weathercock stability caused by addition of vertical surfaces. In the case of a positive sideslip the aircraft would yaw more quickly to the right, hence the higher $C_{n_\beta}$ term. As a result the left wing increases in speed and induces a right roll increasing the Dutch roll effect [18]. Table (13) shows $C_{n_\beta}$ increased by 48% from adding the LVT. The strut-fins increased yaw stiffness by approximately 8%. These effects seem reasonable as the yaw stiffness derivative is strongly influenced by the size of the vertical tail.

| Lateral Derivatives | Baseline | LVT | Strut-fins | LVT + Strut-fins |
|---|---|---|---|---|
| $C_{y_\beta}$ | -0.4688 | -0.5658 | -0.5651 | -0.6602 |
| $C_{l_\beta}$ | -0.1437 | -0.1374 | -0.1378 | -0.1309 |
| $C_{n_\beta}$ | 0.0302 | 0.0449 | 0.0325 | 0.0472 |
| $C_{y_p}$ | -0.1066 | -0.1111 | -0.1066 | -0.1111 |
| $C_{l_p}$ | -0.5147 | -0.5147 | -0.5147 | -0.5147 |
| $C_{n_p}$ | -0.0019 | -0.0019 | -0.0019 | -0.0019 |
| $C_{y_r}$ | 0.2180 | 0.2829 | 0.2288 | 0.2937 |
| $C_{l_r}$ | 0.1552 | 0.1552 | 0.1552 | 0.1552 |
| $C_{n_r}$ | -0.0344 | -0.0452 | -0.0344 | -0.0452 |

Table (13) Non-Dimensional Lateral Stability Derivatives for Different Configurations.

The LVT made yaw damping , $C_{n_r}$ , more negative by 31% and the strut-fins had no effect. At first glance we expect the LVT be more stabilizing than the strut-fins in the Dutch roll mode. Yaw damping is the most important derivative for determining Dutch roll stability. It is important to note a balance between yaw damping and dihedral derivative, $C_{l_\beta}$, is required to achieve good Dutch roll characteristics. The different configurations reveal the tradeoff: adding the LVT degrades the dihedral derivative in terms of stability while improving the yaw damping derivative. The dynamic stability analysis should reveal which effect dominates.

### 5.2.8. Trim

Trimming the aircraft was critical for both the dynamic stability and turn analysis. Calculations for three types of steady state maneuvers were performed: steady state straight and level flight, steady state level turn, and steady state pull up maneuver. Steady state means angular rates in addition to aircraft forces and moments remain constant throughout the maneuver. The trim angle off attack for straight and level flight was used to linearly interpolate the stability derivatives and induced drag used directly for the stability model. The steady state angle of attack, sideslip angle, control surface deflections and angular rates were required for the stall analysis. They were used to trim HASC model through a range of hypothetical bank angles. Then HASC was used to examine the spanwise lift distribution to see where stall might occur first. The same approach was used for the steady state pull up maneuvers for 1.25, 1.5 and 2 g's respectively.

The trim equations came from the aircraft equations of motion with respect to the stability axis. The equations used to trim for steady level flight were the same as the equations used for a steady level turn with a few exceptions. For straight and level flight the bank angle was set to zero, the load factor, *n*, was set equal to one and all of the angular rates and moments were zero. In general these equations assume the aircraft has adequate control power and the servos generate enough torque to maintain adequate control surface deflection [18].

Some assumptions were made to simplify the problem. First, the equations assumed flow remained attached over the wings. Since the purpose of the turn trim was to see where stall developed first and not to predict actual turn performance this assumption had minimal impact on the results. Another assumption was that the stability x-axis stayed in the same plane throughout the turn. Conveniently the stability derivatives were computed with respect to stability axes and worked nicely for these calculations. The roll rate, $p$, was assumed to be zero. For the steady state turn you must bank angles were selected prior to solving the equations [18].

Roskam's steady state turning flight equations were used to find the trim conditions. Roskam included a term to account for the effect of the horizontal tail incidence angle, but those terms were neglected as the tail incidence angle for VA-1 was zero. These equations would need modification for a twisting rear wing or inclined horizontal tail. First finding the load factor $n$, as $n = 1/\cos\varphi$ where positive $\varphi$ is the bank angle with the right wing down. The steady state pitch and roll rates, $q$ and $r$ rad/s respectively, can then be found as $q=g/u_1(n-1/n)$ and $r=(g/nu_1)\sqrt{n^2-1}$ where g is the gravitational constant and $u_1$ is the steady state velocity in ft/s [[18]:224-230].

Next we turn our attention to the trim angle of attack and elevator deflection angle for the steady state turn. The following equations were found by separating the longitudinal aerodynamic force and moment equations from the lateral equations. Assuming the aircraft had enough thrust to maintain the respective steady state condition, the remaining longitudinal equations could be solved with the following:

$$(15) \quad \begin{bmatrix} C_{L_\alpha} & C_{L_{\delta e}} \\ C_{m_\alpha} & C_{m_{\delta e}} \end{bmatrix} \begin{Bmatrix} \alpha \\ \delta e \end{Bmatrix} = \begin{Bmatrix} nC_{L_{trim}} - C_{L_0} - C_{L_{i_h}} i_h \\ -C_{m_0} - C_{m_q} \frac{cg}{2u_1^2}(n - \frac{1}{n}) \end{Bmatrix}$$

where $C_{L_{trim}}$ was the trim lift coefficient when L=W, $C_{L_0}$ was the lift coefficient at zero angle of attack, $C_{m_0}$ was the moment coefficient at zero angle of attack, $c$ was mean geometric chord in feet, $\alpha$ was the angle of attack in radians and $\delta e$ the elevator deflection angle, also in radians [18]. The term $i_h$ was the incidence of the horizontal tail while $C_{L_{i_h}}$ was the change in lift coefficient with respect to change in horizontal tail incidence angle. The tail incidence for VA-1 was zero, but the tail incidence terms could perhaps be expanded for future use with a twisting rear wing. Note that positive elevator deflection means trailing edge down. Note once again, for steady level flight, when $n = 1$ the bottom right term on the right hand side become zero. At this point enough is known for trim in straight and level flight as the sideslip angle, aileron deflection and rudder deflection are all zero.

To complete the steady state turn trim we need to account for the sideslip angle, $\beta$, aileron deflection angle, $\delta a$, and rudder deflection angle, $\delta r$. From the lateral aerodynamic force and moment equations Roskam provides the following system of lateral equations[[18][18]:224-230]:

$$(16)\quad \begin{bmatrix} C_{y_\beta} & C_{y_{\delta a}} & C_{y_{\delta r}} \\ C_{l_\beta} & C_{l_{\delta a}} & C_{l_{\delta r}} \\ C_{n_\beta} & C_{n_{\delta a}} & C_{n_{\delta r}} \end{bmatrix} \begin{Bmatrix} \beta \\ \delta a \\ \delta r \end{Bmatrix} = \begin{Bmatrix} -C_{y_r} \dfrac{bg \sin\phi}{2u_1^2} \\ \dfrac{(I_{zz} - I_{yy}) g^2 \sin^3\phi}{QSbu_1^2 \cos\phi} - C_{l_r} \dfrac{bg \sin\phi}{2u_1^2} \\ -C_{n_r} \dfrac{bg \sin\phi}{2u_1^2} \end{Bmatrix}$$

Recall $Q$ was used for dynamic pressure in $lb_f/ft^2$ to avoid confusion with the pitch rate $q$.

The equations were solved with a MATLAB script file and simple matrix manipulation[[48]]. First, the equations were input into the form $Cx = b$, where $C$ was the matrix of non-dimensional stability derivatives, $x$ contained the unknown trim angles for the longitudinal or lateral equations. Then the term on the right hand side was pre-multiplied by the inverse of $C$, $x = C^{-1}b$, to find the steady state trim angles in radians. The angles were converted to degrees for ease of use later in the analysis.

Using the non-dimensional stability derivatives computed from HASC data for the LVT the trim conditions for bank angles of 0, 50 and 55 degrees were computed and presented in Table (14). For all cases the roll rate, $p$, was zero. For the zero bank angle the trim angle of attack was 2.36 degrees. This was the trim angle of attack for steady level flight and was used to interpolate the non-dimensional stability derivatives used for the model.

Since the stability derivatives had some mild non-linearities, the trim calculations for straight and level flight were iterated a couple of times. The first guess for trim angle of attack was made by simply computing the angle of attack that corresponded to the lift coefficient where lift equaled weight. The stability derivatives for $C_{L\alpha}$ and $C_{m\alpha}$ were interpolated and fed into the trim equations above for straight and level flight. This of course did not account for elevator deflection and the next solution provided a more realistic angle of attack. By repeating the process until the trim angle of attack did not change by more than 0.01 degrees the aircraft was considered trimmed for straight and level flight. The rest of the non-dimensional stability derivatives were then found at the trim angle of attack and used for the dynamic stability model.

The steady state level turn trim conditions were not iterated in the same manner. The turn would require interpolating between more variables and quickly becomes much more complicated. Again, the purpose of the trim for turning flight was to examine spanwise lift distribution. Iterating would only cause minor changes in small control deflections and have little effect on the local lift coefficient. In addition, the trim angle of attack only slightly increased from straight and level flight. As a result the stability derivatives used to find straight and level flight were also used to find the trim conditions for each bank angle.

| Bank Angle | 0 | 50 | 55 | (deg) |
|---|---|---|---|---|
| Pitch rate, $q$ | 0.00 | 25.51 | 32.70 | (deg/s) |
| Yaw rate, $r$ | 0.00 | 21.41 | 22.90 | (deg/s) |
| Angle of Attack, $\alpha$ | 2.37 | 5.82 | 6.96 | (deg) |
| Sideslip Angle, $\beta$ | 0.00 | -0.43 | -0.66 | (deg) |
| Elevator Deflection Angle, $\delta e$ | -10.69 | -15.57 | -17.06 | (deg) |
| Aileron Deflection Angle, $\delta a$ | 0.00 | 6.11 | 8.93 | (deg) |
| Rudder Deflection Angle, $\delta r$ | 0.00 | 9.47 | 12.01 | (deg) |

Table (14) Steady State Turn Trim Conditions used for HASC input.

### 5.2.9. Dynamic Stability

Dynamic stability of VA-1 was evaluated in the cruise flight condition for each configuration. VA-1 was assumed to be a rigid body and aeroelastic effects were neglected to simplify the model. Lateral and longitudinal flight dynamics were decoupled into two three-degree of freedom state space models of the form $\dot{x} = Ax + Bu$. The $A$ and $B$ matrices contained the dimensional stability derivatives and $x$ was a state vector and $u$ was a control vector. The corresponding eigenvalues of each system were used to determine the damping and natural frequencies of each flight mode. Longitudinal flight modes included the short period and phugoid modes. Lateral modes included roll, Dutch roll and spiral modes. The data for each mode was compared against longitudinal and lateral flying qualities to determine which combination of surfaces was best for inherent dynamic stability of the airframe.

Since stick-fixed stability was evaluated, the control matrix, $B$, was not needed. The longitudinal $A$ matrix was estimated using dimensional derivatives and assumed $Z_q$ and $Z_{\dot{w}}$ were negligible. The dimensional derivatives are with respect to the body fixed reference frame. To review the dimensional derivative nomenclature, $X$, $Y$ and $Z$ correspond to forces in the body axis $x$, $y$ and $z$ directions. Variables $L$, $M$ and $N$ represent the aerodynamic moments about the $x$, $y$ and $z$ axes. The subscripts $u$, $v$ and $w$ represent a derivative with respect to velocity in the $x$, $y$ and $z$ directions on the body axis. For these derivatives, subscripts $p$, $q$ and $r$ represent the dimensional derivatives with respect to the angular rates about the $x$, $y$ and $z$ body axes respectively. For example, the derivative $Z_q$ would be the change in aerodynamic force in the z-direction with respect to a change in pitch rate, $q$ and is typically small for conventional fixed-wing aircraft. The subscript $\beta$ is the derivative with respect to sideslip angle and the subscript $1$ represents the initial unperturbed condition. The gravitational constant is denoted as $g$ [19]. The longitudinal A matrix was:

$$(17) \qquad A=\begin{bmatrix} X_u & X_w & 0 & -g \\ Z_u & Z_w & u_1 & 0 \\ M_u+M_{\dot{w}}Z_u & M_w+M_{\dot{w}}Z_w & M_q+M_{\dot{w}}u_1 & 0 \\ 0 & 0 & 1 & 0 \end{bmatrix}$$

and the corresponding states $x = [\Delta u\ \Delta w\ \Delta q\ \Delta\theta]^T$ [[19]:149]. The lateral modes were found with the following dimensional coefficient matrix:

$$A=\begin{bmatrix} \frac{Y_\beta}{u_1} & \frac{Y_p}{u_1} & -\left(1-\frac{Y_r}{u_1}\right) & \frac{g\cos\theta_0}{u_1} \\ L_\beta & L_p & L_r & 0 \\ N_\beta & N_p & N_r & 0 \\ 0 & 1 & 0 & 0 \end{bmatrix} \quad (18)$$

with the following states x = $[\Delta\beta\ \Delta p\ \Delta r\ \Delta\varphi]^T$ [[19]:195].

MATLAB was used to solve for the eigenvalues of the *A* matrices. Each A matrix had four associated eigenvalues. The longitudinal A matrix produced two short period and phugoid eigenvalues. The lateral A matrix produced a roll mode eigenvalue, usually the largest in magnitude, a complex conjugate pair of eigenvalues for Dutch roll and one smaller real eigenvalue for the spiral mode. The real and imaginary parts of the eigenvalues were used to compute the different handling quality criteria for each mode. The natural frequency was $\omega_n=\sqrt{\mathrm{Re}^2+\mathrm{Im}^2}$ and damping ratio was $\zeta=\cos\left(\tan^{-1}\left(\frac{\mathrm{Im}}{\mathrm{Re}}\right)\right)$. The eigenvalue real component was equal to $\zeta\omega_n$. Negative real eigenvalue components indicated a stable mode.

### 5.2.10. Dynamic Stability Criteria

General dynamic stability requirements for lateral and longitudinal modes were referenced in MIL-STD-1797A Appendix A [20]. MIL-STD-1797A was written primarily for manned aircraft so the criteria are inexact. For simplicity, this research focused on stick-fixed stability. Specific parameters used to determine flying quality levels depended on aircraft class and flight phase category.

Aircraft class takes into account aircraft size and weight. A small fighter aircraft has different stability requirements than a large heavy transport. The flight phase category takes into account pilot task requirements during different phases of flight. For example takeoff and cruise flight have different task requirements and impose different types of workloads for the pilot.

VA-1 did not easily fit any of the aircraft categories for determining flying qualities. As a result, the VA-1 was measured against criteria for class II, medium weight aircraft with low to moderate maneuverability. The reconnaissance portion of the mission would fall under flight phase Category A and the cruise flight condition into Category B. In general Category A is more restrictive than Category B and for areas where VA-1 met Category A requirements it also met Category B requirements [20].

The parameters used to judge longitudinal flight quality included short period and phugoid damping ratios and the control anticipation parameter (CAP). Parameters used to measure lateral flight quality varied according to the lateral modes: roll, spiral and Dutch roll. Spiral mode was evaluated against a minimum time to double amplitude. Roll mode was measured against a maximum roll time constant. Dutch roll was evaluated with three different criteria: damping ratio, natural frequency and the product of the two.

The levels used to quantify the flyability of the aircraft correspond to Cooper-Harper handling qualities scale. Level 1 criteria means the flying quality is satisfactory for the mission flight

phase. Level 2 means the flying qualities are acceptable, but either pilot workload is increased or mission performance is degraded with respect to the task, or a combination of the two. Level 3 signifies the need for significant work as it means the pilot workload is considered excessive, mission performance is inadequate or a combination of the two [20]. Any VA-1 configuration meeting level 2 or 3 would need further investigation.

### 5.2.11. Longitudinal Dynamic Stability

The results show VA-1 has good dynamic stability. Longitudinal flight characteristics were measured against short period and phugoid criteria shown in Table (15). All four configurations had virtually the same short and long period characteristics. Table (16) shows longitudinal stability parameters for VA-1 with the LVT attached. Phugoid damping ratio was the primary measure for the phugoid mode. Phugoid damping was right at the minimum, 0.04, for level 1 flight quality [20].

| **Longitudinal Flying Qualities** | | | | | |
|---|---|---|---|---|---|
| | **Short Period** | | | | **Phugoid** |
| | Categories A and C | | Category B | | All Categories |
| **Level** | $\zeta_{sp}$ min | $\zeta_{sp}$ max | $\zeta_{sp}$ min | $\zeta_{sp}$ max | |
| 1 | 0.35 | 1.3 | 0.3 | 2 | $\zeta$>0.04 |
| 2 | 0.25 | 2 | 0.2 | 2 | $\zeta$>0 |
| 3 | 0.15 | (-) | 0.15 | (-) | $T_2$>55 s |

Table (15) Longitudinal Flying Qualities[[19]]

| **Mode** | **Variable of Interest** | **LVT** | **Units** |
|---|---|---|---|
| Short Period | Damping Ratio, $\zeta_{sp}$ | 0.85 | (-) |
| | Natural Frequency, $\omega_n$ | 6.72 | (rad/s) |
| | Control Anticipation Parameter, CAP | 3.78 | $(1/g/s^2)$ |
| Phugoid | Damping Ratio, $\zeta$ | 0.04 | (-) |

Table (16) VA-1 Longitudinal Dynamic Stability of Different Configurations.

VA-1 was stable with respect to the short period mode. Normally the short period mode is examined using the control anticipation parameter, CAP, and short period damping ratio. CAP accounts for how the pilot sitting in the plane senses the aircraft attitude response to a commanded pitch input to change the flight path angle. Typically the pilot senses this feedback through his inner ear and corrects his input accordingly [18]. Since the VA-1 pilot observes the vehicle while standing on the ground, the CAP may not be as important in predicting flying qualities. CAP is commonly used to measure longitudinal stability, however and is included for comparison value. CAP was defined as $\omega_{n_{sp}}^2 \Big/ (n/\alpha)$ for simplicity [20]. The subscripts sp

denoted short period natural frequency and units were $1/g/s^2$, where g was g-force. The denominator $n/\alpha$ was found with $n/\alpha = u_1 C_{L_\alpha} QS/g$ where $u_1$ was the unperturbed freestream velocity in ft/s, $C_{L_\alpha}$ is the aircraft lift curve slope, $Q$ is dynamic pressure in $lb_f/ft^2$, $S$ is total wing area in $ft^2$ and $g$ is the gravitational constant.

The short period damping ratio, 0.85 for all cases, fell well within the specified range for Level 1 handling in Categories A and B. CAP was compared with specific ranges depending on the short period damping. For a short period damping ration of 0.85 CAP should be between 0.085 and 3.6 for Level 1 in Category B or between 0.28 and 3.6 for Level 1 in Categories A and C. CAP and damping ratio only supported Level 2 for categories A and B as CAP was approximately 3.8, too high for Level 1 but well within the upper limit of 10 for Level 2 [18]. Figure (46) and Figure (47) show how CAP and short period damping together make VA-1 level 2 with respect to this requirement. Once again, VA-1 is unmanned which means CAP requirements do not have the same significance as they would for piloted aircraft. Because CAP does not carry as much weight for this aircraft and the other longitudinal stability parameters show level 1 handling qualities, VA-1 is inherently stable with respect to longitudinal stability.

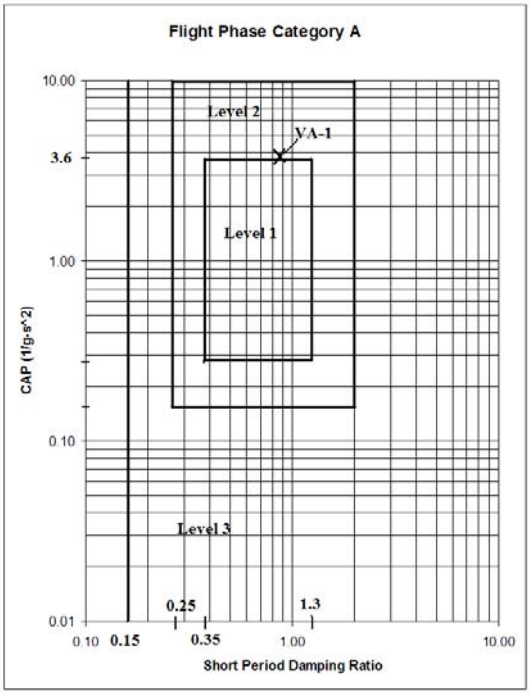


Figure (46) MIL-STD 1797A Criteria for Flight Phase Category A[[20]]

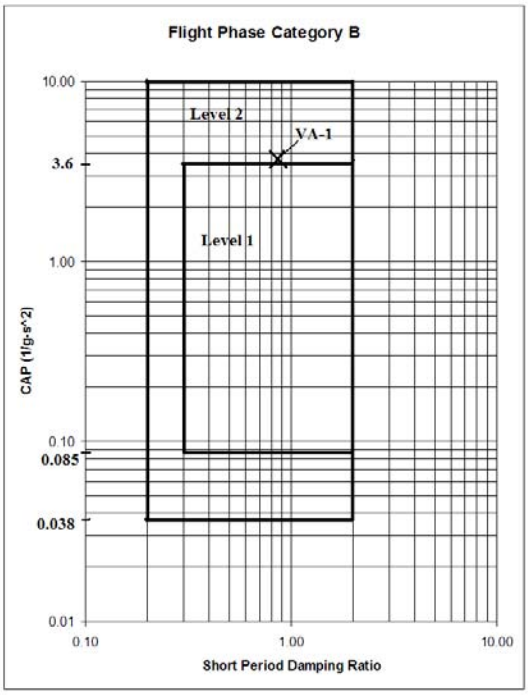


Figure (47) MIL-STD 1797A Criteria for Flight Phase Category B[[20]]

### 5.2.12. Lateral Dynamic Stability

All VA-1 configurations met level 1 handling criteria for every lateral mode. Table (17) lists the lateral stability parameters and their associated mode for each configuration. The results for spiral mode will be discussed first, followed by the roll mode and finally Dutch roll.

The spiral mode results disagreed with Bowman's prediction of an unstable spiral mode for the baseline configuration [21]. The spiral mode was stable for the baseline configuration as its eigenvalue had a negative real part. All other configurations had spiral mode eigenvalues with positive real parts and were unstable in the spiral mode.

Table (17) shows the time to double amplitude denoted with an asterisk for configurations with unstable spiral modes: LVT, strut-fins and LVT+strut-fins. The baseline configuration lists time to half amplitude. Aircraft, however, can be unstable in spiral mode and still meet a level 1 flight quality [19]. Table (18) shows the minimum time to double amplitude for Category A Level 1 flight qualities is 12 seconds. All configurations exceeded this requirement.

| Mode | Variable of Interest | Baseline | LVT | Strut-fins | LVT+ Strut-fins | Units |
|---|---|---|---|---|---|---|
| Spiral | Time to Double* or Half Amplitude ,$T_d$ | 107.63 | 61.30* | 96.77* | 28.69* | (s) |
| Roll | Time constant , $\tau$ | 0.05 | 0.05 | 0.05 | 0.05 | (s) |
| Dutch roll | Damping Ratio, $\zeta$ | 0.22 | 0.24 | 0.23 | 0.25 | (-) |
| | $\zeta\omega_n$ | 0.62 | 0.81 | 0.69 | 0.88 | (rad/s) |
| | Natural Frequency, $\omega_n$ | 2.85 | 3.34 | 2.94 | 3.45 | (rad/s) |

Table (17) VA-1 Lateral Dynamic Stability for Different Configurations

| Category | Minimum Time to Double Amplitude (s) | | |
|---|---|---|---|
| | Level 1 | Level 2 | Level 3 |
| A and C | 12 | 8 | 4 |
| B | 20 | 8 | 4 |

Table (18) MIL-STD 1797A Recommended Spiral Mode Stability [32]

| Roll Mode | | | | |
|---|---|---|---|---|
| Category | Class | Maximum Roll Time Constant (s) | | |
| | | Level 1 | Level 2 | Level 3 |
| A | I,IV | 1 | 1.4 | 10 |
| | II,III | 1.4 | 3 | 10 |
| B | All | 1.4 | 3 | 10 |
| C | I,II-C,IV | 1 | 1.4 | 10 |
| | II-L,III | 1.4 | 3 | 10 |

Table (19) MIL-STD 1797A Recommended Roll Mode Stability [32]

| Dutch Roll Mode | | | | | |
|---|---|---|---|---|---|
| Level | Category | Class | **Min $\zeta$** (-) | **Min $\zeta\omega_n$** (rad/s) | **min $\omega_n$** (rad/s) |
| 1 | A (CO, GA, RR, TF, RC, FF, AS) | I, II, III, IV | 0.4 | 0.4 | 1 |
| | A | I, IV | 0.19 | 0.35 | 1 |
| | | II, III | 0.19 | 0.35 | 0.4 |
| | B | All | 0.08 | 0.15 | 0.4 |
| | C | I, II-C, IV | 0.08 | 0.15 | 1 |
| | | II-L, III | 0.08 | 0.1 | 0.4 |
| 2 | All | All | 0.02 | 0.05 | 0.4 |
| 3 | All | All | 0 | (-) | 0.4 |

Table (20) MIL-STD 1797A Recommended Dutch Roll Stability [32]

The roll mode time constants for all configurations were well below the maximum roll time constant, 1 second, for Level 1, Category A handling [19].

The Dutch roll mode also turned out to be stable in cruise, Category B, for all configurations. Table (20) shows the requirements for Dutch roll. Note there are two rows for Category A. The abbreviation RC stands for reconnaissance so the top was applied. To meet Level 1 Category A for criteria in the Dutch Roll mode, the minimum damping allowed was 0.4. The best VA-1 Dutch roll damping is 0.25 for the LVT+strut-fins configuration. So for reconnaissance this particular plane is Level 2. For cruise, Category B, however, all configurations easily exceeded the Level 1 requirement.

An important conclusion to be drawn from these results is that VA-1 does not need the LVT or strut-fins for stable flight as the baseline configuration meets Level 1 handling qualities for cruise flight in all modes. This means there is opportunity to reduce weight and drag by removing the LVT. This would reintroduce the problem of protecting the propeller during rotation on takeoff and landing. It is recommended the aft wheel configuration be restored as shown in Figure (14).

Thus, the VA-1 would takeoff without rotating the plane. The angle of attack could be adjusted with the adjustable front wheel strut. VA-1 could then accelerate to the trim speed corresponding to the angle of attack and simply rise off the ground. Rotation would be more difficult to control during landing.

### 5.2.13. Preliminary Stall Analysis

#### 5.2.13.1. Evaluation Method

On its last flight VA-1 landed hard while recovering from what appeared to be a stall developed in a right hand turn. Before continuing flight tests it is important to know which bank angles are

likely to cause a stall and where the stall first occurs. In reality the turn was not likely a true steady state turn, but a steady state level turn will be used to simplify the analysis.
Turn trim conditions, such as control surface deflection and angular rates for roll, pitch and yaw were determined with methods discussed in the trim chapter and put into the HASC input deck. HASC VORLAX output files were used to compute section lift coefficients for the front and rear wings to illustrate a spanwise lift distribution. Sections of the wing that exceeded the two-dimensional maximum lift coefficient of 1.2 were considered stalled. Three dimensional sections would stall before this point so these computations are only an approximation of the stall. The goal was to find the approximate bank angle where a significant section of the wing might stall and the location of initial stall along the wing.

### 5.2.13.2. Section Lift Coefficient

To simplify the spanwise lift distribution results the term section is introduced. HASC uses surfaces, panels and subpanels for bookkeeping. The term section is intended to be a spanwise strip of the forward or rear wing. Some sections were composed of only one panel, while sections with control surfaces were made up of two panels. The joint was considered its own section. Figure 1 shows the location of each wing section along the right wing. The left wing was divided into similar sections, only in reverse order from root to tip.

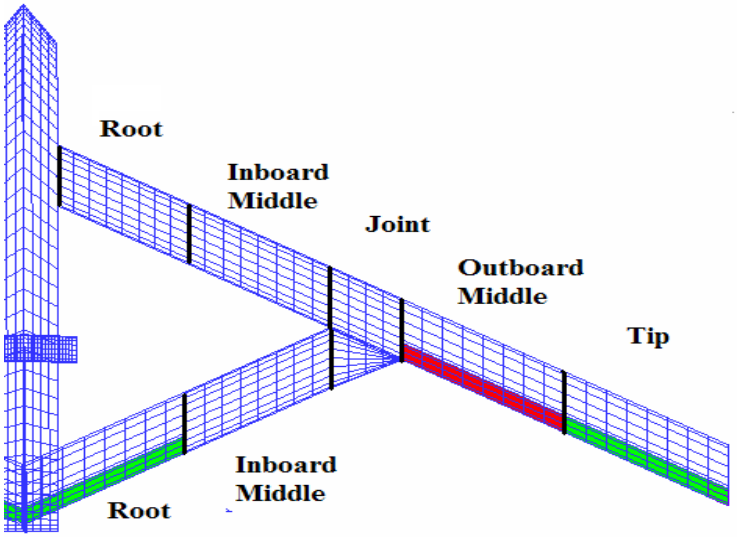


Figure (48) Figure 1. VA-1 Spanwise Wing Sections

The section lift coefficient was computed for two cases. In the first case the panel area and section area were the same. This method was used for the front wing root and inboard middle sections, as well as the aft wing inboard middle section. The second case required finding the section lift coefficient for sections composed of two panels. The front wing tip and outboard middle sections along with the rear wing root fell into this category. The equation for the case where the panel area equals the section area is discussed first.

The VORLAX output from HASC tabulated the local lift coefficient for each panel, non-dimensionalized using total wing area. Each panel lift coefficient could then summed together to find the total lift coefficient for the complete aircraft. The equation for panel lift coefficient would be $C_{L_i} = L_i / QS$ where $L_i$ is the panel lift in $lb_f$, $Q$ is the dynamic pressure in $lb_f/ft^2$ and $S$ is the total wing reference area in $ft^2$. The subscript $i$ represents the panel number.

For this analysis local lift coefficient with respect to the section area is desired. The general equation for section lift coefficient is then $C_{L_{section}} = L_{section} / QS_{section}$ where $L_{section}$ is the lift and $S_{section}$ is the area for the respective wing section. For wing sections composed of one panel, $L_i = L_{section}$ and $S_i = S_{section}$. To convert the panel lift coefficient to section lift coefficient, the panel lift coefficient was divided by the panel surface area, $S_i$, and multiplied by total area, $S$:

$$C_{L_{section}} = C_{L_i} \frac{S}{S_i} \tag{19}$$

Where $S/S_i = S/S_{section}$.

The calculation differed for sections composed of two panels. For example, the wing tip section is composed of two panels: a trailing edge device and an adjacent upstream panel. For illustration purposes, let's assign trailing edge device and the adjacent upstream panels to i = 1 and 2 respectively. First add the lift coefficients, non-dimensionalized with total wing area, together to get $C_{L_1} + C_{L_2} = (L_1 + L_2)/(QS)$. Then multiply both sides by $S/(S_1+S_2)$ to end up with the equation used to find the section lift coefficient for sections with two panels:

$$C_{L_{section}} = \frac{\left(C_{L_1} + C_{L_2}\right) S}{\left(S_1 + S_2\right)} \tag{20}$$

which is equivalent to $(L_1+L_2)/(Q(S_1+S_2))$ or $L_{section}/QS_{section}$. With equations for sections with one and two panels respectively, a spanwise lift coefficient distribution was created.

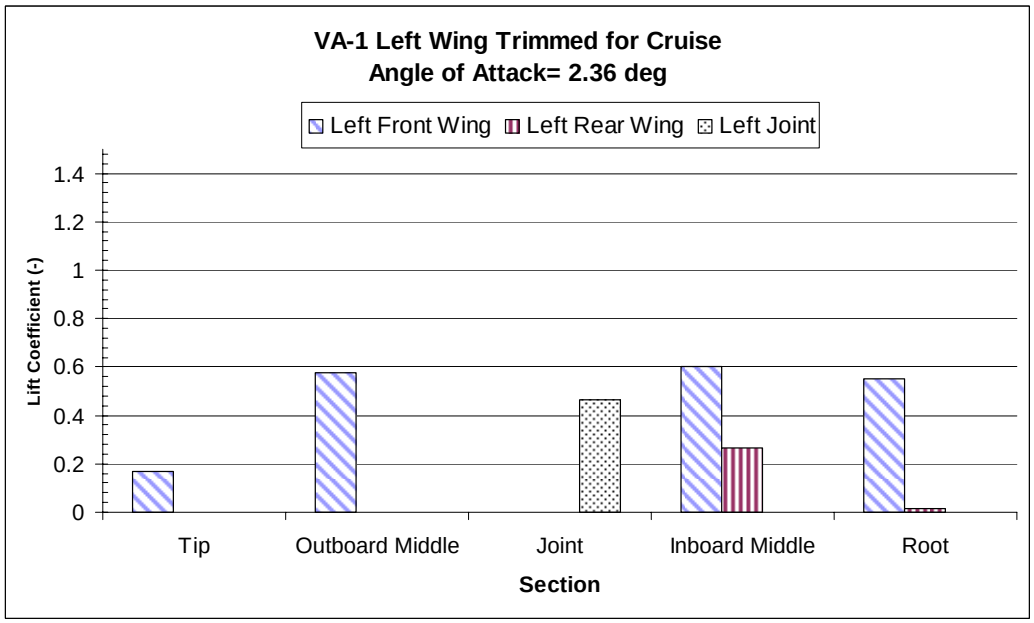


Figure (49) VA-1 Left Wing Lift Coefficient Distribution for Straight and Level Flight.

Figure (49) shows the lift coefficients for each spanwise section when VA-1 is trimmed for straight and level flight. In straight and level flight the right wing lift coefficient distribution mirrors the left. Figure (50) and Figure (51) show the section lift coefficients for the left and right wings respectively when VA-1 is trimmed for level right hand turn with 50 degrees of bank. The outboard middle section on the left front wing approaches stall first. Figure (52) and Figure (53) show the outboard middle section exceeds the airfoil's maximum lift coefficient and potentially stalls at 55 degrees of bank.

The results make sense as the ailerons were located at the outboard middle wing sections. In a right had turn the left aileron is deflected trailing edge down to increase the local lift coefficient and effect the turn. The aileron on the right wing is deflected trailing edge up so that the aileron section inside the turn reduces the local lift. Thus it makes sense that the right wing does not approach stall before the left wing in a trimmed right hand level turn. The relatively lower lift coefficients for the front wing tips and rear wing roots were partly due to the fact that these sections included elevator control sections. During the bank all elevator control surfaces were moved trailing edge up, reducing the local lift for each rear wing root and front wing tip section.

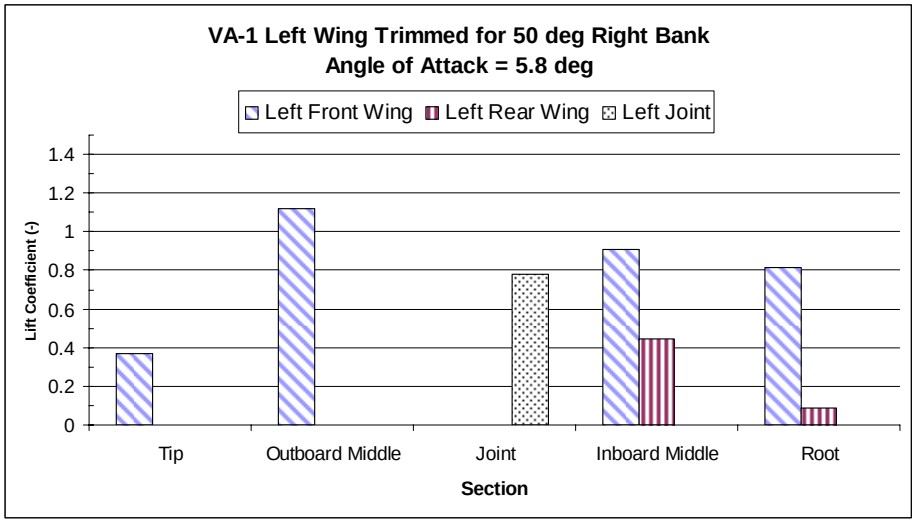


Figure (50) VA-1 Left Wing with 50 Degree Bank Angle

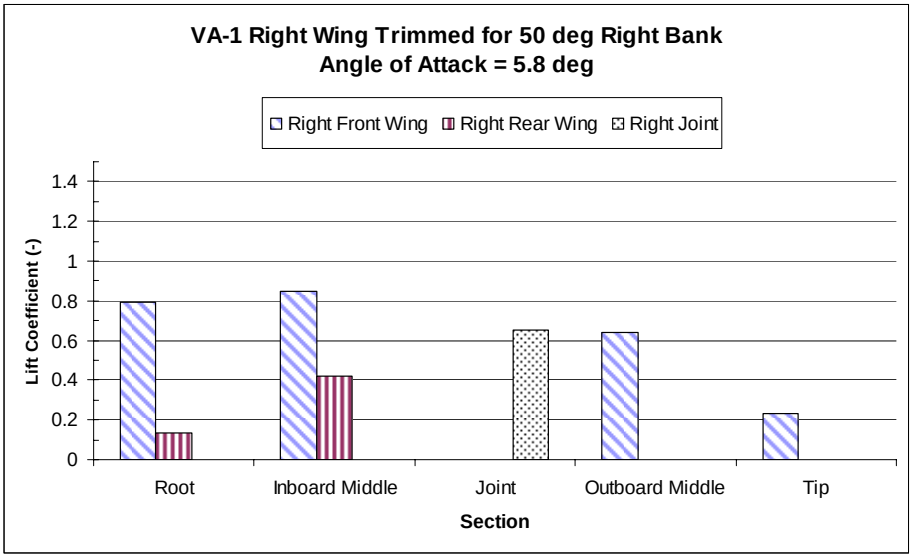


Figure (51) VA-1 Right Wing with 50 Degree Bank Angle

These results do not agree the flight test video which showed the inboard wing buffet, suggesting the wing inside the turn stalled first. The difference was possibly due to a combined turn and descending effect. On a descending right turn aircraft rolls into the turn, or right wing down. This roll rate causes a local increase in the effective angle of attack on the inside wing, which could contribute to an inside wing stall [22]. To explore this effect the HASC input deck trimmed for a steady level 50 degree right hand turn was given a 20 deg/s right roll rate to see the effective change in angle of attack on the wings in the descending turn. This was not enough to get the inside wing sections to stall, but several right wing panels increased in lift coefficient by approximately 0.1 suggesting an increase in local angle of attack.

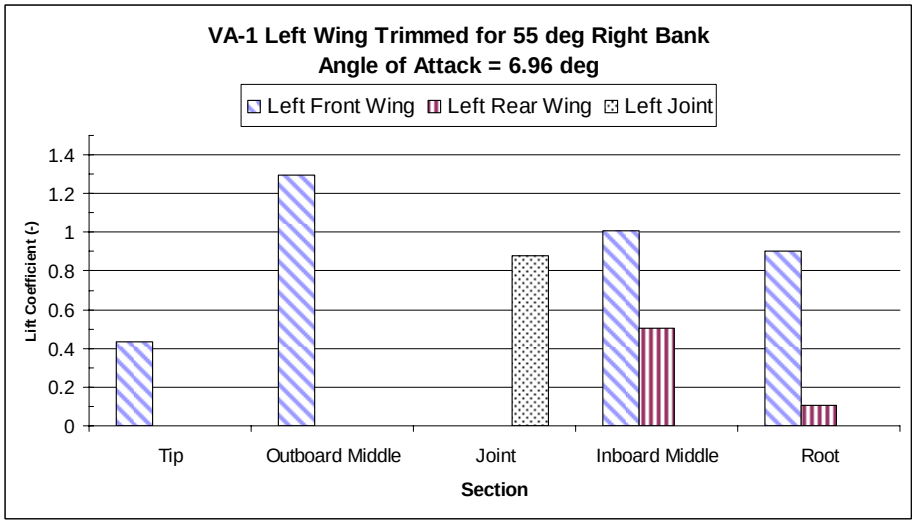


Figure (52) VA-1 Left Wing with 55 Degree Bank Angle

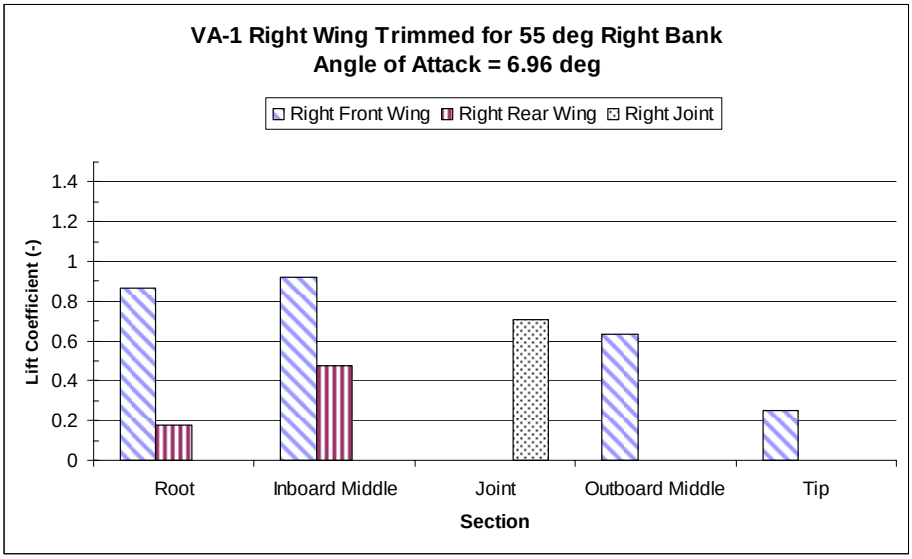


Figure (53) VA-1 Right Wing with 55 Degree Bank Angle

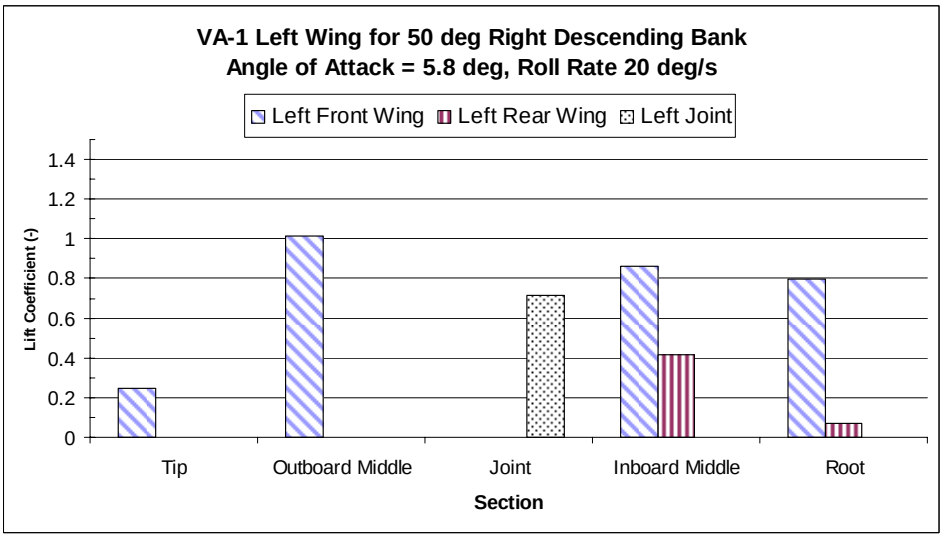


Figure (54) VA-1 Left Wing with 50 Degree Bank Angle and 20 deg/s Roll Rate

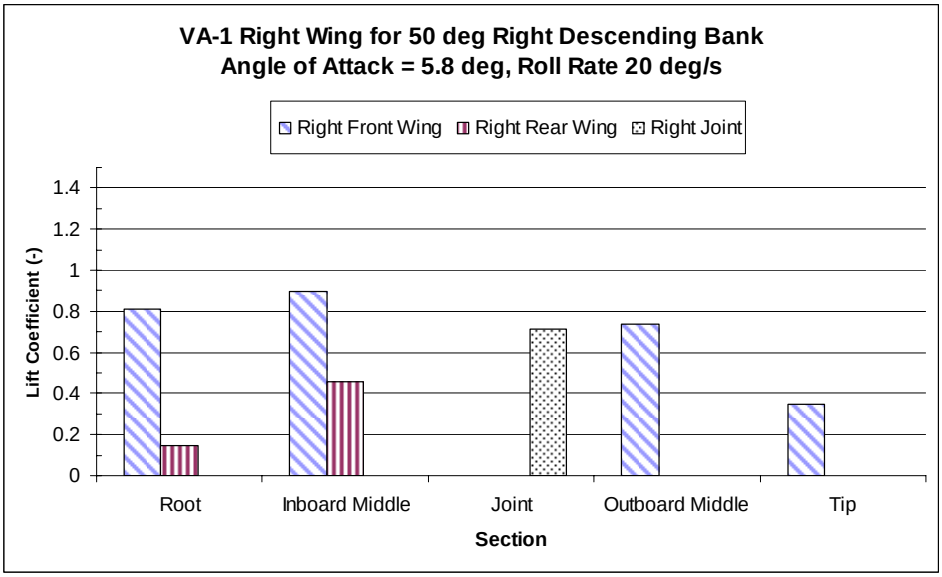


Figure (55) VA-1 Right Wing with 50 Degree Bank Angle and 20 deg/s Roll Rate

For trimmed level turning flight, the stall occurs between 50 and 55 degrees of bank. In this case, stall appears to begin at the outboard middle section of the wing outside the turn. In general when the wing outside the turn stalls first, recovery is relatively easy as the aircraft would simply roll itself out of the turn. Since the pilot does not have a real time bank angle indicator from which to read bank angle a good rule of thumb for future flight tests might be to avoid banking more than 45 degrees when possible. The 45 degree bank angle limitation also provides some margin for error as distance and viewing angle would make judging 45 degrees of bank difficult.

Wing tip stall is typically avoided to preserve aileron effectiveness, which aids stall recovery by preventing loss of aircraft control. In the turning maneuver, stall first occurs inboard of the tip. Unfortunately this is still where the aileron is located. Some standard procedures to prevent stall over the ailerons would be geometrically twisting the wing section or adding a leading edge slot or slat to increase the stall angle of attack for the aileron portion of the wing [17].

For descending turns the inside wing can stall first, especially if the airspeed is low in the turn. Recovering from the condition where the wing inside the turn stalls is much more difficult because the turn quickly becomes steeper due to loss of lift on the inside wing, and the airplane may enter a spiral dive [22]. This complicates recovery as the aircraft loses altitude quickly and may have lost control surface effectiveness needed to recover. Clearly the inside wing in the turn stalling is the more severe condition. More research should be done with regard to how to predict stall in descending turns.

Refer to Jason Bowman's report, completed prior to flight and before McClelland's thesis, not published, presented here as Appendix C.

## 5.3. Propeller Analysis

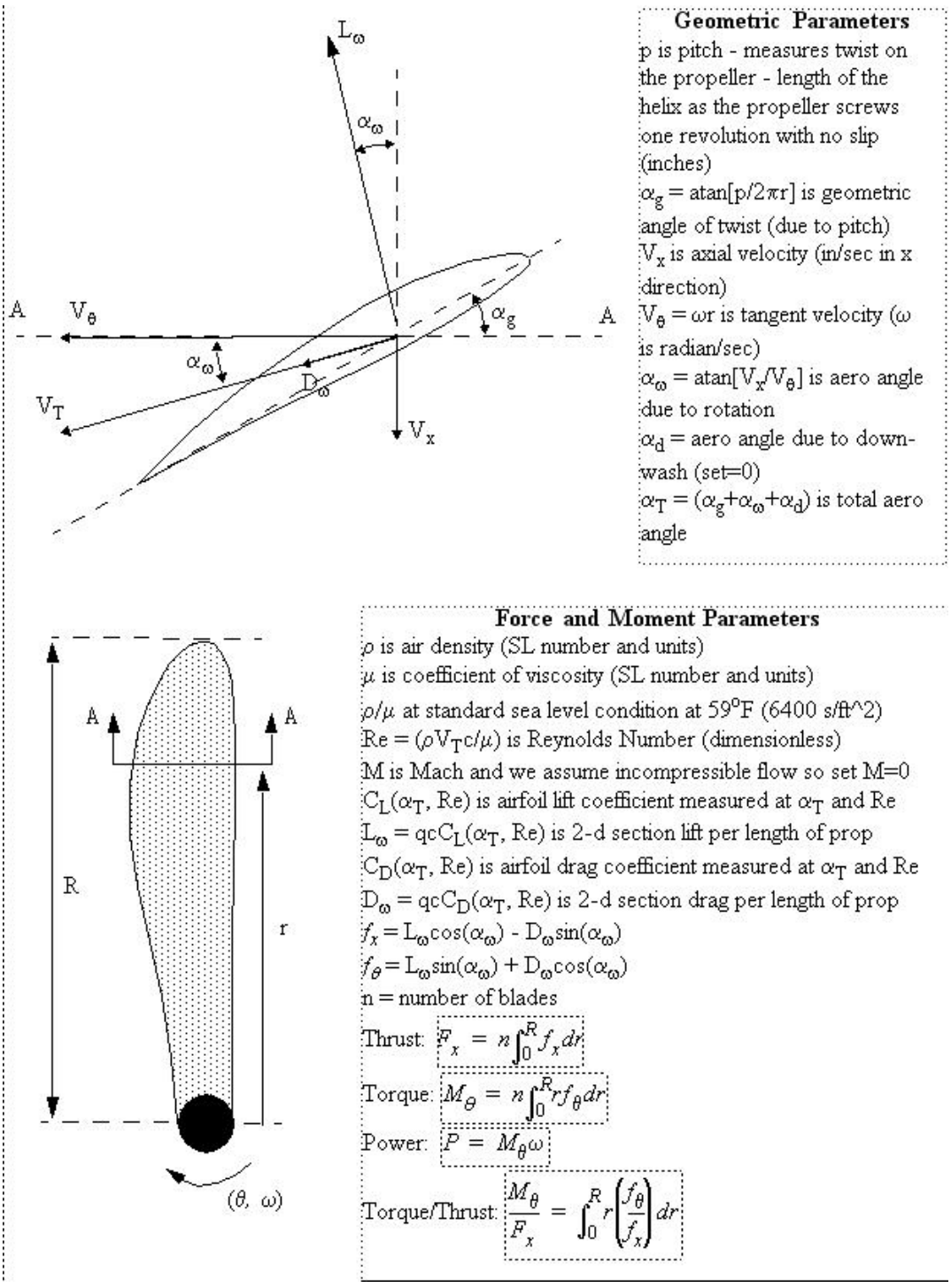


Figure (56) Propeller Analysis - I

**Small Angle Assumptions**

Let $H = L_\omega/D_\omega$ represent the lift over drag ratio and set all angles to be a small value

$$\frac{f_\theta}{f_x} \approx \frac{H\alpha_\omega + 1}{H - \alpha_\omega} \approx \frac{H(V_x/V_\theta) + 1}{H - (V_x/V_\theta)} = \frac{HV_x + \omega r}{\omega r H - V_x} \tag{1}$$

Substitute this into the expression for the torque/thrust:

$$\frac{M_\theta}{F_x} = \int_0^R r\left(\frac{f_\theta}{f_x}\right)dr = \int_0^R \left(\frac{HV_x r + \omega r^2}{\omega Hr - V_x}\right)dr = \int_0^R \left(\frac{HV_x r}{\omega Hr - V_x}\right)dr + \int_0^R \left(\frac{\omega r^2}{\omega Hr - V_x}\right)dr \tag{2}$$

From CRC #30

$$\int\left(\frac{r}{a+br}\right)dr = \left[\frac{r}{b} - \frac{a}{b^2}\log(a+br)\right] \tag{3}$$

From CRC #33

$$\int\left(\frac{r^2}{a+br}\right)dr = \frac{1}{b^3}\left[\frac{(a+br)^2}{2} - 2a(a+br) + a^2\log(a+br)\right] \tag{4}$$

Let $\bar{V} = (V_x - H\omega R)$ and $\bar{\omega} = H\omega R$. Evaluating the first element of Equation (2):

$$\int_0^R \left(\frac{HV_x r}{\omega Hr - V_x}\right)dr = HV_x\left[\frac{R}{H\omega} - \frac{V_x}{(H\omega)^2}[\log\bar{V} - \log\bar{\omega}]\right] \tag{5}$$

Evaluate the second element of Equation (2)

$$\int_0^R \left(\frac{\omega r^2}{\omega Hr - V_x}\right)dr = \frac{-\omega}{(H\omega)^3}\left[\frac{\bar{V}}{2} - 2\bar{V}V_x + \left[\frac{3}{2} + \log\bar{V} - \log V_x\right]V_x^2\right] \tag{6}$$

Use equations (5) and (6) to evaluate the torque to thrust ratio in equation (2) for a given $V_x$ and $\omega$ and pitch. Also, set L/D to be some average constant for all chord sections (this approximation may be good enough for our level of analyis here).

**Special Cases:**

Let R = 15 in, p = 28 in, $\alpha_g = 16^o$, $\omega$ = 2870 RPM = 300 r/s, $V_x$ = 25 MPH = 440 in/s

With calculations for r = 15 in, $\alpha_\omega = -5.58^o$ and $\alpha_T = 10.4^o$. This is close to stall condition (check Re at this local propeller speed). If we go slower (make $V_x$ less), then $\alpha_T$ increases and the propeller will certainly stall.

Let R = 14 in, p = 18 in, $\alpha_g = 11.56^o$, $\omega$ = 2390 RPM = 250 r/s, $V_x$ = 25 MPH = 440 in/s

With calculations for r = 14 in, $\alpha_\omega = -7.16^o$ and $\alpha_T = 4.40^o$. This is far from the stall condition.

(1) $\alpha_T$ for airfoil section stall

(2) $\alpha_T$ for airfoil section zero lift (no thrust)

(look at how angle decreases with increasing speed and how stall happens at low speed)

Figure (57) Propeller Analysis - II

# 6. GROUND TESTING

## 6.1. Radio Control Range Test

### 6.1.1. Test Objective:

It is crucial that the Joined Wing vehicle maintains controllability. The radio transmission is a critical link in vehicle control. Objective of this test is to demonstrate radio transmission range to assure control of the airplane over the entire test area. Sufficient range and interference-free communication between the radio transmitter and receiver are demonstrated with various vehicle orientations and incidences.

### 6.1.2. Approach:

The range test will be conducted by two individuals. One person will remain stationary with the Joined Wing Demonstrator while the other person, holding the controller, walks away from the plane to a distance of approximately 4000 feet. The person standing with the plane will use a two-way radio to communicate with the controller, confirming all inputs given to the plane. This will also allow us to guarantee the two-way radios cause no interference with the radio control system. The airplane attendants will reorient the vehicle several times and retest the radio reception.

This test will be conducted in concert with the Vehicle Flight Worthiness Test as the vehicle is driven down a runway where later flight-testing will take place. The test must take into consideration that the structural reinforcement bars imbedded in the runway (Ree-Bar) will carry the signal. Therefore, the test must be conducted with the transmitter and vehicle off to the side of the runway.

**Success Criteria**: Radio range established for 4000 ft.

## 6.2. Propulsion Testing

The MaxCim MegaMax brushless DC motor is a recent development. Test data is not available. Neither is test data available for RC propellers that are compatible with the MegaMax motor. The data that is available does not directly tell us how much thrust to expect and the power duration is also unknown. The motor and propeller were tested by AFRL/VAA in the vertical wind tunnel facility at WPAFB Area B.

Data obtained from these tests determined which prop to use and motor speed setting for optimizing flight times. Nine different props were wind tunnel tested using the MegaMax motor. Prop diameters ranged from 28” to 20” inches, and prop pitch ranged from 28 to 10. The props and motor were mounted in the center of the tunnel on a load cell which measured the thrust at various rpm and tunnel speed up to 45 mph.

### 6.2.1. Test objectives:

- Determine which propeller to use for flight-testing
- Identify optimal RPM for any vehicle speed in the range 0 to 45 mph.

### 6.2.2. Data Measured:

Amperage, velocity, thrust, duration

### 6.2.3. Approach:

Use Vertical Wind Tunnel to test each propeller from x rpm to x rpm with wind velocity between 0 to 45 mph.

### 6.2.4. Success Criteria/Results:

Of all the propellers tested, the 28-18 propeller provided the best overall thrust. The 28-18 propeller will be installed on the vehicle for flight-testing. Static thrust (wind off) was measured at 11.5 lbs. Thrust at 45 mph was measured at 4.5 lbs.

Data was also obtained from these tests to help determine how much flight time each battery pack could provide. Battery power at full throttle with 45 mph velocity lasted 4.5 minutes. The flight time at reduced power may be as long as 10 minutes final report is expected from AFRL/VAA.

All ground testing will be completed before taxi and flight testing. The ground test description is included in the test plan in order to build confidence in the integrity of the proposed flight test program. The SRB is not responsible for the safety and execution of these relatively simple and safe ground tests.

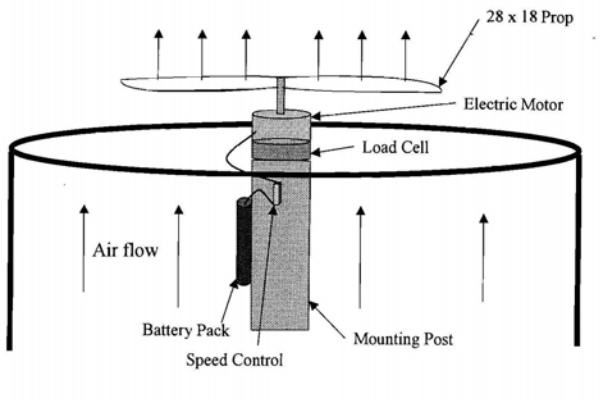


Figure (58) Propeller Test Set-Up

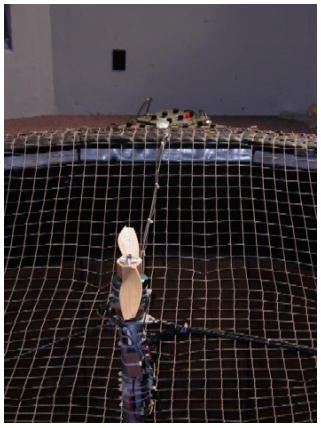

Figure (59) Propeller Calibration Test in Vertical Wind Tunnel Facility

| Date | Run | Test Point # | Prop size | Tunnel Velocity mph | Prop rpm | Batteries | Misc. Info. | Data Processed |
|---|---|---|---|---|---|---|---|---|
| 15-Apr-03 | 1 | 1-36 | 28-18 | 0, 20, 28, 35, 40, 45 | 0-2500 | 3 each lead acid | | X |
| 15-Apr-03 | 2 | 37-72 | 27-20 | 0, 20, 28, 35, 40, 45 | 0-2500 | 3 each lead acid | | |
| 16-Apr-03 | 3 | 73-108 | 27-18 | 0, 20, 28, 35, 40, 45 | 0-2500 | 3 each lead acid | | |
| 16-Apr-03 | 4 | 109-144 | 26-10 | 0, 20, 28, 35, 40, 45 | 0-2500 | 3 each lead acid | | |
| 16-Apr-03 | 5 | 145-180 | 25-10 | 0, 20, 28, 35, 40, 45 | 0-2500 | 3 each lead acid | | |
| 16-Apr-03 | 6 | 181-216 | 24-10 | 0, 20, 28, 35, 40, 45 | 0-2500 | 3 each lead acid | | |
| 16-Apr-03 | 7 | 217-252 | 22-10 | 0, 20, 28, 35, 40, 45 | 0-2500 | 3 each lead acid | | |
| 17-Apr-03 | 8 | | 28-18 | 45 | 2500 | 36 each Ni-MH (pack B) | Speed Control Tripped off | |
| 17-Apr-03 | 9 | | 28-18 | 45 | 2500 | 36 each Ni-MH (pack B) | Speed Control Not reset | |
| 17-Apr-03 | 10 | | 28-18 | 45 | 2500 | 36 each Ni-MH (pack B) | Speed Control Tripped off | |
| 17-Apr-03 | 11 | | 28-18 | 45 | 2500 | 36 each Ni-MH (pack B) | Endurance Runs | |
| 17-Apr-03 | 12 | | 28-18 | 45 | 2500 | 36 each Ni-MH (pack A) | Endurance Runs | |
| 18-Apr-03 | 13 | 287-322 | 28-28 | 0, 20, 28, 35, 40, 45 | 0-2500 | 3 each lead acid | | |
| 18-Apr-03 | 14 | 323-358 | 20-10 | 0, 20, 28, 35, 40, 45 | 0-2500 | 3 each lead acid | | |
| 18-Apr-03 | 15 | | 28-18 | 45 | 2500 | 36 each Ni-MH (pack B) | Endurance Runs | X |
| 18-Apr-03 | 16 | | 28-18 | 28 | 2034 | 36 each Ni-MH (pack A) | Endurance Runs | |
| 18-Apr-03 | 17 | | 28-28 | 45 | 2500 | 36 each Ni-MH (pack B) | Endurance Runs | |

Table (21) Joined-Wing Propeller Test Cases in Vertical Wind Tunnel 15-18 April 2003

| Date | Time | Filename | Test Point # | Prop size | Type of Battery | Tunnel Velocity mph | Pulse width millsec | Pulse Freq | RPM | Thrust lb | Battery Voltage | Battery Current | Delta Thrust | Total Thrust |
|---|---|---|---|---|---|---|---|---|---|---|---|---|---|---|
| 4/15/2003 | 12:47p | 2003-04-15-1247-16.scl | 1 | 28-18 | Lead Acid | 0.00 | 1.0 | 0.0 | 0 | 5.60 | 37.00 | 0.99 | | 0 |
| 4/15/2003 | 12:48p | 2003-04-15-1248-10.scl | 2 | 28-18 | Lead Acid | 0.00 | 1.2 | 33.8 | 1014 | 7.61 | 36.76 | 2.61 | 2.02 | 2.02 |
| 4/15/2003 | 12:49p | 2003-04-15-1249-05.scl | 3 | 28-18 | Lead Acid | 0.00 | 1.3 | 45.9 | 1377 | 9.41 | 36.22 | 4.89 | 1.80 | 3.81 |
| 4/15/2003 | 12:49p | 2003-04-15-1249-45.scl | 4 | 28-18 | Lead Acid | 0.00 | 1.4 | 57.7 | 1731 | 11.59 | 35.72 | 8.58 | 2.18 | 5.99 |
| 4/15/2003 | 12:50p | 2003-04-15-1250-22.scl | 5 | 28-18 | Lead Acid | 0.00 | 1.5 | 66.0 | 1980 | 13.58 | 35.34 | 12.96 | 1.99 | 7.98 |
| 4/15/2003 | 12:51p | 2003-04-15-1250-59.scl | 6 | 28-18 | Lead Acid | 0.00 | 1.6 | 79.4 | 2382 | 17.12 | 34.32 | 22.15 | 3.54 | 11.52 |
| 4/15/2003 | 01:01p | 2003-04-15-1301-52.scl | 7 | 28-18 | Lead Acid | 20.40 | 1.0 | 0.0 | 0 | 5.68 | 36.94 | 0.91 | | 0.08 |
| 4/15/2003 | 01:02p | 2003-04-15-1302-34.scl | 8 | 28-18 | Lead Acid | 20.40 | 1.2 | 35.9 | 1077 | 6.38 | 36.83 | 1.93 | 0.70 | 0.79 |
| 4/15/2003 | 01:03p | 2003-04-15-1303-16.scl | 9 | 28-18 | Lead Acid | 20.40 | 1.3 | 47.5 | 1425 | 7.87 | 36.34 | 4.62 | 1.49 | 2.28 |
| 4/15/2003 | 01:04p | 2003-04-15-1304-05.scl | 10 | 28-18 | Lead Acid | 20.40 | 1.4 | 57.4 | 1722 | 9.59 | 35.75 | 8.52 | 1.72 | 4.00 |
| 4/15/2003 | 01:04p | 2003-04-15-1304-36.scl | 11 | 28-18 | Lead Acid | 20.40 | 1.5 | 65.3 | 1959 | 11.32 | 35.29 | 13.11 | 1.73 | 5.72 |
| 4/15/2003 | 01:05p | 2003-04-15-1305-08.scl | 12 | 28-18 | Lead Acid | 20.40 | 1.6 | 77.8 | 2334 | 14.49 | 34.22 | 23.05 | 3.17 | 8.90 |
| 4/15/2003 | 01:07p | 2003-04-15-1307-24.scl | 13 | 28-18 | Lead Acid | 28.92 | 1.0 | 0.0 | 0 | 5.10 | 36.81 | 0.92 | | (0.50) |
| 4/15/2003 | 01:08p | 2003-04-15-1307-56.scl | 14 | 28-18 | Lead Acid | 28.92 | 1.2 | 41.5 | 1245 | 5.56 | 36.78 | 1.62 | 0.47 | (0.03) |
| 4/15/2003 | 01:08p | 2003-04-15-1308-28.scl | 15 | 28-18 | Lead Acid | 28.92 | 1.3 | 49.5 | 1485 | 6.62 | 36.57 | 3.54 | 1.06 | 1.03 |
| 4/15/2003 | 01:09p | 2003-04-15-1309-02.scl | 16 | 28-18 | Lead Acid | 28.92 | 1.4 | 59.8 | 1794 | 8.35 | 35.79 | 7.68 | 1.72 | 2.75 |
| 4/15/2003 | 01:09p | 2003-04-15-1309-35.scl | 17 | 28-18 | Lead Acid | 28.92 | 1.5 | 67.8 | 2034 | 10.07 | 35.24 | 12.60 | 1.73 | 4.48 |
| 4/15/2003 | 01:10p | 2003-04-15-1310-08.scl | 18 | 28-18 | Lead Acid | 28.92 | 1.6 | 79.0 | 2370 | 12.89 | 34.32 | 21.97 | 2.81 | 7.29 |
| 4/15/2003 | 01:11p | 2003-04-15-1311-11.scl | 19 | 28-18 | Lead Acid | 35.43 | 1.0 | 0.0 | 0 | 4.74 | 36.66 | 0.91 | | (0.85) |
| 4/15/2003 | 01:11p | 2003-04-15-1311-51.scl | 20 | 28-18 | Lead Acid | 35.43 | 1.2 | 48.0 | 1440 | 4.90 | 36.74 | 1.25 | 0.16 | (0.70) |
| 4/15/2003 | 01:12p | 2003-04-15-1312-20.scl | 21 | 28-18 | Lead Acid | 35.43 | 1.3 | 53.3 | 1599 | 5.65 | 36.63 | 2.60 | 0.75 | 0.05 |
| 4/15/2003 | 01:12p | 2003-04-15-1312-50.scl | 22 | 28-18 | Lead Acid | 35.43 | 1.4 | 61.9 | 1857 | 7.11 | 36.24 | 6.12 | 1.46 | 1.51 |
| 4/15/2003 | 01:13p | 2003-04-15-1313-30.scl | 23 | 28-18 | Lead Acid | 35.43 | 1.5 | 69.9 | 2097 | 8.70 | 35.20 | 10.93 | 1.59 | 3.10 |
| 4/15/2003 | 01:14p | 2003-04-15-1314-01.scl | 24 | 28-18 | Lead Acid | 35.43 | 1.6 | 81.0 | 2430 | 11.48 | 34.46 | 20.41 | 2.78 | 5.88 |
| 4/15/2003 | 01:14p | 2003-04-15-1314-52.scl | 25 | 28-18 | Lead Acid | 40.92 | 1.0 | 0.0 | 0 | 4.40 | 36.66 | 0.92 | | (1.19) |
| 4/15/2003 | 01:15p | 2003-04-15-1315-29.scl | 26 | 28-18 | Lead Acid | 40.92 | 1.2 | 49.2 | 1476 | 3.94 | 36.85 | 0.11 | (0.47) | (1.66) |
| 4/15/2003 | 01:16p | 2003-04-15-1316-07.scl | 27 | 28-18 | Lead Acid | 40.92 | 1.3 | 57.8 | 1734 | 5.17 | 36.70 | 1.96 | 1.24 | (0.42) |
| 4/15/2003 | 01:16p | 2003-04-15-1316-41.scl | 28 | 28-18 | Lead Acid | 40.92 | 1.4 | 65.4 | 1962 | 6.49 | 36.36 | 5.08 | 1.32 | 0.90 |
| 4/15/2003 | 01:17p | 2003-04-15-1317-18.scl | 29 | 28-18 | Lead Acid | 40.92 | 1.5 | 72.0 | 2160 | 7.82 | 35.48 | 9.05 | 1.33 | 2.22 |
| 4/15/2003 | 01:17p | 2003-04-15-1317-54.scl | 30 | 28-18 | Lead Acid | 40.92 | 1.6 | 83.5 | 2505 | 10.53 | 34.61 | 18.72 | 2.71 | 4.94 |
| 4/15/2003 | 01:18p | 2003-04-15-1318-48.scl | 31 | 28-18 | Lead Acid | 45.76 | 1.0 | 0.0 | 0 | 4.28 | 36.63 | 0.92 | | (1.31) |
| 4/15/2003 | 01:19p | 2003-04-15-1319-38.scl | 32 | 28-18 | Lead Acid | 45.76 | 1.2 | 51.1 | 1533 | 3.44 | 36.90 | 0.49 | (0.84) | (2.15) |
| 4/15/2003 | 01:20p | 2003-04-15-1320-17.scl | 33 | 28-18 | Lead Acid | 45.76 | 1.3 | 61.4 | 1842 | 4.80 | 35.75 | 1.50 | 1.36 | (0.79) |
| 4/15/2003 | 01:20p | 2003-04-15-1320-53.scl | 34 | 28-18 | Lead Acid | 45.76 | 1.4 | 67.6 | 2028 | 5.96 | 36.19 | 4.03 | 1.15 | 0.36 |
| 4/15/2003 | 01:21p | 2003-04-15-1321-27.scl | 35 | 28-18 | Lead Acid | 45.76 | 1.5 | 75.3 | 2259 | 7.55 | 35.54 | 8.70 | 1.59 | 1.95 |
| 4/15/2003 | 01:22p | 2003-04-15-1322-02.scl | 36 | 28-18 | Lead Acid | 45.76 | 1.6 | 85.3 | 2559 | 9.94 | 34.72 | 17.45 | 2.39 | 4.34 |

Table (22) Joined-Wing Propeller Test Results in Vertical Wind Tunnel 15-18 April 2003

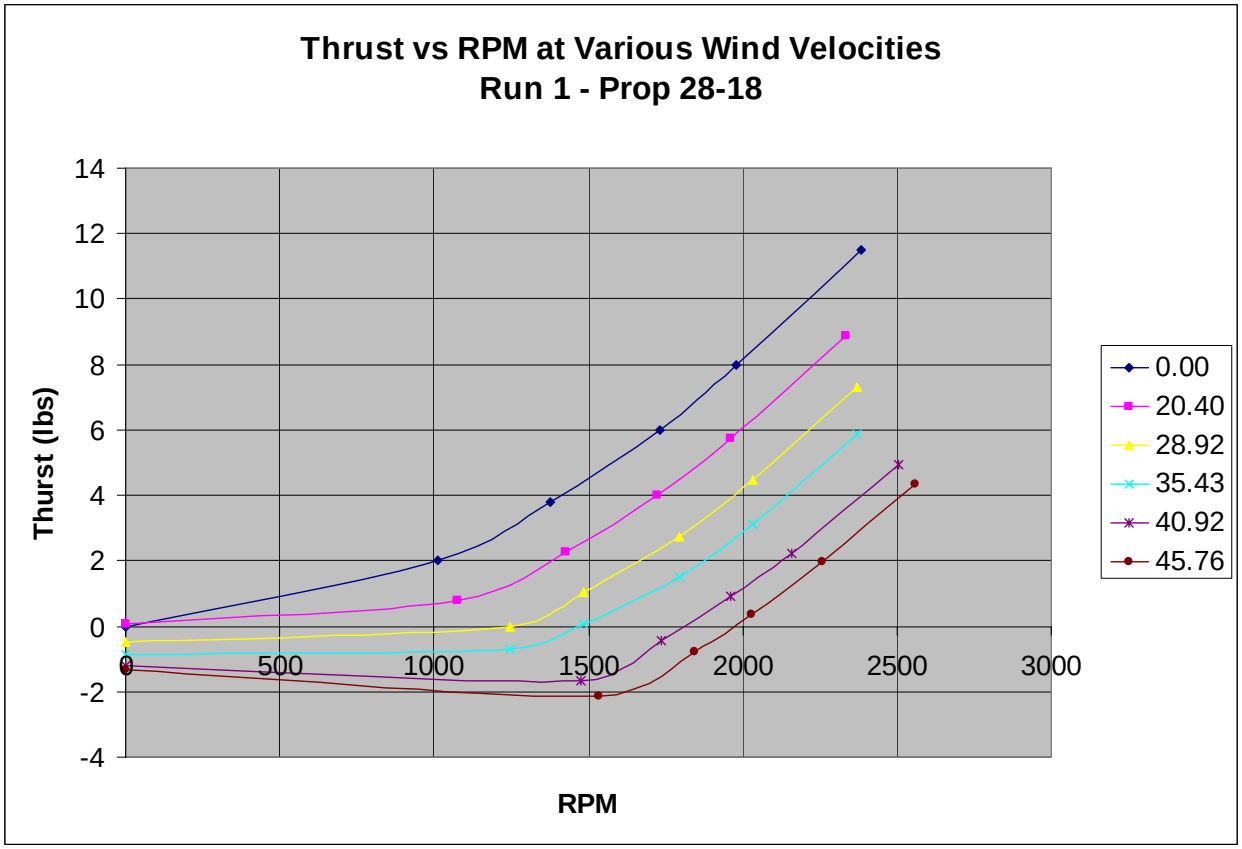


Figure (60) Thrust vs RPM at Variois Wind Velocities Run 1 – Prop 28-18

| Date | Time | Filename | Test Point # | Prop size | Type of Battery | Tunnel Velocity mph | Pulse width millsec | Pulse Freq | RPM | Delta Time (Minutes) | Thrust lb | Delta Thrust (lbs) | Battery Voltage | Battery Current (Amps) | Delta Thrust | Total Thrust |
|---|---|---|---|---|---|---|---|---|---|---|---|---|---|---|---|---|
| 4/18/2003 | 11:35a | 2003-04-18-1135-18.scl | | 28-18 | 36 - NiMH | 0 | | | | **0** | 6.59 | - | 48.33 | 0.95 | | |
| 4/18/2003 | 11:36a | 2003-04-18-1135-55.scl | | 28-18 | 36 - NiMH | | | | | **0.62** | | | | | | |
| 4/18/2003 | 11:36a | 2003-04-18-1136-13.scl | | 28-18 | 36 - NiMH | | | | | **0.92** | 17.49 | 10.91 | 36.48 | 22.65 | | |
| 4/18/2003 | 11:36a | 2003-04-18-1136-29.scl | | 28-18 | 36 - NiMH | 45.76 | | | | **1.18** | | | | | | |
| 4/18/2003 | 11:37a | 2003-04-18-1136-46.scl | | 28-18 | 36 - NiMH | 45.76 | | | | **1.47** | 13.58 | 7.00 | 37.10 | 22.02 | | |
| 4/18/2003 | 11:37a | 2003-04-18-1137-03.scl | | 28-18 | 36 - NiMH | 45.76 | | | | **1.75** | 11.71 | 5.12 | 38.06 | 20.06 | | |
| 4/18/2003 | 11:38a | 2003-04-18-1138-01.scl | | 28-18 | 36 - NiMH | 45.76 | | | | **2.72** | | | | | | |
| 4/18/2003 | 11:38a | 2003-04-18-1138-29.scl | | 28-18 | 36 - NiMH | 45.76 | | | | **3.18** | 10.70 | 4.11 | 38.69 | 19.68 | | |
| 4/18/2003 | 11:39a | 2003-04-18-1138-59.scl | | 28-18 | 36 - NiMH | 45.76 | | | | **3.68** | 10.56 | 3.97 | 38.63 | 19.68 | | |
| 4/18/2003 | 11:39a | 2003-04-18-1139-19.scl | | 28-18 | 36 - NiMH | 45.76 | | | | **4.02** | | | | | | |
| 4/18/2003 | 11:39a | 2003-04-18-1139-34.scl | | 28-18 | 36 - NiMH | 45.76 | | | | **4.27** | | | | | | |
| 4/18/2003 | 11:39a | 2003-04-18-1139-50.scl | | 28-18 | 36 - NiMH | 45.76 | | | | **4.53** | | | | | | |
| 4/18/2003 | 11:40a | 2003-04-18-1140-04.scl | | 28-18 | 36 - NiMH | 45.76 | | | | **4.77** | 10.23 | 3.65 | 38.37 | 19.47 | | |
| 4/18/2003 | 11:40a | 2003-04-18-1140-34.scl | | 28-18 | 36 - NiMH | 45.76 | | | | **5.27** | | | | | | |
| 4/18/2003 | 11:40a | 2003-04-18-1140-55.scl | | 28-18 | 36 - NiMH | 45.76 | | | | **5.62** | 10.01 | 3.42 | 38.02 | 19.19 | | |
| 4/18/2003 | 11:41a | 2003-04-18-1141-34.scl | | 28-18 | 36 - NiMH | 45.76 | | | | **6.27** | | | | | | |
| 4/18/2003 | 11:42a | 2003-04-18-1142-04.scl | | 28-18 | 36 - NiMH | 45.76 | | | | **6.77** | 9.59 | 3.01 | 37.21 | 18.44 | | |
| 4/18/2003 | 11:42a | 2003-04-18-1142-38.scl | | 28-18 | 36 - NiMH | 45.76 | | | | **7.33** | | | | | | |
| 4/18/2003 | 11:43a | 2003-04-18-1143-05.scl | | 28-18 | 36 - NiMH | 45.76 | | | | **7.78** | 8.88 | 2.29 | 35.31 | 16.63 | | |
| 4/18/2003 | 11:43a | 2003-04-18-1143-20.scl | | 28-18 | 36 - NiMH | 45.76 | | | | **8.03** | | | | | | |
| 4/18/2003 | 11:43a | 2003-04-18-1143-35.scl | | 28-18 | 36 - NiMH | 45.76 | | | | **8.28** | | | | | | |
| 4/18/2003 | 11:44a | 2003-04-18-1144-02.scl | | 28-18 | 36 - NiMH | 45.76 | | | | **8.73** | 7.48 | 0.89 | 31.02 | 12.53 | | |
| 4/18/2003 | 11:44a | 2003-04-18-1144-19.scl | | 28-18 | 36 - NiMH | 45.76 | | | | **9.02** | 6.75 | 0.16 | 28.67 | 10.22 | | |
| 4/18/2003 | 11:44a | 2003-04-18-1144-41.scl | | 28-18 | 36 - NiMH | 45.76 | | | | **9.38** | | | | | | |
| 4/18/2003 | 11:45a | 2003-04-18-1145-00.scl | | 28-18 | 36 - NiMH | 45.76 | | | | **9.70** | | | | | | |
| 4/18/2003 | 11:45a | 2003-04-18-1145-19.scl | | 28-18 | 36 - NiMH | 45.76 | | | | **10.02** | | | | | | |
| 4/18/2003 | 11:46a | 2003-04-18-1146-08.scl | | 28-18 | 36 - NiMH | 45.76 | | | | **10.83** | | | | | | |
| 4/18/2003 | 11:46a | 2003-04-18-1146-12.scl | | 28-18 | 36 - NiMH | | | | | **10.90** | | | | | | |

Table (23) Propeller Test Results – Duration

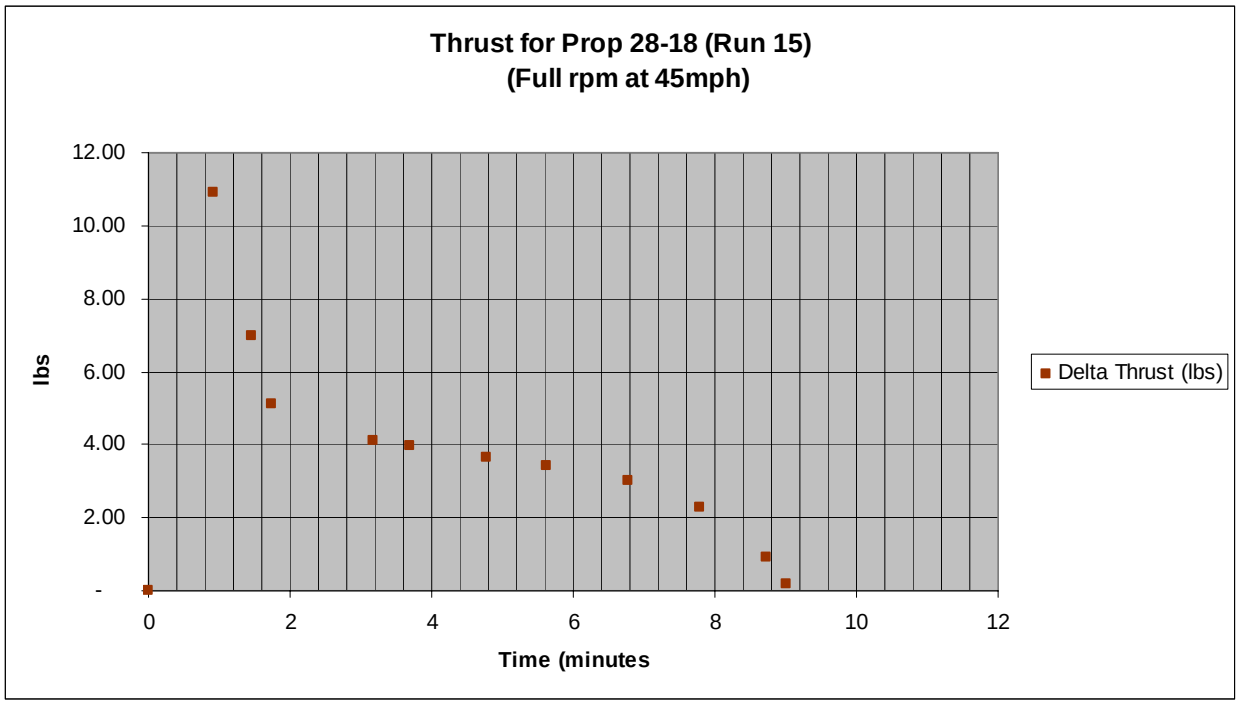


Figure (61) Thrust for Propeller 28-18 – Run 15

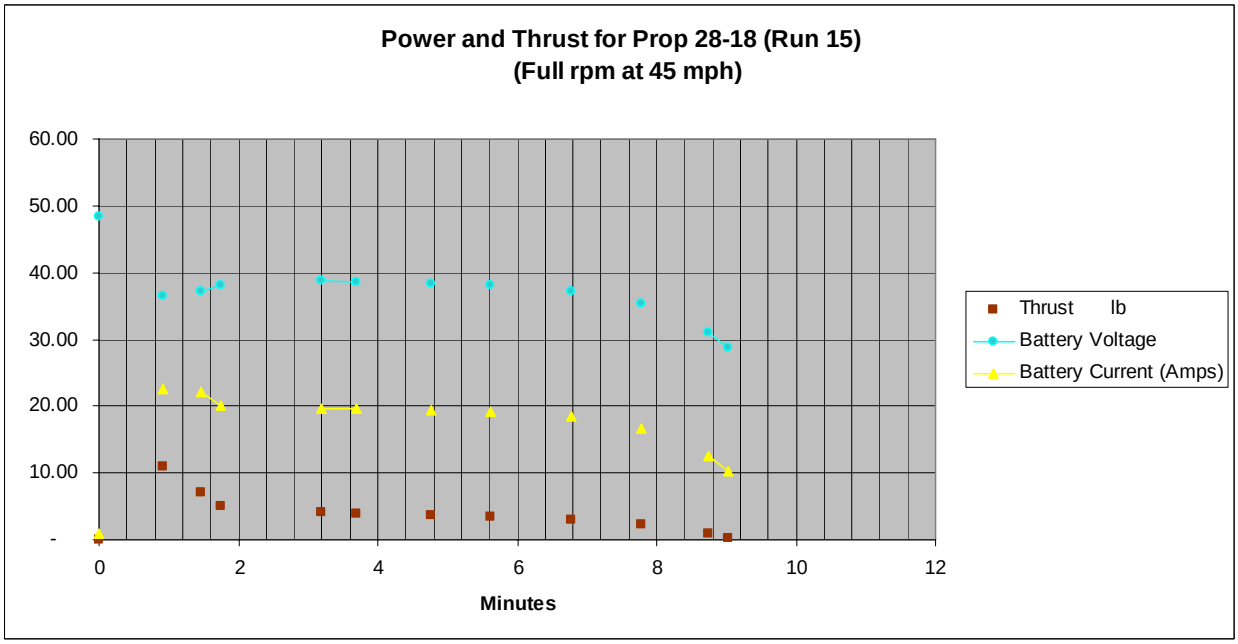


Figure (62) Power and Thrust for Propeller 28-18 – Run 15

Project: AFRL/VA Joined-Wing Scaled Prototype Design

Goal: Match motor/propeller parameters - with expected airplane flight parameters

Set cruise speed at 25 mph (set takeoff speed at 10 mph).

Estimate the vehicle weight (W)

Trim the vehicle in lift and pitch (no thrust)

Calculate the drag at trim setting

Equate drag to thrust required

Select a propeller - be sure propeller is not stalled at takeoff and flies efficiently at cruise with sufficient excess thrust available for acceleration.

For this thrust, cruise velocity and propeller ask prop manufacturer for bench tested torque data.

For this torque, identify the voltage and current setting on motor.

Question: is this voltage between 50% and 80% - to assure excess power available.

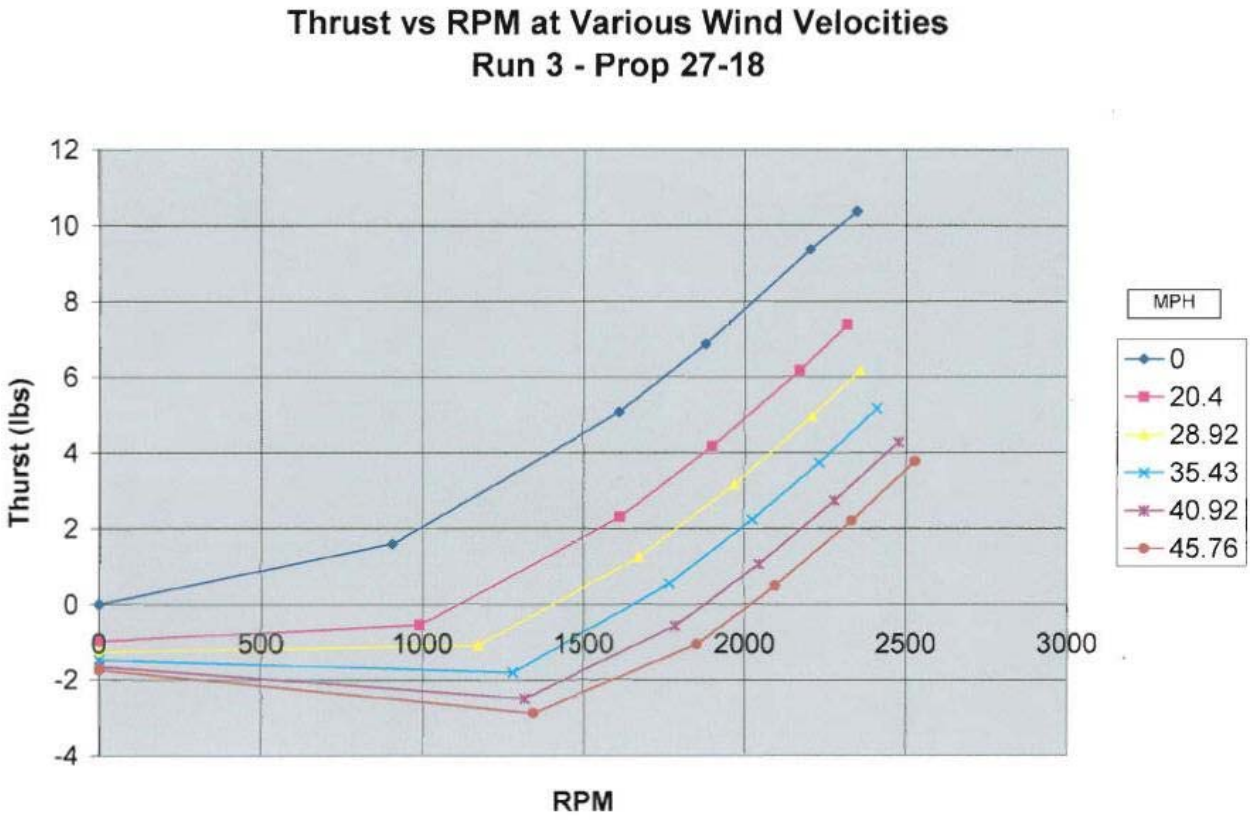


Figure (63) Thrust vs RPM at Various Wind Velocities Run 3 – Prop 27-18

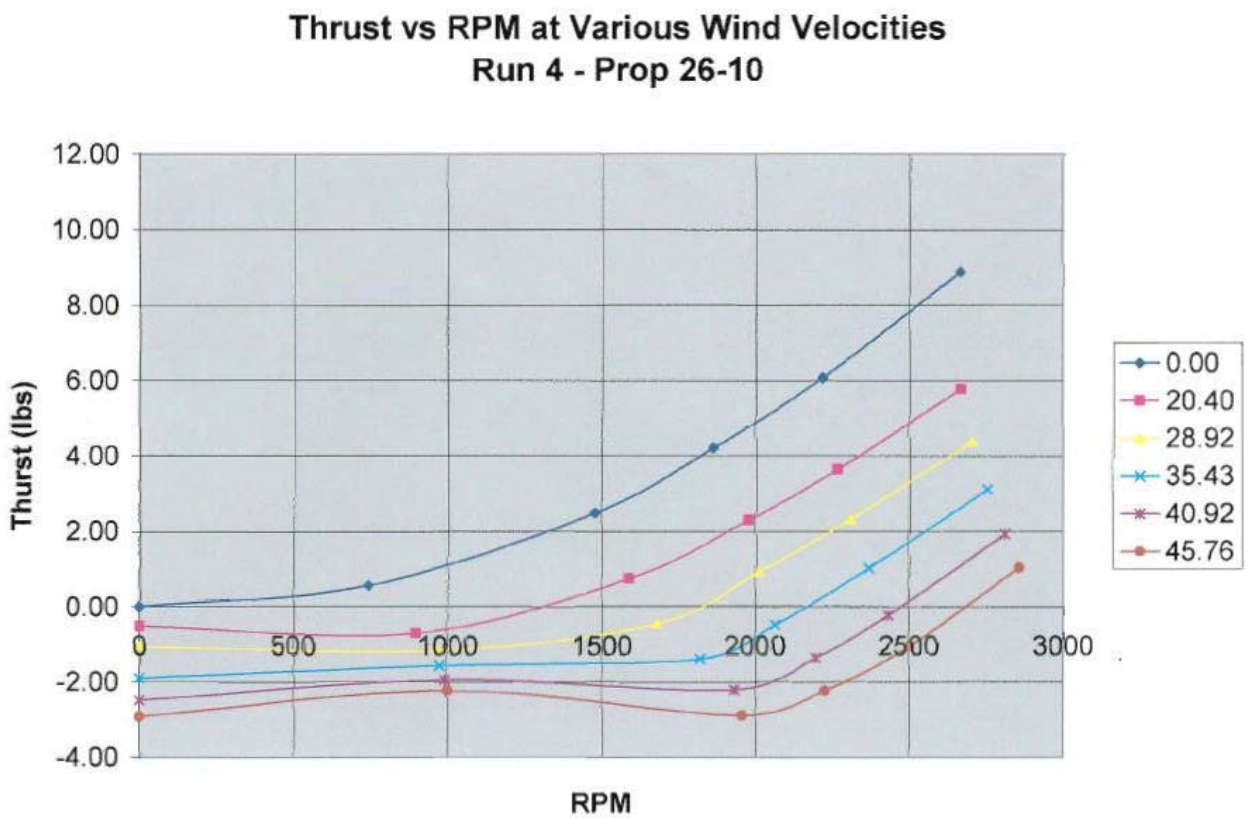


Figure (64) Thrust vs RPM at Various Wind Velocities Run 4 – Prop 26-10

## 6.3. Structural Testing

As indicated, there was immediate concern at the time of model delivery. The wing structure was excessively flexible. The immediate thought was the possibility of aeroelastic flutter. Since the wings were considered to be defective, there was little concern for their loss. A flutter test was developed as described below. Management approval for the test was not granted, possibly out of a concern for safety. Probably, that was a good thing, but for a different reason.

We engaged in a static load test which, taken to failure, provided experimental validation for redesigning the wing. Only the wing carry-through structure was lost. Thus, the wing structure could be easily modified. The modification was possible because of the low cost foam, wood and fiberglass technology.

The second static load test followed an extensive structural redesign effort that involved extensive analysis (described in Section 5.1 on Structural Analysis). This test passed. All tests are described here.

A drop test was devised in order to safely establish the ability to take a hard landing. This drop test is described here. In the end, the test team voted unanimously that this test would not reduce the flight test risk and it was not conducted. The risk was not reduced because the landing criteria could not be established for lack of precedent. This is discussed below.

### 6.3.1. Flutter Test

A flight test was out-of-the-question with the model that was delivered. The wings were excessively flexible. It was clear that the airplane was not safe to fly. We considered expedient and safe approaches to clear the model for flight worthiness. There was little concern if the wing structure was lost.

Thus, a flutter clearance test was devised. A wooden frame was constructed in the bed of a truck. This is shown in Figure (65). The model was secured to the top of the frame. It was clear that the wings could break away from the fuselage. A test plan was devised to avoid the possibility of personal injury.

Figure (65) Joined-Wing Model Mounted on Truck Bed for a Captive Flutter Test

An aeroelastic (flutter) analysis was never planned. High stiffness was a design requirement for this model in order to avoid the possibility of flutter. When the model was delivered, the wing structure was surprisingly and excessively flexible. Clearly, we did not have an airplane that was stiff. It failed the high stiffness requirement. A redesign effort was necessary to create a stiff wing. However, it was not easy to make the case without hard evidence in the form of analysis or failed test. The analysis would require extensive load-deflection test to generate the stiffness data required for a flutter analysis. The time required to generate an analysis was excessive, considering that the analysis data would simply prove the model was not flight worthy and would have to be redesigned. Therefore, we chose to fail the wing in a captive flutter test. The point of the test was mostly to prove the lack of aeroelastic flight worthiness without harm to the test team.

The captive flutter test did not go forth. This section is simply reported for future reference.

### 6.3.2. Wing Maneuver Load Test

#### 6.3.2.1. Wing Maneuver Load Criteria for the Static Structural Test

With a minimum of 200 ft turning radius allowed in this test plan, we are required to simulate maneuvers for (L/W = n = 1.3) with safety margin of 1.5. Therefore, this test will simulate 2.0g pull-up. With a vehicle weight of 26 lbs (including the wings), our conservative approach is to evenly apply a total of 52 lbs over the full span, front and back.

| Turning radius = 500 ft | | | Turning radius = 400 ft | | | Turning radius = 200 ft | | |
|---|---|---|---|---|---|---|---|---|
| V(mph) | θ (deg) | n | V(mph) | θ (deg) | n | V(mph) | θ (deg) | n |
| 50 | 18.47 | 1.054 | 50 | 22.64 | 1.080 | **50** | **39.84** | **1.300** |
| 40 | 12.07 | 1.023 | 40 | 14.97 | 1.037 | 40 | 28.13 | 1.130 |
| 30 | 6.86 | 1.007 | 30 | 8.55 | 1.013 | 30 | 16.74 | 1.050 |
| 25 | 4.77 | 1.003 | 25 | 5.97 | 1.008 | 25 | 11.81 | 1.024 |

Table (24) Vehicle Load Factor Variability With Respect to Velocity and Turning Radius

#### 6.3.2.2. Approach

The wing-maneuver load test will be conducted in a frame with the vehicle suspended by the wheel struts. Aerodynamic load will be simulated with the weight of sandbags. Load will be applied in an incremental approach maintaining a nearly constant distribution over the wings. Four discrete load increments will be tested - [13, 26, 39 and 52] lbs.

If, during the process, we determine the wing cannot withstand more load, the decision will be to terminate the test and restrict the vehicle velocity according to the above table B.2.1.1.

#### 6.3.2.3. Data Collection

The wing tip deflection will be measured at each load increment. (This provides another reason to fix all free-play and glue the wings to the fuselage and tail.)

A photographic record will be maintained of all testing.

#### 6.3.2.4. Risk and Success Criteria

No instrumentation will be employed. Therefore, we will not know how much strain has been induced at any point. Go/No-Go decisions will be based on experience, visual inspection and audibles. In the event a failure is seen or heard, testing will be terminated, repairs will be made and testing will be repeated. The test is a success if the wings withstand an equivalent 2-g maneuver load.

#### 6.3.2.5. Equipment List

- Custom frame to suspend the vehicle upside-down. (Need graphic)
- 60 Calibrated Sandbags @ 1 lbs.
- Ruler (measure deflection for the record)
- Digital Camera (take pictures for the record)

#### 6.3.2.6. Results of First Static Structural Test

Although the original wing was fabricated with modular parts, the resulting free-play was noteworthy. Free-play included a bending and twisting motion. Not only was there a concern for dynamic uncertainty, structural failure was a possibility. The connecting screws were not well centered and delamination of the unidirectional tow was a concern. Consequently, we made a

decision to glue all modular parts for maximum stiffness and structural integrity. We could not take a chance on structural failure where the model was designed to explore rigid vehicle flight.

The first loading at which measurements were recorded is 20 pounds, 10 pounds on each the right and left wing. This resulted in a wing tip displacement of 8 inches at either tip. The second set of measurements was taken at a loading of 40 pounds. This resulted in a tip displacement of 21 inches on both sides.

Upon nearing the target test weight, considerable creaking sounds pointed to possible failure. The test was aborted at 46 pounds when the deflection was far too great and signs of structural failure were evident. The weights were removed and the wings were inspected.

As shown in the following pictures in Figure 8, the displacement of the tip was far from linear with respect to the wing loading.

| Increment | Applied Load (lbs) | Tip Displacement Left (in) | Tip Displacement Right (in) |
|---|---|---|---|
| 0 | 0 | 0.00 | 0.00 |
| 1 | 20 | 8.00 | 8.00 |
| 2 | 40 | 21.00 | 21.00 |
| 3 | 46 | NM | NM |

Table (25) Static Load Test Displacement Results

Load Increment 0 | Load Increment 1 | Load Increment 2

Figure (66) Successive Loadings of VA-1 Static Load Test

Through inspection, it was found that parts of the wing construction had become delaminated and structural integrity of the joint between the wing and fuselage had been severely compromised.

Prior to testing, the lap joints connecting the wing to the fuselage carry-through spar had been reinforced with epoxy adhesive. During the test, much of the epoxy connecting the spars was damaged and cracked. Also, the bulkhead in which the carry-through spar was mounted was delaminated. As discussed before, the bulkhead was constructed of three layers. The outer two layers were no longer glued to the inner layer in the area surrounding the carry-through spar, and the carry-through spar was free to twist within the bulkhead. This freedom led to the excessive deflection of the wing upon substantial loading.

It was determined that the wing, upon loading - with its attachment to the fuselage via a single carry-through spar, attempted to twist at the wing root until the carry through spar acted as a prying member. The spar was able to pry apart the three sections of the plywood bulkhead as well as the glue that reinforced the lap joints within the wing.

After becoming free to twist within the bulkhead, the wing was more free to flatten out into a plane (consisting of three points: the fore root, the aft root, and the wing merge), causing the moment of inertia of the wing sections with respect to that plane, as a bending plane, to be reduced. This effectively erased the truss-like characteristics of the joined-wing design and allowed the wing to transition into a simple cantilever, slightly skewed from simple vertical deflection.

The static load test revealed obvious failure in the structural design of the VA-1. This failure is focused in the region of the fore wing root. The original design shows a need for structural improvement in the connection of the fuselage and the fore wing sections. As the bulkhead within the fuselage was delaminated, along with the spar lap joints, it would be impractical to clear the vehicle for further testing. These two malfunctions severely inhibit the ability of the wings to support the loads needed for even the simplest of flight maneuvers.

#### 6.3.2.7. Results of Second Static Structural Test

Following structural modification, the wing was again tested for 2-g maneuver load. The sequence of events is depicted in Figure (67).

Figure (67) Second Static Structural Test

The test was a success. At the time of this report, measured wingtip deformation data was misplaced. However, clearly the wing resisted the load with 42 bags @ 1 pound. The deformation was scaled from the photo. Wingtip deformation was approximately 5 inches. The airplane was considered structurally sound.

Figure (68) Top View of Simulated Load with 1 Pound Sand Bags

Figure (69) Team for the Successful Strucural ReTest, Elizabeth Mikolaj, Amar Bhungalia, Max Blair, John McNees, Mike Ooten

### 6.3.3. Vehicle Drop Test

Anyone familiar with the design of inexpensive model airplanes knows to design to withstand hard landings. This means the airplane is either not severely damaged or can be readily repaired. The drop test was designed as a sanity check from a structures perspective to make sure the plane's nose gear, propeller, and flexible wings can withstand a hard landing without major damage. As a result, overall structural integrity would be assessed and the possibility of a propeller strike (on landing) would be explored. Again, the drop test was developed, but not carried out.

The vehicle is designed with aluminum struts in the rear, protecting the propeller. The Joined-Wing vehicle, with its pusher prop design, uses these struts to protect the propeller from ground strike on takeoff and landing. These struts are designed to splay and deform on a hard landing,

thus providing for shock absorption. This introduces the potential for prop-strike on a hard landing, something that must be explored.

The vehicle is designed with a single steerable strut in the front fashioned from a round rod. The rod is free to plunge with elastic recoil provided by a stiff spring. This provides shock-absorbing ability in the front of the airplane. With the aft wheel struts so far behind the vehicle center of mass, the nose is likely to slap the ground in a free rotation immediately after the rear wheels have touched down.

The objective of the vehicle drop test was to demonstrate landing load durability and strike free landing under specified conditions.

#### 6.3.3.1. Landing Criteria for the Vehicle DropTest

There is very little guidance on requirements development for sink rates applied to RC airplane design. Most RC airplanes lack the instrumentation to record this data and for those that might, it seems unlikely this data is available or even applicable to our joined-wing vehicle. The X-35C design landing sink rate at 18 ft/sec may provide our most extreme precedent, slightly less than a controlled crash.

Ref: [http://www.codeonemagazine.com/archives/2001/articles/arp_01/x35c/ ]

The X-35C is designed to survive carrier landings, which tend to be more severe than typical Air Force landings. In numerical terms, when a pilot flies the X-35C on a carrier landing, the rate at which the aircraft hits the runway, called the sink rate, is approximately eleven feet per second. The aircraft is designed to withstand a sink rate of almost eighteen feet per second. By comparison, the typical sink rate for an X-35A landing, the conventional takeoff and landing variant of the JSF demonstrator, was around two feet per second.

Lacking clear guidance and relevant precedence, the drop test will incorporate some element of exploration which will be used to advise the pilot in planning for the approach to landing.

| Terminal Sink Rate (ft/sec) | Delta Time (sec) | Drop Height (ft) |
|---|---|---|
| 18 | 0.56 | 5.0 |
| 12 | 0.37 | 2.2 |
| 6 | 0.19 | 0.6 |
| 2 | 0.06 | 0.1 |

Table (26) Drop Heights to Meet Sink Rate Criteria

#### 6.3.3.2. Vehicle Drop Test Approach

The drop test was to consist of two incremental tests. First is the nose drop to test the free rotation shock absorption. Second is the whole vehicle drop to test the rear strut shock absorption. In both cases, the wings will also experience a structural dynamic reaction which must be tracked and considered.

#### 6.3.3.2.1. Nose-Drop:

The nose of the plane will be lifted off the ground then released, thus allowing the nose to drop to the ground. The nose will first be lifted up 6 inches, then 12 inches, 18 inches, and 24 inches (max). Stop testing before forward strut spring bottoms out.

#### 6.3.3.2.2. Vehicle-Drop:

The entire vehicle will be raised off the ground and released. The vehicle will be lifted up 6 inches, then 12 inches, 18 inches, and 24 inches, as the test director deems prudent. Stop testing before forward strut spring bottoms out. Caution: fuselage structure not analyzed for this test. Will probably want to stop at 12 inch drop simulating an approximately 9 ft/sec sink rate.

#### 6.3.3.2.3. Risk and Success Criteria

No instrumentation will be employed. Therefore, we will not know how much strain has been induced at any point on the struts or the wings. Go/No-Go decisions will be based on experience, visual inspection and audibles. In the event a failure is seen or heard, testing will be terminated, repairs will be made and testing will be repeated. The test would be successful when the maximum drop height has been reached.

## 6.4. Tests to Measure Vehicle Moments of Inertia [50]

Miller researched a method for experimentally measuring aircraft inertia to within 1% of the actual value [9]. Hardware was built to limit oscillation to two dimensions and improved the accuracy of the measurements. Due to time and budget limitations the exact same hardware was not recreated for the VA-1.

In the report Miller utilized two methods to measure inertia: pendulum method and a bifilar torsion pendulum. In both tests the aircraft was suspended by two cables. The pendulum method swung the aircraft side to side like a pendulum on a clock. The bifilar torsion pendulum measurement involved twisting the vehicle in a circular motion so that the center of mass remained equidistant between the suspension cables at all times. By measuring the axis of rotation relative to the attachment points and timing a predetermined number of oscillations the mass moment of inertia was calculated [9]. The VA-1 inertia measurement was based on this approach with some modifications discussed later.

The purpose of this chapter is to discuss the method used to experimentally determine the inertia of VA-1. Inertia data along with non-dimensional stability derivatives are used to find dimensional stability derivatives used for the stability model. VA-1 inertia about the roll, pitch and yaw axes was measured using a twist test approach based on Miller's NACA TR 531. The fundamental premise of the test involved suspending an object from two points equidistant from the object's center of gravity. After the object was rotated by a small angle about its center of gravity and released the period of oscillation was measured. The period, combined with other geometric dimensions, was then be used to calculate inertia. Miller called this a bifilar torsion pendulum [9].

VA-1's large 14 ft. wingspan required a large open space to twist freely without obstruction or damage to the wings. The test was conducted in a large open room in AFRL's Bldg 65 at WPAFB as a result. A level I-beam, part of a crane, 23 feet off of the ground provided the ceiling attachment points. Nylon chords were tied to eye-bolts that were secured to the I-beam

with I-beam clamps. Four clamps were spaced at specified intervals based on how the aircraft was suspended for each test so that the chord would be perfectly vertical when attached to VA-1. The cord attachment points were 29, 32 and 64.5 in. apart for the roll, yaw and pitch tests respectively. Cords were secured to VA-1 in different locations and manners depending on which test was being performed. Figure (70) shows VA-1 suspended to measure inertia about the roll axis.

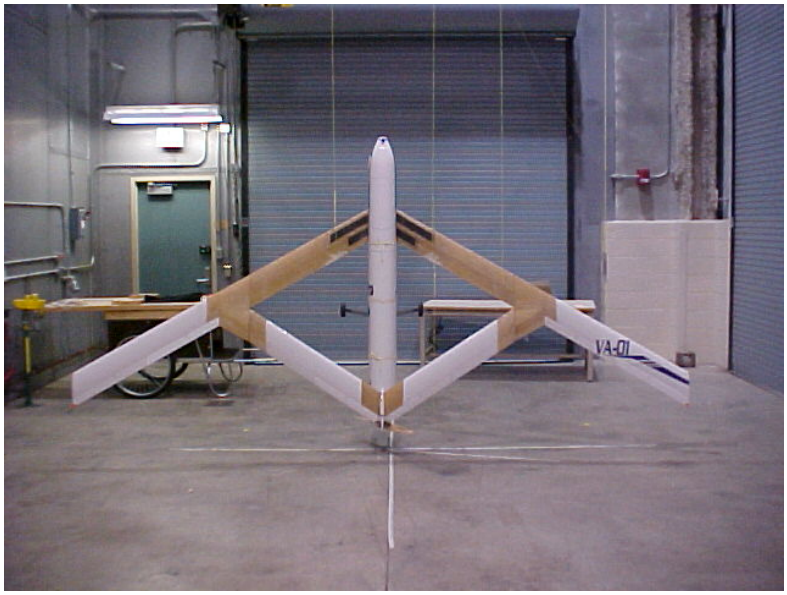


Figure (70) VA-1 Roll Inertia Twist Test Setup.

### 6.4.1. A Swinging Bar Validation Test

A cylindrical steel bar of uniform density was tested to verify the equation worked and the test setup could predict theoretical inertia within 10% uncertainty. The metal bar weighed 22.2 lbs, was 80.125 in. long and had a 1.125 in. diameter. Due to the length of the bar relative to its diameter, the theoretical inertia was calculated with the slender rod equation I = (1/12)mL2 where m was mass in slugs and L was length in feet [9]. The theoretical inertia was found to be 2.56 slug-ft$^2$ with an uncertainty of 0.01 slug-ft$^2$. The experimental inertia, from the twist test, turned out to be 2.49 slug-ft$^2$ with an uncertainty of 0.04 slug-ft$^2$. Also note the measured inertia had the close in magnitude to VA-1 inertias. The experimental measurement showed a difference of 3% from the theoretical measurement and the test was found to be adequate for the purpose of this research.

The aircraft was measured with almost exactly the same procedures as the bar, except the orientations were different. Figure (70) illustrates how the bar was suspended from two cables with its center of gravity equidistant between the two attachment points. The bar's short axis, at the center of gravity, ran parallel to the vertical chords. The bar was then rotated about its c.g. to an initial position where its long axis was approximately ten degrees from the equilibrium position. The bar was carefully released and a stopwatch simultaneously started. The bar then twisted away from its initial release point and subsequently changed direction and returned. At the instant of this change in direction, one cycle or oscillation was counted. The moment the object hit a predetermined number of oscillations, 50 cycles for the bar test, the stopwatch was

stopped and the period was averaged over 50 cycles. This method, except for equipment setup, matched the NACA TR 351 almost exactly [9].

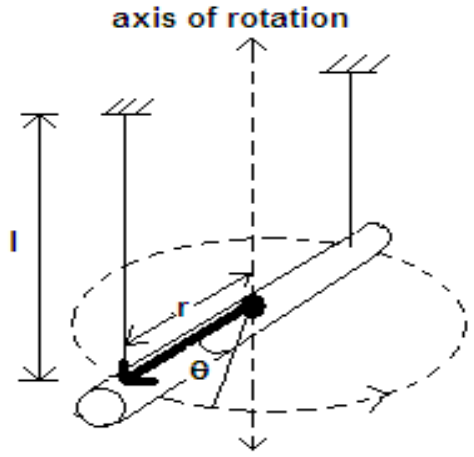


Figure (71) Twist Tests Setup for a long cylindrical bar.

The data was reduced in the following manner. The period was combined with weight, hanging length and radius of rotation to calculate the inertia about the measured axis with the following equation:

$$I = \frac{W}{l}\frac{r^2 P^2}{4\pi^2} \tag{21}$$

Where W is the weight in $lb_f$, r is the radius of rotation in feet, P is the period in seconds, l is the hanging length in feet, I is the mass moment of inertia in slug-$ft^2$.

This equation is not exactly the same as the inertia equation used for the bifilar torsion pendulum in Miller's report. His report [9] used a value of 16 in place of the 4. Miller used the distance between the cables instead of the radius from the center of gravity to one cable. Substituting a (d/2) for r would yield the exact same equation. The version in this research was preferred as it helps illustrate the location about which the body twists. The interested reader is referred to Appendix B for a detailed derivation.

## 6.5. Tests for Measuring Moments of Inertia on VA-1

The airplane was seriously damaged and repaired following the second flight test.

Care was taken to match the internal configuration of VA-1 to that used for flight test so the measured inertia would match the flight test inertia. The aircraft was made with low density materials and redistribution of mass inside the fuselage could change both the inertia and the center of gravity. Batteries and the hand held GPS receiver were installed in the fuselage. The 28 in. propeller, damaged in the hard landing, was not used for the test. The closest available substitute, a 27 in. diameter propeller, was reattached to the shaft in its place. These components affected both weight and c.g., which in turn affected the inertia calculations.

The c.g. was first re-measured by hanging VA-1 from one chord tied around the fuselage and finding the point where the plane would balance on its own. Next, VA-1 was suspended by one chord at two separate attachment points in the same plane. A plumb line was hung from the attachment points and the angles of intersection with the fuselage marked. The center of gravity was marked where the two lines crossed. This method had the added benefit of finding the $z_{c.g.}$ location. Both methods came within one inch of each other in the longitudinal direction and the $x_{c.g.}$ was marked 46.75 in. aft of the nose. This value was forward from the flight test value by approximately one inch.

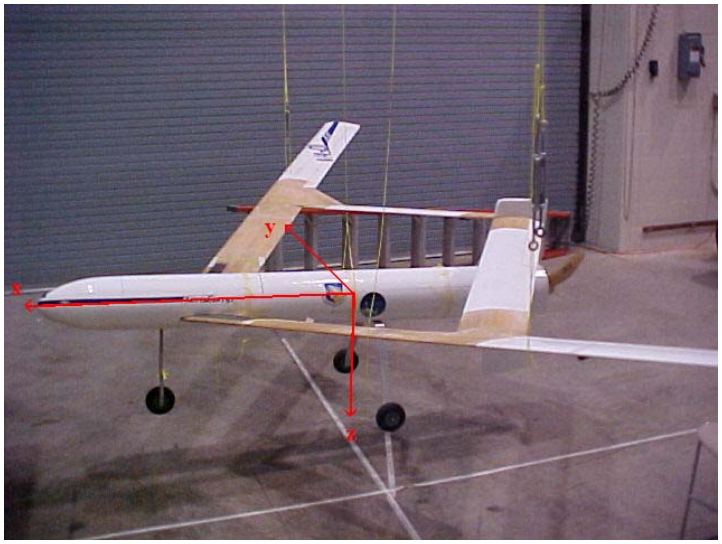


Figure (72) Center of Gravity Measurement with Body Axes Labeled.

VA-1 was suspended in three different orientations to measure three different inertias: $I_{xx}$ , $I_{yy}$, and $I_{zz}$ for roll, pitch and yaw respectively. Inertia was measured about the aircraft body axes, anchored at the aircraft center of gravity shown in Figure (72). The x-axis pointed out the nose, the y-axis pointed towards the starboard wing and the z-axis pointed down. The cross product of inertia, $I_{xz}$, was assumed to be negligible due to aircraft symmetry and was not measured. The other cross product of inertia, $I_{xy}$, was assumed to be close to zero. For each test, the attachment method and location varied to ensure the c.g. was placed equidistant between the two chords.

For the yaw inertia test, VA-1 was suspended by tying chords around the fuselage with wings and fuselage parallel to the ground. Figure (73) shows the yaw inertia test setup. The chords attached to the crane were then connected to the fuselage chords while the plane sat on a table. When the table was removed the plane was suspended with the fuselage level to the ground.

Figure (73) VA-1 Yaw Inertia Twist Test Setup.

To capture roll inertia, chords were tied directly to the wings so that that the c. g. in both the y and z directions was centered between the attachment points. Figure (70) shows the roll test setup. Wing dihedral limited this distance and the radius of rotation was the smallest of the three configurations. The chords were taped down to the wings to minimize travel during the test. As the plane twisted in this configuration, the wings moved normal to the airflow. Drag was a concern but the effects were difficult to predict. Significant twisting seemed to end almost completely after five oscillations, which suggested significant damping existed in the system. The five oscillation limit was highly repeatable.

Meirovitch's treatment of damping and logarithmic decrement was used to estimate damping and its effect on the period [23]. The logarithmic decrement gives insight into the amount of damping encountered during the roll inertia test. The equation for logarithmic decrement is $\delta = (1/n)\ln(x1/xn+1)$, where $\delta$ is the logarithmic decrement, x1 is the amplitude of the first peak and xn+1 is the amplitude of the fifth peak. The variable x can also be thought of as the magnitude of the displacement of the cord attachment point from the equilibrium position. The integer, n, is the cycle number of the last peak minus the cycle number of the first peak. Because the roll twist test appeared to stop after five cycles assume a 99% decrease in amplitude over five cycles. The fifth cycle has magnitude $x5 = 0.01x1$ where the subscripts represent the cycle number. For this case n =4 and $\delta = 1.1513$. Damping ratio, $\zeta$, can then be computed using the logarithmic decrement:

$$\zeta = \frac{\delta}{\sqrt{(2\pi)^2 + \delta^2}} \qquad (22)$$

For roll test the estimated damping ratio was 0.18. The damped natural frequency, $\omega_d$, is related to the undamped natural frequency, $\omega_n$, by $\omega_d = \omega_n\sqrt{1-\zeta^2}$ and $\omega_d = 0.9836\omega_n$ [[23]].

The inertia equation assumed that damping was small and the damped period was virtually the same as the undamped period. When damping seems significant, the undamped period, $P_n$, can be found from the observed or damped period, $P_d$. In general, the period, P, is related to frequency, $\omega$, by $P = 2\pi/\omega$. The damped period can be computed with $P_d = 2\pi/\omega_d$. By substitution $P_d = 2\pi/(0.9836\omega_n)$. Because $\omega_n = 2\pi/Pn$ we find $P_n = 0.9836\ P_d$. For the roll inertia test the observed period is approximately 1.6% smaller than the undamped period. This means the inertia is smaller by a factor of $0.9836^2$ and decreases the computed inertia by approximately

3.3%. Before accounting for damping, the roll inertia comes out to be 3.29 slug-ft$^2$. After correcting for damping the roll inertia is approximately 3.18 slug-ft$^2$ [23].

To capture pitch inertia the plane was suspended sideways with the fuselage parallel to the ground. The center of gravity, in the z direction, was not directly on the fuselage centerline. Simply tying the chords around the fuselage would have allowed the aircraft to tilt or wobble during the test. Eye bolts were installed in the fuselage along the x-y plane at the $z_{c.g.}$ location.

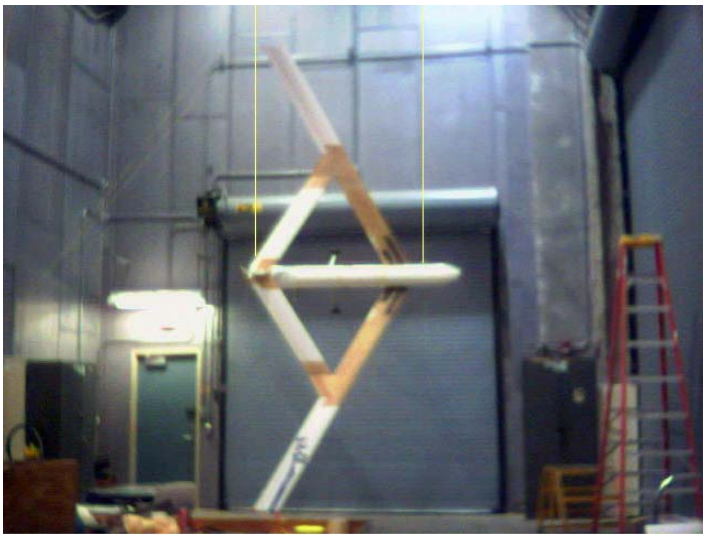

Figure (74) VA-1 Pitch Inertia Twist Test Setup.

To increase the accuracy of the results, a high number of oscillations were measured when possible. For example, during the yaw inertia measurement three sets of fifty oscillations were timed. The total time divided by the total number of oscillations was then the average period, which was used for the inertial computation. This approach worked well for both the yaw and pitch inertias. The roll inertia, however, damped out almost completely in five oscillations so the period was adjusted for damping prior to inertia computation. These results are listed in Table (27). A description of the uncertainty analysis is given in Appendix B.

| Axis | Inertia (slug-ft$^2$) | Uncertainty (slug-ft$^2$) |
|---|---|---|
| Roll, $I_{xx}$ | 3.18 | 0.06 |
| Pitch, $I_{yy}$ | 2.58 | 0.06 |
| Yaw, $I_{zz}$ | 5.04 | 0.09 |

Table (27) Table 1. VA-1 Twist Test Results.

Potential sources of error came from a variety of sources. The aircraft c.g. did not remain perfectly centered during the test. Small side to side and front to back oscillations, called secondary oscillations, were noted. A possible cause may have been the non-zero cross products of inertia about the x-y plane. The manner of release also seemed to impact the magnitude of secondary oscillation. At time test conductors accidentally imparted a velocity component during release. Tests were repeated according to the subjective criteria that secondary oscillations seemed too large. Some type of release mechanism may reduce this effect.

A slight difference in hanging lengths on each side of the aircraft may also affect the results as the axis about which the aircraft rotated should run precisely through the center of gravity. A level was used to ensure the hanging lengths were as even as possible.

The nylon chords stretched significantly, 6-8 in., from the weight of the plane. The chord may have been a source of damping, but the effects seemed insignificant. In addition the inertia of the chords was neglected in the analysis. Other errors may have come from errors in c.g. measurement.

Finally, drag from the twisting motion may have impacted the roll, but damping measurements suggested otherwise. Simple equations for damping were used to correct the period of the roll test for the damping effect. For the pitch and yaw configurations damping was obviously negligible as the aircraft easily reached 50 oscillations for both tests.

### 6.5.1. Center of Mass Test

#### 6.5.1.1. Test objective:

Measure the vehicle weight and establish the center of mass.

#### 6.5.1.2. Specific test goals:

The center of mass must be forward of the aerodynamic center

#### 6.5.1.3. Needed data:

Location of center-of-mass along the fuselage length.

#### 6.5.1.4. Data collection:

Measure weight on each wheel separately.

#### 6.5.1.5. Risk:

Low. Must not change vehicle mass following this test.

#### 6.5.1.6. Success Criteria:

Center of mass is determined.

# 7. Flight Test

The following section addresses, Flight Test Planning,

## 7.1. Flight Test Planning

Flight-testing is scheduled to commence during the month of August 2003 and will continue periodically over the next 12-18 months. All affected organizations will be notified at least 24 hours before any flight-test. Flights will most likely be between 0700 and 1000 due to better weather conditions in the morning hours.

### 7.1.1. Data Requirements

The data requirements are minimal. Trajectory data relates to structural loads. The power consumed is roughly extracted from battery usage.

- Atmospheric - temperature, pressure, wind
- Static Thrust at launch
- Point of takeoff - linear measurement along runway
- Time of flight
- GPS measurements - ground speed - options:
- Still photography and video

The following data requirements are future options that are anticipated to become available:

Attitude and ground speed with modified Palm Pilot

### 7.1.2. Instrumentation

Instrumentation is kept to a bare minimum to reduce cost risks during the initial flight testing phase. The only on-board instrument is the GPS receiver for tracking vehicle position. No telemetry. All trajectory data is down-loaded to a laptop computer while the vehicle is stationary. Power consummation is approximated by battery drain. Static thrust gauge will be incorporated in a simple launch/release mechanism at point of departure.

Figure (75) Garmin GPS Receiver

### 7.1.3. TEST MANAGEMENT, RESPONSIBILITIES AND SUPPORT

#### 7.1.3.1. Management Procedures:

The procedures described herein shall be used in the course of all AFRL/VAS in-house flight testing as defined in AFRLI 99-101. While AFRLI 99-101 describes the overall organizational requirements, the lack of specific guidance related to the effective management of the execution phase required additional direction. An effective test results from a well choreographed team of support personnel working toward the same, well-defined objective. The following requirements provide the effective management visibility and control, while giving the test group an organized methodology reducing potential risk during the execution phase.

#### 7.1.3.2. Test Scheduling

Prior to test execution, but after test plan approval, a test kick-off meeting is suggested. This meeting will provide an opportunity to brief all participants the overall test plan. Following the kick-off meeting, the test is executed through a series of repetitive approval-execution-review cycles. Each of these cycles will be termed "missions" for the remainder of this document.

#### 7.1.3.3. Test Cards

##### 7.1.3.3.1. Test Card Content:

The card deck of approved test points for a given mission must provide a clear description of all activities pertinent to a given mission's execution. Test Cards are provided in Appendix C.

**Go-No Go Conditions**. All requirements mandatory for test execution must be clearly identified on the test cards. Those items required for the entire test should be identified on a cover page, while test point specific requirements can be identified on each individual test point card.

**Communications**. All communication requirements shall be clearly identified before testing begins. Clear, unambiguous terminology must be briefed during the pretest briefing for possible anticipated situations. For example:

**"Knock it off"**: Stop current test point and obtain safe condition.
**"Terminate, terminate, terminate"**: Immediately stop the test.

**Build-Up Approach**. Care must be taken to ensure the test points flow in a methodical sequence with previous test points providing the foundation for future test points.

**Data Recording**. When possible, predetermined locations for data entry should be provided directly on the test cards.

##### 7.1.3.3.2. Test Card Review and Approval Sequence:

The test card review cycle provides management the necessary insight into the daily operation of the test team. All mission card decks shall be reviewed for technical content at the division level. The approved test plan will then be submitted to the Technical Review Board (TRB) and Safety Review Board (SRB) for their review as specified in References [24] (AFRL Test Program) and [25] (AFRL Test Guide).

**Test Team Author**. The test team will create the complete mission card deck.

**Branch Level Review**. Once complete, the mission card deck will be reviewed by the Branch Chief. This can be delegated.

**Division Approval**. Once branch review is complete, the division chief (or assigned approval authority) will approve the test mission.

**Technical Review Board**. Reviews proposed test program for technical merit and approach at Directorate Chief Scientist level.

**Safety Review Board.** Reviews proposed test program for safety at the Directorate Commander Level. Provides final recommendation to commander.

#### 7.1.3.4. Test

##### 7.1.3.4.1. Prebrief and Walk-Through.

All test procedures shall be briefed to the entire test team during a prebrief immediately prior to test execution on the same day as the test. All active participants are required to attend. Each participant must understand their specific responsibility.

##### 7.1.3.4.2. Test Execution.

Execute the briefed procedures! Only those procedures approved and briefed shall be performed.

##### 7.1.3.4.3. Test Debrief.

The debrief serves two purposes. The first is a thorough review of the test itself. All test points accomplished shall be reviewed for last minute comments and verification of satisfactory completion. Secondly data quality is scrutinized. During the post-test debrief, verify all data recorded was adequate for successful completion.

#### 7.1.3.5. Management Responsibilities:

The Joined-Wing vehicle is the property and responsibility of AFRL. Management responsibilities are carried by the following individuals:

The flight test will be managed with the following team:

| Joined-Wing Test Team Personnel | | |
|---|---|---|
| Role | Primary | Secondary |
| Test Director | Max Blair (AFRL/VASD) | TBD Mike Pilkenton (AFRL/VAS) |
| Vehicle Technician | Santiago Panzardi (AFRL/PR) | Hank Baust (AFRL/VAA), Joe Mekina (ASC/ENFT), John McNees (Wylie) |
| Pilot | Keith Numbers (AFRL/VAA) | Mike Pilkenton (ASC/YCA) |
| Safety | Amar Bhungalia (AFRL/VASD) | Maggie Skujins (AFRL/VA) |
| Ground Controller | Lanny Jines (AFRL/VA) | TBD |

Table (28) Joined-Wing Test Team Personnel

Although the vehicle fabricator carries no management responsibility, they are listed as key sources of information:

Vehicle Fabrication: (primary) Mr. Ed Noble, for AeroComposites Inc.

(modifications) Mr. John McNees, Wylie/AFRL/SN

Note: With calm weather being a major test constraint, we will be challenged to find all the primary personnel available on any given suitable test date.

#### 7.1.3.6. Test Plan Deviation Authority

No deviations from the test plan are authorized. Only the test director and pilot together have the authority to make joint decisions and adjustments that result in immediate actions within the scope of the Joined-Wing Flight Experimentation Test Plan. Adjustments are not authorized where there is disagreement. Allowable adjustments might involve weather conditions, lack of certain equipment, lack of certain Joined-Wing component functionality, change in personnel, or number of personnel required. Additional guidance is expected from Safety Review Board and Technical Review Board.

### 7.1.4. Flight Termination (Kill) Procedures

The large trapezoid-shaped area in Figure (76) and Figure (77) will be demarcated with orange traffic cones. Four spotters will be responsible for monitoring each of the boundaries of the test area. The spotters will be equipped with radio communication and thereby required to signal any observation of the airplane approaching or crossing the border. Should the vehicle approach the 200 ft caution zone, a spotter will radio a warning to the test director. If the vehicle crosses the "kill" perimeter, the spotter will radio the "kill" command to the test director, who will then tell the operator to terminate the flight. The test director will stand beside and immediately relay any caution or "kill" commands to the operator. The ground controller will also stand with the operator to ensure that airspace protocol is observed.

It is also important to note that vehicle velocity will be limited to approximately 50 miles per hour (level flight), flying altitude will not be greater than 400 feet (proximity to airport), and maneuvers will not be performed at an altitude less than 50 feet.

The PCM radio receiver is programmable to a fail-safe mode in the event radio signal is lost. There are different opinions on what constitutes a safe pre-programmed setting. One extreme wants the airplane to cut power and continue flying level. This provides smooth operation through radio glitches and still brings the airplane down in the event of substantial failure. The other extreme wants the airplane to cut power and execute a death spiral. For this test program, the fail safe-mode will execute engine off and a slow turn. Outboard flaps and aft wing elevators (both are primary pitch effectors) will go into opposing settings in order to slow the airplane. Inboard wing flaps (ailerons) will effect the gentle roll. While we are cleared to fly to 400 ft altitude, incremental testing will be done at 50 feet and below for the sake of safety. Therefore, the airplane will have little possibility of gliding out of the test area.

### 7.1.5. CONSTRAINTS AND LIMITATIONS

- Battery power for the main propulsion system is limited to ten minutes maximum. Several battery packs are recommended to minimize down time due to recharging. Each recharge is expected to require 30 minutes.

- Battery power for the radio and receiver are limited to one hour duration.
- Personnel Availability (volunteers)
- Control authority limits turning performance
- Weather Conditions

### 7.1.6. SUPPORT REQUIREMENTS

- A successful test requires the presence of the vehicle technicians. (more details, max)
- Safety spotters are required to support the test.

### 7.1.7. DATA PROCESSING:

Data is processed from the GPS receiver to software on the laptop. Vehicle g forces and loads will be estimated based on GPS data.

### 7.1.8. DATA ANALYSIS:

Data will be analyzed in light of maneuver requirements.

### 7.1.9. TEST SCHEDULE AND TIME OF DAY FOR SPECIFIC TESTS

The test area must be scheduled for one week at a time in order to capture good flying weather.

The test area is currently available for the following time windows:

12-16 April 2004
17-21 May 2004
14-18 June 2004

No flights between 11:00 and 13:00 (lunch hour)

The time of day will likely fall in the early morning when winds are most calm. This situation is most likely to occur after weather fronts have passed and we are in a high pressure region. This can be tracked days in advance with on-line weather services.

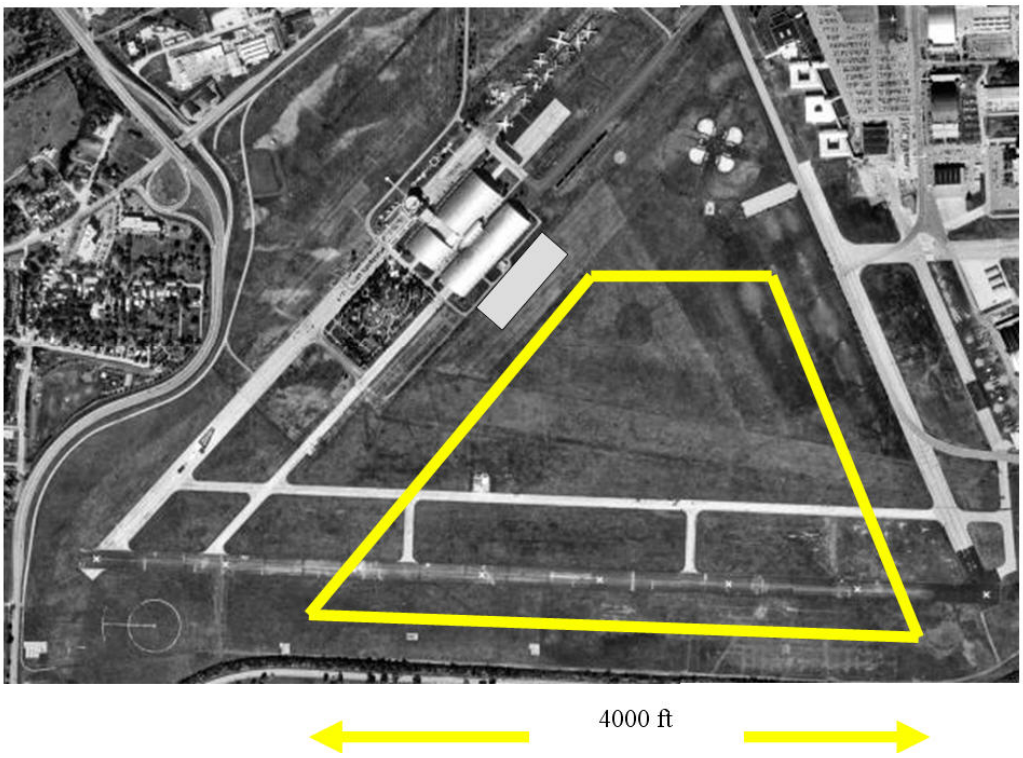


Figure (76) Aerial View of Test Site

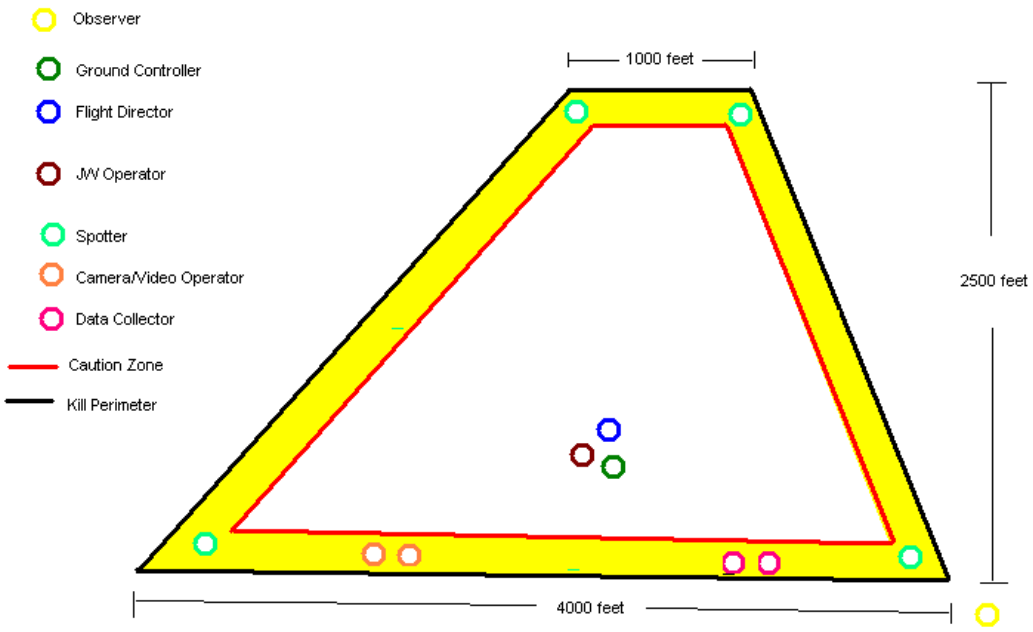


Figure (77) Schematic of Flight Test Site

## 7.2. TEST LOCATION AND TEST BOUNDARIES

All phase I-A testing will be performed at Wright-Patterson AFB. This reduces risk for government-owned test articles as long at the test article stays within the boundaries. Any test

can be performed as many times as needed on as many days as needed to capture the required data. Phase I-A flight-testing will take place at Wright-Patterson Air Force Base, Ohio. Flight testing at WPAFB allows the testing to proceed with less scheduling anxiety and ready availability of volunteers for test support. An aerial view and schematic are presented as Figures 4 and 5. To assure the proposed test area would be large enough for the Joined-Wing vehicle to safely maneuver, analysis was done to predict turning performance. For a turning radius of 200 feet, with the vehicle traveling at 50 mph (max speed), a bank angle of 40 degrees is required. This creates a load factor of L/W = n = 1.3. With a 50% factor of safety, we require 2.0 g static load test (for steady pull-up). (See Appendix C.2.1 - Maneuver Loads)

The area highlighted in the figure will be laid out with traffic cones prior to testing. Spotters will be stationed at the corners. We do not anticipate flying close to the border. The largest footprint involves a smooth turn from takeoff to the north of the runway with a 500 ft radius. The region south of the test area is bordered by trees and a fence along Col. Glenn Highway. The highway is approximately 800 feet from the runway.

### 7.2.1. TEST CONDITIONS:

Weather Sensitivities: Considering the large span and light weight of the test vehicle, ambient wind is a serious constraint. All testing will be done with sustained winds less than 5 mph, gusts less than 5 mph, no precipitation and visibility exceeds one mile with 1000 ft ceiling.

## 7.3. PHASE I-A FLIGHT-TEST OBJECTIVES, APPROACH and SUCCESS CRITERIA:

This section will explain the five main objectives of Phase I-A. These objectives proceed incrementally beginning with the establishment of basic vehicle taxi capability, establishing front strut settings for direct-lift take-off, matching aerodynamic center with center of mass, and finally demonstrating minimal flight turning capability. Once simple bank and turn capability has been demonstrated, the vehicle is ready for further investment and higher risk with the insertion of expensive instrumentation, data acquisition and telemetry.

The science of flight testing fixed-wing aircraft is covered in reference 2.6. This textbook addresses traditional manned flight. The present test plan addresses an uninhabited air vehicle (UAV) of small scale and low cost for research. This test plan is an extremely rough adaptation of classical flight testing while keeping within scope of resources allocated.

This section will also list the data needed to meet each objective, the planned execution of each test, the risks associated with each test, and the success criteria in meeting each objective. A learning curve is expected.

There are five tests planned and described below:

- Basic Taxi and Team Operations
- Establish Front Strut for Best Take-Off
- Establish Aerodynamic Center
- Demonstrate Banking Ability
- Establish Basic Turning Capability

### 7.3.1. Objective I: Basic Taxi and Team Operations

Establish Basic Vehicle Taxi Capability and Team Operations. We would like to see quick acceleration, good lateral stability (does not want to roll over), sensitivity of the nose gear (controllability) and propeller torque effect. This test also provides clearance for possible (but not likely) flap flutter and for possible interference between onboard GPS and radio control system. Test ability to verify adequate thrust at moment of launch. The vehicle has two footprints described in section 3 (Test Item Description). The objective in this test is to observe the different dynamic characteristics.

#### 7.3.1.1. Data:

These are the various data quantities requiring test measurements

##### 7.3.1.1.1. Atmospheric:

Current temperature and barometric pressure are used to calculate atmospheric density, required for calculating dynamic pressure.

##### 7.3.1.1.2. Distance:

Distance along ground roll is required to mark point of lift-off. This is used along with GPS data to point out velocity at lift-off.

#### 7.3.1.1.3. Velocity:

Measured with on-board GPS unit and hand calculated for sanity check (with stopwatch and measured distance).

#### 7.3.1.1.4. Video & Camera:

Record all tests with video camera and digital camera.

### 7.3.1.2. Test Execution:

[brackets indicate settings at repeated intervals]

- Configure vehicle with aft wheels in aft-most position.
- Set front strut to negative angle of attack (-4 deg).
- Unload the wings with pre-set pitch down control
- Execute Pre-Flight Checklist
- Power up system to [half/full] throttle - verify thrust @ RPM
- Check and verify minimum static thrust and release on command.
- Accelerate down the runway at [half / full] throttle and without lift off
- Cut the throttle at [100 ft / 200 ft] and roll out airplane
- Measure distance of roll-out
- Taxi turns and maneuvers back to starting point
- Download GPS data - note the acceleration (more is good)
- Record data (test card listing)
- Repeat the process until batteries are drained
- Measure total time in powered mode
- Replace battery pack and recharge used batteries
- Repeat process replacing and recharging batteries
- Repeat with aft wheels in forward position

### 7.3.1.3. Observations:

The airplane will experience regularly repeated bumps in the runway. Observe the wing response. How much deformation? How much damping? Observe the fuselage response. Does the airplane remain pointed straight? How much do the wheel struts deform? Does the fuselage bounce off the ground? Does the fuselage bounce with increased angle of attack (tendency to take-off prematurely)? Is the GPS data clean? Does there seem to be interference from the GPS on the radio control system (will have to operate with and without GPS receiver turned on). Record Modified Cooper-Harper Rating. How does the airplane dynamics vary with main landing gear in forward and aft positions.

### 7.3.1.4. Risks

- Flutter: See Appendix X for resolution
- Structural Failure on bumps
- Vehicle Tip Over upon turning

#### 7.3.1.5. Success Criteria:

This experimental period is considered successful when the operator and crew have become familiar with taxi operations and on-site battery recharging operations. The vehicle must demonstrate freedom from interference, external or onboard GPS. Success is declared when all observed data has been recorded on paper and with cameras and data downloaded from GPS to the laptop. The team will then be sufficiently prepared for the next objective, test hops, to determine the front strut setting.

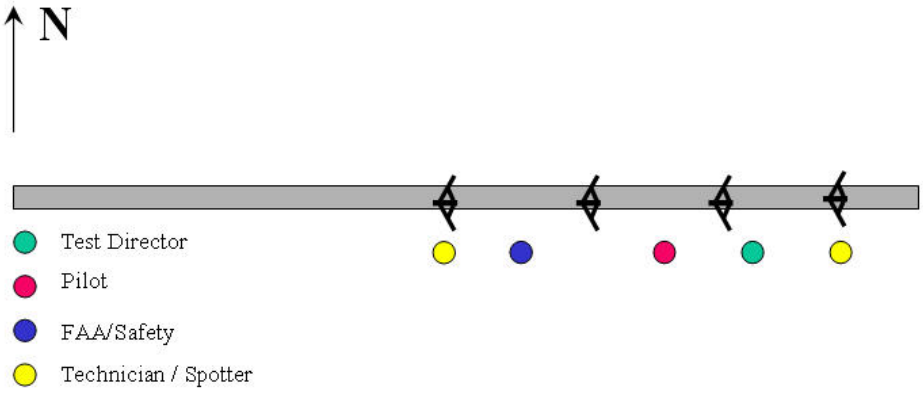


Figure (78) Test Personnel Positioned for Observation

### 7.3.2. **Objective II:** Establish Front Strut for Best Take-Off

Establish front strut settings (angle) for direct-lift takeoff. Vehicle is designed to cruise at 0 degrees angle of attack. Unknowns are ground-effect aerodynamics. Will generate the relationship between takeoff velocity and angle setting. Quick takeoff capability is desired in order to minimize separation between pilot and vehicle at point of departure. Cruise velocity will be reached (in ground vicinity), thus clearing for flap flutter without excessive risk to the overall vehicle. Stall-free envelope for trimmed level flight will be opened as velocity is reduced on landing. Pilot will develop doublet inputs for early stall indication. Explore the different takeoff modes with main landing gear forward and main landing gear aft.

#### 7.3.2.1. Data:

These are the various data quantities requiring test measurements

##### 7.3.2.1.1. Atmospheric:

Current temperature and barometric pressure are used to calculate atmospheric density, required for calculating dynamic pressure.

##### 7.3.2.1.2. Distance:

- Distance along ground roll is required to mark point of lift-off. This is used along with GPS data to point out velocity at lift-off. Repeat and record distance and takeoff velocity for different strut settings. Also measure landing spot for correlation with GPS velocity.

#### 7.3.2.1.3. Transmitter Control Settings:

- How many clicks on the control stick (for each test). Alternatively, program the transmitter computer for maximum throttle setting and then pilot can simply push the throttle all the way.

#### 7.3.2.1.4. Velocity:

- Measured with on-board GPS unit and hand calculated.

#### 7.3.2.1.5. Video & Camera:

- Record all tests with video camera and digital camera.

### 7.3.2.2. Test Execution:

Set front strut. Accelerate down the runway, Cut throttle when vehicle barely gets off ground (less than 3 feet). Measure velocity and distance traveled at moment of liftoff. Record the value.

- Set main landing gear aft.
- Set front strut
- Execute Pre-Flight Checklist
- Power up - check thrust for minimum thrust - RPM check
- Accelerate down the runway
- Liftoff with altitude less than 3 feet
- Measure distance to takeoff
- Adjust throttle to sustain level flight at 3 feet.
- Record throttle setting for future reference
- For flutter run, increase speed while maintaining 3 feet altitude.
- Cut throttle, land and roll out airplane, measure point of touchdown
- Return to launch point
- Download GPS data
- Correlate points at takeoff and landing - note respective velocity.
- Repeat the process until operator has exhausted test settings for front strut.
- Repeat with main landing gear forward.

### 7.3.2.3. Observations:

Observe the wing deformation at lift-off. Observe the angle of attack on landing and the rotation rate on touchdown. How far does the front strut spring compress on landing? Any damage to vehicle? Correlate with drop test results to estimate rotation rate. Record Modified Cooper-Harper Rating. Make notes toward expanding stall-free envelope.

### 7.3.2.4. Risks

- Flutter: See paragraph 19.1 for resolution
- Structural Failure: See paragraph 19.2 for resolution
- Vehicle Stability and Controllability: paragraph 19.3 for resolution

#### 7.3.2.5. Success Criteria:

Success is realized when there is enough data to create a plot correlating strut setting, throttle setting, takeoff distance and takeoff velocity. This plot is used by the Test Director and Operator who must agree on the front strut and throttle settings for takeoff. These settings must sustain the minimum operational airborne velocity without concern for wing stall.

### 7.3.3. **Objective III:** Establish Aerodynamic Center and correct Center of Mass.

This is an incremental test beginning with "best estimate" (based on analysis) for center of mass. The five pound battery pack will serve as the adjustable payload. The center of mass is adjusted aft in small increments until pilot declares pitch stability has degraded the controllability. Center of mass is also incrementally adjusted forward until pilot declares pitch control authority has been marginalized. The aft and forward limits for center of mass will be noted. Following flight testing, the center of mass range will also be ink-marked on the airplane in the laboratory using the balance system. This data is required for future flights with modified payload. Continue to manage the stall envelope with records of velocity range in trimmed flight. Pilot will consider execution of standard doublets to test response. Modified Cooper-Harper will be basis of evaluation.

#### 7.3.3.1. Data:

##### 7.3.3.1.1. Atmospheric:

Current temperature and barometric pressure are used to calculate atmospheric density, required for calculating dynamic pressure.

##### 7.3.3.1.2. Distance:

Distance along ground roll is required to mark point of lift-off. This is used along with GPS data to point out velocity at lift-off.

##### 7.3.3.1.3. Velocity:

Measured with on-board GPS unit.

##### 7.3.3.1.4. Position:

Payload (battery pack) position measured

##### 7.3.3.1.5. Video & Camera:

Record all tests with video camera and digital camera.

#### 7.3.3.2. Test Execution:

- Set initial center of mass.
- Set main landing gear aft.
- Establish center of mass 6 inches forward of calculated aerodynamic center
- Execute Pre-Flight Checklist
- Power up and verify minimum thrust exceeded @ RPM
- Accelerate down the runway

- Liftoff with altitude less than 5 feet
- Operator rapidly establishes pitch trim
- Operator assessment of pitch control
- Land airplane
- Adjust center of mass (battery pack payload) by 1 inch. Mark and index the location to cross reference with pilot assessment.
- Repeat the process until enough data is available to determine optimal center of mass location
- Mark preferred payload location on vehicle for future reference
- Establish and mark center of mass range (associated with payload range) when airplane is back in laboratory and placed on balancing system.
- Repeat with main landing gear forward.

#### 7.3.3.3. Observations:

Does the airplane diverge when pilot releases the controls (as the center of mass is moved aft)? Can the pilot trim the airplane with adequate range of pitch control (as center of mass is moved forward)? Record Modified Cooper-Harper Rating. Continue to manage the stall envelope by noting the trimmed velocity range.

#### 7.3.3.4. Risks

- Structural Failure: See paragraph 19.2 for resolution
- Vehicle Stability and Controllability: paragraph 19.3 for resolution

#### 7.3.3.5. Success Criteria:

Success is realized when the center of mass range has been established to pilot satisfaction.

### 7.3.4. Objective IV: Demonstrate Rolling Ability

This test is conducted at altitude of approximately 25 feet. Velocity maintained "slightly" below flutter clearance established during high speed runs down runway in test 11.2. Velocity maintained "significantly" above minimum velocity for trimmed vehicle (tests 11.2 and 11.3) to avoid wing tip stall. Adjust (redundant) control surface ratios. (see section 3). Begin to form Modified Cooper-Harper handling qualities rating scale for UAV (see end of text). Incrementally repeat the test until a maximum roll angle of approximately 40 degrees is achieved. Adjust the control surface mixing as required to achieve adequate rolling power. This test increases risk to the airplane while increasing safety with flight line over runway at low altitude. Pilot will be more capable of ditching the airplane without incurring liability or personal injury. Pilot will be challenged to takeoff, roll and land from a single standing position - thus making it important to position the pilot to maximize control on all phases of the flight. Explore the effect of main landing gear forward and aft with additional vertical tail installed and removed.

#### 7.3.4.1. Data:

##### 7.3.4.1.1. Atmospheric:

Current temperature and barometric pressure are used to calculate atmospheric density, required for calculating dynamic pressure.

##### 7.3.4.1.2. Velocity:

Measured with on-board GPS unit.

##### 7.3.4.1.3. Video & Camera:

Record all tests with video camera and digital camera.

#### 7.3.4.2. Test Execution:

- Set main landing gear aft - no auxiliary vertical tail.
- Set front strut and center of mass as determined above.
- Execute Pre-Flight Checklist
- Power up and verify minimum thrust exceeded @ RPM
- Accelerate down runway until liftoff at pre-determined minimum operational flight speed.
- Mark point of takeoff for correlation with GPS.
- Rise to 25 feet altitude and sustain at minimal velocity using throttle setting noted earlier.
- Continue flight path down the runway, while rolling the airplane left and right with increasing amplitude beginning with roll angle of approximately 5 degrees.
- Land airplane at maximum range allowable and roll-out
- Download and store GPS
- Optional: adjust control surface ratios to meet pilot satisfaction.
- Repeat test until roll angle of approximately 40 degrees is achieved.
- Repeat test with main gear forward and auxiliary vertical tail installed (must have vertical tail installed to avoid tail strike).

#### 7.3.4.3. Observations:

Take notes on roll angle achieved and corresponding velocity. (See Cooper Harper Scale) Pilot ratings: Report on tendency of airplane to spiral-in as indicated through analysis. Vehicle responsiveness. Record Modified Cooper-Harper Rating.

#### 7.3.4.4. Risks

- Vehicle Stability and Controllability: paragraph 19.3 for resolution

#### 7.3.4.5. Success Criteria:

Success is realized when the airplane has executed simple rolling doublets with 10 degrees amplitude.

### 7.3.5. Objective V: Establish Basic Turning Capability

This test is conducted at altitude of approximately 50 feet. Velocity maintained as in test 11.4. Continue to form Modified Cooper-Harper handling qualities rating scale for UAV (see end of text). Incrementally repeat the test until a turning radius of 200 feet at established safe velocity is achieved. This requires a roll angle of 40 degrees to execute. (see Appendix B). When cleared, explore different control surface mixes with emphasis on key question: Can we fly without the aft wing pitch effector to the benefit of structural design (Ref 2.1).

#### 7.3.5.1. Data:

##### 7.3.5.1.1. Atmospheric:

Current temperature and barometric pressure are used to calculate atmospheric density, required for calculating dynamic pressure.

##### 7.3.5.1.2. Distance:

Distance along ground roll is required to mark point of lift-off. This is used along with GPS data to point out velocity at lift-off.

##### 7.3.5.1.3. Velocity:

Measured with on-board GPS unit.

##### 7.3.5.1.4. Video & Camera:

Record all tests with video camera and digital camera.

#### 7.3.5.2. Test Execution:

- Lay out cones in 500 ft radius from operator with spotters
- Set main landing gear aft - no auxiliary vertical tail.
- Set front strut and center of mass as determined above.
- Execute Pre-Flight Checklist
- Power up and verify minimum thrust exceeded @ RPM
- Accelerate down runway until liftoff at pre-determined minimum operational flight speed.
- Record point of takeoff for correlation with GPS.
- Rise to 50 feet altitude and sustain at minimal velocity using throttle setting noted earlier.
- Bank the airplane and turn through 360 degrees with 500 ft radius.
- Land airplane and roll-out
- Download and store GPS
- Pending acceptable stability and controllability, repeat from (11.5.2.3) with new control surface ratios until pilot identifies the best mix. Verify ability to fly with aft wing pitch effector locked (programmed) out.
- Repeat test with main gear forward and auxiliary vertical tail installed (must have vertical tail installed to avoid tail strike).

### 7.3.5.3. Observations:

Report on tendency of airplane to spiral-in as indicated through analysis. Record Modified Cooper-Harper Rating. Note approach and landing.

### 7.3.5.4. Risks

- Vehicle Stability and Controllability: paragraph 19.3 for resolution

### 7.3.5.5. Success Criteria:

Success is realized when the airplane has executed three takeoffs and three landings at the same point with a 200 ft radius turn in between. Verify ability to fly with aft wing control flap programmed out. Controllability assessment can not be easily achieved precisely with level of instrumentation – pilot opinion is involved.

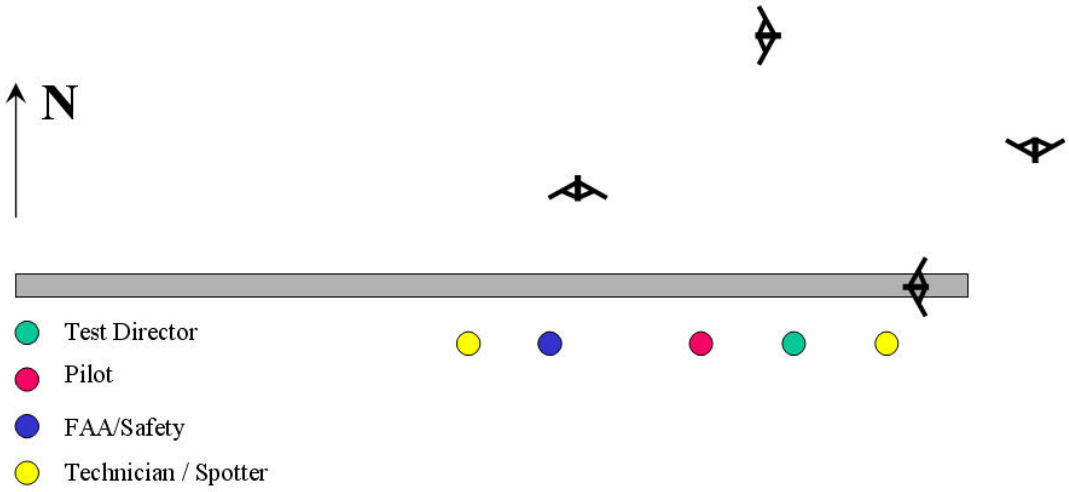


Figure (79) Test Personnel Positioned for Observation During Objective V

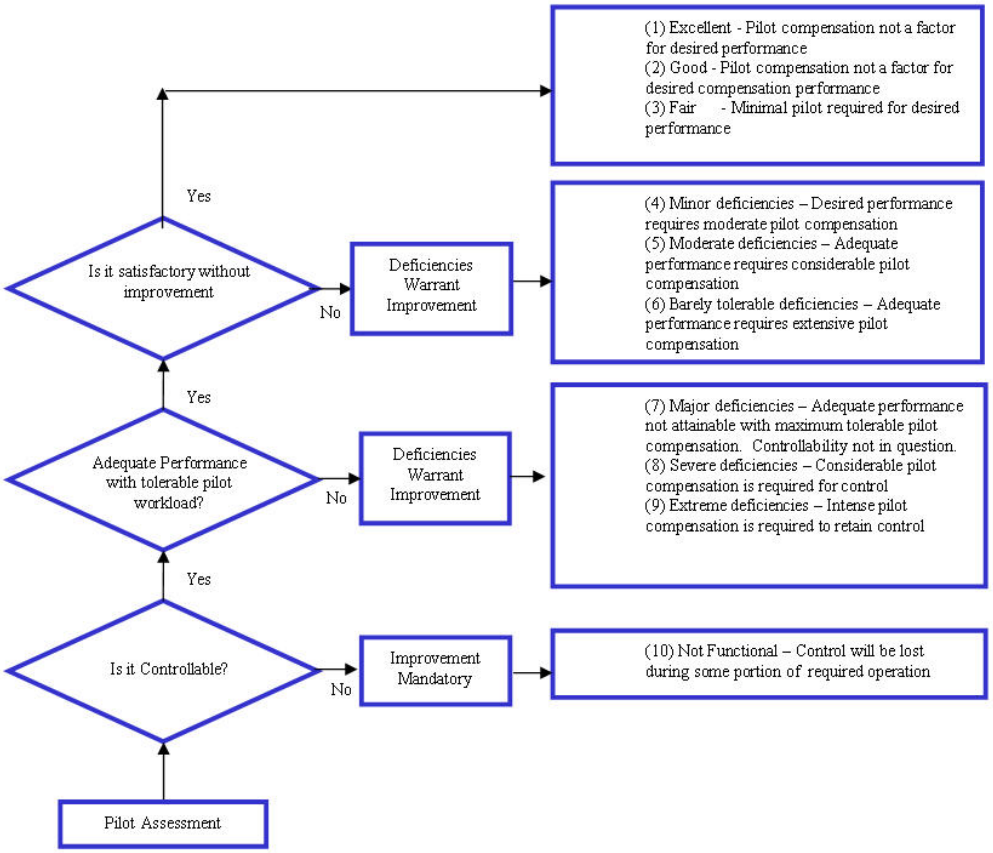


Figure (80) Cooper-Harper (MCH) for AFRL Flight Testing

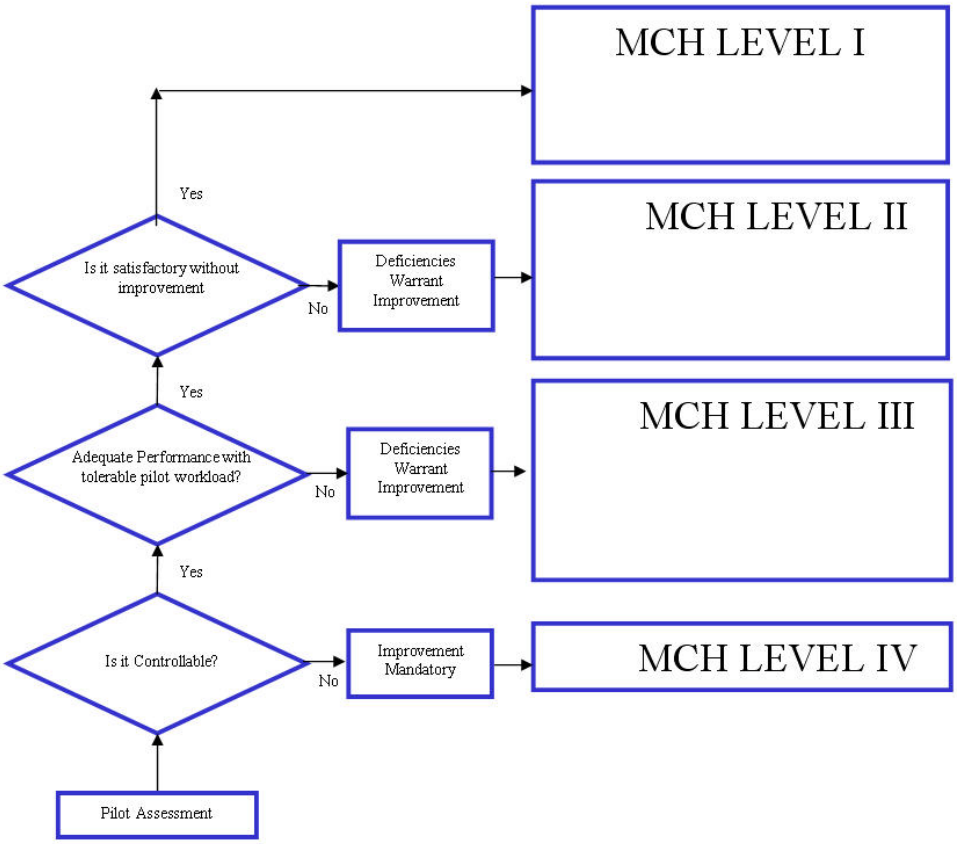


Figure (81) Modified Cooper-Harper (MCH) for AFRL Flight Testing

## 7.4. PREREQUISITE GROUND TESTING TO SUPPORT PHASE I-A FLIGHT TEST ACTIVITIES

A series of simple ground tests will precede the flight tests. Ground testing is conducted in order to assure adequate thrust, sufficient structural integrity and aeroelastic stability. The goal of this program is to assure a safe flight envelope. The goal is not to correlate with high fidelity analysis. This low cost (low risk) testing is limited to go/no-go criteria assuming a limited set of critical loads. All ground tests will be completed before flight-testing begins. Each of the following tests is conducted following the successful conclusion of the previous testing. Successful completion of all these ground tests indicates the vehicle is prepared for Phase I-A flight-testing.

- Appendix B1: Propulsion Calibration Test
- Appendix B2: Vehicle Structural Load Testing
- Appendix B3: Radio Control Range Test
- Appendix B4: Vehicle Center of Mass Test

## 7.5. PHASE I-A FLIGHT-TEST SECURITY and SAFETY CONCERNS:

List safety concerns that directly influence the test plan and call out sections in safety plan. Be sure to distribute read and implement the entire safety plan before execution of the test plan.

- Identify responsible lead and establish procedure for controlling entry and exit to the flight test area. No visitors will be authorized within the test area while testing is in progress.
- Resolve radio communications (test commands, specific phrases, eliminate chatter/confusion, etc)
- Make sure each participant understands his/her role for the specific test.
- Make sure participants understand “kill” procedures.
- Make sure participants are familiar with the test area, especially the “kill” perimeter.
- Make sure to have a pre-test briefing to insure all participants are aware of the potential hazards.
- Make sure there is no interference between the controller, the handheld radios, the GPS unit, radar gun, etc.
- Make sure the test area is secure (only test participants are allowed) before testing begins.
- Make sure to notify all potential users of the test area.
- Make sure all frequencies needed for the test are available and clearly displayed. Scan the environment for interference-free radio operation.
- Make sure all participants have adequate protective gear, if needed. Remote spotters stand next to automobile for protection from uncontrolled aircraft.
- Make sure the Test Director has a cell phone to use in case of emergency.

### 7.5.1. PHASE I-A RISK ASSESSMENT / CONTAINMENT OPTIONS:

List all approaches to contain risk. Engineering design issues discussed here. Test Hazard Analysis (THA) provided in Appendix G.

#### 7.5.1.1. Aeroelastic Flutter

For the modified vehicle, flutter is most probable (but not likely) for the flaps and elevons.

##### 7.5.1.1.1. Uncertainties

- Unsteady Aerodynamic Loads
- Structural Stiffness
- Mass Distribution

##### 7.5.1.1.2. Approaches to Risk Assessment

- Analysis: Flutter analysis is time consuming. Flow over control surfaces is not easily modeled with gaps and separated flow. For flow dominated by low Reynolds Number physics, linear methods are far from reliable.
- Wind Tunnel Testing: Very likely to indicate the problems with flutter in the flight testing program. This is very expensive to set up and run with instrumentation. Flutter occurrences in wind tunnels have been known to cause damage to the wind tunnel facility.
- Restrained Test: At first, this seemed to be a good approach to clear for flutter without incurring high risk. However, with the modified wing (very stiff), wing flutter is now only a remote possibility with flap flutter a more likely concern.
- High Speed Taxi Test (recommended): The vehicle taxi test will take the vehicle close to cruise speed (max - get these estimates from Jason). In essence, the vehicle will be cleared from flap flutter up to the speed encountered in the taxi testing.

##### 7.5.1.1.3. Approach Selected and Rationale:

Vehicle takeoff speed will be close to cruise speed (max - calculate estimated takeoff speed). High speed taxi testing will therefore capture flap and elevon flutter.

#### 7.5.1.2. Structural Failure

##### 7.5.1.2.1. Uncertainties

- Critical Load Set: Limited to 2G pull up load (safely pull maneuver within the test area) and landing load.
- Material Properties: Balsa properties have 50% variance which closely tracks material density. Foam for the foam core wings is very low density and engineering data is not available.
- No real-time data (no telemetry)

##### 7.5.1.2.2. Approaches to Risk Assessment

- FEM Analysis: This has been completed (see appendix). The material stiffness properties were calibrated to match total wing deflection.
- Static Load Testing: This has been completed for 2G maneuver load (2G pull-up) and the drop test. This covers uncertainties with respect to material failure properties.

##### 7.5.1.2.3. Approach Selected and Rationale:

The combination analysis and ground test was the selected approach.

#### 7.5.1.3. Stability and Control

##### 7.5.1.3.1. Uncertainties:

- Aerodynamic stability derivatives
- Magnitude of risk - controllability

##### 7.5.1.3.2. Approaches to Risk Management:

- Analysis presented in Appendix A-2: Indicates marginal yaw control power and tendency to execute spiral instability. Aerodynamic modeling is unreliable at low Reynolds numbers.
- Incremental approach in expanding turning performance: Following simple takeoff and landings in a straight line, the vehicle will include some small amplitude bank and turn oscillations. Incrementally increase amplitude at low altitude.

##### 7.5.1.3.3. Approach Selected and Rationale:

Selected the incremental approach to expanding turning ability with pilot warned of tendency to spiral and will halt testing increments when behavior becomes marginalized.

## 7.6. TEST CARDS

Test card content, review and approval, prebrief, execution and debrief were discussed in section 6.1.2 of the test plan. The following five test cards represent the contents of section 11 of the test plan. Each test card represents minimum requirements for each test. As such, they are carefully crafted.

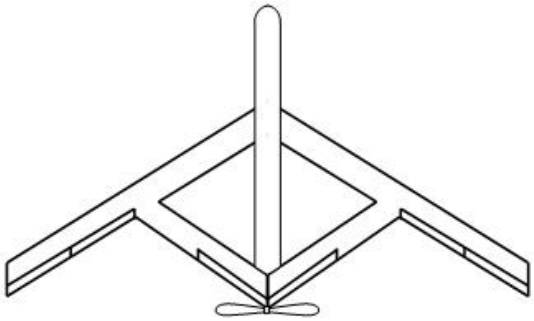

**Joined-Wing Vehicle 1-A Flight Test**

TEST: 1
TITLE: Taxi Test
CARD: 1/1

**OBJECTIVE:** Establish basic vehicle taxi capability and team operations. Establish rolling distance takeoff and landing. Test 2 wheel configurations (forward and aft) and note ground maneuvering dynamics.

**DATA REQUIREMENTS:**
Atmospheric conditions: temp, pressure
Distance of takeoff and landing roll distance
Position/Velocity profile of airplane
Time in powered mode

**SAFETY:**
Execute Safety Checklist

**PROCEDURES:**
1) Set wheel configuration and strut setting
2) Follow preflight & operational checklists
3) Power up, measure static thrust, release
4) Accelerate down runway at partial throttle
5) Unload wings with pitch down control
6) Cut throttle at 200 ft and roll out airplane
7) Measure distance of roll out
8) Taxi turns & maneuvers back to starting point
9) Download GPS data
10) Repeat process until batteries are drained.
11) Record total time in powered mode
12) Repeat process
13) Replace & recharge battery packs as needed

**EQUIPMENT:**
Airplane & Toolbox
Airplane Transport Wagon
Spare Batteries, Charger (Motor and RC)
RC Transmitter
GPS unit (alternate: Palm Telemetry Unit)
Laptop with GPS map software loaded
Digital Camera
VHS Camera
Tape measure or equivalent

**PERSONNEL:**
Test Director
Pilot
Range Officer / Ground Controller
Safety Officer
Vehicle Technician
2 Data Collectors
2 Spotters
VHS Video Camera Grip

Figure (82) Test Card 1: Taxi Test

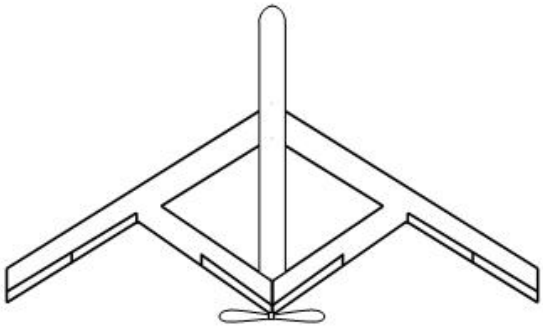

**Joined-Wing Vehicle 1-A Flight Test**

TEST: 2
TITLE: Strut Setting
CARD: 1/1

**OBJECTIVE:** Establish the relationship between direct lift takeoff and front wheel strut setting. Explore aft wheel strut position and practicality of takeoff rotation.

**DATA REQUIREMENTS:**
Atmospheric conditions: temp, pressure
Distance of roll out
Position/Velocity profile of airplane
Time in powered mode

**SAFETY:**
Execute Safety Checklist

**PROCEDURES:**
1) Set wheel configuration & center of mass
2) Set front strut
3) Adjust vehicle control settings
4) Follow preflight and operational checklists
5) Power up, confirm full thrust, accelerate
6) Cut throttle as wheels unload < max visual
7) Mark/Measure departure point
8) Roll out airplane & measure distance
9) Taxi turns & maneuvers back to starting point
10) Download GPS data
11) Repeat process until batteries are drained
12) Record total time in powered mode
13) Replace batteries & recharge used batteries

**EQUIPMENT:**
Airplane & Toolbox
Airplane Transport Wagon
Spare Batteries, Charger (Motor and RC)
RC Transmitter
GPS unit (alternate: Palm Telemetry Unit)
Laptop with GPS map software loaded
Digital Camera
VHS Camera
Tape measure or equivalent

**PERSONNEL:**
Test Director
Pilot
Range Officer / Ground Controller
Safety Officer
Vehicle Technician
2 Data Collectors
2 Spotters
VHS Video Camera Grip

| Parameter | Run 1 | Run 2 | Run 3 | Run 4 | Run 5 |
|---|---|---|---|---|---|
| Vehicle Layout | | | | | |
| Throttle Setting | | | | | |
| Rolling Distances | | | | | |
| GPS data (Y/N) | | | | | |
| Time Powered | | | | | |
| MCH Rating | | | | | |

notes:
Vehicle layout: encode(gear, control, prop, tail, cg)
GPS data: denote data file
Time Powered: denote battery recharge
MCH denotes ability to manage takeoff-roll

Figure (83) Test Card 2: Strut Setting

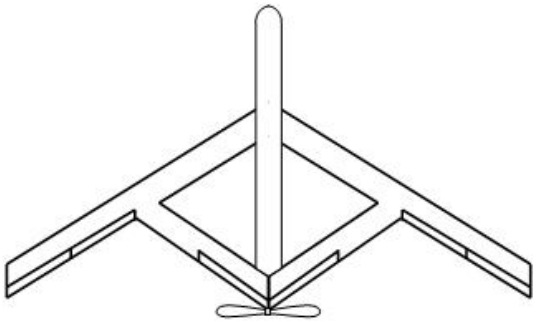

**Joined-Wing Vehicle 1-A Flight Test**

TEST: 3
TITLE: Aerodynamic Center
CARD: 1/1

**OBJECTIVE:** Adjust the center of mass for longitudinal stability.

**DATA REQUIREMENTS:**
Atmospheric conditions: temp, pressure
Distance of roll out
Position/Velocity profile of airplane
Center of mass increments and range
Time in powered mode

**SAFETY:**
Execute Safety Checklist

**PROCEDURES:**
1) Set wheel configuration (record data)
2) Adjust center of mass (record data)
3) Follow preflight and operational checklists
4) Accelerate down runway at full throttle
5) Liftoff to altitude less than five feet
6) Establish pitch trim
7) Land airplane (no turn)
8) Return taxi to starting point
9) Operator assessment of pitch control
10) Download GPS data
11) Adjust center of mass per operator assessment
12) Repeat process until batteries are drained
13) Measure total time in powered mode
14) Replace batteries & recharged used batteries

**EQUIPMENT:**
Airplane & Toolbox
Airplane Transport Wagon
Spare Batteries, Charger (Motor and RC)
RC Transmitter
GPS unit (alternate: Palm Telemetry Unit)
Laptop with GPS map software loaded
Digital Camera
VHS Camera
Tape measure or equivalent

**PERSONNEL:**
Test Director
Pilot
Range Officer / Ground Controller
Safety Officer
Vehicle Technician
2 Data Collectors
2 Spotters
VHS Video Camera Grip

| Parameter | Run 1 | Run 2 | Run 3 | Run 4 | Run 5 |
|---|---|---|---|---|---|
| Vehicle Layout | | | | | |
| Throttle Setting | | | | | |
| Rolling Distances | | | | | |
| GPS data (Y/N) | | | | | |
| Time Powered | | | | | |
| MCH Rating | | | | | |

notes:
Vehicle layout: encode(gear, control, prop, tail, cg)
Throttle Setting: record for brief cruise condition
GPS data: denote data file
Time Powered: denote battery recharge
MCH denotes ability to control pitch

Figure (84) Test Card 3: Aerodynamic Center

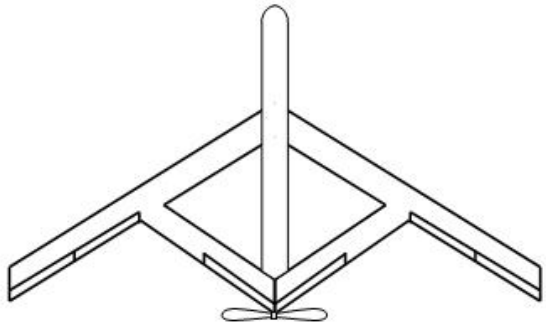

**Joined-Wing Vehicle 1-A Flight Test**

TEST: 4
TITLE: Rolling Ability
CARD: 1/1

**OBJECTIVE:** Safely expand ability to maneuver with a series of flights with incrementally increased rolling doublets along a nominally straight trajectory. Prelude to initiating turn in test 5.

**DATA REQUIREMENTS:**
Atmospheric conditions: temp, pressure
Position/Velocity profile of airplane
Guesstimate of vehicle attitude (roll angle)
Time in powered mode

**SAFETY:**
Execute Safety Checklist

**PROCEDURES:**
1) Set wheel configuration and center of mass
2) Program new control surface ratios
3) Follow preflight and operational checklists
4) Accelerate down runway at full throttle
5) Lift off and rise to 25 ft altitude
6) Roll doublets left and right along runway
7) Keep within pilot comfort zone visual contact
8) Descent, landing and rollout, taxi to launch pt
9) Download GPS data
10) Repeat process until batteries are drained
11) Measure total time in powered mode
12) Replace batteries & recharge used batteries
13) Repeat process (pending adequate controllability)

**EQUIPMENT:**
Airplane & Toolbox
Airplane Transport Wagon
Spare Batteries, Charger (Motor and RC)
RC Transmitter
GPS unit and Palm Telemetry Unit
Laptop with GPS map software loaded
Digital Camera
VHS Camera
Tape measure and protractor (for roll angle)

**PERSONNEL:**
Test Director
Pilot
Range Officer / Ground Controller
Safety Officer
Vehicle Technician
2 Data Collectors
2 Spotters
VHS Video Camera Grip

| Parameter | Run 1 | Run 2 | Run 3 | Run 4 | Run 5 |
|---|---|---|---|---|---|
| Strut Setting | | | | | |
| Throttle Setting | | | | | |
| Rolling Distances | | | | | |
| GPS data (Y/N) | | | | | |
| Time Powered | | | | | |
| MCH Rating | | | | | |

notes:
Vehicle layout: encode(gear, control, prop, tail, cg)
Throttle Setting: record for brief cruise condition
GPS data: denote data file
Time Powered: denote battery recharge
MCH denotes ability to roll - record roll angle

Figure (85) Test Card 4: Rolling Ability

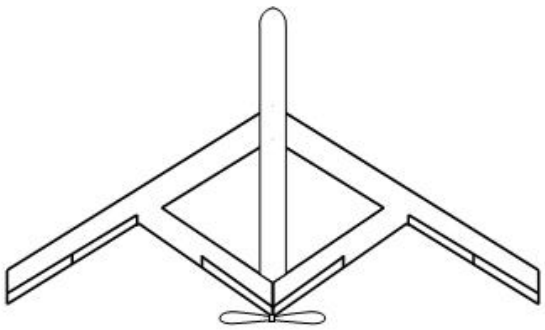

**Joined-Wing Vehicle 1-A Flight Test**

TEST: 5
TITLE: Full Turning Ability
CARD: 1/1

**OBJECTIVE:** Demonstrate capability to takeoff, rise, execute 200 ft radius turn, approach and land

**DATA REQUIREMENTS:**
Atmospheric conditions: temperature, pressure
Position/Velocity profile of airplane
Time in powered mode

**SAFETY:**
Execute Safety Checklist

**PROCEDURES:**
1) Execute preflight checklist
2) Mark circle limits with cones - for pilot queue
3) Set wheel configuration and center of mass
4) Accelerate down runway at full throttle
5) Lift-off and rise to 50 ft altitude
6) Bank and turn with established radius
7) Approach and landing and rollout
8) Download GPS data
9) Program new control surface ratios
10) Repeat process until batteries are drained. Reduce radius incrementally until 200 ft radius is reached.
11) Measure total time in powered mode
12) Replace batteries & recharge used batteries

**EQUIPMENT:**
Airplane & Toolbox
Airplane Transport Wagon
Spare Batteries, Charger (Motor and RC)
RC Transmitter
GPS unit and Palm Telemetry Unit
Laptop with GPS map software loaded
Digital Camera
VHS Camera
Tape measure

**PERSONNEL:**
Test Director
Pilot
Range Officer / Ground Controller
Safety Officer
Vehicle Technician
2 Data Collectors
4 Spotters
VHS Video Camera Grip

| Parameter | Run 1 | Run 2 | Run 3 | Run 4 | Run 5 |
|---|---|---|---|---|---|
| Strut Setting | | | | | |
| Throttle Setting | | | | | |
| Rolling Distances | | | | | |
| GPS data (Y/N) | | | | | |
| Time Powered | | | | | |
| MCH Rating | | | | | |

notes:
Vehicle layout: encode(gear, control, prop, tail, cg)
Throttle Setting: record for brief cruise condition
GPS data: denote data file
Time Powered: denote battery recharge
MCH: ability to bank and turn - record turn radius

Figure (86) Test Card 5: Full Turning Ability

## 7.7. Checklists

### 7.7.1. Equipment Checklists

#### 7.7.1.1. Safety Equipment Checklist

- Orange cones-used to demarcate the flight test area
- Handheld radios-used for communication between spotters and test director
- Cellular phone-available to contact fire/police department if necessary
- Signs-to be posted warning unauthorized personnel to keep out
- Sunscreen and water-for personnel safety

#### 7.7.1.2. Joined-Wing Vehicle Equipment Checklist

- Joined-Wing vehicle
- Assortment of propellers
- Garmin GPS receiver
- Additional batteries for vehicle
- Tool box
- Radio transmitter
- Field Charger (for batteries)
- Voltmeter

#### 7.7.1.3. Data and Recording Equipment Checklist

- Video Camera
- Digital Camera
- Laptop Computer
- Wind anemometer
- Wind sock
- Stopwatch
- Thermometer
- String (1000 ft length & calibrated to measure 50 ft increments)
- Barometer (The 88$^{th}$ Air Base Wing Weather Squadron has a Kestrel 4000 to loan)
- Static thrust gauge (hand-held digital fish scale measured on nose before takeoff)
- Tachometer (propeller RPM)
- RC Frequency Scanner

### 7.7.2. Procedure Checklists:

#### 7.7.2.1. Communication/Notification Checklist

- Hold a pre-flight meeting with the operator, test director, spotters, and any other people decided by the test director.
  - Outline the goals of the flight test.
  - Review flight plan – sequence of planned patterns.
  - Identify and discuss all known safety hazards.
  - Inform team that the area is to be evacuated if the vehicle crashes. Brief team on 911 procedure - Must specify that we are on Wright-Patterson Air Force Base.
  - Specify video needs/expectations with video-operator.
  - Specify digital photographic needs/expectations with camera-operator.
  - Specify needed velocity measurements with radar-operator.
- Make sure a ground-controller (a graduate of FAA or military ground school) is present.
- Notify Mr. Bob Pinkus (ASC/LPK, 255-3507 x3061) of the tests, so he can let concerned AMA members know that we will be using the airfield.
- Notify Base Operations to let them know about our tests. Specify maximum altitude of test – below 400 feet (Airfield Management Office 257-6206 or 6207).
- Notify base fire department before test (Station 4: 255-3820).
- Notify the Air Force Museum of the tests (Theresa Lacey 255-8046 x311).
- Notify AFRL/PA 656-9876 of tests so they can address any public inquiries.
- Notify Maj. Walt Jackson (ASC/SEF, 254-3386), the base flight safety officer, of the test dates so he may observe the tests if he wishes. (It is not mandatory that he be present at the test.)
- Notify Chris Bozada (AFRL/SNDI ) and his pilot, John McNees, to make sure they aren't flying their RC helicopter on the same day.
- Notify Lt Kirk Olson (AFRL/SN) and his "Rodent Aloft" program to make sure they aren't flight-testing on the same day.

**Safety Checklist**

- Cell phone for test director immediate use to call for help.
- Place a warning sign at the gate entrance to the test area.
- Clear runway of obstacles (use broom to sweep obstacles larger than 1/8 in).
- Mark all significant potholes on the runway with orange cones.
- Verify test personnel are safely positioned to achieve desired results as agreed.
- Perform radio checks between spotters, operator, and program manager.

### 7.7.3. Operational Checklists:

#### 7.7.3.1. Weather Constraints

- Sustained winds must be less than 5 mph.
- Gusts must be less than 5 mph.
- No precipitation or fog.
- Must have better than one-mile visibility and 1000 ft ceiling.

#### 7.7.3.2. Battery Checklist (day before flight)

- Radio receiver batteries cycled several times
- Main power batteries cycled and recharged (prefer three units)

#### 7.7.3.3. Joined-Wing Pre-Flight Checklist

- Visually inspect control links, push-pull rods and all other flight control components.
- Manually operate all flight control and throttle servos to ensure ease of operation.
- Visually inspect propeller.
- Inspect propeller shaft for missing and loose hardware.
- Inspect all support equipment such as landing gear, batteries, motor and speed controller for damage or missing hardware.
- Inspect electrical system. Check all wiring, switches, and batteries for damage.
- When applicable, check payload added to vehicle for proper and secure installation.
- Have a second test team member (experienced in R/C) repeat all inspection steps. This step is mandatory before the maiden flight and before all flights at Wright field.

#### 7.7.3.4. Start-Up Sequence

- Check wind direction – establish takeoff direction – select runway.
- Place vehicle at launch position.
- Perform Range check to 4000 ft (extent of the flight test area).
- Check voltages on vehicle receiver batteries and power batteries.
- Check voltage of radio transmitter batteries.
- Turn on GPS receiver (optional)
- Turn on vehicle receiver – note possible interference – abort if necessary.
- Turn on radio transmitter – note effect on vehicle receiver.
- Perform all flight control checks for proper direction and motion of left and right elevons and rudder as well as nose wheel steering.
- Perform controller range check, with antenna collapsed, at a minimum of 100 feet extending all the way out to 4000 feet. Perform this check on the grass to reduce interference with iron rebar in runway.
- Start engine at idle.
- Repeat range check at engine idle position.

#### 7.7.3.5. Normal Shut-Down Sequence

- Shut off engine.
- Turn off vehicle receiver, then radio transmitter.
- Turn off GPS receiver.

## 7.8. Operational Perspective on Position Descriptions

- Test Director (Blair)
    - Nerve center for monitoring communications/radio input
    - Watches all operators
    - Stands next to pilot and issues directives as required.
    - Announces "clear", “rolling”, "takeoff", "approach", "land" over radio.
        - "Clear": Announced test id#, watch to see if runway is clear - check for feedback from safety - give pilot go-ahead
        - “Rolling”: pilot has initiated ground roll
        - "Takeoff": watch to see if takeoff spot is marked
        - "Approach": watch to see if runway is clear - inform the pilot
        - "Land": watch to see if landing spot is marked and timed
- Pilot (Numbers / Pilkenton)
    - Flies the airplane - responds only to test director and airplane test plan
    - Assigns Modified Cooper-Harper ratings
- Range Officer / Ground Controller (Jines)
    - Stands with pilot and test director
    - Observes all FAA regulations are being met (altitude etc)
    - Records Modified Cooper-Harper ratings
- Safety Officer (Bhungalia)
    - Watches for unauthorized people in test area
    - Approaches suspects
    - Clear runway of debris
- Vehicle Technician (Baust or Panzardi)
    - Vehicle transport
    - Vehicle setup
    - Sets the strut
    - Measure static thrust before takeoff
    - Maintain battery charge rotation
    - Replace main power batteries
    - Vehicle storage
- Launch Site Data Collector (Canfield)
    - Synchronize clock with GPS unit
    - Starts stopwatch on ground-roll initiation
    - Marks each takeoff - records time from stopwatch and watch
- Down Range Data Collector (McCabe)
    - Start stopwatch on takeoff
    - Mark landing spot - records time on stopwatch
- GPS Data Collector (TBD)

    - After vehicle is at rest with power off and locked
    - Hook laptop into GPS and download data
- Technical Video (McNees, alt: Baron, Baust)
    - Keeps technical video for later review
- Marketing Video (Carol Young hires)
    - Intermittent video of people and airplane - generates image of organization
- Border Safety Spotters (CGO)
    - Configuration depends on test
    - Stands by automobile at test border
    - In constant radio contact
    - Announce warning and kill commands to test director
    - Not required after flight characteristics established.

## 7.9. TEST HAZARD ANALYSIS

### 7.9.1. Hazard #1 - Controlled Vehicle Crash

#### 7.9.1.1. Cause:

Unexpected vehicle response due to unmodeled analysis or pilot induced response [e.g. Vehicle Stall induced at low speed due to inadequate thrust available]

#### 7.9.1.2. Effect:

Legal liability in event of damage or injury or death. Note: no hazardous materials involved.

#### 7.9.1.3. Controls/Minimizing Procedures:

The vehicle is fabricated with styrofoam, balsa, plywood, and mylar sheet and standard hobby adhesives. Equipment on board include batteries, electric motor, speed controller, and servo motors. In the event of a crash, these materials and components may be spread across WPAFB property.

#### 7.9.1.4. Corrective Actions & Emergency Procedures

Call 911 and others on official call list

### 7.9.2. Hazard #2 - Runaway Vehicle Crash

#### 7.9.2.1. Cause:

Radio contact is lost or radio batteries lose power

#### 7.9.2.2. Effect:

Airplane flies indefinitely without control until power is lost or contacts immoveable object (it crashes) or both.

#### 7.9.2.3. Controls/Minimizing Procedures:

The vehicle has a rotary propeller and the vehicle itself can reach velocities of approximately 50 miles per hour. If control of the vehicle is lost, significant damage to persons or property can result from the impact of collision.

The aircraft will be flown over an open field on the airfield, a safe distance from any building. The test involves hovering and simple turning maneuvers, not high speed or aerobatic flight. The vehicle will be flown at speeds of no more than 50 miles per hour. A 3000 x 1500 foot region will be marked off with traffic cones and four spotters will ensure that the vehicle stays within that area. Should the vehicle approach the perimeter of said area, a spotter will notify the pilot by radio to bring the aircraft back toward the center. The spotters themselves will be stationed well outside the area, at least 50 feet from their assigned corners. A pre-programmed kill sequence will be automatically activated if the vehicle receiver fails to respond to the controller. Routine inspection procedures to ensure the mechanical integrity of the vehicle will be followed.

There is little to no chance that the vehicle with PCM (pulse code modulated) controller can fly for any considerable distance on its own if communication with the controller is broken with the vehicle at 100 ft altitude. The pre-programmed PCM fail-safe mode is motor idle and controls to neutral. The rational is that oftentimes there are radio glitches with subsequent radio restoral. This fail-safe mode will bring the airplane down slowly with an actual radio failure and will not destroy the plane in case of momentary radio failure.

#### 7.9.2.4. Corrective Actions & Emergency Procedures

If the vehicle crashes, it is anticipated that the above precautions ensure that no damage or injury will result. For a worst-case scenario, a cellular telephone will be on hand to notify emergency crews.

### 7.9.3. Hazard #3 - Vehicle loses main Power

#### 7.9.3.1. Cause:

Failed main batteries - main batteries prematurely drained (note main power and receiver power are separate battery units)

#### 7.9.3.2. Effect:

Power drain happens slowly and in that circumstance, the airplane will naturally force a controlled landing. In the event the power loss is sudden, the controller will be forced to land in the open field.

#### 7.9.3.3. Controls/Minimizing Procedures:

Batteries will be kept charged and back-up batteries will be on-hand. It is difficult to measure total charge remaining. We will have a good idea of operational duration following taxi tests. The propulsion system has been wind tunnel tested (with flight batteries installed) and duration at full throttle and 45 mph was approximately 5 minutes. No flight will begin with less than 80%

thrust available. Measurement will take place immediately before release for takeoff. All flights will take place within the control zone.

#### 7.9.3.4. Corrective Actions & Emergency Procedures

The airplane will be landed immediately following power loss or any sign of inadequate power.

### 7.9.4. Hazard #4 - Vehicle becomes aerodynamically unstable

#### 7.9.4.1. Cause:

Death Spiral or improper center of mass.

#### 7.9.4.2. Effect:

The airplane will be unstable and subsequently uncontrollable with large deviations. At best, the operator can hope for a controlled crash in the field. At worst, the vehicle will experience an uncontrolled crash.

#### 7.9.4.3. Controls/Minimizing Procedures:

The vehicle test plan is designed to clear the airplane with respect to instabilities at low altitude at the earliest point possible. Once cleared, the potential hazard to is minimized to irrelevance. These tests will be conducted far from the test area boundary. The vehicle operator is instructed to cut power in any case where an unstable vehicle is approaching the test area boundary. It is the operators discretion whether to execute the PCM mode (which could cause an unstable vehicle to become more unstable).

#### 7.9.4.4. Corrective Actions & Emergency Procedures:

The pilot will be briefed on possible vehicle behavior and will not be surprised.

### 7.9.5. Hazard #5 - Vehicle becomes aerodynamically uncontrollable

#### 7.9.5.1. Cause:

Control surface effectiveness is inadequate (e.g. rudder)

#### 7.9.5.2. Effect:

The airplane will be uncontrollable but stable. At best, the operator can hope to maneuver the vehicle for a landing. At worst, the vehicle will experience an uncontrolled crash.

#### 7.9.5.3. Controls/Minimizing Procedures:

Same as hazard #4.

#### 7.9.5.4. Corrective Actions & Emergency Procedures:

Same as hazard #4.

## 7.10. WHAT-IF LIST

### 7.10.1. What if: The airplane goes out of the test area (but not off base).

a) **Soft Landing** - NO personal injury or property damage:
   (i) No immediate action required. Optional: Contact Maggie Skujins (AFRL T&E) by voice or email within 24 hrs.
b) **Hard Landing** with personal injury or property damage:
   (i) Telephone the following immediately:
      (a) AFRL/VA Safety Officer (see below)
         (i) Safety Officer will call appropriate officials
      (b) Branch (AFRL/VASD)
      (c) Division (AFRL/VAS)
      (d) SRB (Safety Review Board) Chairperson
   (ii) Complete Test Safety Mishap Worksheet (in test plan) immediately.
      (a) Denote times on form as calls are made

### 7.10.2. What if: The airplane goes off the base.

a) Telephone AFRL/VA Safety Officer (see below)
   (i) Notify of the event
   (ii) Leave test site cell phone number
   (iii) Safety Officer will call appropriate officials
b) Flight Test Director personally seeks out airplane landing location
c) Telephone
   (i) AFRL/VA Safety Officer (again) - notify with location and status
   (ii) Branch (AFRL/VASD) - notify with situation and status
   (iii) Division (AFRL/VAS) - notify with situation and status
   (iv) SRB (Safety Review Board) Chairperson - notify with situation and status
d) Complete Test Safety Mishap Worksheet (in test plan) immediately.
   (i) Denote times on form as calls are made

## 7.11. Unplanned Scenarios

### 7.11.1. Scenario #1 - Intruder blunders into test area during flight testing

**Situation A:** Flight testing is going well with airplane in control with sufficient battery reserve to loiter five minutes. No perceived threat to airplane or personnel.

**Action:** Safety director leads the intruder off the field. Test director instructs the pilot to fly away from the incursion and loiter until notice. Safety officer informs test director when situation controlled at which time the test director instructs the pilot to land the airplane with normal approach. If situation extends past the three minute mark - see situation B below.

**Situation B:** Flight testing is going well with airplane in control without sufficient battery reserve to loiter five minutes. No perceived threat to airplane or personnel.

**Action:** Safety director leads the intruder off the field. Test director instructs the pilot to land the airplane at a spot on runway furthest from the incursion.

**Situation C:** Flight testing is going well with airplane in control. Perceived threat to airplane or personnel.

**Action:** Safety director leads the intruder off the field. Test director instructs the pilot to land the airplane immediately at any open spot in the field, regardless of possible damage to the airplane. Safety issue overrides vehicle life.

### 7.11.2. Scenario #2 - Emergency flight termination declared

**Situation A:** The spotter has declared the airplane has exited the test area and test director has informed the pilot to turn off transmitter.

**Action:** Flight director draws a trajectory on where airplane is headed. If the airplane lands in test area with less than moderate damage, no follow-up. If airplane heads out of test area, follow the checklist.

## 7.12. Flight Test Execution

In 2004 the AFRL Air Vehicles Directorate designed, built, and flew a scaled radio-controlled joined-wing aircraft, called VA-1, to explore general airworthiness of a joined-wing configuration.

The weather was a significant factor in scheduling. Essentially, the project manager had to look at the on-line weather forecast every day to check for low winds and wind direction.

Could not follow

### 7.12.1. Test Date (09 August 2004) Radio Range Testing

Called the test team personnel and rolled the airplane out on the runway at far point accompanied by CB radio person. Range test on CB radio passed. Range test on airplane control radio passed. Airplane returned to laboratory.

### 7.12.2. Test Date (11 August 2004) Taxi Testing

Required low wind from any direction. Airplane could not take off with any cross winds (certainly less than 5 mph). The smallest cross wind easily rolled the airplane upon liftoff. If you can feel the cross wind, it is too strong.

The VA-1 was significantly under-powered. The pilot struggled to hop the airplane off the ground, but could not sustain the takeoff. It was clear that we could not simply follow the test cards directly. Our entire focus would be to get the airplane airborne.

Many taxi tests: Finally got airborne (several feet altitude for a distance of perhaps 20 feet). Test guidance called for pilot to cut power immediately to induce landing and avoid flight. The net result was a rapid pitch-down and hard landing.

Hard Landing – Tail Damaged – Repaired by volunteer crew (Pilkenton and Panzardi)

### 7.12.3. Test Date (25 August 2004) Flight Test – Card 5

Several taxi attempts to take off. Success finally attained. Two circuits and soft controlled landing. Great success and much relief. Many thanks to the pilot Mike Pilkenton.

Following the successful flight, there was a conflict on whether to complete the flight test program. The program manager was very concerned that the vehicle was seriously under-powered. Clearly, the flight test pilot exerted influence as deputy division chief and was successful in ordering a second test flight.

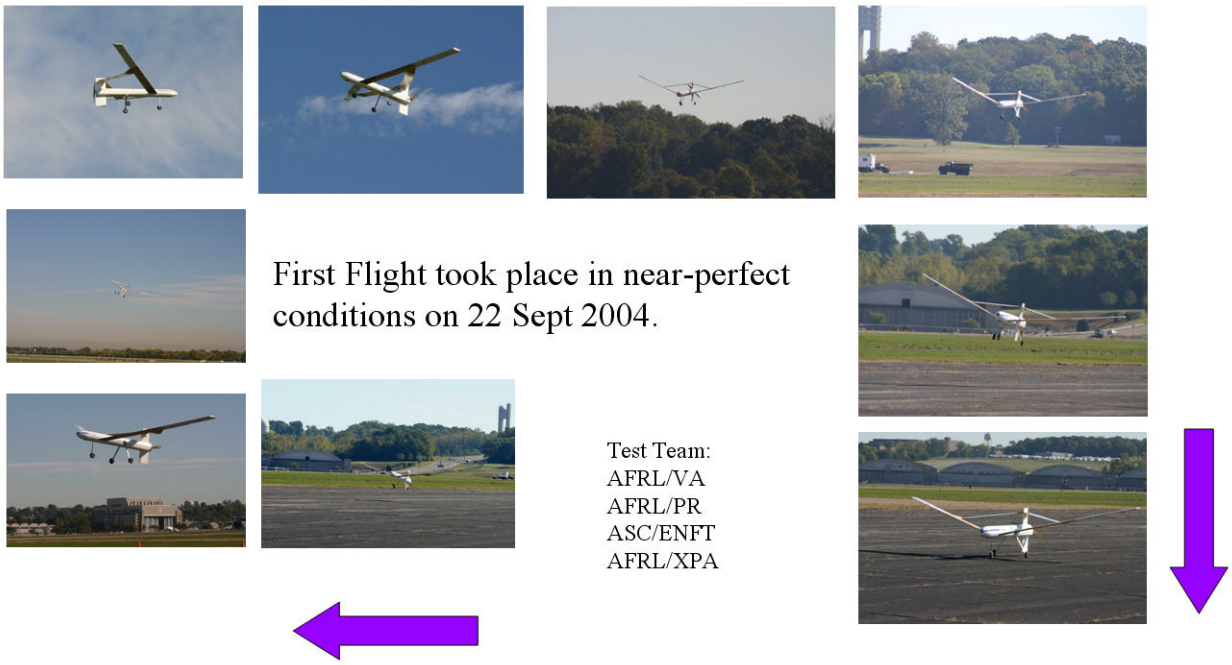


Figure (87) Sequence of Photos Depicting the First and Successful Flight

### 7.12.4. Test Date ( 22 September 2004) Flight Test – Card 5

The flight test video shows the following sequence of events leading to the hard landing. During a shallow right turn the starboard wing dipped slightly. The right hand bank became steeper as VA-1 lost altitude. VA-1 began to simultaneously pitch up and level its wings. Almost as soon as the wings became level, a loss of airspeed was noted and VA-1 descended quickly in an apparent stall while maintaining a small pitch angle. The plane was just beginning to pitch over when the ground came rushing up and the plane rotated as though to land on the main landing gear. Figure 1 shows VA-1 immediately prior to the hard landing.

The intent of this research is to shed light on the potential causes or contributing factors that led to the hard landing. As a result of the incident, questions arose regarding the dynamic stability and stall characteristics of VA-1. The apparent trigger event that led to the hard landing was the starboard wing dip in the shallow turn. The exact cause of the wing dip was unknown. Possible causes included a wind gust, pilot input, or a stall. Due to limited telemetry data it was difficult to figure out for sure.

On the day of the test winds were light and wind gusts unlikely. This potential cause will not be addressed in this study. If the aircraft was inherently unstable and difficult to fly, that increases the likelihood that pilot input may have been a contributing factor. A dynamic stability analysis would give insight into how difficult the plane was to fly. Insight into the stall of the inside wing in the turn theory could be studied by analyzing wing lift distribution with a vortex-lattice method computer code. This analysis would give the flight test team information to assess the risk of any potential future testing.

On another note, since VA-1 seemed underpowered despite having the most powerful electric motor practicable, methods to reduce drag were also requested. As a result the drag of the LVT and landing gear fairings were evaluated and their effect on stability considered.

Flight tests were suspended after the model landed hard after a stall during a turn maneuver.

## 7.13. Flight Test Data

The test team included two amateur photographers and two amateur videographers. Hundreds of photos and 6 video streams were recorded. The key photos are shown above in Figure xxx. The stall and hard landing are show below in Figure (88).

Figure (88) VA-1 Sequence After Stall was Encountered and Before Hard Landing

Data from the GPS unit is shown in the graph in Figure (89).

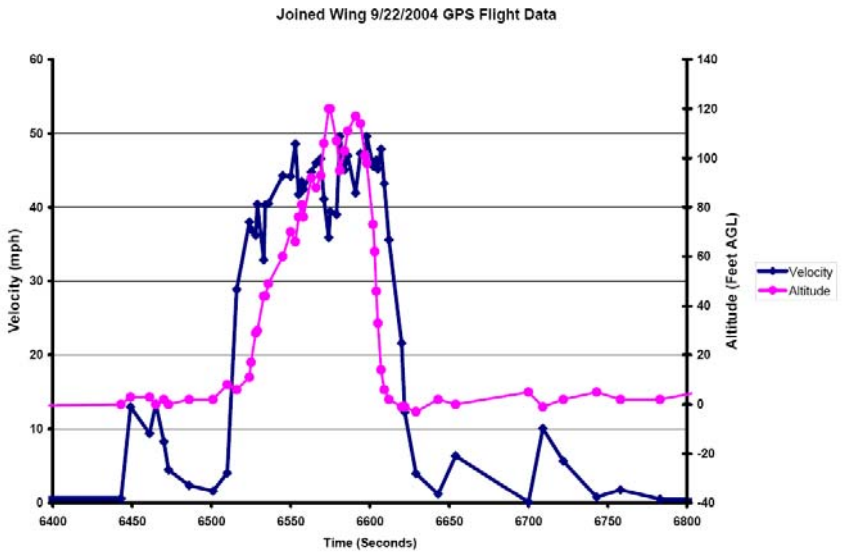


Figure (89) Velocity and Altitude Data from the First and Successful Flight Test

A special unit based on a Personal Digital Assistant (PDA e.g. Palm Pilot) was modified to collect GPS data. The modified PDA was installed on board for the second flight. It could not be made to function. It was removed. The flight test was conducted without any data recorder.

## 7.14. NOTES COLLECTED DURING PROGRAM DEVELOPMENT

Unanswered Questions

What is the minimum area for the kill zone that allows us to safely maneuver the vehicle without going outside the kill zone. Currently set at 3000 ft by 1500 ft.

What is the minimum altitude we can work within? What agreement does RAM have with WPAFB on maximum altitude?

Special Factors to Consider:

While the vehicle scale is unusually large, the weight definitely falls within the 55 lb limit set by the Academy of Aeronautics – the designated authority for FAA where RC sport flight is concerned.

The Joined-Wing concept will possibly be tested by the fabricator at a private facility of their choice. This is a necessary part of model development because there is the real possibility the vehicle controllability will need attention and modifications will be required before delivery to AFRL.

Responsibility and liability will rest with the fabricator until delivery. Responsibility and liability will transfer to WPAFB after model is officially delivered and ready to fly at WPAFB.

This is a research project. Failure is a real possibility. In spite of our best efforts – the kill zone is not an actual barrier – but rather a zone of operations outside of which we plan appropriate corrective (but not fail safe) action.

Worst Case Scenarios:

Airplane control is lost – airplane continues to fly out of sight and crashes far away and causes loss of life. What do we do? TBD

Since we will keep the altitude as low as possible (below 400 ft by AMA rules, normally 100 ft), it is likely an uncontrolled airplane will quickly crash within the WPAFB property – especially with pre-set failure mode in PCM radio gear (Max – find out how to say this intelligently)

Most likely outcome from a crash:

This has been experienced by many amateur RC fliers at the WPAFB RAM facility – including myself. We pick up pieces and go home. No hazardous materials beyond the NiCad batteries that will remain contained in any foreseeable scenario.

Pilot Visual of 14 ft aircraft at 3000 ft range – can he see it?

Early morning or late evening is usually the best time regarding wind. Depending on where the flight line is set up, sun location can be a problem for visibility. The current RAMS flight line faces towards Gate 22B, and in the morning the sun is right in our eyes. Moving to one of the other runways solves this problem.

1 mile visibility is plenty. If the radio is functioning properly, it will have range far in excess of visibility requirements. Typical RC operations are around a few hundred yards downrange...any farther and it becomes difficult for the pilot to discern the vehicle attitude.

Finally, has anyone weighed this beast lately with all the structural mods and data acquisition stuff. What is the current wing loading? I think good flying models in this size are about 25-30 oz/ft^2, but I'll double check that. Also, lateral stability is a major issue...have any mods been consider to increase yaw damping?

Your wind criteria seem to dictate early morning testing.

What's the max range from aircraft to ground controller? 1 mile vis is low when you're looking up into the sky for a small white thing.

Just a comment. Commanding roll does change heading ~ the lazyS that I talked about. I would NOT want to start off with a coordinated roll/yaw input to try to prevent heading change. Make sure that it is understood that the first test would be a roll one way and roll back at least to wings level, or even back to runway 'centerline' and then wings level. Can build up from that.

I had a thought for the test plan. One of the straight away hops could include a pilot commanded wing roll (without heading change) to check roll rate before we get into the turning flight phase. I figure a 30 deg bank to the left and right would do it. Maybe could consider a yaw input during another run as well.

I have some concerns with flight testing an unmanned vehicle at WPAFB. I still believe this flight testing should be conducted at a different, less populated area. Col Glen highway and the Air Force museum are too close to the proposed flight test area.

It is my understanding that most or all of the control systems and related equipment for the test vehicle are single thread - no back-up systems. I am assuming one transmitter, one receiver, one antenna for transmit and one antenna for receive, etc., for example. I also assume that there is no second battery back-up system for emergency situations - in the aircraft or the ground station.

To my knowledge, the transmitter frequencies are normal model airplane frequencies that anyone can have access to - including kids residing at Page Manor with model cars, air planes, and boats.

The joint wing test plan states that Col Glen highway is 800 ft from the runway and the test boundaries (from figure 4) appear to be half way or 400 ft to Col Glen highway. Following the Flight Termination (kill) Procedures indicated, the spotter will radio a warning the test director when the vehicle reaches the 200 ft caution zone. At 50 mph (73 ft / sec), rough calculations would indicate the test vehicle is 5 or 6 seconds from Col Glen highway. To my understanding, all the safety procedures and fail-safe procedures provided assume the pilot has control of the test vehicle. What happens if the pilot does not have control of the vehicle? The procedures indicate the PCM radio receiver is programmable to a fail-safe mode in the event radio signal is lost. This test fail safe will execute engine off and a slow turn. A failure on the aircraft (battery, electric actuator, etc) may not allow the fail safe to be implemented. Other information provided indicates a turning radius of 200 ft equates to a 2.0g turn at a bank angle of 40 degrees. A 2g turn seems a hard load on the test vehicle for the first flight.

The Flight Termination and (kill) Procedures indicate that the test is cleared to 400 ft altitude, and incremental testing will be done at 50 ft and below for the sake of safety. My concern is that Murphy's law is always with us. At some point in time, either the first flight or some other flight, the potential is always there for a failure to occur - especially with a new R&D airframe and a single thread system. Is AFRL ready to answer the questions about a mishap near WPAFB that has the potential for injury to non AFRL personnel?

Again, I think this is a great program with many potential payoffs. My comments above only indicate some of the potential failures or problems that can occur with flight testing new and innovative concepts. My concerns relate to a 26 pound vehicle traveling at 73 ft/sec and the public areas around WPAFB are only 10 to 20 seconds away at best. I strongly urge the flight test team to conduct the flight testing at a remote area.

You may or may not know that AFRL/VACC had an in-house Unmanned Research Vehicle (URV) effort. During the 15 or so years that VACC conducted research using the URVs I had several hats, some at the same time. Program Manager, Flight Test Director, Developing safe places to fly, Project lead for vehicle development, vehicle subsystems design and safety, Frequency Allocations, Ground Station Development, Vehicle and subsystems Pre-flight checks, are a few of my responsibilities during the URV efforts. Most of the flight testing was accomplished with vehicles developed in-house. The first type vehicle, Lambda, weighed 250 lbs with a wing span of 14 ft and a payload of 25 lbs. The second type vehicle, Gamma, weighed 500 lbs with a wing span of 18 ft and a payload of 150 lbs.

I've reprogrammed the radio as follows:

| Tx Channel | Joined Wing Function |
|---|---|
| Throttle | Throttle |
| Aileron | Inboard Aileron Y Harness |
| Elevator | Aft Elevator Y Harness |
| Rudder | Rudder |
| Gear | empty |
| Aux 1 | Left Outboard Elevator |
| Aux 2 | Right Outboard Elevator |
| Aux 3 | Nose Steering |

I've reset all the dual rates and volumes to 100%, no expo, and set the subtrims to zero.

I've set up the following mixing:

| | |
|---|---|
| Mix 1 | Rudder -> Aux 3, always on….slaves nose gear to rudder |
| Mix 2 | empty |
| Mix 3 | Elev -> Aux 1, always on…slaves left outboard elevator to aft elevator |
| Mix 4 | Elev -> Aux 2, always on…slaves right outboard elevator to aft elevator |
| Mix 5 | Ail -> Aux 1, switch on…slaves left outboard elevator to aileron in emergency |
| Mix 6 | Ail -> Aux 2, switch on…slaves right outboard elevator to aileron in emergency |

This is the only way I could think to do the emergency ailevator control mode with the current servo wiring setup. I'm not sure if you can control a slaved channel with two separate driver channels…I guess we'll see.

I have a briefing over at AFMC HQ from 1330-1430 today, and I'll be busy getting ready for that this morning. I may go do a quick test of the mixing setup around lunch time, but plan to be over there at 1500 to really start working the setup.

# 8. The Next Step: An Aeroelastically-Scaled Flight Test [34]

This Section presents design plans for a low-cost aeroelastically scaled flight test concept that will significantly reduce developmental risk for a joined-wing SensorCraft variant. Initial flight tests and plans for aeroelastic scaling on a half-span wind tunnel model and full-span remotely piloted model are discussed. One of these test vehicles will provide the opportunity to modify and calibrate existing aeroelastic test practices to account for non-linear structural responses. Non-linear scaling procedures will focus on replicating deflections due to the worst case flight conditions in the envelope, the gust response. Linear scaling will be based on dynamic response at this condition to include investigation of flutter instabilities. To the degree that all linear elastic dynamics are scaled, the geometric nonlinear deformations should scale automatically.

Scaled aeroelastic models are often associated with flutter clearance and are considered critical in developing new aircraft configurations and typically involves the development and testing of dynamically and aeroelastically scaled wind tunnel models prior to full-scale prototype development. Rather than flutter, the scaled aeroelastic model proposed here should target its scaling procedure to replicate the critical dynamic gust response.

Conventional wisdom tells us that experimental aeroelasticity is expensive and typically involves flight testing of the full-scale aircraft. Modern aircraft may benefit from an increased emphasis on wind-tunnel testing of scaled models. In this Section, the proposed scaled aeroelastic model is inexpensive from a materials perspective. And the low aircraft cost will be dominated by the cost of electronics. Cost growth will be primarily driven by the time required to design the flight vehicle and time to carry out the test plan.

This Section describes how the classical aeroelastic scaling laws are applied when developing scaled models. Scaling a model such that it is dynamically similar to an aircraft requires that its characteristics under steady loads match those of the aircraft. A model that is statically scaled to flight vehicle deflects to the same shape and with scaled magnitude under scaled static loads. Relevant assumptions, restrictions, limitations and implications of this methodology are also discussed.

## 8.1. Scaled Flight Test Conceptual Design Concept

The Boeing Company has focused significant effort in the design of a joined-wing concept to meet the agreed performance requirements by the SensorCraft team. While the mission of the Air Force Research Lab is strictly *technology development*, the SensorCraft team serves that mission by integrating technology concepts into a larger system. The Boeing SensorCraft concept represents their integrating concept. The various technologies address (a) ISR Sensor Performance (b) High Altitude Propulsive Capability (c) Aero-Performance Enhancements (d) Emerging Structural Concepts. The Boeing Joined-Wing configuration is a bold step forward in the realm of research and development. This configuration naturally accommodates a persistent 360-degree field of view for sensor development. Other unsubstantiated benefits include increased pitch authority for enhanced aeroservoelastic stability. However, there are also technical risk factors involving unprecedented aeroelastic response modes with inherent geometric non-linearities.

The aeroelastic response of the joined-wing is not well established and a number of validation tests should be considered. Full-scale testing for any large SensorCraft vehicle is likely risky and

expensive. Reduced scale testing may provide significant confidence in our ability to safely operate SensorCraft vehicles.

The geometric non-linearity of a joined-wing structure affects all aspects of the design.

So what kind of aeroelastic testing would best serve to advance joined-wing technology at this point in time? The traditional approach is to design/build/test an aeroelastically scaled wind tunnel model. Carefully controlled conditions in the wind tunnel reduce test risk factors. At the same time, wind tunnel testing is fairly expensive and the environment is somewhat artificial.

An aeroelastically scaled flight test article would not be tested in a carefully controlled environment. However, gusty conditions are readily found and may be measured. Indeed, the sport of slope soaring for gliders depends on a regular source of updraft to operate. Aeroelastic flight testing may be feasible where wind direction is steady and predictable. Steady wind over large ground obstacles provide a regular source of updraft suitable for flight testing gust alleviation technologies.

New electronic and propulsion technologies are flooding the scaled flight market in the form of autonomous flight systems, data acquisition systems, sensors, telemetry and even jet turbine engines. It may prove economically desirable to produce an aeroelastically scaled flight test representation of the Boeing joined-wing SensorCraft. The first step toward such a conclusion calls for a conceptual design study. The purpose of this paper is to produce such a design.

Another approach may produce a single scaled design that could be wind-tunnel tested (half-span) for calibration and flight tested for validation. In any case, this paper offers a conceptual design of a low cost (low risk) aeroelastically scaled flight test concept in order to support management planning with future tests of SensorCraft technologies.

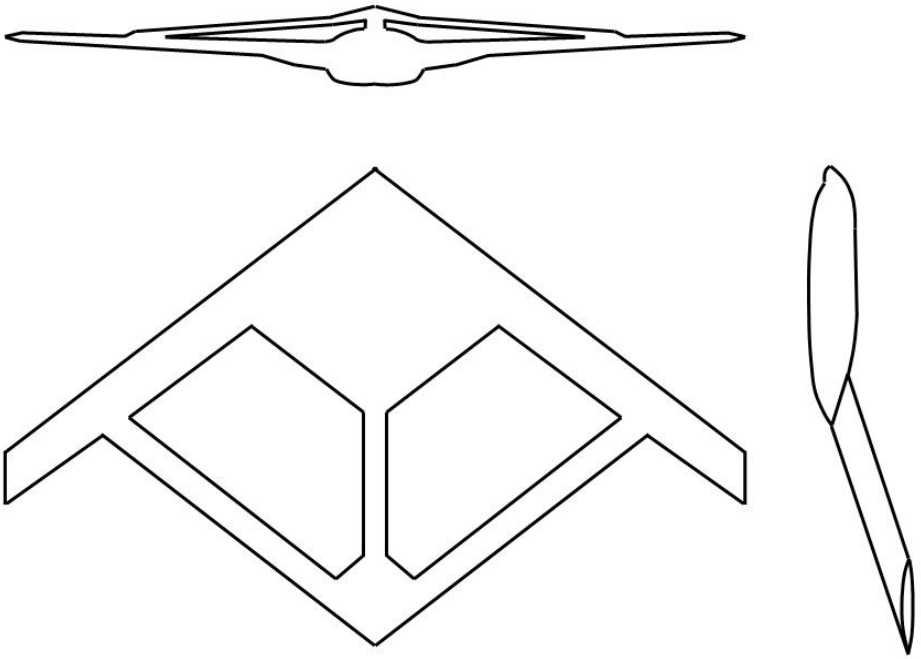

Figure (90) Three-View Schematic of Boeing SensorCraft

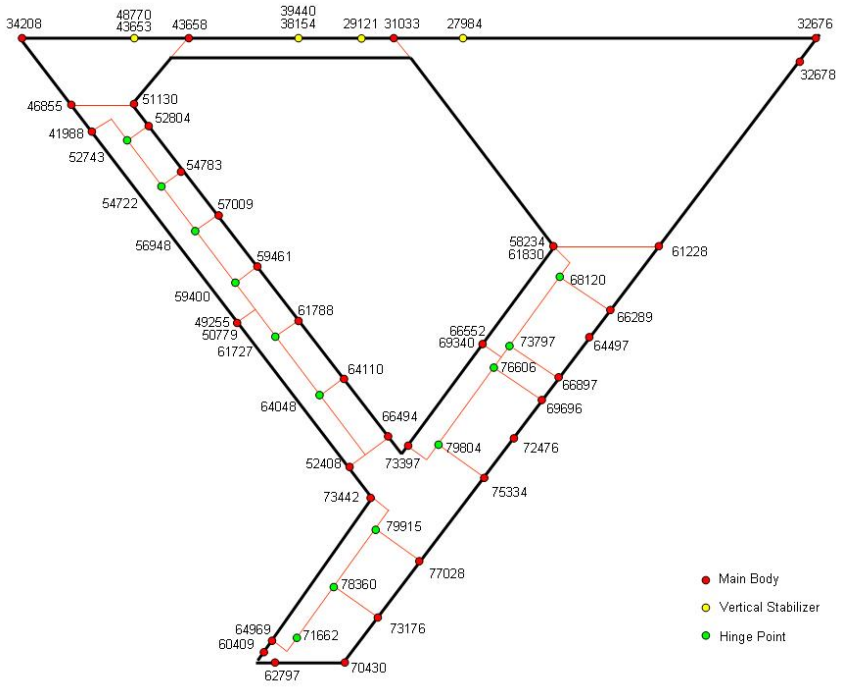


Figure (91) Reduced Eigenvector Set for Scaling

### 8.1.1. Baseline Model

Figure (90) is an accurate three view sketch of the Boeing joined-wing concept. The wings span 150 ft tip-to-tip. Boeing has completed extensive design study involving aerodynamic and structural optimization. The Boeing Company delivered an extensive finite element model to the AFRL as their input to the AFRL Joined-Wing research team. The AFRL in-house team has reduced that model to a more manageable set in order to simplify the scaling process as discussed below. Key points are located in Figure (91). The first three modes of vibration are depicted in Figure (92). Table (29) lists the free vibration frequencies for the baseline FEM with a fixed point on the fuselage. Clearly, there are many closely spaced frequencies that present aeroelastic challenges. The aeroelastic scaling procedure is described in the following section.

The joined-wing configuration does not lend itself to a natural separation between symmetric and anti-symmetric aeroelastic modes. We can artificially enforce a vertical plane of symmetry to generate symmetric modes of vibration. However, the remaining modes of vibration tend to oscillate the vertical tail in a lateral (i.e. not anti-symmetric) direction. This asymmetric quality motivates us to avoid half-plane wind tunnel models or at least account for this movement with a roller-type support. Thus, it can move fore, aft and vertically along the wind tunnel wall.

When it comes to reducing uncertainty and risk with joined-wing technology, we need to consider all the possible modes of uncertainty. Flight testing the joined-wing will reveal response mechanisms associated with lateral gust input. Of course, the risk factors increase with flight testing. However, with a proper design study, the cost of flight testing may prove advantageous. Many factors come into play including choice of flight test facility.

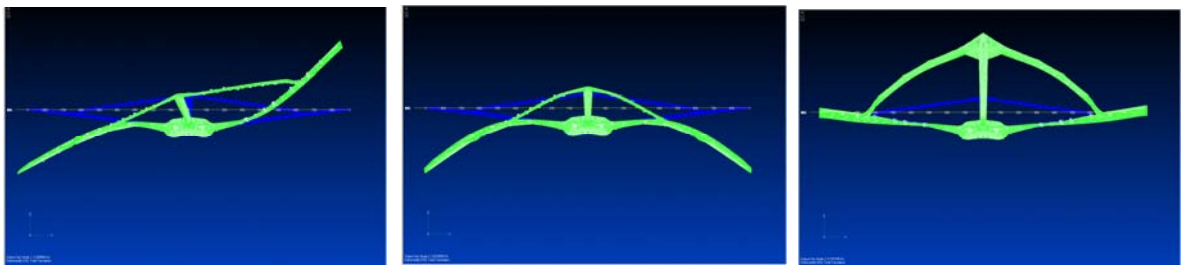

Figure (92) First Three Mode Shapes for Scaling

| Mode | Frequency (HZ) |
|---|---|
| 1 | 3.995681E-01 |
| 2 | 6.786585E-01 |
| 3 | 7.537054E-01 |
| 4 | 1.234790E+00 |
| 5 | 1.536691E+00 |
| 6 | 1.634070E+00 |
| 7 | 2.039813E+00 |
| 8 | 2.195891E+00 |
| 9 | 3.311272E+00 |
| 10 | 3.503062E+00 |

| Mode | Frequency (HZ) |
|---|---|
| 11 | 4.141252E+00 |
| 12 | 4.749025E+00 |
| 13 | 5.003888E+00 |
| 14 | 5.321827E+00 |
| 15 | 5.857614E+00 |
| 16 | 5.859805E+00 |
| 17 | 5.868320E+00 |
| 18 | 5.875937E+00 |
| 19 | 5.876733E+00 |
| 20 | 5.880007E+00 |

Table (29) SensorCraft Natural Frequencies

## 8.2. Design of the Scaled Flight Article

In addition to scaling based on physics, aeroelastic testing requires the development of a flight-worthy concept. The AFRL-led team is developing design processes that account for both perspectives simultaneously. A flight test concept requires consideration of all flight metrics beginning with vehicle weight, thrust, drag, trim and 3 axis maneuverability including takeoff, cruise and landing operations in unsettled atmosphere.

Figure (93) Oblique View of In House Scaled Concept

Figure (94) Three-View of In-House Scaled Concept

The scaled configuration will closely resemble the aerodynamic shell of the full scale concept depicted in Figure (93) and Figure (94). The interior structural layout will not resemble the full-scale design. An aeroelastic scaled design will reproduce the exterior deformations under scaled aerodynamic loads. The scaled design is not intended to reproduce the structural load paths or to scale structural failure. As indicated later, the scaled aerodynamic design is achievable on the basis of linear aerodynamic theory. With this in mind, the scaled aeroelastic response will not be significantly altered with choice of airfoil thickness, an important design freedom where wing flexibility is a challenge to achieve. The concept depicted in Figure (94) will require jet propulsion, either in the form of a pair of ducted fans or a pair of more powerful micro-jet turbines. Specifications for an assortment of micro-jets are presented in Table (30).

| AMT-USA<br>Cincinnati OH | AT180 SP | AT280 SP | AT400 | AT450 |
|---|---|---|---|---|
| Diameter (in) | 3.9 | 4.7 | 4.7 | 5.1 |
| Length (in) | 8.9 | 10.6 | 10.6 | 10.6 |
| Weight (lbs) | 3.1 | 4.6 | 5.1 | 5.3 |
| Thrust (Lbf @ KRPM) | 20 @ 152.6 | 30 @ 117.5 | 38 @ 115.5 | 45 @ 112.0 |
| Max Rotation (KRPM) | 159.0 | 121.0 | 117.5 | 112.0 |

Table (30) Specifications on an Assortment of Micro-Turbines from AMT-USA

### 8.2.1. Aeroelastic Scaling

Experimental testing provides hard evidence for designs based on ideas and expectations. Scaled testing provides significant cost reduction while reducing uncertainty. But these savings come

with a compromise, because the art of scaled testing is based on Computational Physics. In other words, a scaled test is no better than the faith one puts in a "governing" set of equations. This faith is actually substantiated with the formalized processes of verification and validation. In the developments that follow here, we assume the scaling is "governed" by the differential equations associated with Continuum Mechanics. Computational Physics views the world in terms of kinematics and dynamics that can, in turn, be decomposed into a system of equations that relate any output to any input.

For the joined-wing concept, there is significant uncertainty associated with geometric non-linear structures undergoing large deformation in a maneuvering aerodynamic state. The strategy for a scaled flight experiment is rationalized in the following paragraphs.

Conversely, given a set on non-dimensional equations, the key to the non-dimensional formulae are the dimensional characteristics. If one constructs a reduced scale model with the same non-dimensional parameters as the full-scale article, then the equations of motion will be the same. Thus, the response of the reduced scale model will be identical to the response of the full scale model in the context of the scientific principles that create the "governing" equations.

With high-speed computers, we are able to solve these "governing" equations with significant accuracy, thus avoiding many tests altogether. However, scaled testing is still very useful for a number of reasons.

- Validation and calibration of computational models
- Uncover unexpected phenomena
- Test run for development of competent and coordinated test team for full scale article.

Scaled testing involves a number of trade considerations between cost and accuracy. In general, all effects cannot be scaled with the same test model. Aeroelastic scaling is a combination of geometric scaling, structural scaling and aerodynamic scaling. One of the predominant effects that benefit with scaling is the aerodynamics. In the context of the SensorCraft program, what physical mechanics can we reasonably expect to scale with test models? We start looking at the non-dimensional aerodynamic parameters.

In the past, aeroelastic scaling has been utilized in the design of static aeroelastic wind-tunnel models. For instance, the Forward-Swept Wing tests were used to validate computational aeroelastic optimization programs and led to the X-29 Flight Test Program. Two wind-tunnel models were designed, built and tested with material distribution that scales static aeroelastic deformation. While little is reported on the scaling strategy, one can refer to [40] [Bisplinghoff et. al. 1955] Chapter 11 for a formal description of similarity laws. With aeroelastic scaling, the structural loads arise with aerodynamic pressures that can be modeled with an aerodynamic system of equations. The (linear or non-linear) aerodynamic system can be non-dimensionalized and the system inputs (boundary conditions to the PDE) are functions of non-dimensionalized geometry. Thus, input for the combined aerodynamic and structural (i.e. aeroelastic) system is cast in terms of displacements (e.g. flap setting etc).

### 8.2.2. Stiffness Scaling

We are given a full-scale baseline structure that deforms under load. In this study, we are interested to design a geometrically scaled test model with scaled deformation in response to scaled pressure. The deformation scaling is determined by the geometric scale. Subsequently, we

design the model with a new material distribution. At the same time, we are required to determine a scaled load distribution that produces the scaled deformation. Thus, the scaled model can be designed such that both full and scaled articles deform identically under scaled loads.

Careful attention must be given to the development of scaled models that mimic geometrically non-linear structures. An extended discussion on geometric non-linear beam structures is published in [38] and [39]. Free vibration modes and mode shapes can be scaled [41]. The mechanics of beam buckling can also be scaled [41]. However, in a scaling procedure for which every free vibration mode (and model shape) is perfectly scaled, then it is likely (but not proven) the stiffness properties will be scaled to replicate both vibration and buckling phenomena. However, in a practical scaling procedure, relatively few modes can be scaled and therefore it makes sense to focus on scaling the lowest free vibration frequencies and modes AND simultaneously the lowest modal buckling loads and modes. With beam buckling scaled, we are able to extrapolate and explore the role of geometrically non-linear structures in an aeroelastic system. If it is not practical to scale vibration and buckling modes simultaneously, then it might be possible to scale linear loads that re-create the critical buckled shapes.

### 8.2.3. Aerodynamic Scaling

For aerodynamically scaled wind tunnel models, the geometric accuracy and atmospheric composition are desirable design attributes. The quality of these attributes is constrained by the cost of model fabrication and the test facility operation. The aerodynamic scaling procedure is derived from computational aerodynamics and the associated partial differential equations (PDE). The design of the aerodynamically scaled model may be governed by small disturbance incompressible linear potential PDE for the simplest case. A scaled model based on the Navier-Stokes PDE's is much more difficult to achieve.

The Navier-Stokes equations are non-dimensionalized in terms of Reynolds Number (viscous effects) and Mach Number (compressibility effects). Reynolds number is $Re = \rho VL/\mu$. Thus, for an airplane flying at high altitude (low $\rho$) and large chord (high L), we are able to maintain Re with a much smaller model (low L) at low altitude (high $\rho$). Mach is the ratio of vehicle speed (V) and speed of sound (c). Thus for an airplane flying at high altitude (low $c = c_0$) at velocity $V_0$, we can maintain Mach scaling with a model flying at low altitude (high $c = c_1$) at velocity $V_1 > V_0$ or $V_1 = V_0\, c_1/ c_0$ . For Reynolds scaling we enforce $\rho_1\, c_1 L/\mu_1 = \rho_0\, c_0 L/\mu_0$ .

Each row in Table (31) represents a different scaled design, flown at sea level. Each scale mimics an incrementally higher altitude baseline (full scale) design through geometric and mass scaling. Air density $\rho$ and viscosity $\mu$ vary with altitude.

For geometric scaling, we consider both the scale of the model AND the attitude of the model with respect to the flow. While this is trivial for wind tunnel testing, in scaled flight testing we must trim the vehicle at the same attitude for both full and scaled condition. Thus, at low altitudes (high density and high dynamic pressure), more weight is required to achieve the same trimmed angle of attack.

| Flight Test Altitude (km/kft) | Geometric Scale Factor (%) | Wing Span (ft) | Wing Chord (in) | Scaled Weight (lbs) | Vehicle Volume (in3) / Density (lb/ in3) |
|---|---|---|---|---|---|
| 0/0 | 7.8 | 15.6 | 7.68 | 1.24E4 | 7.26E+3 / 1.71E+0 |
| 3/10 | 10.3 | 20.6 | 10.03 | 1.49E4 | 1.67E+4 / 8.91E-1 |
| 6/20 | 13.8 | 27.6 | 13.58 | 1.75E4 | 4.02E+4 / 4.35E-1 |
| 9/30 | 19.1 | 38.2 | 18.80 | 2.25E4 | 1.06E+5 / 2.11E-1 |
| 12/40 | 28.2 | 56.4 | 27.75 | 3.09E4 | 3.43E+5 / 9.00E-2 |
| 20/65 | 100.0 | 200.0 | 98.43 | 1.25E5 | 1.53E+7 / 8.10E-3 |

Table (31) Consequences of Aerodynamic Scaling for Flight Testing

In Table (31), it is clear that as the geometric scale is reduced, combined Reynolds Number and Mach scaling becomes prohibitive for flight testing. But it is not so much a problem with Reynolds Number and Mach as is achieving the correct vehicle attitude. For the baseline model at high altitude, the vehicle is at high angle-of-attack to achieve sufficient lift for trimmed level flight. In order to achieve the same high angle-of-attack in trimmed flight for the scaled flight test requires a very heavy vehicle to offset the very dense air at low altitude (consequently high dynamic pressure and the very high lift).

We are constrained to geometrically scaled flight models that are inexpensive to build and operate. We are considering $1/8^{th}$ geometric scale on the Boeing SensorCraft baseline with a 165-foot span. The resulting 21-foot span vehicle is significantly constrained on the level of scaling that can be achieved in flight test. In effect, our aerodynamic scaling will be governed by the small disturbance linear potential PDE. This means we are admitting linear superposition at modest angles-of-attack. Yet, these limited physics are adequate to begin low-cost exploration of flight mechanics for an aeroelastically scaled joined-wing SensorCraft in gust conditions. We believe this proposed scaled flight test will validate evolving design and analysis techniques related to the aeroelastic response of a Joined-Wing SensorCraft. Indeed, the proposed simplifications still result in a significantly complex aeroelastic flight system.

For aeroelastically scaled models we start with standard aerodynamic scaling parameters that non-dimensionalize the (generalized) aerodynamic loads and the boundary conditions (due to deformation). Subsequently, the structural dynamic components are scaled to create a system of non-dimensional aeroelastic equations of motion. The non-dimensional equations of motion for the full scale aeroelastic baseline can also represent a reduced scale aeroelastic model. Thus, the scale model will replicate the aeroelastic response of the full scale within the limits assumed by physics as represented by the equations of motion.

So, we start by scaling the aerodynamic aspects of our aeroelastic experiment according to the linear small disturbance potential PDE, derived in Reference [59] and in Reference [40] as equation (5-44) and shown here in non-dimensional form with $\bar{\phi}(x,y,z,t)$ representing the velocity potential.

(23) $$(1-M^2)\bar{\phi}_{\xi\xi}+\bar{\phi}_{\eta\eta}+\bar{\phi}_{\zeta\zeta}-2M^2\bar{\phi}_{\xi\tau}-M^2\bar{\phi}_{\tau\tau}=0$$

The boundary condition for this PDE simply enforces tangential flow over the vehicle surface (in addition to special wake conditions). The pressure on the vehicle surface is used to calculate

loads on the structural model. Once this PDE is solved for the potential field $\phi(x,y,z,t)$ , the pressure is simply computed with derivatives with respect to time and $\xi$ as follows.

$$\bar{p} = \bar{\phi}_\tau + \bar{\phi}_\xi \tag{24}$$

The non-dimensional scaling parameters were derived using the Buckingham Pi Theorem discussed in Reference [40] Chapter 11-3 and Appendix A of Reference [60]. The non-dimensional quantities (with over-bar) are related to dimensional counterparts as follow:

$$\bar{p} = \frac{p}{\rho U^2}; \qquad \xi = \frac{x}{b}; \quad \tau = \frac{tU}{B}; \quad \bar{\phi} = \frac{\phi}{UL}; \quad k = \frac{\omega b}{U} \tag{25}$$

The non-dimensional aerodynamic force coefficient $C_i$ (in the direction of Cartesian component $x_i$) in equation (26) is an integral of the pressure over the area $A(\xi, \eta)$. Parameters $\xi$ and $\eta$ span the surface. Here, we cast the non-dimensional pressure as a function of $\xi$ and $\eta$. Also, $J$ is the Jacobean transformation that relates the differential area in physical coordinates to $[d\xi\, d\eta]$. The parameter $A_R$ is the reference area. The unit vector $n$ is the surface normal at $(\xi, \eta)$. The unit vector $x_i$ is the Cartesian unit vector pointing in direction associated with aerodynamic force coefficient $C_i$.

$$C_i = \left(\frac{1}{A_R}\right) \int_{A(\xi,\eta)} \left\{ \left[ \hat{n} \bullet \hat{x}_i \right] \bar{p}(\xi,\eta) J d\xi \right\} d\eta \tag{26}$$

In order to simplify the meaning of equation (26), we simply exemplify for a wing in the x-y plane. The non-dimensional lift coefficient for a force in the z direction is:

$$C_L = \left(\frac{1}{A_R}\right) \int_{A(x,y)} \bar{p}(x,y) dA \tag{27}$$

While we have some intuitive sense of forces and aerodynamic force coefficients, the concept of generalized forces is not commonly appreciated. The need for generalized forces arises with structural dynamics and is firmly based on energy methods. Each component of generalized force is associated with the energy that arises with the associated generalized displacement. In aeroelastic solutions, the common practice is to incorporate the smallest set of modal displacements as the basis for the set of admissible generalized displacements.

Thus, the set of aerodynamic forces is enlarged to include not only rigid lift, drag, sideforce and moments, but also includes a generalized (or modal) force for each admissible modal displacement. The mode shape associated with rigid plunge is simply a unit displacement everywhere in the z direction. Thus, equation (26) actually represents a generalized force associated with rigid plunge for $i$=3. For a simple bending shape, the associated generalized force for bending is achieved by weighting equation (26) by the bending displacement function $\vec{W}_I(\xi,\eta)$.

$$C_I = \left(\frac{1}{A_R}\right) \int_{A(\xi,\eta)} \left\{ \left[ \hat{n} \bullet \vec{W}_I(\xi,\eta) \right] \bar{p}(\xi,\eta) J d\xi \right\} d\eta \tag{28}$$

### 8.2.4. Working with Modal Coordinates – The Homogeneous Solution to the PDE

At this point, we shift back to the equations of motion in order to fold in the aerodynamic forces. Equation (29) represents a classical linear dynamic system with two generalized coordinates ($x_1$ and $x_2$) and any time varying force $f_1(t)$ and $f_2(t)$. The units on $x_1$ may be either linear displacement or rotation. Independently, $x_2$ may be either displacement or rotation. The force $f_i(t)$ could be a harmonic forcing functions with amplitude $Q_1$ and $Q_2$. The stiffness terms $k_{ij}$ are generalized stiffness terms and $m_{ij}$ are generalized mass normalized to the total mass.

$$(29) \quad \begin{bmatrix} m_{11} & m_{12} \\ m_{21} & m_{22} \end{bmatrix} \begin{Bmatrix} \ddot{x}_1(t) \\ \ddot{x}_{21}(t) \end{Bmatrix} + \begin{bmatrix} k_{11} & k_{12} \\ k_{21} & k_{22} \end{bmatrix} \begin{Bmatrix} x_1(t) \\ x_2(t) \end{Bmatrix} = \begin{Bmatrix} f_1(t) \\ f_2(t) \end{Bmatrix} = \begin{Bmatrix} Q_1 \\ Q_2 \end{Bmatrix} e^{i\omega t}$$

The classical solution to a linear systems of partial differential equations is to first solve the homogenous (unforced) system, then the particular (forced) solution and finally address the undetermined constant coefficients in the total solution (combined unforced and forced) by enforcing the initial conditions. The homogeneous system PDE is

$$(30) \quad \begin{bmatrix} m_{11} & m_{12} \\ m_{21} & m_{22} \end{bmatrix} \begin{Bmatrix} \ddot{x}_1(t) \\ \ddot{x}_{21}(t) \end{Bmatrix} + \begin{bmatrix} k_{11} & k_{12} \\ k_{21} & k_{22} \end{bmatrix} \begin{Bmatrix} x_1(t) \\ x_2(t) \end{Bmatrix} = \begin{Bmatrix} 0 \\ 0 \end{Bmatrix}$$

Using the method of separation of variables, the solution is cast into the following eigenvalue problem

$$(31) \quad \left[ -\omega^2 \begin{bmatrix} m_{11} & m_{12} \\ m_{21} & m_{22} \end{bmatrix} + \begin{bmatrix} k_{11} & k_{12} \\ k_{21} & k_{22} \end{bmatrix} \right] \begin{Bmatrix} X_1 \\ X_2 \end{Bmatrix} e^{i\omega t} = \begin{Bmatrix} 0 \\ 0 \end{Bmatrix}$$

The eigenvalues $\omega_i$ and the associated eigenvectors $[U] = \lfloor \{u_1\} \{u_2\} \rfloor$ provide a basis for transformation $[U]$ to a system of modal coordinates such that

$$(32) \quad \lfloor X_1, X_2 \rfloor^T = [U] \lfloor \delta_1, \delta_2 \rfloor^T$$

Each eigenvector in [U] can be scaled as desired with a constant. The units in [U] are consistent with whatever is required to transform dimensional $X_i$ non-dimensional $\delta_i$. Equation (31) is transformed with Equation (32) by pre-and-post multiplying with the orthonormalized-scaled $[U]^T$ to produce the following:

$$(33) \quad \frac{1}{m_R} \left[ -\omega^2 \begin{bmatrix} 1 & 0 \\ 0 & 1 \end{bmatrix} + \begin{bmatrix} \omega_1^2 & 0 \\ 0 & \omega_2^2 \end{bmatrix} \right] \begin{Bmatrix} \delta_1 \\ \delta_2 \end{Bmatrix} e^{i\omega t} = \begin{Bmatrix} 0 \\ 0 \end{Bmatrix}$$

Parameter $m_R$ is the reference (or total) mass. The mass and stiffness representations for the joined-wing in Figure (93) generated the modal transformation of Equation (32) and thereby forming Equation (33). The eigen-solution to the eigenvalue problem in Equation (31) is the basis for the transient component of the total solution starting from the initial condition. In a similar fashion to equation (9), an eigenvalue for buckling may be formed.

$$(34) \quad \left[ \begin{bmatrix} k_{11} & k_{12} \\ k_{21} & k_{22} \end{bmatrix} \right] - \lambda \begin{bmatrix} k_{G11} & k_{G12} \\ k_{G21} & k_{G22} \end{bmatrix} \begin{Bmatrix} \overline{X}_1 \\ \overline{X}_2 \end{Bmatrix} = \begin{Bmatrix} 0 \\ 0 \end{Bmatrix}$$

where the terms $k_{Gij}$ represent the geometric stiffness. The geometric stiffness effect may be incorporated into the aeroelastic response, as well. This paper addresses the design of a scaled model that replicates the aeroelastic gust response. This is primarily driven by the solution to the PDE for the aeroelastic system.

### 8.2.5. Solving the Aeroelastic Equations in Scaled Form

Next, we form a linear system of PDE for the aeroelastic system. A classical aeroelastic system replaces the force amplitude terms in Equation (29) with harmonic forces in terms of non-dimensional complex (real and imaginary components) aerodynamic influence coefficients $\bar{Q}_{ij}(k)$.

$$(35) \quad \left[\begin{bmatrix} k_{11} & k_{12} \\ k_{21} & k_{22} \end{bmatrix} - \lambda \begin{bmatrix} k_{G11} & k_{G12} \\ k_{G21} & k_{G22} \end{bmatrix} - \omega^2 \begin{bmatrix} m_{11} & m_{21} \\ m_{12} & m_{22} \end{bmatrix} - qA \begin{bmatrix} \bar{Q}_{11}(k) & \bar{Q}_{12}(k) \\ \bar{Q}_{21}(k) & \bar{Q}_{22}(k) \end{bmatrix}\right] \begin{Bmatrix} X_1 \\ X_2 \end{Bmatrix} e^{i\omega t} = \begin{Bmatrix} 0 \\ 0 \end{Bmatrix}$$

Each row in equation (35) is in units of a generalized force. A generalized force is related to a generalized displacement through integration. For example, a lift force is a generalized force associated with vertical displacement. A moment is a generalized force associated with a small rotation.

Each scalar in each matrix represents a generalized force per generalized displacement. For example, the quantity $[qA\,\bar{Q}_{ij}(k)]$ is in units of force/length (load/displacement). Thus, each $qA\bar{Q}_{ij}(k)$ is an aerodynamic sensitivity of non-dimensionalized force with respect to displacement. For example, if our aeroelastic system represents a simple airfoil with $x_1$ representing vertical plunge and $x_2$ representing airfoil twist, then the quantity $[qA\,\bar{Q}_{12}(k)]$ is the lift due to twist or for static conditions, the standard lift curve slope (or the lift due to angle-of-attack). The argument $k$ is the reduced frequency $k = (\omega b/U)$. The reduced frequency $k$ is non-dimensional and represents the number of oscillations in the time it takes to traverse distance $b$ with velocity $U$.

Here, $q = \rho U^2/2$ is the dynamic pressure, $\rho$ is the air density, $U$ is the free stream velocity and A is a reference area such as the wing planform area. The $x_i(t)$ are the system degrees of freedom. With this two degree-of-freedom (dof) matrix equation, we can represent an aeroelastic airfoil section with plunge and pitch degrees of freedom. The same matrix equation could represent a wing with a simple bending ($x_1$) and torsion ($x_2$) generalized degrees of freedom.

The next step in solving ODE equation (35) is to assume the system response is the same harmonic form as the forcing function. The result is a homogeneous equation for the aeroelastic system.

$$(36) \quad \left[\begin{bmatrix} k_{11} & k_{12} \\ k_{21} & k_{22} \end{bmatrix} - \lambda \begin{bmatrix} k_{G11} & k_{G12} \\ k_{G21} & k_{G22} \end{bmatrix} - \omega^2 \begin{bmatrix} m_{11} & m_{21} \\ m_{12} & m_{22} \end{bmatrix} - qA \begin{bmatrix} \bar{Q}_{11}(k) & \bar{Q}_{12}(k) \\ \bar{Q}_{21}(k) & \bar{Q}_{22}(k) \end{bmatrix}\right] \begin{Bmatrix} X_1 \\ X_2 \end{Bmatrix} e^{i\omega t} = \begin{Bmatrix} 0 \\ 0 \end{Bmatrix}$$

Ongoing work uses equation (36) as the basis for scaling the models shown in Figure (91).

### 8.2.6. Controlling the Model

If our aeroelastic system for a wing is appended with a control surface, ignoring geometric stiffness for the time-being, the aeroelastic system takes the following form with $\delta$ representing the control surface displacement.

$$(37)\quad \left[\begin{bmatrix} k_{11} & k_{21} & 0 \\ k_{12} & k_{22} & 0 \\ 0 & 0 & 0 \end{bmatrix} - \omega^2 \begin{bmatrix} m_{11} & m_{21} & m_{13} \\ m_{12} & m_{22} & m_{23} \\ m_{31} & m_{32} & m_{33} \end{bmatrix}\right]\begin{Bmatrix} x_1 \\ x_2 \\ \delta \end{Bmatrix} = qA\begin{bmatrix} Q_{11}(k) & Q_{12}(k) & Q_{1\delta}(k) \\ Q_{21}(k) & Q_{22}(k) & Q_{2\delta}(k) \\ Q_{\delta 1}(k) & Q_{\delta 2}(k) & Q_{\delta\delta}(k) \end{bmatrix}\begin{Bmatrix} x_1 \\ x_2 \\ \delta \end{Bmatrix}$$

Using the same orthonormalized eigenvectors $\{u\}_i$ from the uncontrolled system, we arrive at the non-dimensional equations of motion (EOM) for the controlled system. We should consider designing the scaled system as if the control surface dynamics can be treated as independent input to the system. This is represented in the following EOM.

$$(38)\quad \left[\begin{bmatrix} \frac{b^2\omega_1^2}{U^2} & 0 & 0 \\ 0 & \frac{b^2\omega_1^2}{U^2} & 0 \end{bmatrix} - \left(\frac{b^2\omega^2}{U^2}\right)\begin{bmatrix} 1 & 0 & \overline{m}_{1\delta} \\ 0 & 1 & \overline{m}_{2\delta} \end{bmatrix} - \left(\frac{\rho Ab}{2m}\right)\begin{bmatrix} \overline{Q}_{11}(k) & \overline{Q}_{12}(k) & \overline{Q}_{1\delta}(k) \\ \overline{Q}_{21}(k) & \overline{Q}_{22}(k) & \overline{Q}_{2\delta}(k) \end{bmatrix}\right]\begin{Bmatrix} \delta_1 \\ \delta_2 \\ \delta \end{Bmatrix} = \begin{Bmatrix} 0 \\ 0 \end{Bmatrix}$$

Next, move the input parameters to the right hand side of the EOM as shown here.

$$(39)\quad \left[\begin{bmatrix} \frac{b^2\omega_1^2}{U^2} & 0 \\ 0 & \frac{b^2\omega_2^2}{U^2} \end{bmatrix} - \left(\frac{b^2\omega^2}{U^2}\right)\begin{bmatrix} 1 & 0 \\ 0 & 1 \end{bmatrix} - \left(\frac{\rho Ab}{2m}\right)\begin{bmatrix} \overline{Q}_{11}(k) & \overline{Q}_{12}(k) \\ \overline{Q}_{21}(k) & \overline{Q}_{22}(k) \end{bmatrix}\right]\begin{Bmatrix} \delta_1 \\ \delta_2 \end{Bmatrix} = \left\{\left(\frac{b^2\omega^2}{U^2}\right)\begin{Bmatrix} m_{1\delta} \\ m_{2\delta} \end{Bmatrix} + \left(\frac{\rho Ab}{2m}\right)\begin{Bmatrix} \overline{Q}_{1\delta}(k) \\ \overline{Q}_{2\delta}(k) \end{Bmatrix}\right\}\delta$$

Equation (39) represents the linear aeroelastic system in non-dimensional form. We select parameters for the scaled system such that the reduced frequency, mass-ratio and mode shapes are the same for both scaled and baseline systems.

$$(40)\quad \frac{b_S\omega_S}{U_S} = \frac{b_B\omega_B}{U_B} \qquad and \qquad \frac{\rho_S A_S b_S}{m_S} = \frac{\rho_B A_B b_B}{m_B} \qquad and \qquad \{\overline{u}_S\}_{iS} = \{\overline{u}_S\}_{iB}$$

where subscript S represents the scaled model and subscript B represents the baseline system. The left formula in equation (40) requires a match in non-dimensional modal frequency for the scaled and baseline models. The center formula requires a match in density ratio. The right formula requires a match in non-dimensional mode shapes.

In addition to the linear vibration scaling, we also need to consider scaling the non-linear structural characteristics. The plan for non-linear scaling will be limited to static considerations only. The baseline model has been analyzed for buckling due to gust load input. The critical buckling mode shape will be scaled. The gust load will also be reduced to model scale in order to produce the same scaled deformation as the full-scale baseline. The objective (along with the linear vibration response) is to minimize the difference between the baseline buckling mode shape and the model buckling mode shape. This nonlinear response is the subject of a future paper pending experimental results on a scaled model further exemplifying the procedure.

### 8.2.7. Optimization Procedure for Designing Scaled Modal Responses:

The procedure for frequency-based optimization was verified based on a simple cantilevered and uniform beam. The objective functions for the scaled beam are depicted in Figure (95) along with the first three modes of vibration.

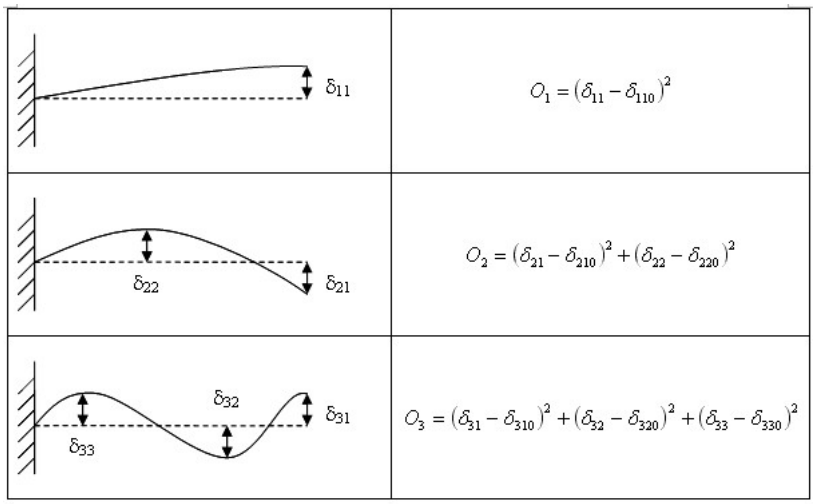


Figure (95) Modes of Vibration for the Equivalent Beam

To begin, we devise a model structure, such as the one depicted in Figure (96) and Figure (97), that is easy to optimize and simple and inexpensive to build. After all, the process requires a number of trial-and-error steps before the manufactured article will actually perform with the desired scaled effect. The skeleton will be composed of many long shims connected tip-to-tail within a bonded sandwich between disks on top and bottom. Design variables for the optimization process include the width of each flexible shim and the mass of each connecting disk.

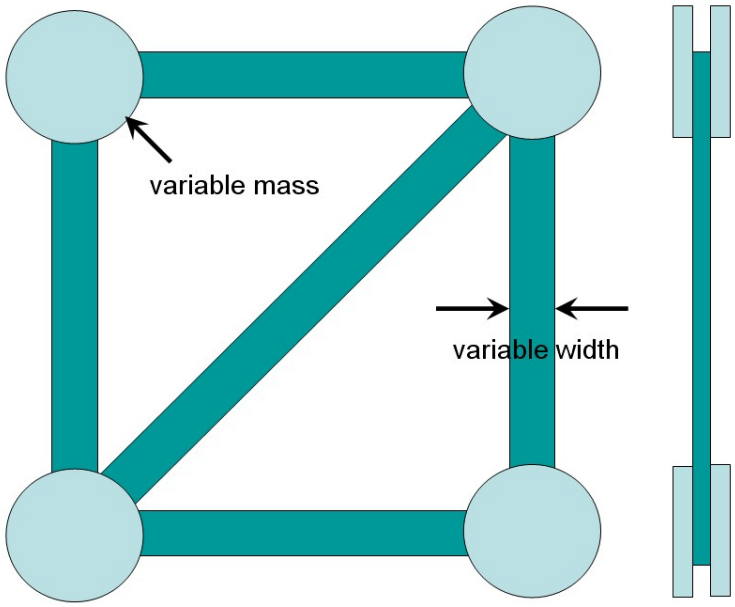


Figure (96) A Structural Cell

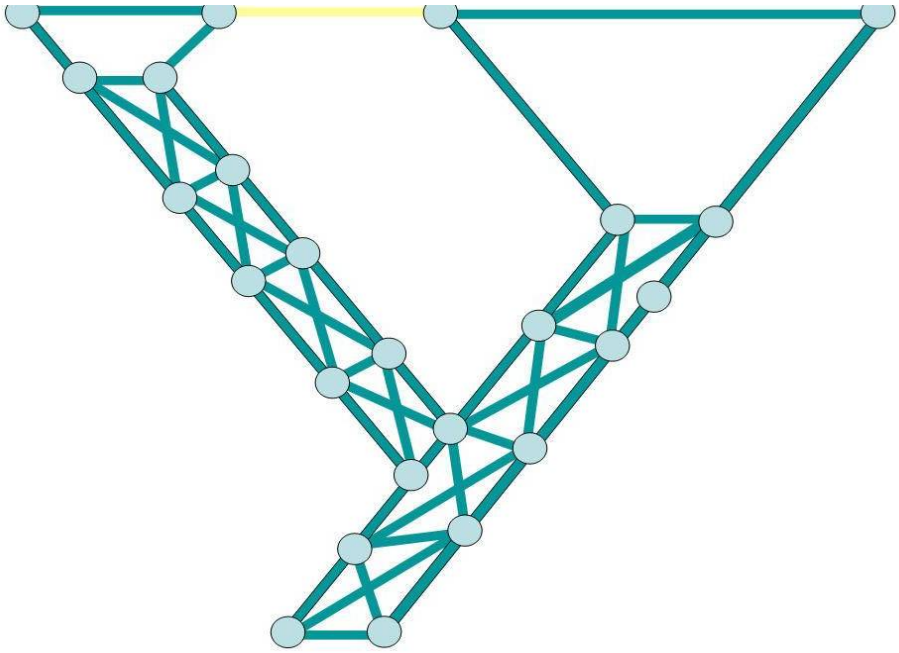

Figure (97) Structural Assembly for Scaled Model

After the optimized scaled design has converged to the desired frequencies and mode shapes, we can begin the process of designing the aerodynamic shell. The shell will be comprised of a foam core with a very thin veneer of fiberglass to harden the skin and protect it from FOD. This sandwich of foam and glass will add significantly to the wing stiffness. However, this is not seen to be a problem because we can arbitrarily scale the airfoil thickness within the rules of thin

air foil theory and the fact that we are scaling the linear potential PDE. With a thinner airfoil section, the influence of the sandwich material will be significantly less. In order to account for the sandwich material in the optimization process, shell elements will be included. The shell stiffness will come entirely from the fiberglass skin. The optimization process is repeated. A number of low-cost models will be fabricated until the desired scaled modal characteristics are attained.

The details up to this point are a review of aeroelastic scaling procedures for linear systems. The joined-wing configuration is dominated by non-linear structural mechanics where design limit loads are concerned. Indeed, this is the major motivation for this conceptual design study.

In principle we will use the same procedure to scale wing buckling that we employed for scaled steady state gust load. Starting with the linear dynamically scaled design constraint, we will proceed to recreate the wing buckling phenomenon under scaled loads. The scaled loads are selected to produce the same linear deformation for the reduced scale as for the full scale at angle-of-attack. In this way, we expect to come fairly close to scaling the static response of the geometrically non-linear dynamic aeroelastic system.

# 9. Conclusions

The joined-wing flight experiment was a success in a number of areas.

1) The joined-wing design concept flight-worthiness was characterized using low cost, and easily repairable materials. Engineering mechanics analysis was kept to a minimum. While conventional wisdom says that analysis is quicker and cheaper than production, the hobby aircraft industry has become very sophisticated with technology, while keeping costs within reach of individual hobbiests. Thus, in many ways, it is cost effective to build cheap and analyze later. In the end, we got what we paid for – the confidence that this joined-wing vehicle can be scaled up in cost.
2) This simple test significantly reduced risk and thereby makes a relatively expensive scaled aeroelastic test conceptually feasible. The additional cost will be found in materials, electronics for data acquisition, and manpower for fabrication and analysis.
3) The AFRL test readiness review process functioned well for the purposes of this test at the Wright-Patterson Air Force Base radio controlled aircraft modelers fun-fly area. However, there were numerous concerns expressed based on real and imagined experiences involving model airplane crashes. These concerns caused logistical challenges involving many spotters and safety control roles during the test of a light radio-controlled airplane. In the end, the geographic convenience of flight testing at Wright-Patterson is offset with regulations. In fact, regulations at Wright-Patterson AFB do not readily support a simple design-build-fly effort that is now common in university aerospace programs.

High speed taxi tests quickly revealed the tendency to roll in the smallest cross-wind as the wheels unloaded. In the latter part of the high speed taxi testing, the airplane went momentarily airborne. The test plan called for the pilot to quickly power-down. The result was a strong pitch-down moment with engine-off.

## 9.1. Flight Testing

The test vehicle was significantly underpowered. Even with our calibrated wind tunnel testing on the propulsion system, our test team was fortunate that the airplane could launch itself from a ground-roll.

Finally, the airplane seems prone to deep stall, as witnessed in the second and final flight. The risk of encountering stall was higher than appreciated with the underpowered (and thus low-speed) design. With hind-sight, the deep stall might have been corrected by cutting power. This guess comes from the high speed taxi test mentioned above and the tendency to nose-down with power loss.

VA-1, despite its unusual joined-wing geometry, is well suited for and dynamically stable in cruise flight. Stable enough, in fact, to remove the LVT without any significant loss of stability. This means we can rule out dynamic instability as a potential contributing factor to the hard landing and focus on the stall. A simple examination of the wing spanwise lift coefficient distribution revealed VA-1 could perform a trimmed bank up to 50 degrees without stalling. For trimmed turns the aileron on the outside wing approaches stall first. Since the trimmed turn did

not represent the events on the flight test video, a descending turn was also briefly considered. Adding a roll rate to the HASC model demonstrated that HASC has the potential to model the change in lift distribution due to a descending turn.

## 9.2. Ground Testing

Wind tunnel testing was critically important to establish available power. It would be even better to wind tunnel test, and thereby calibrate the entire vehicle before flight testing.

The inertia measurement method was a simple low technology method for collecting high quality inertia data about the roll, pitch and yaw axes. Secondary oscillations appeared to affect the results only slightly but leave room for test design improvement. In addition, some kind of release mechanism would be useful for reducing any wobble induced by the testers themselves as they released the airplane from its starting point.

## 9.3. Analysis

Whereas analysis is normally viewed as a cost savings for design certification, analysis was viewed here as a cost driver. However, the dependency on the intuition of the model builder was unfortunate where the structural design was concerned. Standard structural design for joined-wings is very different from traditional sailplane design. SolidWorks for geometry and CosmosWorks for FEM analysis were much appreciated.

However, aerodynamic analysis for Stability and Control proved out the original design for direct-lift takeoff. The same aerodynamic model was able to identify stall onset which was not anticipated. Aerodynamic modeling for takeoff and landing would have effected the design where cross winds caused uncontrollable roll motion. For the fixed propeller design, an aerodynamic analysis would have augmented the wind tunnel results and thereby identify the underpowered condition. Perhaps a different propeller pitch would have prevented the under-powered condition.

HASC was found to be a flexible tool for computing aerodynamic forces and moment coefficients, non-dimensional stability derivatives and unusual control surface combinations. It also came in useful for computing the change in downwash with respect to angle of attack used for the non-dimensional stability derivative computation. The VORLAX output became a useful tool for examining the spanwise lift coefficient distribution along the wings.

Before this research, flying qualities had not been predicted for VA-1 due to the fact the inertia was not measured. Stability derivatives for VA-1 with the LVT did not exist. This research illustrated a method for measuring the inertia of relatively large radio-controlled aircraft. Using HASC to be a simple and effective software application to determine non-dimensional stability derivatives for aircraft of unusual geometry. Subsequent analysis indicated that dynamic instability was likely not a contributing factor to the hard landing. Wing stall was a likely contributor.

The effect of various aerodynamic surfaces of the VA-1 were examined. In order to analyze dynamic stability, the inertia about the three body axes was experimentally measured using a twist test. A VLM program called HASC-95 was used to determine the non-dimensional aerodynamic force and moment coefficients for each configuration. Non-dimensional stability

derivatives for the baseline, LVT, strut-fin and LVT+strut-fin configurations were computed. Non-dimensional derivatives and aircraft inertias were used in the longitudinal and lateral stability models. The stability criteria for each of the longitudinal and lateral modes were compared to flight handling qualities in MIL-STD 1797A and VA-1 was found to have good longitudinal and lateral flying qualities.

## 9.4. Design

Increase the cruise speed, either with increased power or reduced the drag. This would significantly reduce the probability of stall. The pilot requires directives in the event stall is encountered. In the case of the 2nd flight, perhaps the desired airplane angle of attack could have been restored by cutting power (opposite from intuition), as was learned during taxis tests and the first hard landing where severe pitch down was encounted when power was cut..

The LVT was not needed for dynamic stability in cruise flight. Removing the auxilliary vertical tail surface would save weight and reduce drag. Restoring the wheel configuration for direct lift takeoff would also provide protection for the propeller.

Redesign the wing to avoid vehicle roll in crosswinds during takeoff.

Redesign the wing to optimize wing twist and camber in a manner that reduces induced drag. Research is recommended to determine if the potential pitch-up instability near stall angles of attack found on JW-1 would occur on VA-1.

More research is recommended to characterize the stall in descending turns. Adding washout to the wing outside the joint would reduce the local angle of attack and may reduce the tendency for the wing inside the turn to stall during slow descending turns.

# 10. References


[1] David Lucia, "The SensorCraft Configurations: A Non-Linear AeroServoElastic Challenge for Aviation", AIAA-2005-1943, 46th AIAA/ASME/ASCE/AHS/ASC Structures, Structural Dynamics and Materials Conference, Austin TX.

[2] Johnson, F. P. "SensorCraft." AFRL Technology Horizons®, vol 2, no 1 (Mar 01): 10-11 URL: http://www.afrlhorizons.com/Briefs/Dec04/VA0308.html

[3] Wolkovitch, J., "The Joined Wing: An Overview," *Journal of Aircraft*, 23:161-178 (March 1986).

[4] Wolkovitch, J. *Joined Wing Aircraft*, US Patent 3,942,747, March 1976.

[5] Maxwell Blair, Robert A. Canfield, Ronald W. Roberts Jr., "Joined-Wing Aeroelastic Design with Geometric non-Linearity", AIAA Journal of Aircraft, Vol 42, Number 4, July-August 2005, pp 832-848.

[6] Samuels, M. F., "Structural Weight Comparison of a Joined Wing and a Conventional Wing," *Journal of Aircraft*, Vol. 19, No. 6, 1982, pp.485-491.

[7] Gallman, J.W., Kroo, I.M., and Smith, S.C. "Design Synthesis and optimization of Joined-Wing Transports", AIAA-90-3197, presented at the AIAA/AHS/ASEE Aircraft Design, Systems and Operations Meeting, Dayton, OH, 17-19 September 1990.

[8] Smith, S. C., Cliff S.E., and Kroo, I.M., "The Design of a Joined-Wing Flight Demonstrator Aircraft", AIAA Paper 87-2930, AIAA/AHS/ASEE Aircraft Design, Systems and Operations Meeting, St. Louis, MO, 14-16 September 1987.

[9] Miller, M.P. An Accurate Method of Measuring the Moments of Inertia of Airplanes. Technical notes National Advisory Committee for Aeronautics (NACA) Report No. 351. Washington: Langley Memorial Aeronautical Laboratory, 1930.

[10] Kroo, I. M., Gallman, J.W., and Smith, S.C. "Aerodynamic and Structural Studies of Joined-Wing Aircraft." *Journal of Aircraft*, Vol. 28, No.1, January-February 1991, pp. 74-81.

[11] Nangia, R.K., "Towards Designing Novel High Altitude Joined-Wing Sensor-Craft (HALE-UAV)", AIAA-2003-2695, presented at the AIAA/ICAS International Air & Space Symposium, Dayton, OH, 14-17 July 2003.

[12] Rasmussen C.C., *Optimization Process for Configuration of a Flexible Joined-Wing.* MS Thesis, Graduate School of Engineering, Air Force Institute of Technology (AETC), Wright-Patterson AFB, Ohio, March 2004. AFT/GAE/ENY/04-M14.

[13] Craft, Ryan L., *Drag Estimates for the Joined-Wing Sensorcraft.* MS Thesis, Graduate School of Engineering, Air Force Institute of Technology (AETC), Wright-Patterson AFB, Ohio, March 2005. AFT/GAE/ENY/05-J02.

[14] Blair, M. "Technical Review Board: Joined-Wing Technology Demonstrator." Briefing to AFRL/Personnel, WPAFB, OH, May 2004.

[15] Althaus, Dieter and Wortmann, F.X. *Stuttgarter Profilkatalog I*. Braunschweig, Friedr. Vieweg & Sohnn, 1981.

[16] *High Angle of Attack Stability and Control 95*. (HASC95) Computer Software. NASA Langley Research Center, 1995.

[17] Bertin, John J. Aerodynamics for Engineers (4th Edition). New Jersey, Prentice Hall, 2002.

[18] Roskam, Jan. Airplane Flight Dynamics and Automatic Flight Controls: Part I. Lawrence, Design, Analysis and Research Corporation, 1995.

[19] Nelson, R. *Flight Stability and Automatic Control* (2nd Edition). Boston, McGraw Hill, 1998.
[20] Department of Defense. Military Standard Flying Qualities of Piloted Aircraft. MIL-STD-1797A, Washington: Government Printing Office, 30 Jan 1990.
[21] Raymer, Daniel P. Aircraft Design: A Conceptual Approach (2nd Edition). Washington DC: American Institute of Aeronautics and Astronautics, Inc., 1992.
[22] Stinton, D. "Flying Qualities and Flight Testing of the Airplane." Reston, VA, American Institute of Aeronautics and Astronautics, 1996.
[23] Meirovitch, L. "Fundamentals of Vibrations." New York, NY, McGraw-Hill, 2001.
[24] *AFRL Test Program*, Instructions: AFRLI 99-101 Air Force Research Laboratory, 01 August 2002
[25] *AFRL Test Guide*, Pamphlet: AFRLPAM 99-101, Air Force Research Laboratory, 01 June 2002
[26] Nangia, R.K., Palmer, M.E., and Tilmann, C.P., "Planform Variation Effects in Unconventional High Aspect Ratio Joined-Wing Aircraft Incorporating Laminar Flow", AIAA-2005-0243, presented at the 42nd AIAA Aerospace Sciences Meeting and Exhibit, Reno, NV, 10-13 January 2005.
[27] Smallwood, B. *Structurally Integrated Antennas on a Joined-Wing Aircraft*. MS Thesis, Graduate School of Engineering, Air Force Institute of Technology (AETC), Wright-Patterson AFB OH, March 2003. AFIT/GAE/ENY/03-07.
[28] Sitz, J.J., *Aeroelastic Analysis of a Joined Wing Sensorcraft.* MS Thesis, Graduate School of Engineering, Air Force Institute of Technology (AETC), Wright-Patterson AFB, Ohio, March 2004. AFT/GAE/ENY/04-J12.
[29] Roskam, J. "Airplane Design Part IV: Preliminary Calculation of Aerodynamic, Thrust and Power Characteristics." Ottowa, KS, 1990.
[30] Bowman, Jason. "Stability and Control Analysis of the AFRL Radio-Controlled Joined Wing." Report to AFRL/VA personnel, WPAFB, Ohio, 2003.
[31] Bowman, J. "Cruise Velocity Analysis." Report to AFRL/VA personnel, WPAFB, Ohio, 2003.
[32] Yechout, T. R. "Introduction to Aircraft Flight Mechanics: Performance, Static, Stability, Dynamic Stability and Classical Feedback Control." Reston, VA, American Institute of Aeronautics and Astronautics, 2003.
[33] Jones F. Cahill and Dexter H. Stead, "Preliminary Investigation at Subsonic and Transonic Speeds of the Aerodynamic Characteristics of a Biplane Composed of a Sweptback and a SweptForward Wing Joined at the Tips", NACA RM L53L24b, 12 March 1954.
[34] M. Blair, D. Garmann, V. Bond, R. Canfield, P. Pereira, A. Suleman, "Non-Linear Aeroelastic Scaling of a Joined-Wing Concept", AIAA-2007-1887, 3rd AIAA MultiDisciplinary Design Optimization Specialists Conference, 23-26 April 2007, Honolulu, Hawaii
[35] Mark E. Peters, "The Determination of Longitudinal Flying Qualities for Light Weight Unmanned Aircraft", AIAA-1997-3701, AIAA Guidance, Navigation and Control Conference, New Orleans, LA, 11-13 Aug 1997
[36] Mark E. Peters, "Development of a Light Unmanned Aircraft for the Determination of Flying Qualities Requirements", Thesis presented to the Faculty of Purdue University, May 1996.
[37] J. P. Den Hartog, Advanced Strength of Materials, Section 41, "Twist-bend Buckling of Beams", pp. 283-291, McGraw-Hill Book Company, 1952.

[38] Maxwell Blair, “An Equivalent Beam Formulation for Joined-Wings in a Post-Buckled State”, International Forum for Aeroelasticity and Structural Dynamics (IFASD), Stockholm, Sweden, June 2007.
[39] Maxwell Blair, Alfred G. Striz, “Finite Element Beam Assemblies with Geometric Bend-Twist Coupling”, AIAA-2008-1796, 4th AIAA MultiDisciplinary Design Optimization Specialists Conference, 07-10 April 2008, Schaumburg, IL.
[40] Raymond Bisplinghoff, Holt, Ashley, Robert L. Halfman, “Aeroelasticity”, Addison-Wesley Publishing Co, 1955
[41] Bond, V, PhD Thesis AFIT March 2008
[42] Roskam, Jan. Airplane Design: Part VI: Preliminary Calculations of Aerodynamic, Thrust and Power Characteristics. Lawrence, KS, 1990.
Other Useful References:
[43] Reich, G.W., Raveh, D., and Zink, P.S. “Application of Active Aeroelastic Wing Technology to a Joined-Wing SensorCraft”, AIAA-1001-1633, presented at the 43rd AIAA/ASME/ASCE/AHS/ASC Structures, Structural Dynamics, and Materials Conference, Denver, CO, 22-25 April 2002.
[44] Roberts, Ronald. *Sensor-Craft Analytical Certification*, MS Thesis, Graduate School of Engineering, Air Force Institute of Technology (AETC), Wright-Patterson AFB, Ohio, March 2003. AFIT/GAE/ENY/03-06.
[45] Albright, Alan E., Dixon, Charles J., Hegedus, Martin C. “Modification and Validation of Conceptual Design Aerodynamic Prediction Method HASC95 with VTXCHN.”
[46] Riley, William F., Sturges, Leroy D. *Engineering Mechanics: Dynamics (2nd Edition)*. New York, John Wiley and Sons, Inc., 1996.
[47] Stevens, Brian L., Lewis, Frank L. Aircraft Control and Simulation. (2nd Edition). Hoboken, John Wiley and Sons, Inc., 2003.
[48] “MATLAB Version 7.1.0.246(R14) Service Pack (3),” The Mathworks, Inc. 2005.
[49] Hodgkinson, J. “Aircraft Handling Qualities.” Reston, VA, Blackwell Science Ltd., 1999.
[50] William McClelland, “Inertia Measurement and Dynamic Stability Analysis of a Radio-Controlled Joined-Wing Aircraft,” Air Force Institute of Technology MS Thesis AFIT/GAE/ENY/06-M07, March 2006.
[51] John W. Gallman and Ilan M. Kroo, "Structural Optimization for Joined-Wig Synthesis", AIAA Journal of Aircraft, Vol 33, No 01, January-February 1996.
[52] M. H. Shirk, T. J. Hertz, T. A. Weisshaar, “Aeroelastic Tailoring – Theory, Practice and Promise“, AIAA Journal of Aircraft, Vol 23, No 01, January 1986.
[53] Meirovitch, Leonard, *Computational Methods in Structural Dynamics,* Sijthoff & Noordhoff, Rockville, 1980.
[54] Pereira, P, Almeida, L., and Suleman, A., Canfield, R. Bond, V., Blair, M., “Aeroelastic Scaling And Optimization Of A Joined-Wing Aircraft”, 47th AIAA/ASME/ASCE/AHS/ASC Structures, Structural Dynamics and Materials Conference, Honolulu, HI, April 2007.
[55] Mark French, “Design of Aeroelastically Scaled Wind Tunnel Models Using Sensitivity Based Parameter Identification”, PhD Thesis, University of Dayton, August 1993
[56] "Joined-Wing Aeroelastic Design with Geometric non-Linearity", IFASD-AIAA-2003 co-authored with Ronald W. Roberts Jr. and Robert A. Canfield, presented at IFASD International Forum on Aeroelasticity and Structural Dynamics, Amsterdam, The Netherlands, 04-06 June 2003. (Accepted for publication in AIAA Journal of Aircraft - Final Draft Pending)

[57] "Structural Analysis of Joined-Wing Technology Demonstrator", Jason Robinson, AFRL-VA-WP-TR-2004-3048, May 2004,
[58] *Flight Testing of Fixed-Wing Aircraft*, Ralph D. Kimberlin, AIAA Education Series, © 2003.
[59] Max Blair, "A Compilation of the Mathematics Leading to the Double-Lattice Method", WL-TR-95-3022, Air Force Research Laboratory (formerly Wright Laboratory), November 1994.
[60] Arnold M Kuethe and Chuen-Yen Chow, Foundations of Aerodynamics, 3rd edition, John Wiley & Sons, ©1976

## Appendix A: Cruise Velocity Analysis

Reference: "Aircraft Performance Stability and Control" by Perkins and Hage

The component for each vehicle component

| | $C_{D0}$ | $S_{ref}$ ($ft^2$) | D/q ($ft^2$) |
|---|---|---|---|
| wing | 0.007 | 15.2 | 0.106 |
| fuselage | 0.12 | 0.35 | 0.042 |
| vertical tail | 0.008 | 0.75 | 0.006 |
| 3 wheels (3" spheres) | 0.9 | 0.15 | 0.135 |
| Total | | | 0.289 |

Table (32) Component Specifications for Drag and Area

The dynamic pressure q is $\boldsymbol{q = 0.5\rho V^2}$

The drag on a sphere comes from Kuethe and Chow, "Foundations of Aerodynamics"

The formula for total vehicle drag (form and induced components):

$$C_D = C_{D0} + \frac{C_L^2}{\Pi A_R} \tag{41}$$

From the table, we calculate the vehicle $C_{D0}$ (using the wing planform area as the vehicle reference area, $S_0 = 15.2\ ft^2$):

$$C_{D0} = \left.(D/q)\right/_{S_0} = \left(0.289\ ft^2\right)/15.2\ ft^2 = 1.90\times10^{-2} \tag{42}$$

The lift coefficient for level flight :

$$C_L = \frac{W}{qS_0} = \frac{26}{q(15.2)} = \frac{1.71}{q} \tag{43}$$

The aspect ratio is $A_R = b^2/S_0$. We can arrive at a formula for $C_D$:

$$C_D = C_{D0} + \frac{C_L^2}{\Pi A_R} = 1.90\times10^{-2} + \frac{7.22\times10^{-2}}{q^2} \tag{44}$$

The total drag is

$$D = C_D q S_0 = 0.289q + \frac{1.10}{q} = 0.289\left(\frac{1}{2}\rho V^2\right) + \frac{1.10}{\left(\frac{1}{2}\rho V^2\right)} \tag{45}$$

Linear extrapolation of the thrust test results generates the following formula for T(V):

(46) $T = (-0.106)V + 11.5$

Using standard density ($\rho$ = 0.002378 slug/ft$^2$)

Equilibrating thrust and drag allows the calculation of cruise velocity at max thrust:

(47) $$0.289\left(\frac{1}{2}\rho V^2\right) + \frac{1.10}{\left(\frac{1}{2}\rho V^2\right)} = (-0.106)V + 11.5$$

(48) V = 84 f/s or 57 mph.

The drag can now be calculated:

(49) $$D = 0.289\left(\frac{1}{2}\rho V^2\right) + \frac{1.10}{\left(\frac{1}{2}\rho V^2\right)} = 2.56$$

With airplane weight of 26 lbs and calculated drag of 2.56 lbs (@ max cruise V = 84 f/s), the L/D is 10.16.

## Appendix B: Twist Test Equation Derivation and Uncertainty Analysis

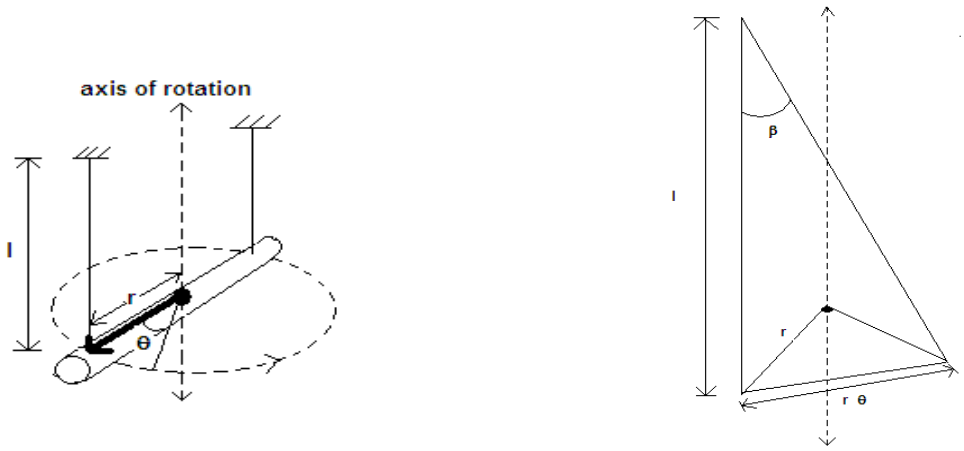


Figure (98) Twist test for a cylinder

Assume a cylindrical bar of uniform density is suspended by two cords of equal length. The dashed line passes through the bar's center of mass and represents the axis about which the mass moment of inertia is to be measured. The bar is twisted $\theta$ radians from it equilibrium position and released. Assuming no external forces act on the bar after release an expression will be derived to find Inertia as a function of the period, $P$.

Assuming each cord is exactly the same length and that the weight is distributed evenly between them so that the tension, $T$, in each chord is ½ $W$. The horizontal component of tension for one cord can be expressed by:

(50) $T_h = ½ W \sin \beta$

where
$T_h$ = horizontal component of tension
$\beta$ = angle between vertical and cable (rad)
$W$ = weight ($lb_f$)

The attachment point follows a circular path. Assuming small angles however, the distance can be estimated using the following relationship:

(51) $$\sin \beta = \frac{r\theta}{l}$$

where
$l$ = cable length (ft)
$r$ = distance from bar c.g. to attachment point (ft)
$\theta$ = angular rotation in horizontal plane (rad)

By substitution the horizontal tension can be calculated from:

(52) $$T_h = \frac{1}{2} W \frac{r\theta}{l}$$

Sum of the moments about the center of rotation yields the key equation:

(53) $$\sum M = I\ddot{\theta}$$

where:
$M$ = moments (ft-$lb_f$)
$I$ = Inertia (slug-$ft^2$)

The sum of the moments are equal to the total horizontal tension times radius of rotation:

(54) $$-2T_h\, r = I\ddot{\theta}$$

Substitute for horizontal tension:

(55) $$-2\left(\frac{1}{2} W \frac{r\theta}{l}\right) r = I\ddot{\theta}$$

Set equal to zero and solve for the second order ordinary differential equation:

(56) $$I\ddot{\theta} + \frac{Wr^2}{l}\theta = 0$$

Divide through by inertia term

(57) $$\ddot{\theta} + \frac{Wr^2}{I\,l}\theta = 0$$

Note the differential equation of the following form:

(58) $$\ddot{\theta} + \omega_n{}^2\theta = 0$$

Solving for natural frequency, $\omega_n$, in units of 1/sec

(59) $$\omega_n{}^2 = \frac{Wr^2}{I\,l}$$

(60) $$\omega_n = r\sqrt{\frac{W}{I\,l}}$$

The period, P, in seconds is related to the natural frequency with the following:

(61) $$P = \frac{2\pi}{\omega_n} = \frac{2\pi}{r\sqrt{\frac{W}{I\,l}}}$$

Solving for Inertia as a function of the period, weight, cable length and radius of rotation:

(62) $$\sqrt{\frac{W}{I\,l}} = \frac{2\pi}{rP}$$

(63) $$\frac{W}{I\,l} = \frac{4\pi^2}{r^2P^2}$$

The following equation can be used to find the inertia:

(64) $$I = \frac{W}{l}\frac{r^2P^2}{4\pi^2}$$

To increase the accuracy of the experiment, the distance, *d*, between the cords was used were $r=d/2$. By substitution the inertia is $I = (Wd^2P^2)/(16\pi^2 l)$.

**Uncertainty Analysis**

To ensure numerical accuracy of the results an uncertainty analysis was conducted. First, the partial derivatives of *I* with respect to the variables *W*, *r*, *P* and *l* was determined. The δ notation signifies the uncertainty for each measurement. For example, $\delta r$ was the uncertainty of the radius of rotation and was estimated to be +/- in.

(65) $$\frac{\partial I}{\partial W} = \frac{r^2P^2}{4\pi^2 l}$$

(66) $$\frac{\partial I}{\partial r} = 2\frac{WrP^2}{4\pi^2 l}$$

(67) $$\frac{\partial I}{\partial P} = 2\frac{Wr^2P}{4\pi^2 l}$$

(68) $$\frac{\partial I}{\partial l} = -\frac{Wr^2P^2}{4\pi^2 l^2}$$

(69) $$\delta I = \sqrt{\left(\frac{\partial I}{\partial W}\delta W\right)^2 + \left(\frac{\partial I}{\partial r}\delta r\right)^2 + \left(\frac{\partial I}{\partial P}\delta P\right)^2 + \left(\frac{\partial I}{\partial l}\delta l\right)^2}$$

# APPENDIX C
# STABILITY & CONTROL ANALYSIS OF THE AFRL RADIO-CONTROLLED JOINED WING

Jason Bowman
Jason.Bowman@wpafb.af.mil
937-904-8060

## Recommendations

The vehicle may not have sufficient yaw stability as is. Even with the addition of winglets, ventral fins, strut fins, and stability augmentation, $C_{n_\beta}$ is just above the value recommended for cruise angles-of-attack for full-scale aircraft at low Mach numbers. At landing angles-of-attack, there may be neutral yaw stability with all of the modifications. Radio-controlled aircraft typically need more stability than full-scale aircraft for the pilot to feel comfortable. The addition of these surfaces also causes a predicted spiral divergence (graveyard spiral) at normal cruising angles-of-attack. It not certain what the time constant is for this divergence.

The vehicle may also be marginally stable in pitch with 4% static margin at the reference CG position (49 inches aft of nose). Both the winglets and strut fins were predicted to increase pitch stability perhaps high enough to be safe. Moving the CG forward may cause trim problems at high sideslips, reduced effectiveness, or if only the rear wing control surface is used.

The rudder may not have enough control power to overcome adverse yaw due to an aileron input. If only the inboard surfaces on the forward wing are used then there should not be a problem. However, the roll time constant may be quite large. The use of both the outboard and inboard surfaces for roll will require pitch/roll mixing on the outboard surface if sufficient trim power is not available from the aft surface. A third strategy is to only deflect the surfaces on the side of the roll. However, this may not be programmable in the radio transmitter.

## Introduction

This document contains stability and control analysis of the AFRL radio-controlled joined wing aircraft. The information presented here includes forces and moments as a function of angle-of-attack and sideslip, control surface force and moment derivatives, damping derivatives, and trimmed elevator positions and vehicle lift coefficient as a function of angle-of-attack. The longitudinal position of the center-of-gravity was also varied for the analysis. A dynamic analysis was not conducted as moment and product of inertia data was not available.

The geometry of the joined wing vehicle is such that typical estimators can not be trusted (the forward wing has aft sweep and positive dihedral, the rear wing has forward sweep and negative dihedral, and they are joined), but the trends are shown in Table 1. It was decided to conduct a vortex lattice analysis using HASC (High Angle-of-Attack Stability and Control) to obtain the necessary stability and control information. Although the high angle-of-attack routines were not used, the normal vortex lattice routines still have some mild non-linearities that are evident in the results.

Table 1: General Effects on Yaw and Roll Stability of Various Features [2]

| Feature | Pitch | Yaw | Roll |
|---|---|---|---|
| Fuselage | - | - | |
| Dihedral | | - | + |
| | | effect increases with $C_L$ | |
| Sweep | + | + | + |
| | | effect increases with $\alpha$ | |
| Thrust | | | |
| tractor | | - | |
| pusher | | + | |

## Geometry

Several views of the actual vehicle are shown in Figure 1. Measurements were taken directly from the vehicle to construct the vortex lattice models.

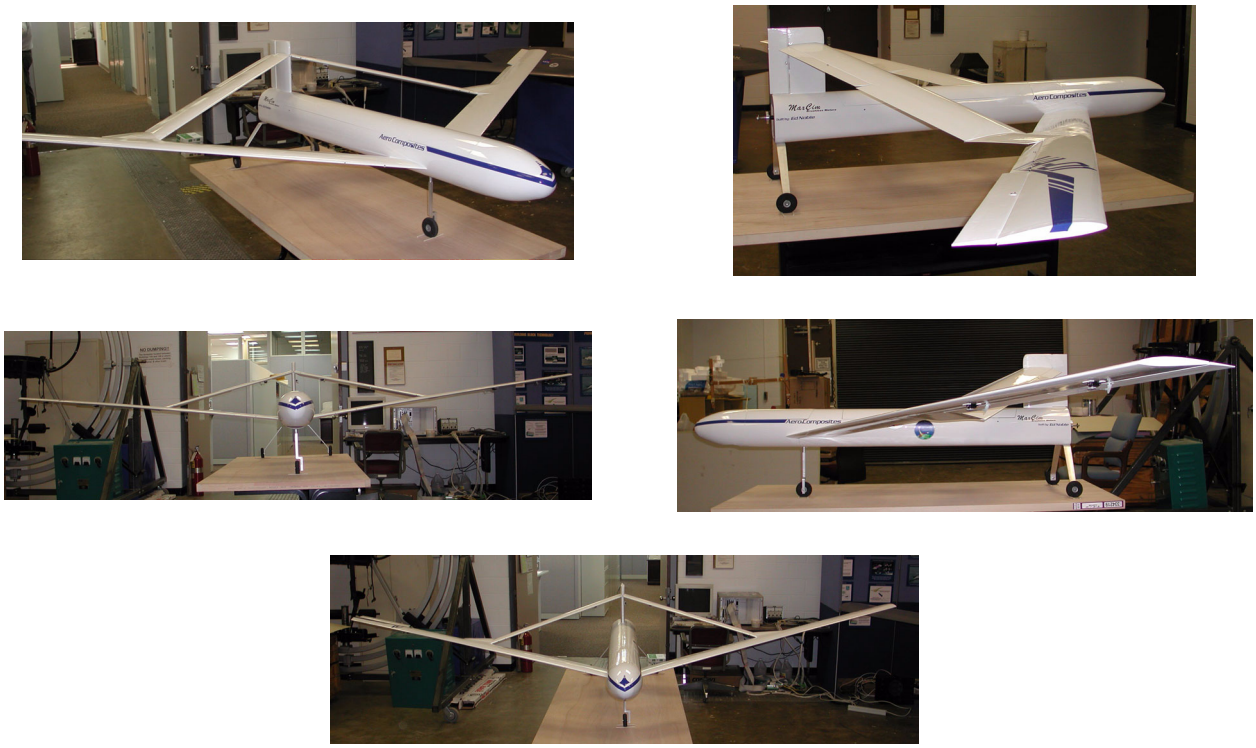

**Figure 1: Several Photos of the Radio-Controlled Joined Wing**

The baseline or reference lattice model is shown in Figures 2 through 5, and its dimensions are shown in Table 2. The reference geometry is the same as the aircraft as currently configured with one exception — the horizontal component of the fuselage, which affects lift and pitching moments, was not included to study the effect of the fuselage on longitudinal stability.

Table 2: Basic Dimensions of the Radio-Controlled Joined Wing

| Dimensions | Value |
|---|---|
| Span | 168 in |
| Area | 2226 $in^2$ |
| Chord | 9.2 in |
| Aspect Ratio | 12.7 |
| Length | 80 in |
| Height | 19.25 in |
| Airfoil | FX60-100 |
| Control Surface Chord | 2.6 in |
| Wing Sweep | 30º |
| Dihedral | +7.5º, -15º |

Additionally, early analysis indicated a potential yaw stability and damping problem. Therefore three additional geometries were considered. On the first modified confutation, two ventral fins were added to the rear of the fuselage. On the second modified configuration, winglets were added since the wingtip longitudinal location was near the vertical tail, which would make them effective in yaw. On the third configuration, small lifting surfaces with symmetric airfoil sections were added over the main landing gear struts.

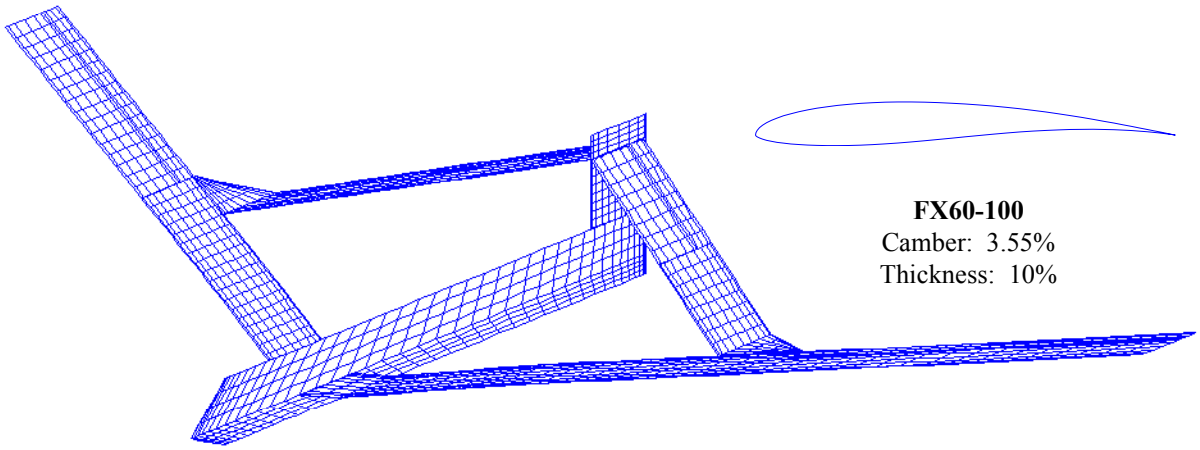


**Figure 2: Reference Geometry**

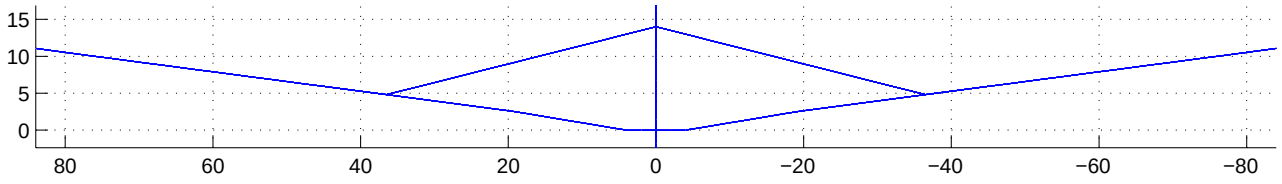


**Figure 3: Reference Geometry Front View**

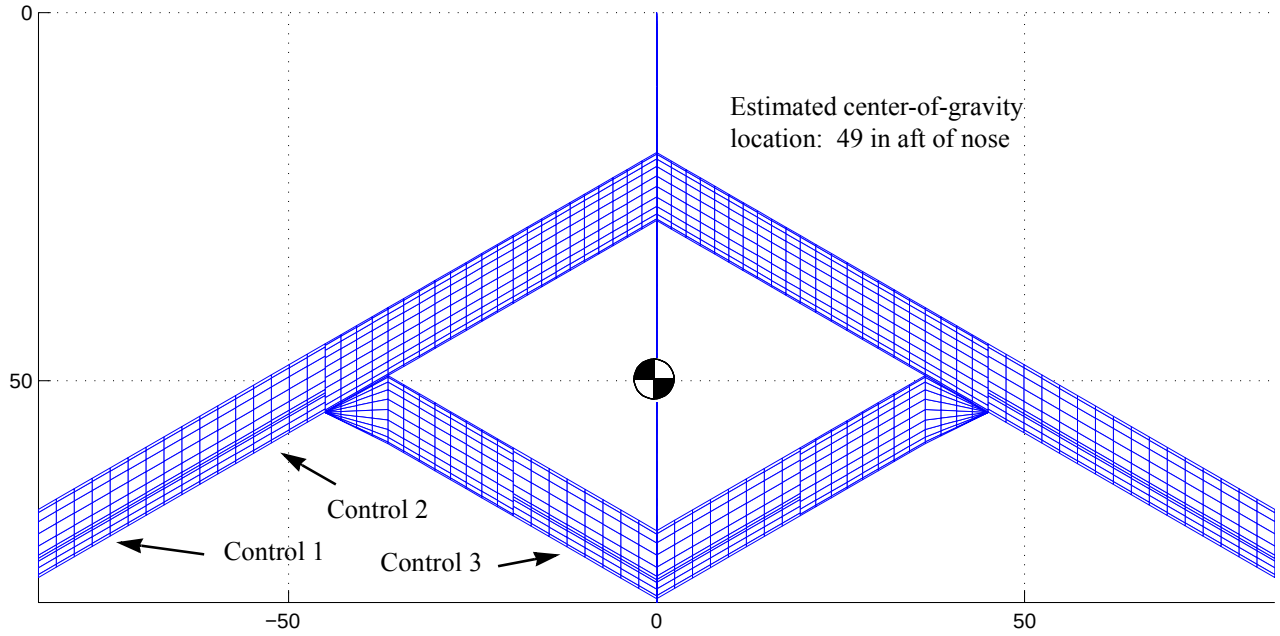


**Figure 4: Reference Geometry Top View**

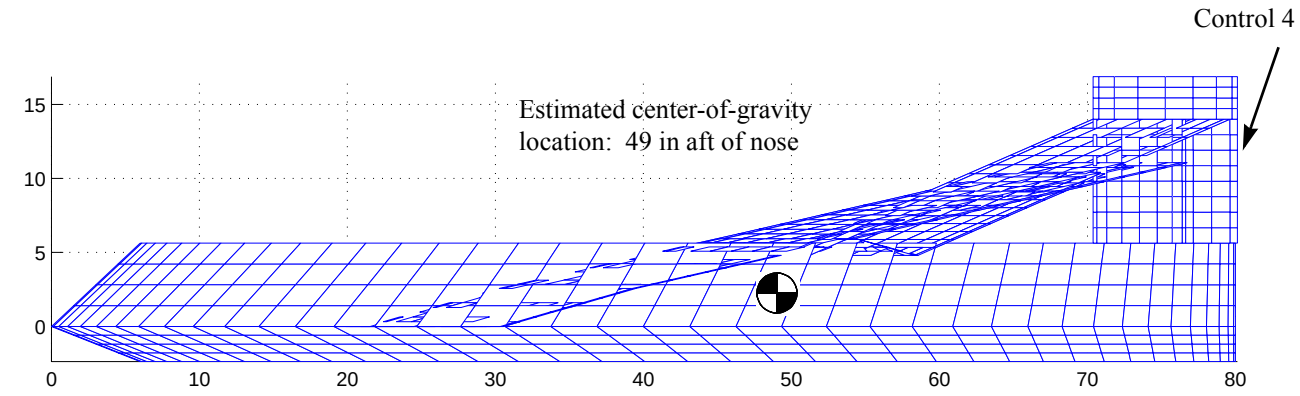


**Figure 5: Reference Geometry Side View**

In Figures 4 and 5, note the position of the control surfaces. As currently configured, the labeled control surfaces have the following functions

Table 3: Control Surface Functions

| Control | Function |
|---|---|
| 1 | Pitch, Mixed Pitch/Roll |
| 2 | Roll |
| 3 | Pitch |
| 4 | Yaw |

The horizontal component of the fuselage was added to determine its effect on pitch stability.

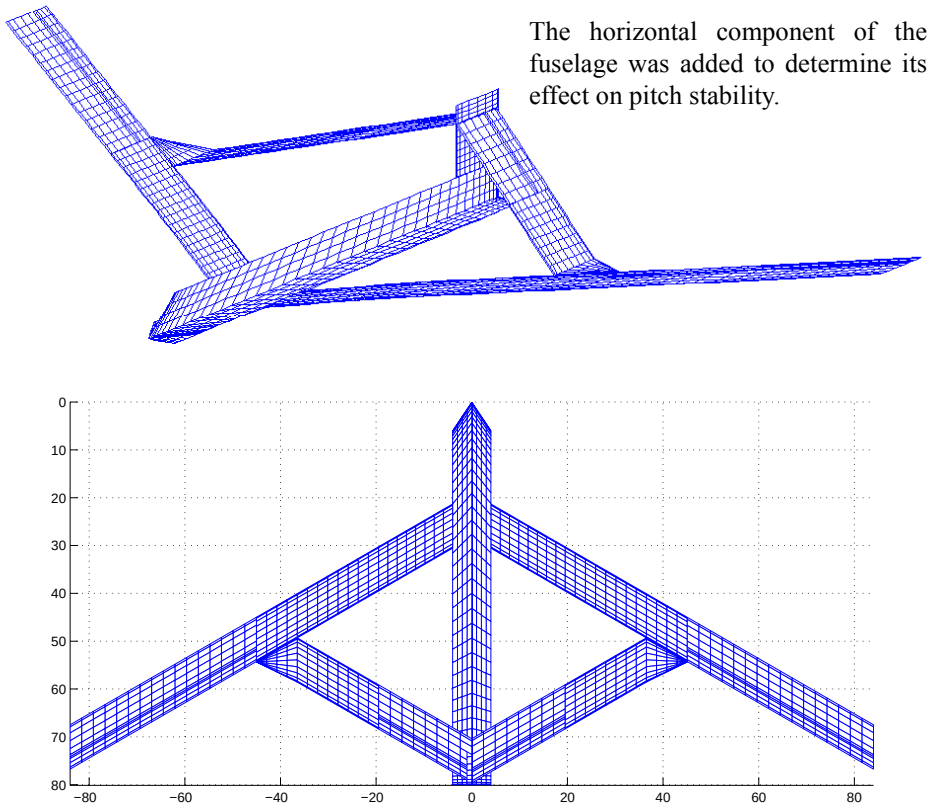


**Figure 6: Reference Geometry + Fuselage**

Early analysis indicated a potential yaw stability problem. Two ventral fins were added to determine their effectiveness in aiding yaw stability.

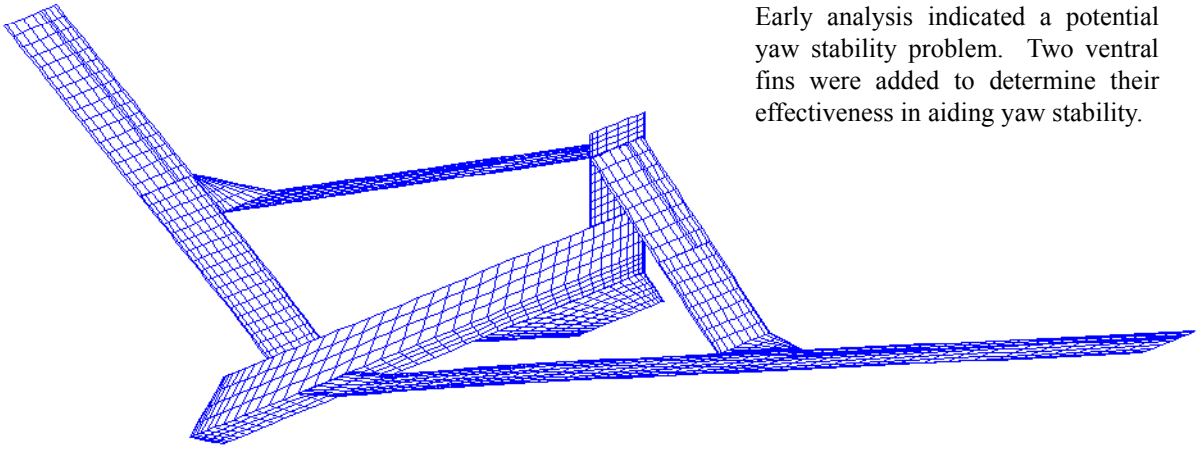

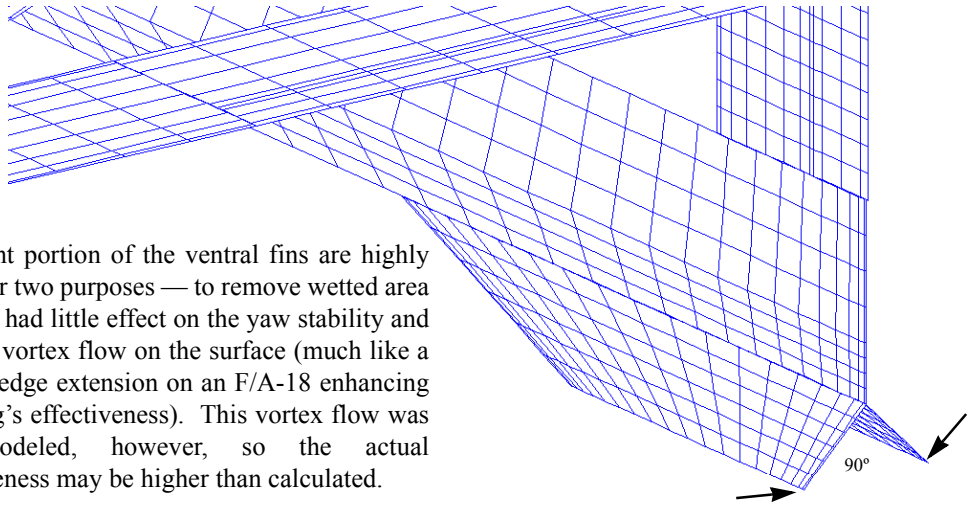


The front portion of the ventral fins are highly raked for two purposes — to remove wetted area where it had little effect on the yaw stability and to force vortex flow on the surface (much like a leading edge extension on an F/A-18 enhancing the wing's effectiveness). This vortex flow was not modeled, however, so the actual effectiveness may be higher than calculated.

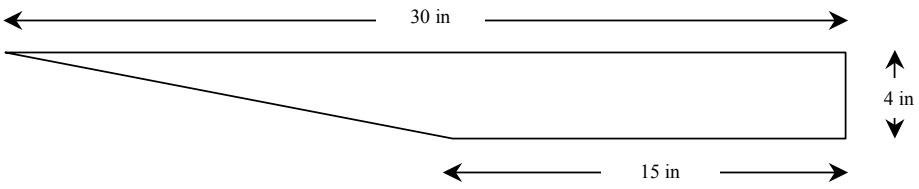


**Figure 7: Reference Geometry + Ventral Fins**

Like the ventral fins, winglets were added to determine if they could improve yaw stability. Each winglet is roughly 70% the size of the primary vertical tail surface. The strut fins, each about 37% of the primary vertical tail, are roughly 33% more effective. This may or may not be a numerical problem.

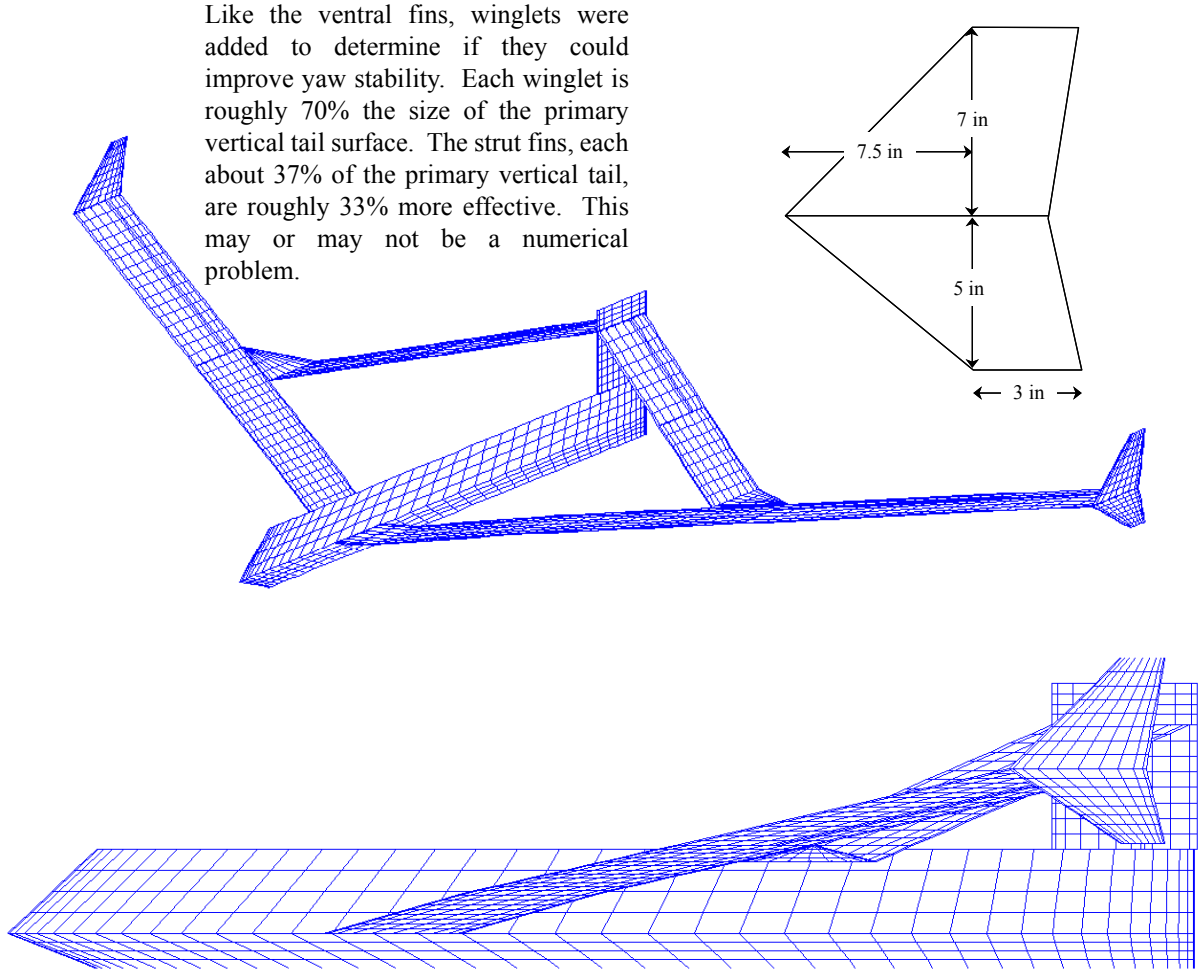


**Figure 8: Reference Geometry + Winglets**

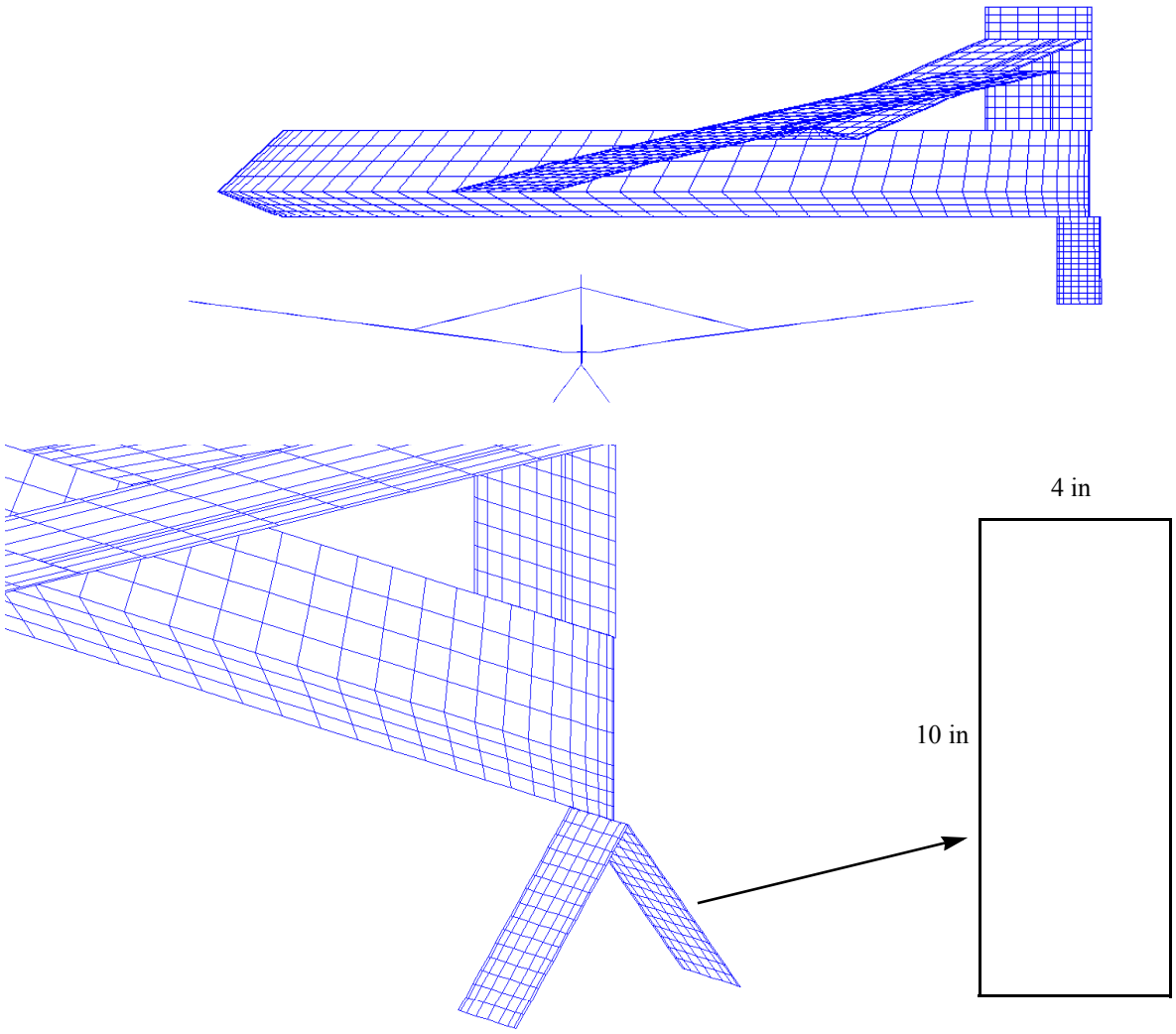


**Figure 9: Reference Geometry + Main Gear Strut Fins**

## Summary of Results

Pitch Characteristics

All of the geometries considered have indistinguishable lift curves, at least as far as the approximations of the vortex lattice indicate. The theoretical value for the lift curve slope was estimated to be $C_{L_{\alpha,\,theory}} \approx 4.8$. However, the calculated value was $C_{L_{\alpha,\,vorlax}} \approx 4.1$. The estimator from [1 eq. 12.6] assumes that there is only one lifting wing. Since the rear wing is in the downwash of the forward wing, it has a reduced lift curve slope much like a conventional aft horizontal tail surface. Because the rear wing is a substantial portion of the vehicle lifting surface, the reduction in lift curve slope on the rear wing is evident in the total lift curve slope. Figure 11 illustrates $C_{L_\alpha}$ for the various configurations as a function of sideslip. Note there is a slight reduction in $C_{L_\alpha}$ with sideslip.

The pitching moment curve slope $C_{M_\alpha}$ is a function of CG position, and, as shown in Figure 12, there is little variation with sideslip. Figure 12 also illustrates the increments in $C_{M_\alpha}$ due to various additions to the baseline geometry. The fuselage is very destabilizing, but surprisingly, the winglets add quite a bit of nose-down pitching moment. It is not certain if this is a real effect or a modeling problem with the vortex lattice method. However, the rolling moment control derivatives indicate that the wing tip is not very effective even without the winglet. So this effect may be accurate. Apparently the winglets modify the pressures on the outer wing panel significantly. The strut fin geometry does not have as strong of an effect on pitching moment as do the winglets.

The static margin varies from +35% to -20% depending on the configuration and CG position. At the reference CG position of 49 inches aft of the nose, the addition of strut fins or winglets should be considered to increase the static margin above the basic value of 4%. Typical well-flying RC aircraft will have static margins in excess of 10%.

The addition of the winglets produces a nose down pitching moment with sideslip. At $\beta = 20°$, an additional nose-down pitching moment coefficient of 0.07 has to be trimmed out. The trim analysis indicates this is not a problem for most conditions.

The pitch strategies included using both the outboard surface on the forward wing (Control 1) and the surface on the rear wing (Control 3) and using only Control 3. The analysis was run assuming first 100% control effectiveness and then 50%. Unsealed hinges and low Reynolds numbers may reduce the effectiveness of the surfaces. The trim analysis was conducted using the vehicle with winglets since the nose-down moments are the most critical for this geometry.

Table 4: Cruise Elevator Deflections for Trim (Baseline + Winglets)

| | 50% Effectiveness | 100% Effectiveness |
|---|---|---|
| Control 3 | -20º to Not trimmable | -10º to -16º |
| Control 1 + Control 3 | -12º to -20º | -6º to -10º |

Flying the vehicle at 20º sideslip or with the addition of the strut fins (but not including the winglets) produces similar results. Using both Control 1 and Control 3 is the best strategy since the deflections for Control 3 alone seem excessive at 50% effectiveness.

The lift and pitch moment damping derivatives are very similar for all of the configurations except when the strut fins are added. Since the fins have a relatively large horizontal component, they add noticeably to the lift and pitching moment when the vehicle has a pitch rate. For cruise angles-of-attack, the strut fins do not appreciably change the lift and pitch moment characteristics. It is only at the higher angles-of-attack, for example when landing, that the difference might be noticeable.

Lateral Characteristics

The main lateral characteristics of interest are the dihedral effect, $C_{l_\beta}$, and the roll damping derivative $C_{l_p}$. There is a complicated set of effects such as wing sweep and dihedral for this vehicle (see Table 1), and before conducting the analysis it was not certain which effect would dominate. As Figure 15 illustrates, each configuration has positive dihedral stability. The winglets, having significant area above the CG, show a marked increase in dihedral stability over the baseline.

The roll damping, being a strong function of vehicle aspect ratio and wing taper ratio, is well predicted by empirical estimators such as those presented in [1 p. 443], which are taken from NACA 868 and 1098. The roll damping derivative is $C_{l_p} \approx -0.53$ at 0º sideslip.

The vehicle roll characteristics show a strong dependence on angle-of-attack (see Figures 31 through 33). The main concern is adverse yaw since the maximum steady roll rate can not be evaluated without moments of inertia. The rudder can provide a maximum yawing moment of about 0.007 assuming 100% effectiveness. Using the inboard surfaces (bilaterally) only (Control 2), the rudder has sufficient power. However, when using both Control 1 and Control 2 bilaterally, the downward deflected side (left aileron for a right roll) produces enough adverse yaw to overpower the rudder at normal flight angles-of-attack. If the surfaces are used unilaterally (only use ailerons on one side), then sufficient rudder power is available except at $\alpha = 10°$ using both Control 1 and Control 2.

Yaw Characteristics

A suspected lack of yaw stability was the factor that prompted this entire analysis. A typical value for $C_{N_\beta}$ for full-scale aircraft ranges from 0.05 to 0.1 at low subsonic speeds. The baseline geometry only achieves a value 5 to 10 times lower. Furthermore, $C_{N_\beta}$ decreases with angles-of-attack above or below the cruise angle-of-attack. At $\alpha = 10°$ with an aft CG, the vehicle is predicted to be unstable in yaw (see Figure 16). Using data taken from Figure16, the additional stability from various devices is presented in Table 5. The most effective is the artificial stability provided by a gyroscope plugged into the yaw channel. This effect was modeled with a rudder gain of 3º deflection for every 1º of sideslip. The winglets are not as effective as the strut fins despite having significantly more area. This effect is probably related to the increase in nose-down pitching moment with the addition of winglets. With stability augmentation and the use of strut fins, the total vehicle yaw stability is roughly $C_{N_\beta} \approx 0.062$, which is probably still too low for good flying qualities (as measured on the Cooper-Harper rating scale).

Table 5: Approximate changes in $C_{N_\beta}$ for Various Additions to the Geometry

| **Geometry** | $\Delta C_{N_\beta}$ |
|---|---|
| Ventral Fins | 0.008 |
| Winglets | 0.015 |
| Strut Fins | 0.022 |
| Rudder<br>3º $\delta_r$ / 1º sideslip | 0.027 |
| Propeller | Unknown but stabilizing in a pusher configuration. See reference [2] |

Assuming 100% rudder effectiveness, the maximum yawing moment available is $C_N \approx 0.007$. Table 6 shows the maximum trimmable sideslip angle with this rudder power.

Table 6: Maximum Trimmable Sideslip

| **Geometry** | **Maximum Trimmable Sideslip** |
|---|---|
| Baseline | 31º |
| Winglets | 14º |
| Strut Fins | 12º |

## Test Matrix

The test matrix included the items listed in Table 7. Note that the CG position can be adjusted to some extent. Therefore a range of positions, ±1 in and ±2 in, were considered to determine the effect on pitch and yaw stability and control.

Table 7: Test Matrix

| Item | Value |
|---|---|
| Longitudinal Center-of-Gravity | baseline: 49 in aft of nose<br>$\Delta x_{CG} = -2, -1, 0, 1, 2$ |
| Angle-of-Attack | -5º to +10º in 1º increments |
| Sideslip | 0º, 10º, 20º |
| Control Deflections | 0º, ±15º, ±30º<br>$\alpha$ = 0º, 5º, 10º<br>$\beta$ = 0º, 10º, 20º |
| Roll Rate | $\frac{pb}{2V_\infty} = 0.049$<br>$\alpha$ from -2º to +10º in 2º increments<br>$\beta$ = 0º, 10º, 20º |
| Pitch Rate | $\frac{qc}{2V_\infty} = 0.003$<br>$\alpha$ from -2º to +10º in 2º increments<br>$\beta$ = 0º, 10º, 20º |
| Yaw Rate | $\frac{\dot{\beta}b}{2V_\infty} = 0.049$<br>$\alpha$ from -2º to +10º in 2º increments<br>$\beta$ = 0º, 10º, 20º |
| Ground Effect | $\frac{h_{root}}{b} = 0.077$ |

## Untrimmed Lift Curve

Equation 1 from [1 eq. 12.6] was used to check the computed lift curve slopes from HASC shown in Figure 10. The value computed from HASC is lower than the theoretical value by about 15%. One reason for the lower lift curve slope is that the rear wing operates in the downwash of the front wing. This phenomenon is known to occur on conventional aft tail surfaces.

$$C_{L_\alpha} = \frac{2\pi AR}{2 + \sqrt{4 + AR^2(1 + \tan^2\Lambda)}} = 4.8 \quad (1)$$

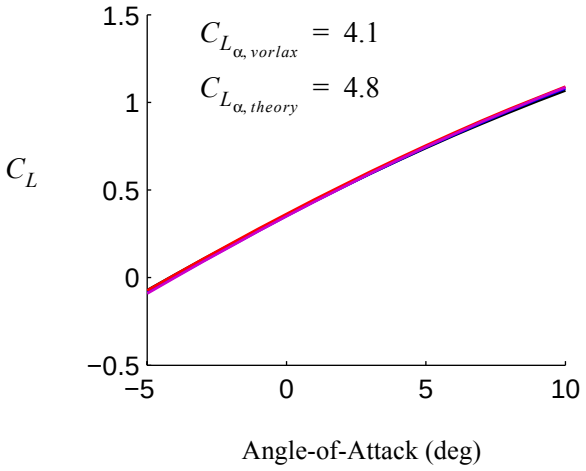


The lift curve of the reference geometry and its derivatives deviate by only small, negligible amounts given the approximations of the geometry and the vortex lattice method.

The computed lift curve slope is somewhat lower than the theoretical value (see eq. 1) of 4.8. This is most likely due to strong downwash from the forward wing on the rear wing. Conventional tail surfaces exhibit the same behavior. Given the slight non-linear shape of the curve, the fit was done over the expect lift coefficient range of 0.3 to 1.0. Using the entire data sets yields a lift curve slope of about 4.4.

**Figure 10: Lift Curves of the Various Geometries**

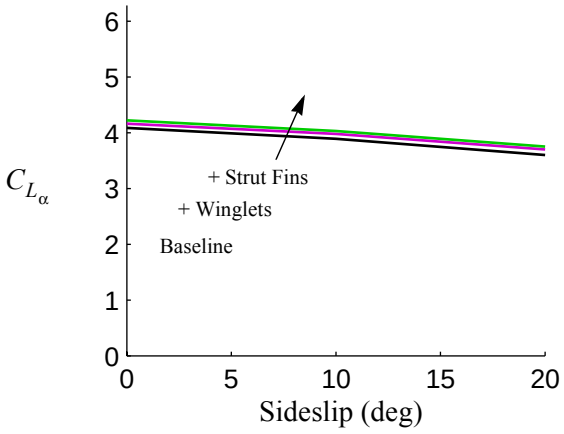


**Figure 11: Lift Curve Slope vs. Sideslip**

## Longitudinal Stability

Figure 12 shows the pitching moment data for the baseline geometry and increments for the various additions. The fuselage is destabilizing (positive increment), the winglets are stabilizing (negative increments), and the Strut Fins are stabilizing, but not as much as the winglets. This behavior is odd. At first glance, the strut fins should be more effective, and it is not clear why the winglets modify the wing pitching moment as much as they do.

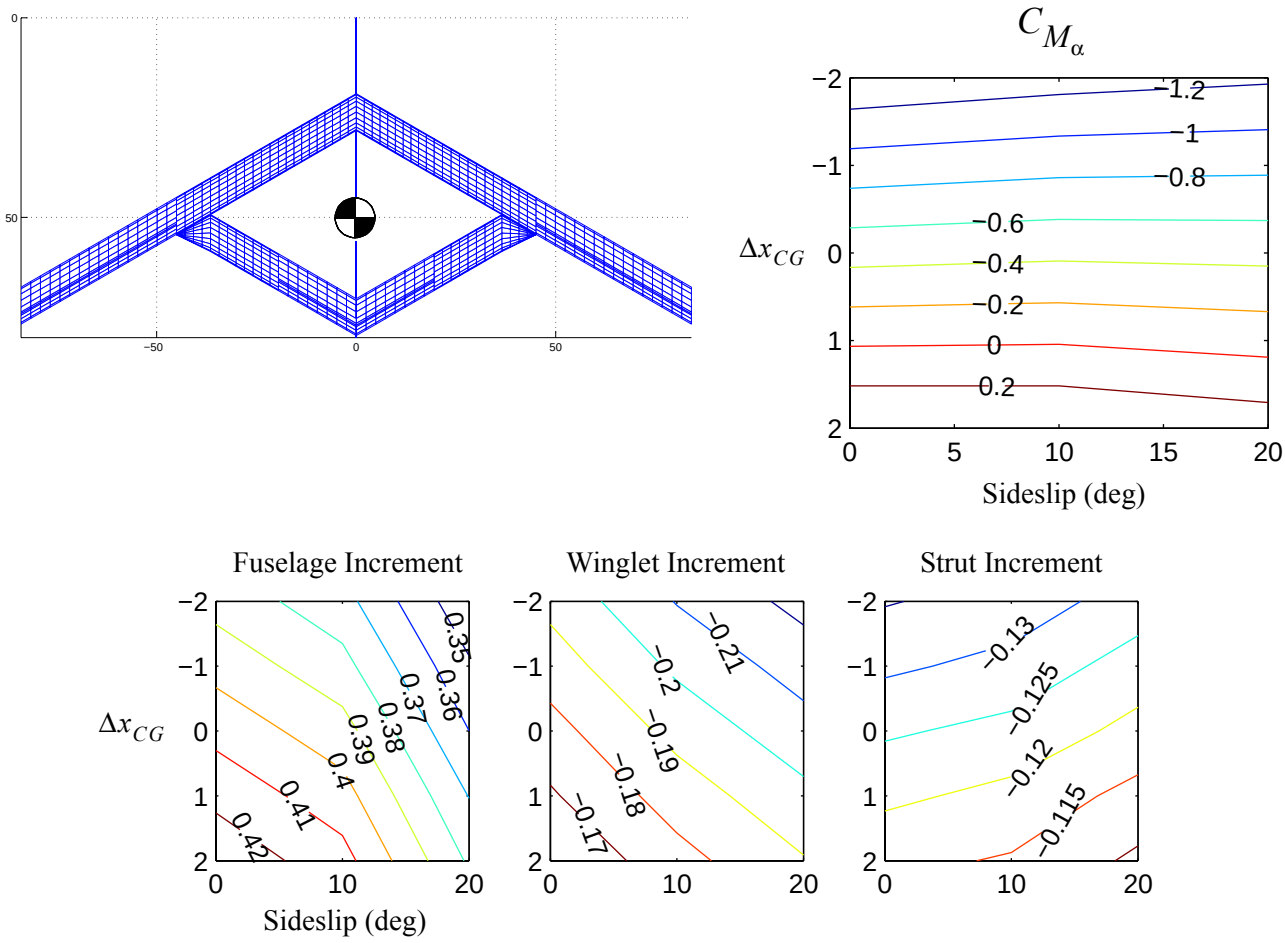


**Figure 12: Pitching Moment Slope with Angle-of-Attack and Increments Due to the Various Components**

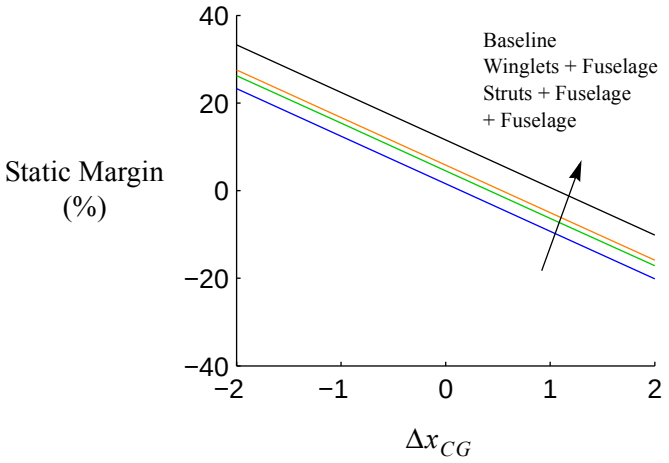


There is a significant difference in the static margin between the baseline and baseline + fuselage geometry. The fuselage is so destabilizing (static margin = 4% at the reference CG position) that the addition of winglets or strut fins for this reason along should be considered unless the CG is shifted forward. Typical RC aircraft will have greater than 10% static margin.

**Figure 13: Static Margin vs. Reference Longitudinal CG Position**

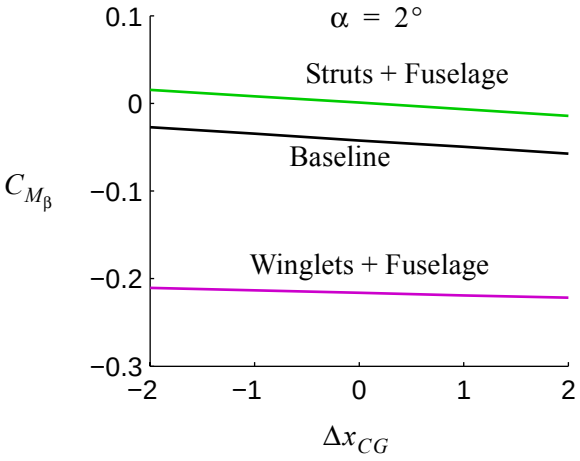


These curves show that there is a potential to pitch with sideslip, especially with the winglet geometry. At 20º sideslip, there would be a change in nose down pitching moment of 0.07, which is a non-trivial change. See the trim plots.

**Figure 14: Change in Pitching Moment due to Sideslip at 2º Angle-of-Attack**

## Lateral Stability

The only lateral derivative measured was the rolling moment due to sideslip, $C_{l_\beta}$, better known as the dihedral effect. Notice the variation with angle-of-attack

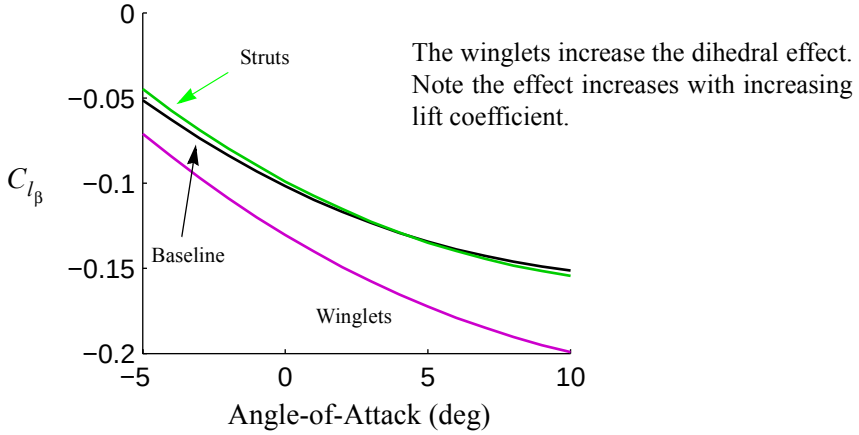


**Figure 15: Change in Rolling Moment with Sideslip (Dihedral Effect)**

## Yaw Stability

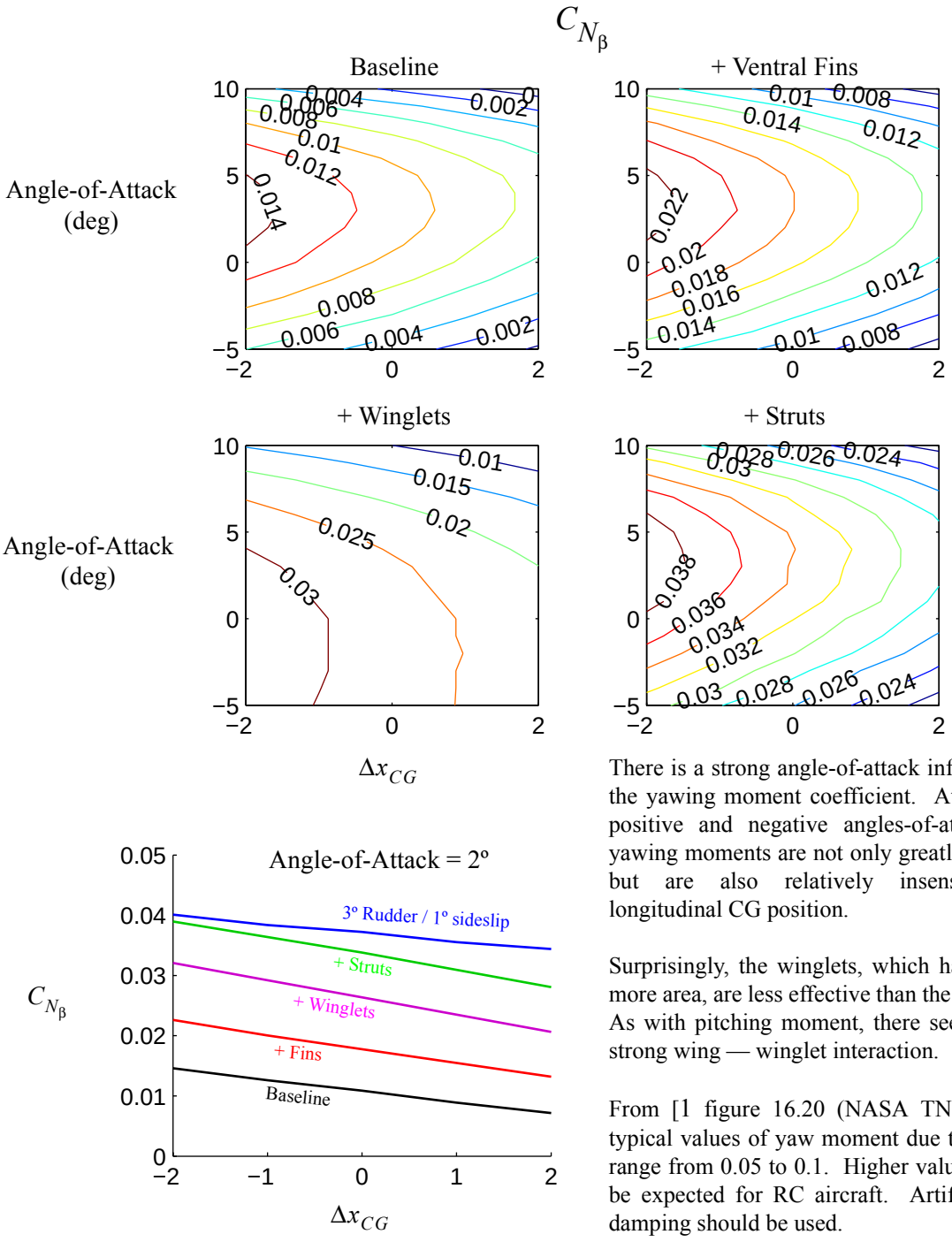


There is a strong angle-of-attack influence on the yawing moment coefficient. At the high positive and negative angles-of-attack, the yawing moments are not only greatly reduced but are also relatively insensitive to longitudinal CG position.

Surprisingly, the winglets, which have much more area, are less effective than the strut fins. As with pitching moment, there seems to be strong wing — winglet interaction.

From [1 figure 16.20 (NASA TN D-423)], typical values of yaw moment due to sideslip range from 0.05 to 0.1. Higher values should be expected for RC aircraft. Artificial yaw damping should be used.

**Figure 16: Yawing Moment Due To Sideslip**

One dynamics mode that can be checked without knowing moments of inertia is the spiral mode stability. Based on the standard spiral mode approximation (sideslip varies slowly, roll rate nearly zero, ignore the product of inertia $I_{xz}$), the criteria for a stable spiral mode is

$$\frac{C_{l_r} C_{n_\beta}}{C_{l_\beta} C_{n_r}} < 1 \tag{2}$$

For spiral stability, the aircraft should have relatively more lateral stability than yaw stability. This quantity is plotted for the baseline, ventral fin, winglet, and strut geometries in Figure 17. Notice that the efforts to increase the yaw stability and damping have created a spiral neutral or divergent mode at normal cruise angles-of-attack. The modified vehicle may be prone to graveyard spirals.

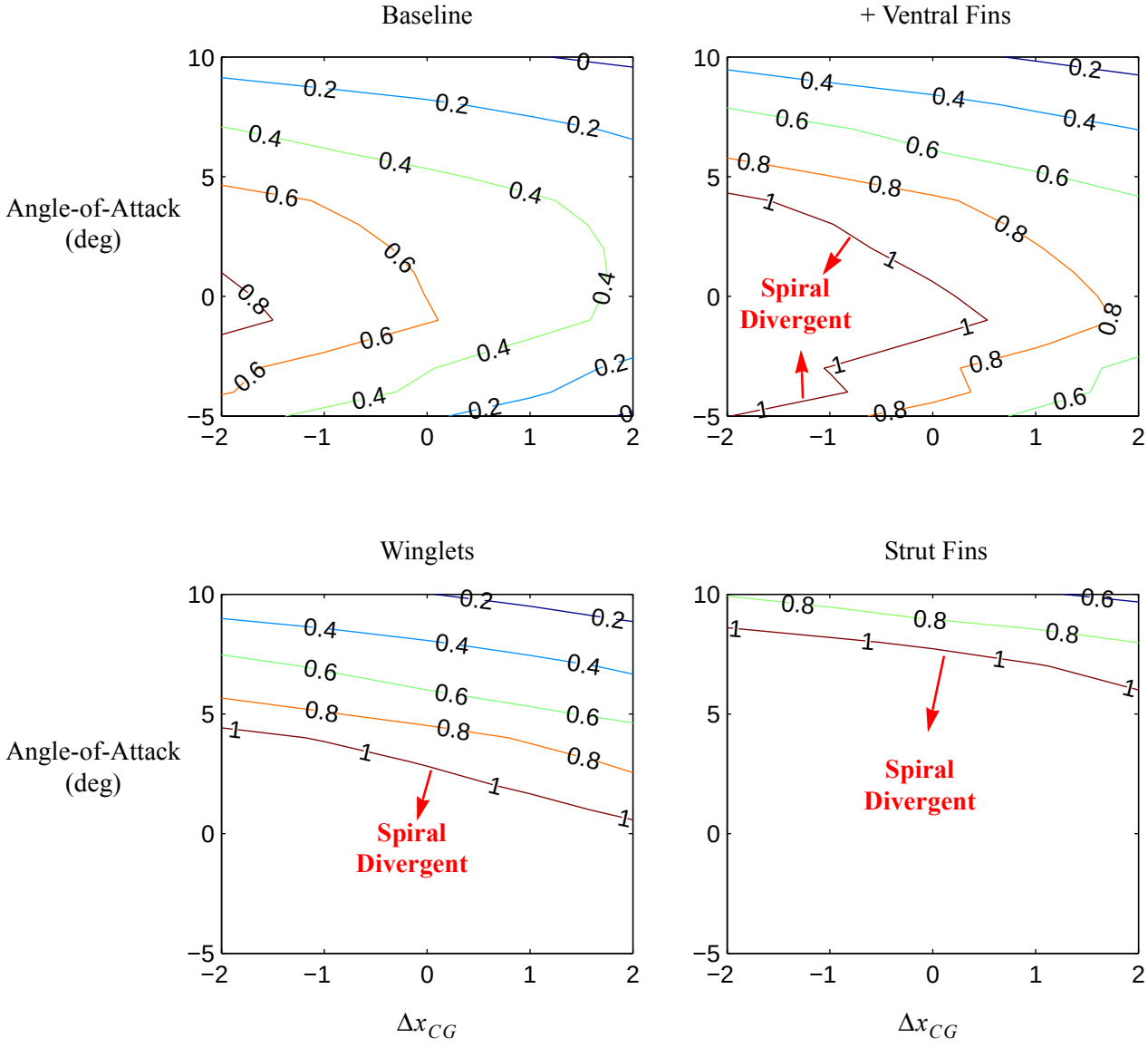


**Figure 17: Spiral Mode Stability**

## Control Derivatives

$$C_{L_\delta}$$

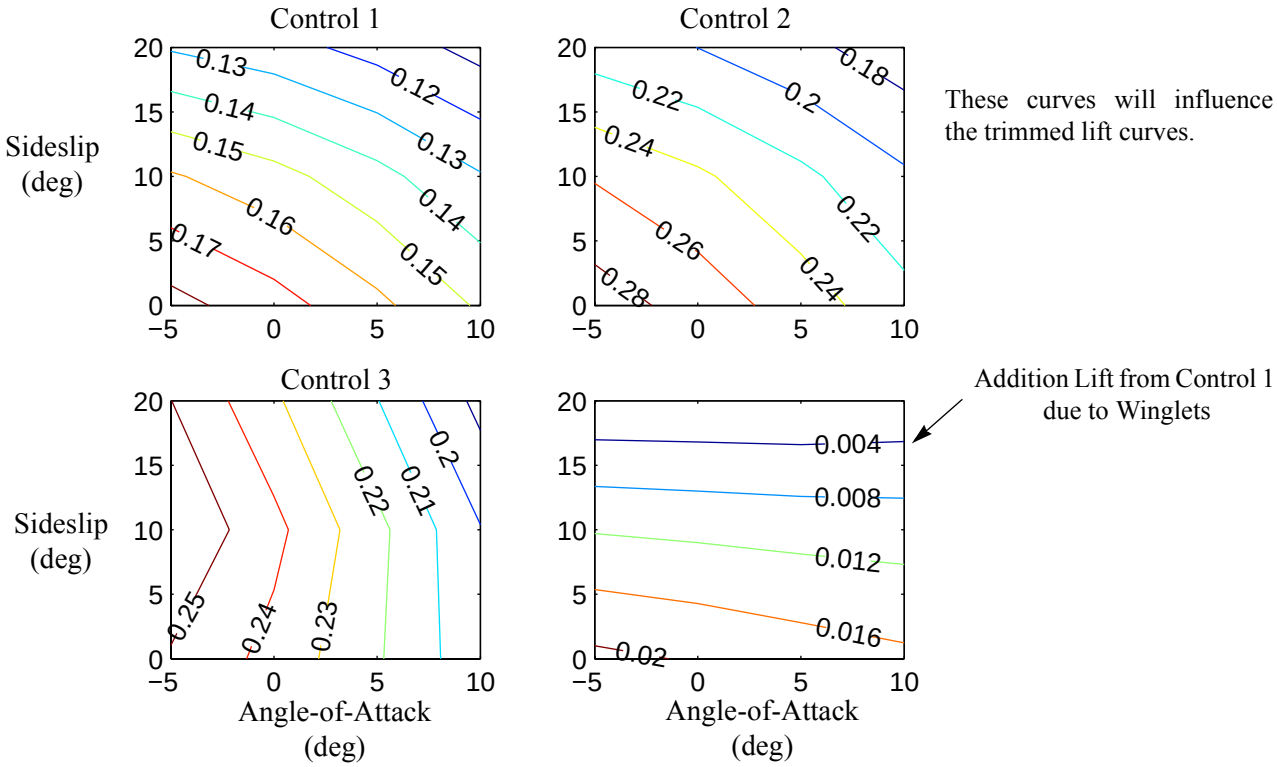


**Figure 18: Change in Vehicle Lift Coefficient with Control Deflection**

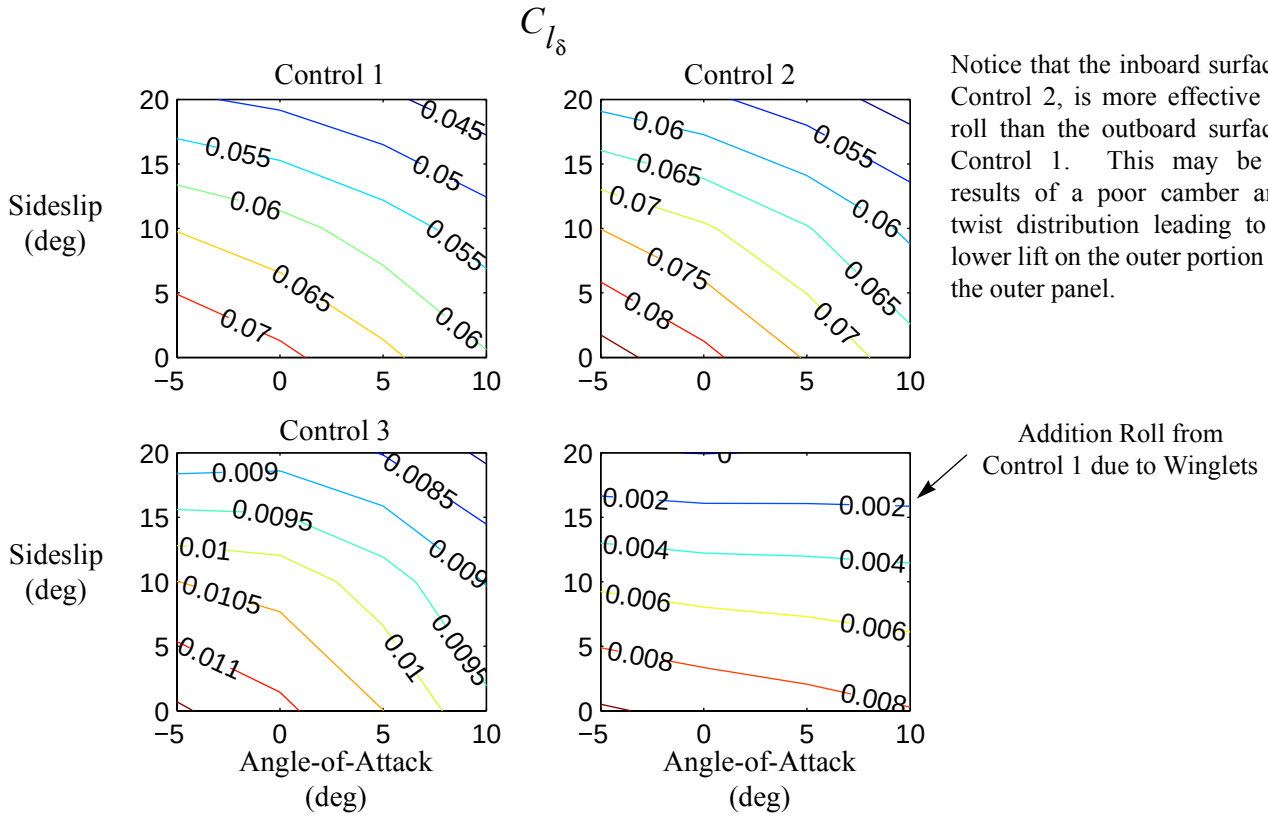


Notice that the inboard surface, Control 2, is more effective in roll than the outboard surface, Control 1. This may be a results of a poor camber and twist distribution leading to a lower lift on the outer portion of the outer panel.

**Figure 19: Change in Vehicle Rolling Moment Due to Control Deflections**

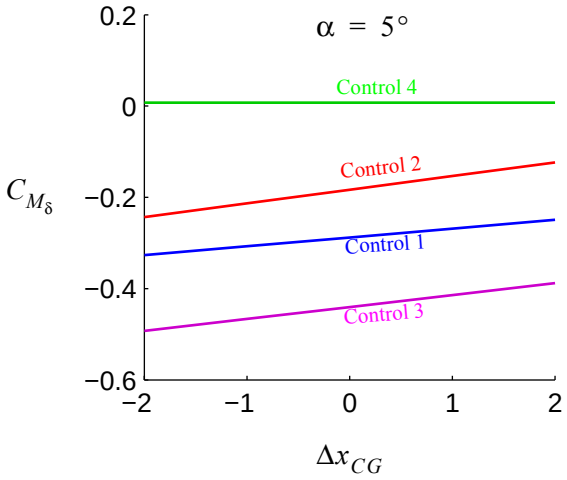


These curves will establish the trim condition for each angle-of-attack.

**Figure 20: Change in Vehicle Pitching Moment Due to Control Deflections**

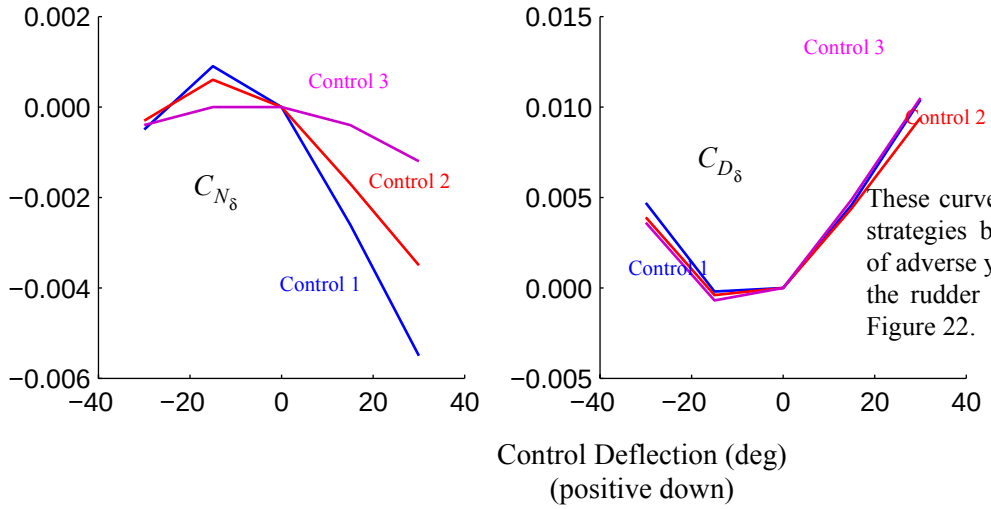


These curves may influence roll strategies because of the effect of adverse yaw and the ability of the rudder to compensate. See Figure 22.

**Figure 21: Change in Vehicle Yawing and Drag Coefficients with Control Deflections**

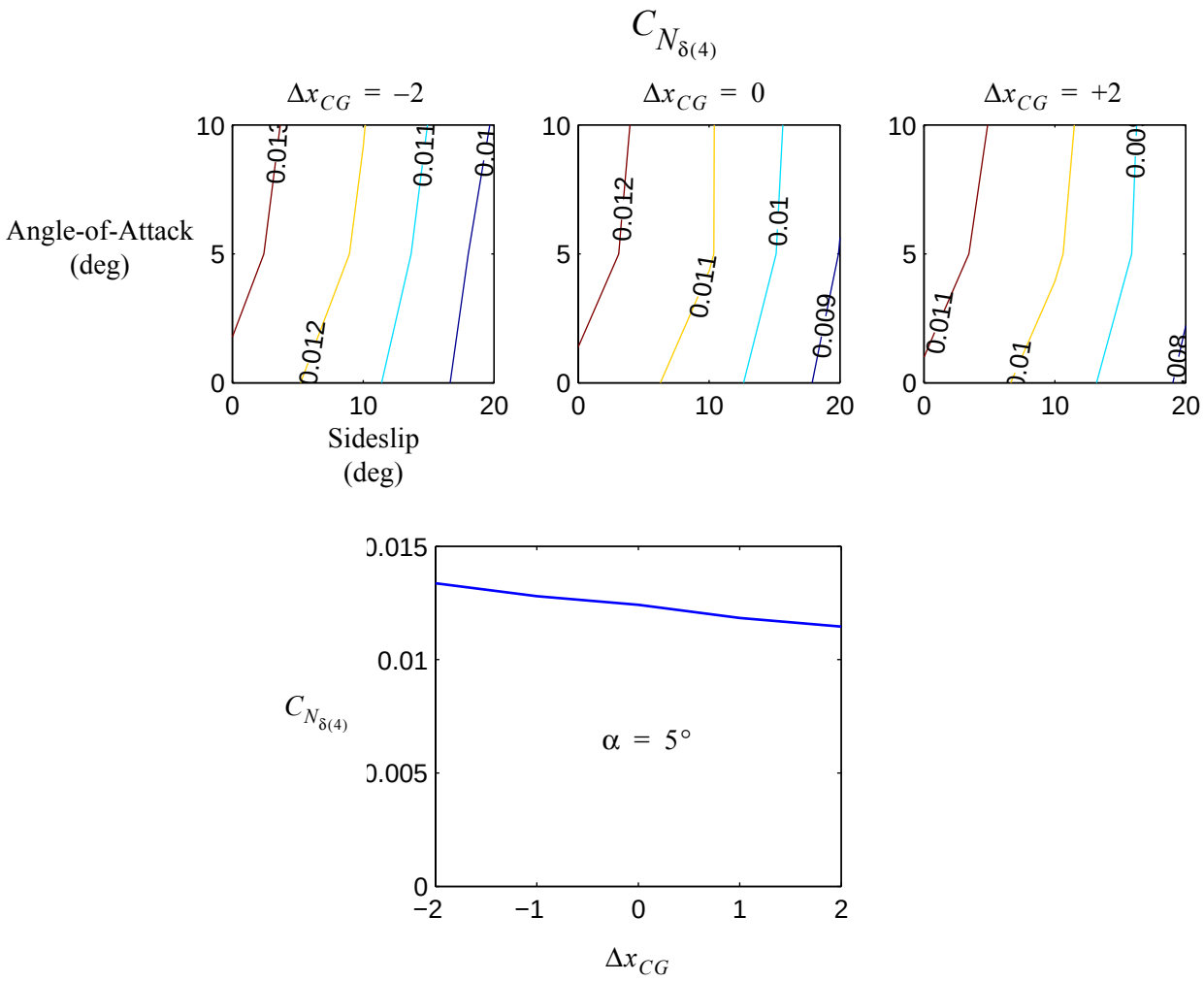


**Figure 22: Change in Yawing Moment Due to Rudder Deflection**

## Rate Derivatives

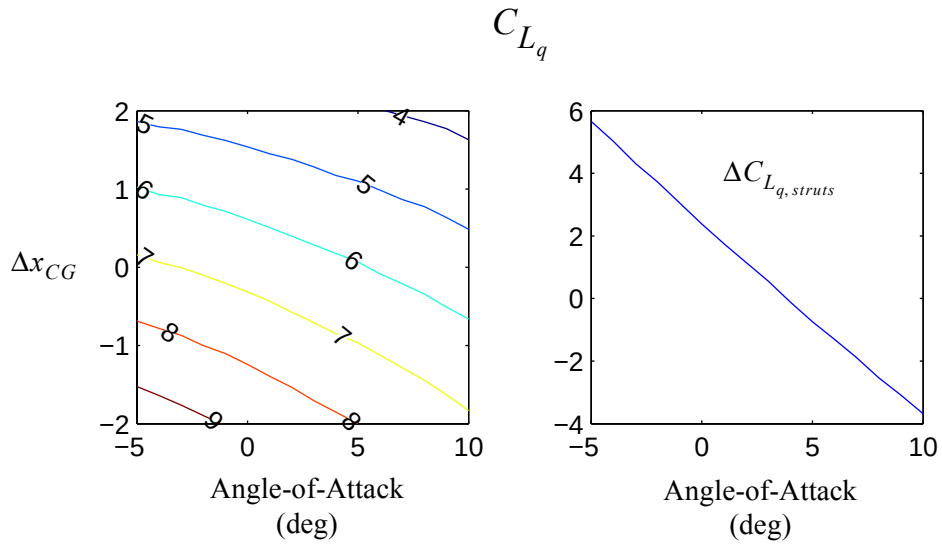


**Figure 23: Change in Lift Coefficient with Pitch Rate**

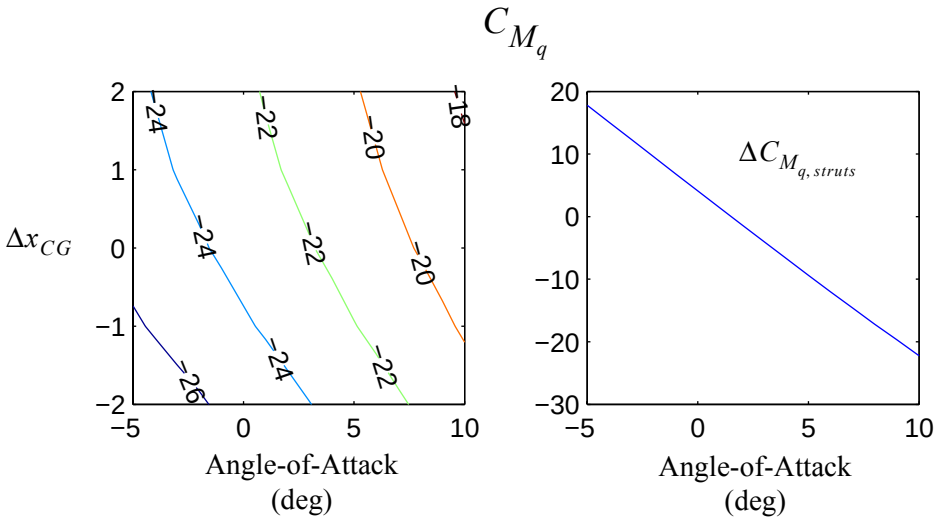


**Figure 24: Change in Pitching Moment Coefficient with Pitch Rate**

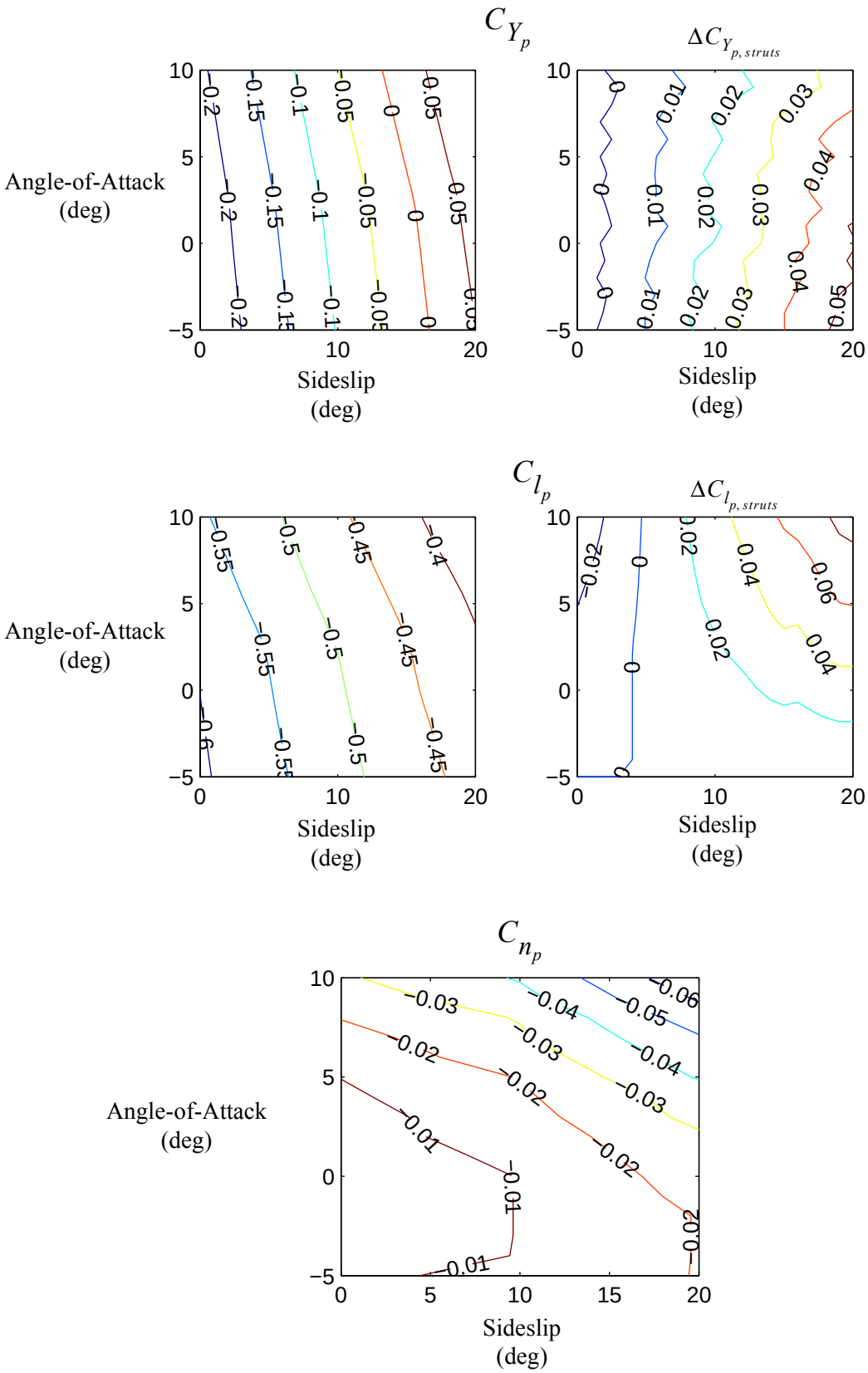


The wiggles in the strut side force coefficient difference plot are numerical noise.

**Figure 25: Change in Side Force, Roll Moment, and Yaw Moment Coefficients with Roll Rate**

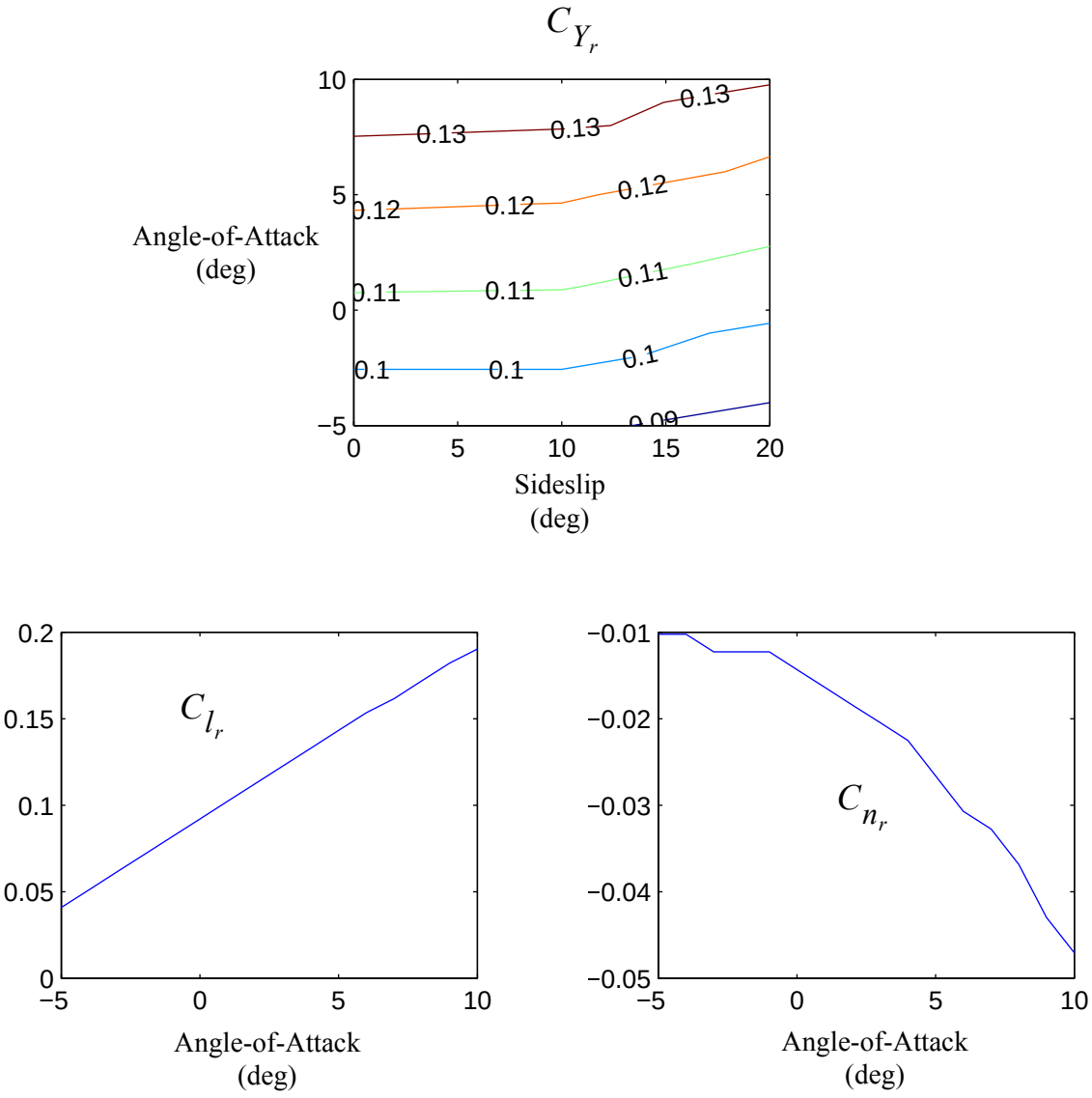


**Figure 26: Change in Side Force, Roll Moment, and Yaw Moment Coefficients with Yaw Rate**

## Control Strategies

For pitch and roll, control strategies have to be developed. That is, if a roll is desired or to trim the aircraft longitudinally, which surfaces should be deflected and by how much?

For pitch, there are two strategies. The first is to use both Control 1 and Control 3 with the same deflection. The second is to use Control 3 only. The first strategy should require smaller deflections on both surfaces compared to the second strategy. Figure 27 illustrates the trimmed elevator deflections and lift coefficients for both strategies. Although strategy 2 requires about double the deflection of Control 3, it is still within the assumed effective range for that surface.

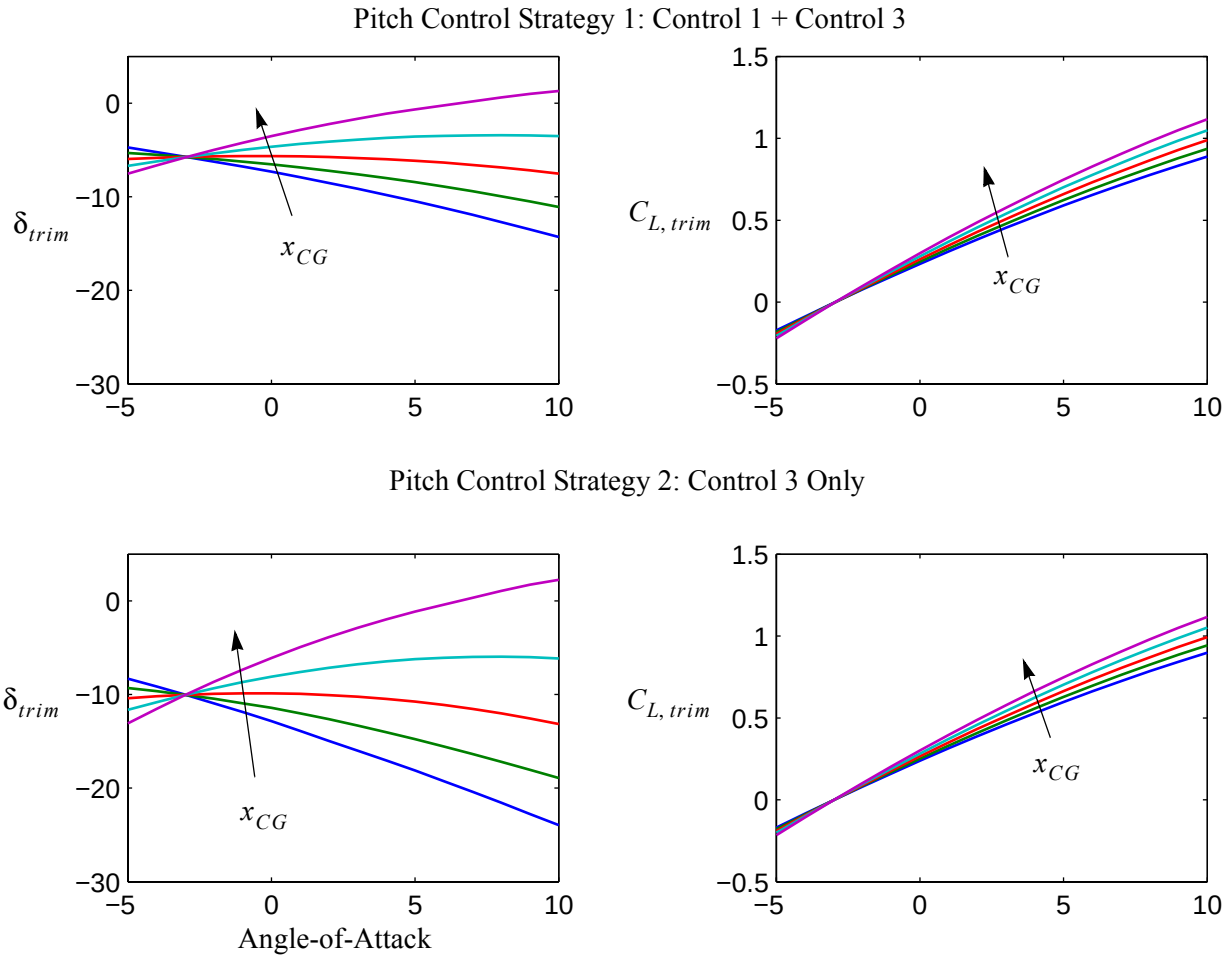


**Figure 27: Trim Elevator Deflections and Lift Coefficients for Surfaces at 100% Effectiveness**

The situation changes somewhat if a 50% control surface effectiveness is assumed. This may be a result of low Reynolds number aerodynamics and unsealed gaps. Figure 28 illustrates the changes with reduced effectiveness. Note that some of the curves are cut off. This indicates that a trim solution could not be found within the ±30º control surface deflection where data was collected. But it also indicates a potential trim problem since deflections greater 30º are probably beyond the stall angle-of-attack for the surface.

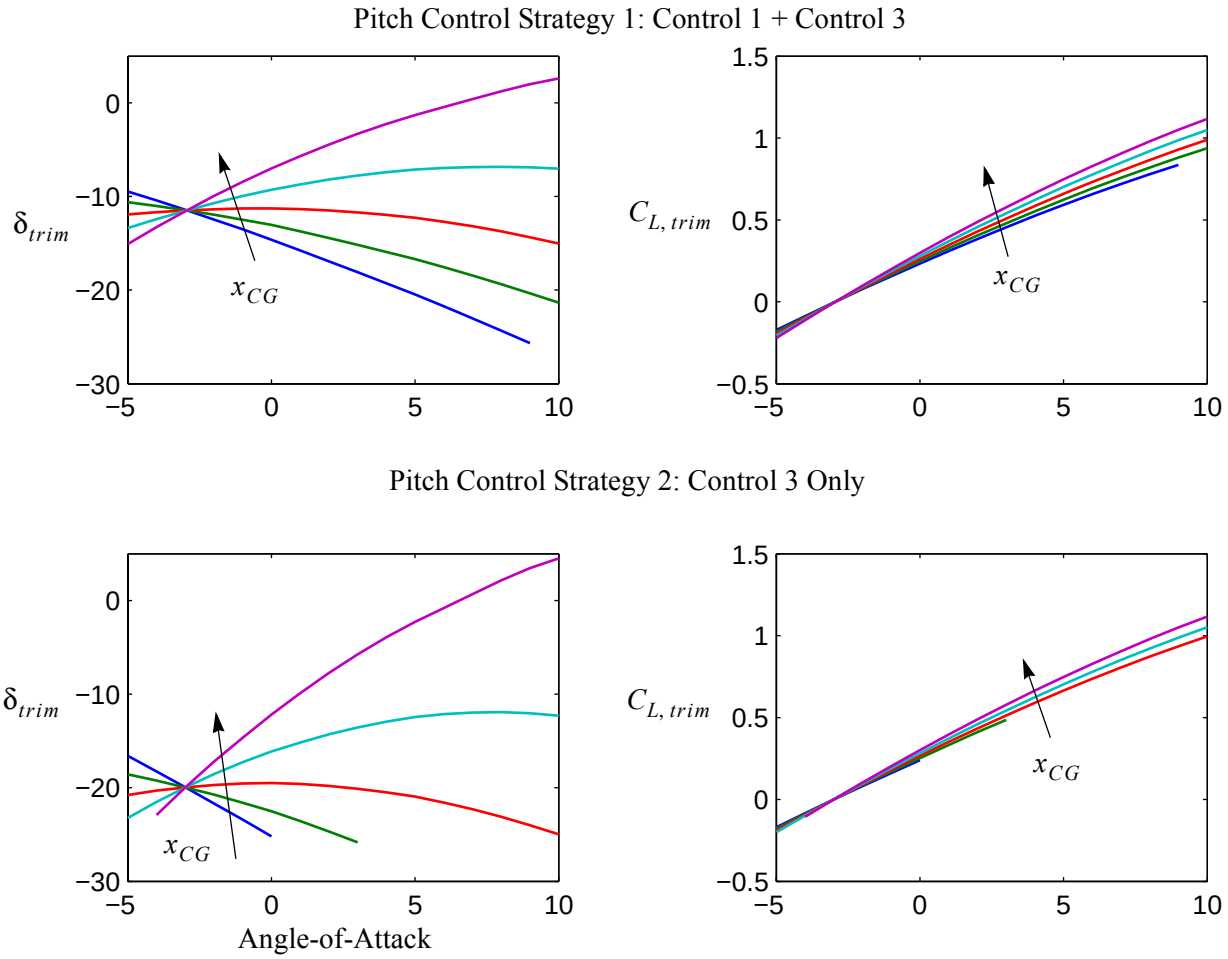


**Figure 28: Trim Elevator Deflections and Lift Coefficients for Surfaces at 50% Effectiveness**

Figure 29 illustrates trim at 20º sideslip. Note that the vehicle may have difficulty trimming at the necessary lift coefficients for CG positions ahead of the reference point.

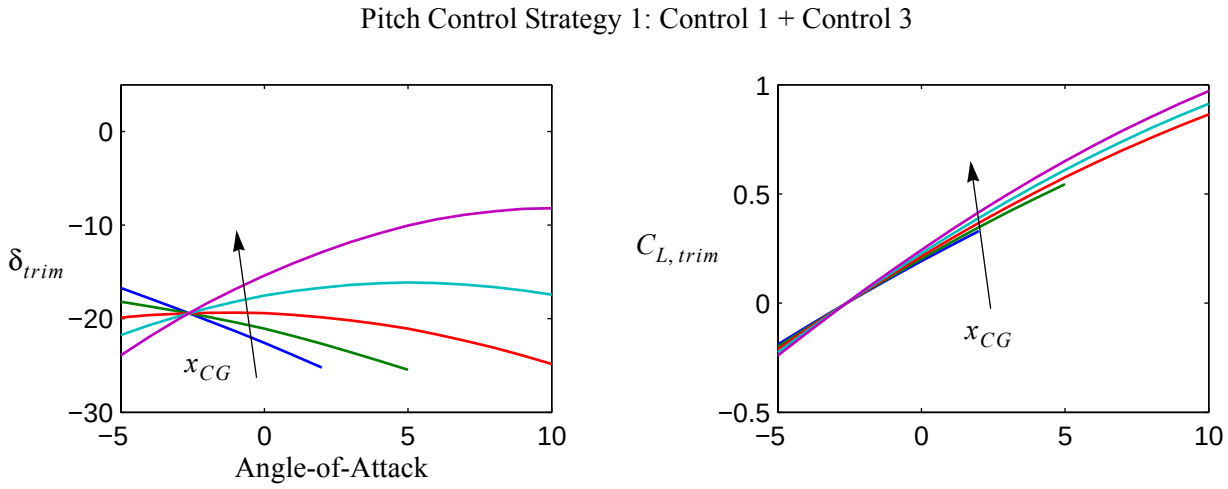


**Figure 29: Trim Elevator Deflections and Lift Coefficients for Surfaces at 50% Effectiveness at 20º Sideslip**

Figure 30 illustrates the trim conditions for the strut fin geometry with 50% control effectiveness.

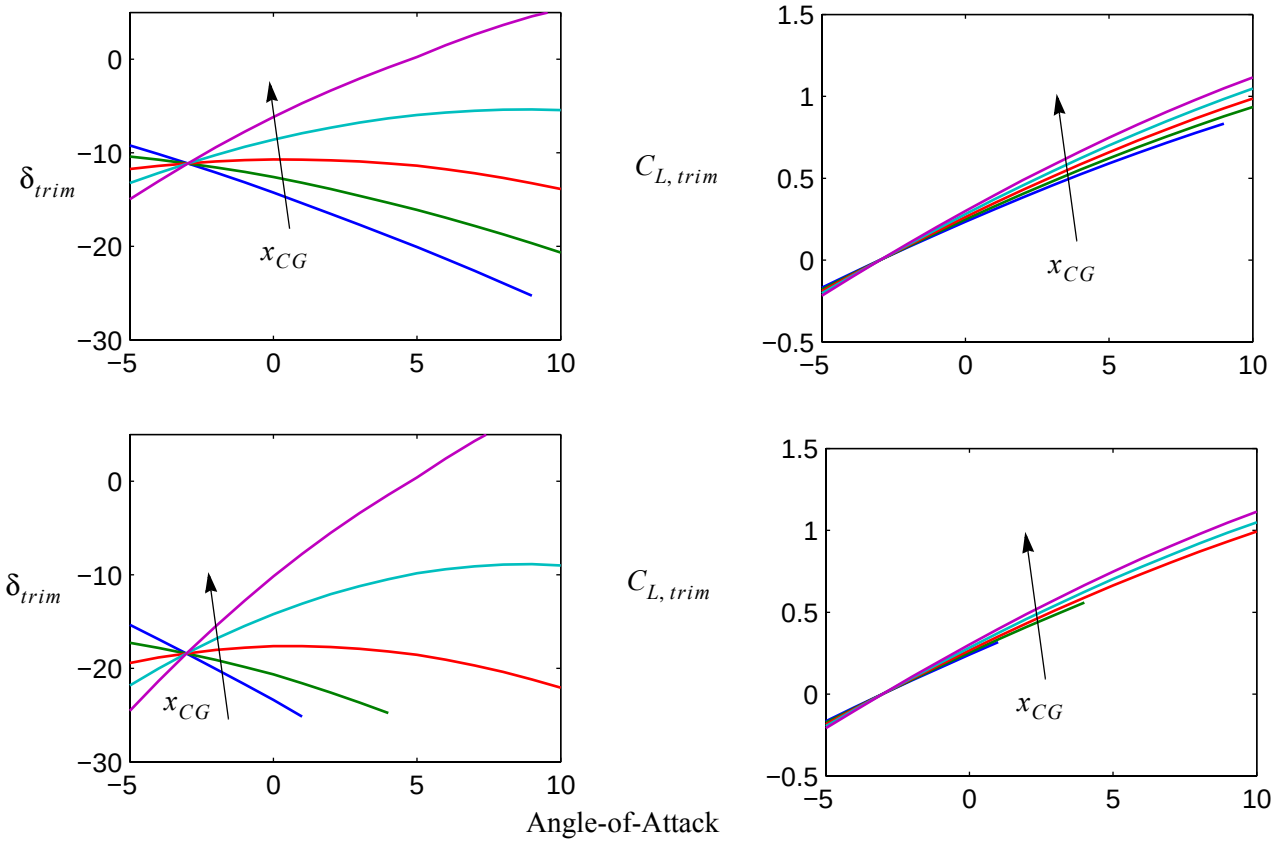


**Figure 30: Trim Elevator Deflections and Lift Coefficients for the + Struts Geometry with Surfaces at 50% Effectiveness**

For roll control, the issue is adverse yaw since the roll rate can not be estimated given the lack of moment of inertia data. If adverse yaw is too high, then it becomes difficult to roll the aircraft. Given the low rudder effectiveness due to its relatively small size, adverse yaw needs to be checked for various control strategies to ensure that the rudder can overcome the adverse yaw or, if it can not, that the adverse yaw is not too large (will prevent roll).

Four strategies will be considered. The first uses Control 1 and Control 2 bilaterally, i.e. Control 1 on both sides of the aircraft is deflected one up and one down. The second only uses Control 2 bilaterally. The third and fourth strategies mirror the first two strategies but only use negative deflections unilaterally, i.e. for a right roll the right aileron is deflected and the left aileron remains neutral. Note that the vehicle lift coefficient decreases since the opposing aileron is not deflected downwards. If the roll time constant is relatively high, an increase in angle-of-attack may be necessary. The maximum decrease in vehicle lift coefficient is approximately 0.25 when both surfaces are used unilaterally. Since the yaw is not symmetric with respect to control deflection and even changes sign for some upward deflections, differential actuation (absolute value of the deflections are not equal) will be considered for strategies 1 and 2.

The results for strategies 1 and 2 are shown in Figure 31. Note that there is a critical point at about -15º deflection (see Figure 21). At this deflection, the induced drag is a minimum for the control surfaces, which increases the adverse yaw. For strategy 1, enough adverse yaw is created that for certain combinations of aileron deflection there is not enough rudder power.

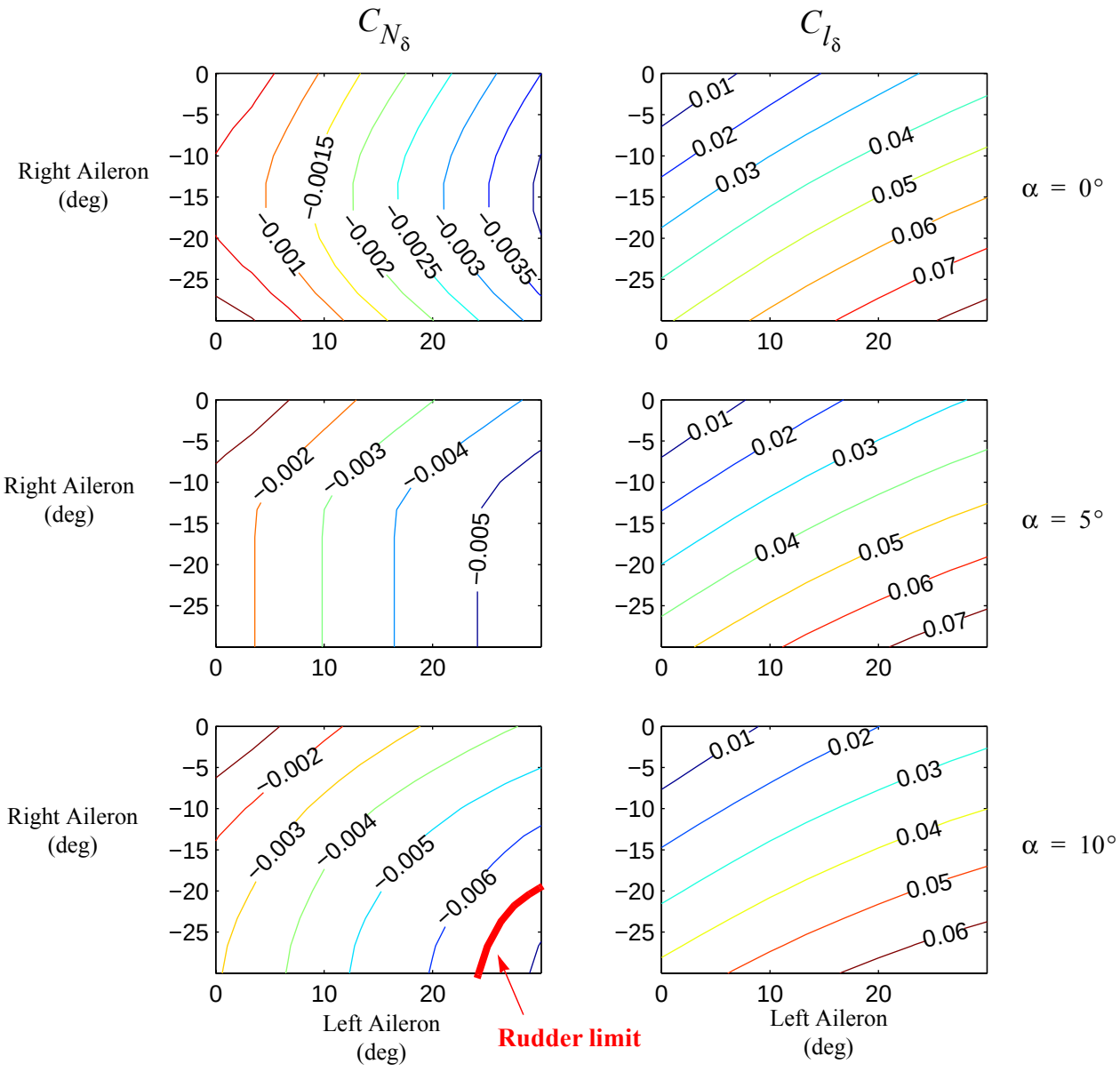


**Figure 31: Roll Control Strategy 1 (Bilateral Control 2)**

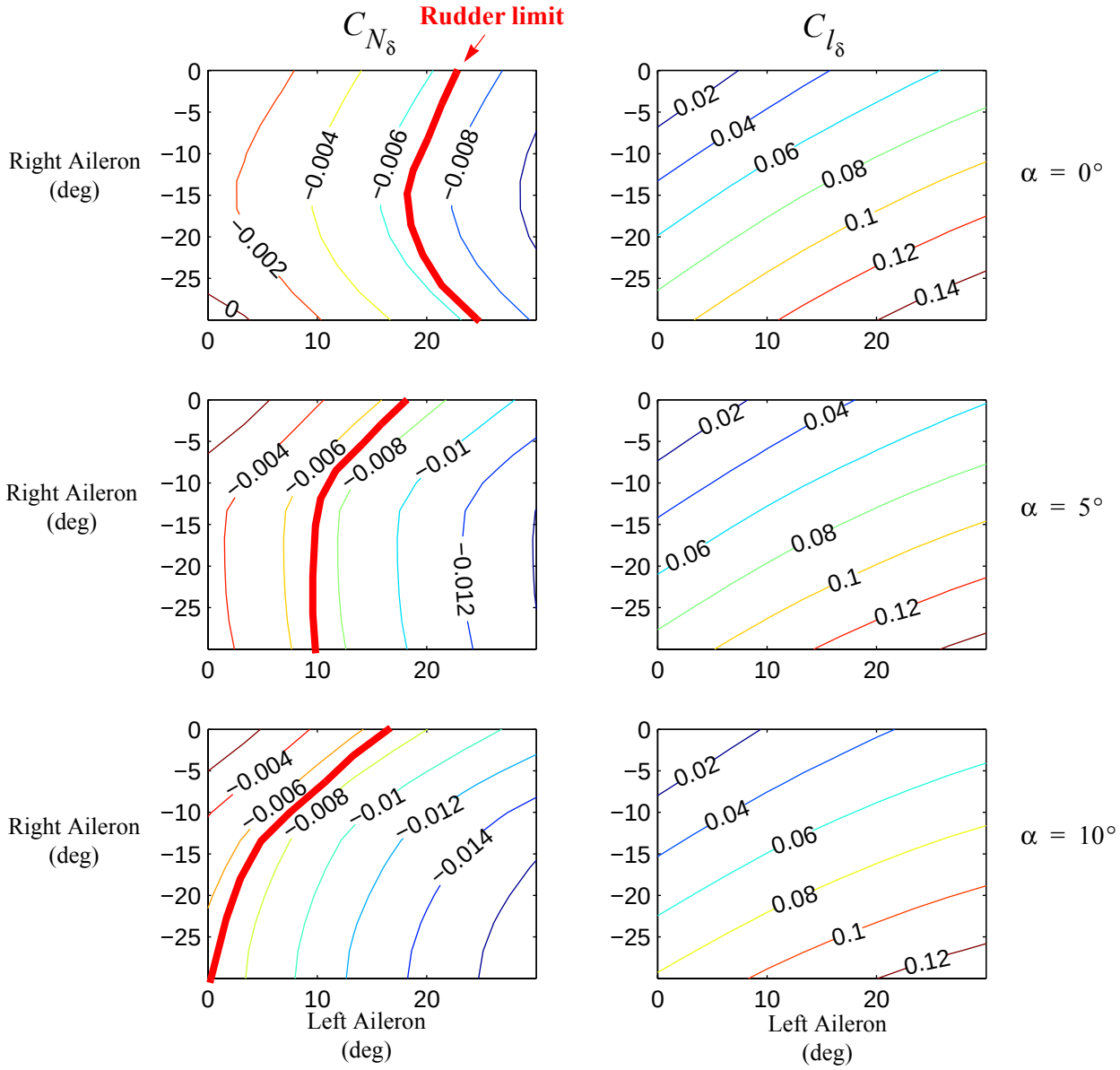


**Figure 32: Roll Control Strategy 2 (Bilateral Control 1 + Control 2)**

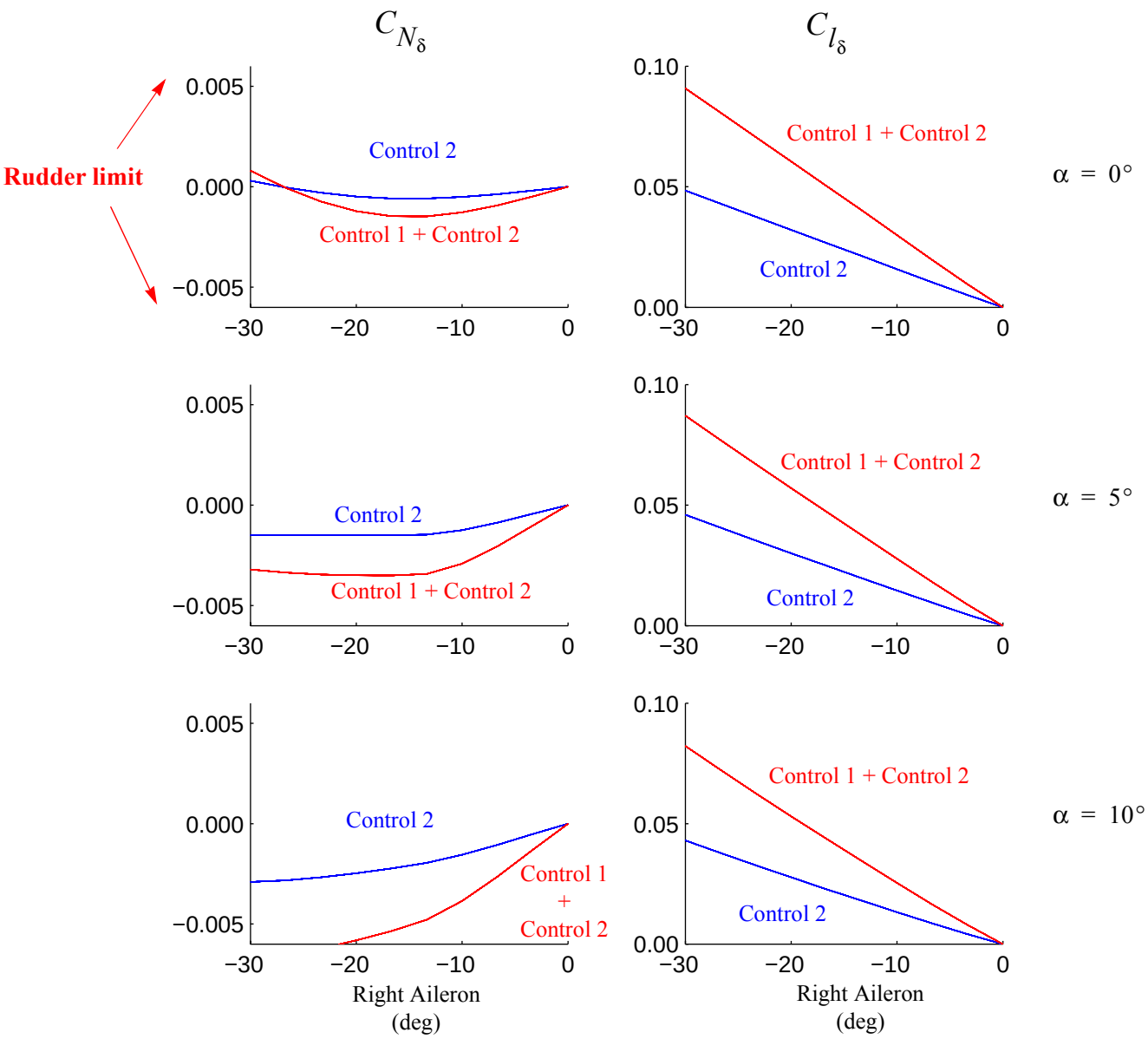


**Figure 33: Roll Control Strategies 3 and 4 (Unilateral Deflection)**

## References

[1] Daniel P. Raymer. Aircraft Design: A Conceptual Approach. AIAA. 1989.

[2] Bandu N. Pamadi. Performance, Stability, Dynamics, and Control of Airplanes. AIAA. 1998.